Advancing Forest Structure Product Validation with Ground, Space and Unmanned Aerial Vehicle Sensors

Benjamin Brede

Propositions

1. Autonomous monitoring is key for remote sensing of forest temporal dynamics.
   (this thesis)

2. Observations from Unmanned Aerial Vehicles are essential to meet requirements of calibration and validation of satellite based forest monitoring.
   (this thesis)

3. Achievability is substituting novelty as the guiding principle for the conception of publications.

4. PhD education nowadays prepares a candidate only to be a scientist, not to be an independent one.

5. Only by re-inventing the wheel, one can really learn how the wheel works.

6. Backup is the health insurance for data scientists.

7. Constantly reminding parents that breast feeding is the best for their child is doing more harm than good.

Propositions belonging to the thesis entitled

"Advancing Forest Structure Product Validation with Ground, Space and Unmanned Aerial Vehicle Sensors"

Benjamin Brede
Wageningen, 21 June 2019

Advancing Forest Structure Product Validation with Ground, Space and Unmanned Aerial Vehicle Sensors

Benjamin Brede

Thesis committee

Promotor
Prof. Dr M. Herold
Professor of Geo-information Science and Remote Sensing
Wageningen University & Research

Co-promotors
Dr J. G. P. W. Clevers
Associate Professor, Laboratory of Geo-information Science and Remote Sensing
Wageningen University & Research

Dr J. P. Verbesselt
Associate Professor, Laboratory of Geo-information Science and Remote Sensing
Wageningen University & Research

Other members
Prof. Dr P. A. Zuidema, Wageningen University & Research
Prof. Dr F. van de Meer, University of Twente, Enschede, The Netherlands
Dr K. Scipal, European Space Agency (ESA), Paris, France
Dr F. Camacho de Coca, EOLAB, Valencia, Spain

This research was conducted under the auspices of the C.T. de Wit Graduate School of Production Ecology & Resource Conservation (PE&RC)

Advancing Forest Structure Product Validation with Ground, Space and Unmanned Aerial Vehicle Sensors

Benjamin Brede

Thesis
submitted in fulfilment of the requirements for the degree of doctor at
Wageningen University
by the authority of the Rector Magnificus
Prof. Dr A.P.J. Mol,
in the presence of the
Thesis Committee appointed by the Academic Board
to be defended in public
on 21 June 2019
at 11 a.m. in the Aula.

Benjamin Brede
Advancing Forest Structure Product Validation with
Ground, Space and Unmanned Aerial Vehicle Sensors
178 pages.

PhD thesis, Wageningen University, Wageningen, The Netherlands (2019)
With references, with summary in English

ISBN 978-94-6343-923-7
DOI 10.18174/473409

Contents

Chapter 1

Introduction

1.1 Motivation

Forests play a crucial role in the functioning of the Earth's climate system, through their role in the carbon, energy and water cycles (Bonan, 2008). A famous example of how these effects have a direct impact on human life and how humans can influence these cycles in turn is the Catskill/Delaware Watershed restoration (Daily and Ellison, 2002). In 1997, the city of New York faced a drinking water crisis due to ageing water purification plants and related bacterial invasion of the drinking water. The construction of a new purification plant was estimated at a cost of \$6–\$8 billion, which would have blown up the New York city communal budget. Instead, the restoration and protection of the forest dominated Catskill/Delaware watershed that provides the drinking water for New York could achieve comparable results at a cost of only \$1.5 billion. In this case, the forested landscape provided an ecosystem service in the form of water purification through interception of rainfall, filtering of pollutants, and water storage. Additionally, forests provide several other services such as carbon sequestration, provision of raw materials, habitats for animals and options for human recreation.

Both above- and below-ground elements of forests contribute to their functionality and service provision. Nonetheless, due to much easier access only above-ground elements are often taken into account when describing forests and assessing their functions. Forest structure can be used as a summarising term for these elements as it can be defined as "[...] the spatial arrangement of the above-ground organs of plants in a [forest]" (Campbell and Norman, 1989). Bongers (2001) further specifies forest texture as "the qualitative and quantitative composition of the vegetation as to different morphological elements" and forest structure as "the spatial arrangement of these elements". In geo-spatial terms texture would describe attributes of canopy elements and structure their location. Important parameters describing forest structure are for example biomass, leaf area, tree height or branch arrangement (Pan et al., 2013).

For the assessment and quantification of these parameters scales matter (Bongers, 2001). Within the canopy, leaves and twigs dominate the description of the canopy structure at scales <1 m, branch arrangement at scales <10 m, crown size, shape and arrangement at scales <100 m, and at landscape level species composition is the prevailing descriptor. Additionally, forest structure is dynamic over time, with different elements having characteristic response intervals. Most traits connected to photosynthesis respond to intra-annual changes of seasons with a periodic behaviour (Lang et al., 2017; Yang et al., 2016), while succession and regrowth after disturbance are directional processes across several years. Responses to climatic changes can affect forest composition over millennia.

In the context of forest structure assessment and monitoring over large areas, Earth Observation (EO) or remote sensing of the Earth has proven a useful tool (Bergen et al., 2009; Pan et al., 2013; White et al., 2016). In principal, EO exploits the effects that

vegetation has on the electromagnetic response of a land surface, no matter whether the surface illumination originates from the sun or from the observation system. However, this leads to the fact that EO is always only providing an indirect measurement of forest structure.

An interesting example for this is the discussion that evolved around the Amazon green-up phenomenon. Several EO-based studies reported a substantial increase in greenness expressed as an increase in Enhanced Vegetation Index (EVI) during the dry season from July to September over large parts of the Amazon rainforest (Huete et al., 2006; Saleska et al., 2007; Samanta et al., 2012; Xiao et al., 2006). This counter-intuitive observation was explained with deep roots that maintain the trees' water supply throughout the dry season. Simultaneously, a change in leaf demography would occur, namely the flushing of new young leaves, which would increase the Near-Infrared (NIR) reflectance of the canopy (Doughty and Goulden, 2008). However, Morton et al. (2014) questioned this hypothesis. They investigated the MODerate-resolution Imaging Spectroradiometer (MODIS) EVI observations underlying most of these studies and found a strong effect of seasonal change in surface anisotropy. These effects are prevalent in surface reflectance and vegetation indices (Sims et al., 2011; Verrelst et al., 2008). Correcting for them led to stable reflectance behaviour and suggested unchanging forest canopy properties. In a follow-up study, Morton et al. (2016) explained seasonal variability of forest productivity observed at eddy fluxtowers with changing light utilisation throughout the canopy that follows from the seasonal change in illumination angles.

The above-mentioned example underlines the need for a complete understanding of the EO signal in response to structural dynamics on the ground in order to allow drawing firm conclusions based on satellite observations. Even more so, it calls for the need for rigorous validation of EO products. Validation in this context should be understood as the "confirmation, through the provision of objective evidence, that the requirements for a specific intended use or application have been fulfilled" (*Quality management systems – Fundamentals and vocabulary* 2015). In this context, the use of biophysical variables instead of vegetation indices should be preferred. This is because biophysical variables are defined independent of the sensing technique and conditions, which should also not affect the observed biophysical variable. This thesis focusses on validation techniques for the two biophysical variables Leaf Area Index (LAI) and Above-Ground Biomass (AGB) that represent forest structure.

The remainder of this chapter is structured as follows: Section 1.2 broadly reviews principal EO techniques related to the retrieval of structural parameters of forests. Section 1.3 introduces (forest) structure products with a focus on LAI and AGB that have evolved based on these technologies, which technologies are used to validate these products and which gaps remain in their validation. Section 1.4 presents new emerging technologies and developments since approximately 2010 that potentially provide solutions to the

encountered calibration and validation challenges. In Section 1.5, the objectives of this thesis are listed that were deducted from these challenges. Finally, Section 1.6 outlines how the objectives were addressed in this thesis and the thesis' structure.

1.2 Forest Structure Retrieval from Remotely Sensed Data

When selecting EO data for the retrieval of forest structural variables, specific regions of the electromagnetic spectrum and sensor characteristics have preferential qualities. Passive, optical sensors sensitive to wavelengths from 350 to 2500 nm are most commonly used, due to their robustness, low cost, data accessibility and intuitive way of signal interpretation, which is similar to the human eye. For example, large scale forest cover assessment has been made possible through routine observations of the Landsat family of satellites (Hansen et al., 2013). However, passive sensor signals carry only limited information about vertical structural variables like LAI when operated at nadir. Multi-angular sampling or exploitation of specific viewing angles is required to overcome this limitation (Chen et al., 2005; Meroni et al., 2004; Roosjen et al., 2018).

Space-borne passive microwave observations at wavelengths from 0.5 to 30 cm have found a much smaller range of applications focussing on vegetation moisture (Barraza et al., 2014b), phenological timing (Jones et al., 2011; Jones et al., 2012) and LAI (Barraza et al., 2014a). Applications with these sensors are limited to biome scales due to the coarse resolution of typically >5000 m, which also makes them difficult to validate with small scale, independent, ground-based measurements.

Signals from active EO technologies, which provide their own target illumination, can be linked more directly to in particular vertical vegetation structure expressed as LAI and AGB. LIght Detection And Ranging (LiDAR) sensors operate in the optical domain at wavelengths in the range of passive, optical sensors. Airborne Laser Scanning (ALS) is used for forest vertical structure assessment, tree height and basal area estimation (Drake et al., 2002) as well as individual tree detection (Duncanson et al., 2014). ALS is used regularly in Europe's Nordic countries for national forest inventories that include tree height and stand delineation (Kangas et al., 2018; Nilsson et al., 2017). Space-borne LiDAR is exploited for continent-scale AGB estimation (Baccini et al., 2012; Baccini et al., 2008; Saatchi et al., 2011). A particular disadvantage of space-borne LiDAR is its discontinuous spatial sampling pattern that produces distinctive ground tracks during single overpasses.

Space- and air-borne Synthetic Aperture Radar (SAR) sensors utilising large wavelengths (>15 cm, L band) are treated as a favourable option to estimate forest AGB wall-to-wall across large areas (Koch, 2010; Santoro and Cartus, 2018). Retrieval based on single images relies on relationships between SAR backscatter coefficients and AGB. Advanced

processing like Polarimetric Interferometric SAR (PolInSAR) allow the retrieval of canopy height, which is closely related to AGB (Villard et al., 2016). Tomographic SAR is also able to resolve the vertical distribution of scattering elements within the canopy similar to LiDAR sensors (Reigber and Moreira, 2000), although both systems are sensitive to different canopy elements according to their exploited spectral domain (Pardini et al., 2018).

Aside from the spectral domain, an important categorisation of forest structure EO technologies is according to their observation platform. The reason for this is that the platform determines the distance to the canopy. This and the finite resolution of digital sensors in turn defines which canopy elements can be resolved. In this context, so called proximal sensing plays a special role. Among these techniques are ground-based sensors that serve to quantify structure at the plot scale and are accepted as means for validation of space- and air-borne observations. For example, lidar-based clinometers are standard instruments in forest mensuration for individual tree height appraisal (Luoma et al., 2017). Terrestrial Laser Scanning (TLS) provides a particular detailed view on the forest canopy that allows the distinction of single branches (Lau et al., 2018), and reconstruction of full trees (Calders et al., 2015b; Gonzalez de Tanago et al., 2018) and canopies (Calders et al., 2018a). Still, these instruments make only indirect measurements of the variable under observation. Especially in the context of LAI estimation this becomes clear: instruments treated as standard for validation practices like the LAI-2000 canopy analyser and Digital Hemispherical Photography (DHP) (Fernandes et al., 2014; Jonckheere et al., 2004) actually measure canopy transmittance. During processing, this quantity has to be interpreted in order to derive the desired LAI.

This brings up a crucial point in the retrieval of forest structure on the basis of EO data. The retrieval always requires a model that connects observation and the desired biophysical variable. This can be a statistical or physical model with arbitrary complexity. In the context of passive, optical EO, Radiative Transfer Models (RTMs) like PROSAIL have been extensively used to retrieve physical canopy and leaf chemical properties (Jacquemoud et al., 2009). However, for application in forests, RTMs like the Discrete Anisotropic Radiative Transfer (DART) or librat models that can represent heterogeneous scenes have been preferred (Calders et al., 2013; Disney et al., 2000; Gastellu-Etchegorry et al., 1996; Malenovský et al., 2008). Probably the most common model for LAI retrieval from below-canopy sensors is the gap fraction model (Weiss et al., 2004).

1.3 Remote Sensing-based Forest Structure Products

Based on available EO technology, a range of scientific products have been developed. The term product is loosely used in literature to refer to both *ad hoc* results as well as systematically produced datasets. Since EO technology has matured over the past decades, monitoring applications are more and more envisaged, so that systematic products

gain in relevance. The products' temporal and spatial resolution vary, but need to be in line with dominant processes in observed variables. For example, LAI in agricultural applications needs to be monitored with sub-weekly resolution to be able to derive meaningful management plans reacting to the crop development (Defourny et al., 2019). The development of global scale products often poses various challenges, because the underlying algorithms needs to be robust and generic to suit a wide range of ecosystems, and processing load is high (Hansen et al., 2013). The Copernicus Land Services contain a palette of vegetation structure products, like tree cover density and LAI (`https://land.copernicus.eu`). Another example for consolidated structure products is the MODIS land product suite (`https://modis-land.gsfc.nasa.gov`).

Leaf Area Index (LAI)

LAI is defined as one half of the vegetation surface area per area horizontal ground (Chen and Black, 1992). It is mostly derived from passive, optical sensors, when global scales are targeted. So far, LAI products have been predominantly based on hectometric EO missions like MODIS due to the availability of high frequency observations and robust algorithms at this scale. Lately, decametric resolution products are targeted based on Copernicus Sentinel-2 (Defourny et al., 2019; Delegido et al., 2011; Verrelst et al., 2013). Production algorithms typically invert RTMs either with Look Up Tables (LUTs) (Myneni et al., 2011) or with Machine Learning Regression Algorithms (MLRAs) like neural networks (Baret et al., 2007).

In order to support LAI product validation efforts, the Committee on Earth Observing Satellites (CEOS) Land Product Validation (LPV) Subgroup has compiled a validation best practice guideline (Fernandes et al., 2014). It was written in order to work towards the Global Climate Observing System (GCOS) targets for global LAI products and therefore typically works with examples of hectometric products. These products cannot be validated directly based on in situ data, because ground reference is typically only representative over (deca)metric scales. Hence, hierarchical upscaling of in situ data should be performed (Figure 1.1).

In this context, the Elementary Sampling Unit (ESU) plays an important role as the smallest spatial unit in the validation chain. The LAI guideline defines ESUs as "[...] contiguous spatial region[s] over which the expected value of LAI can be estimated through in situ measurement[s]" (Fernandes et al., 2014). The ESU size is determined by the maximum within-ESU variability that can be tolerated and hence depends on the spatial LAI variability at the validation site. Taking this into account, the quality of any validation effort is dependent on a number of factors, which each individually can be improved to reach a higher quality validation:

- Spatial within-ESU LAI variability. This can be controlled by choosing homogeneous sites for ESUs, but will be limited by the site conditions.

- The number of established ESUs defines the confidence with which uncertainties can be reported.
- Speed and accuracy of the in situ acquisition method.
- Resources available for the validation effort. These will most likely be given and/or be limited.

Wide reaching validation efforts have been undertaken in different projects with varying spatial and temporal coverage. For example, the BEnchmark Land Multisite ANalysis and Intercomparison of Products (BELMANIP) project collected in situ observations from 371 ESUs across the globe from dedicated campaigns and existing experimental networks for validation of hectometric products (Baret et al., 2006). However, these special efforts are rare. Systematic acquisition of LAI is performed within ecosystem networks like the Integrated Carbon Observation System (ICOS) in Europe and the National Ecological Observatory Network (NEON) in the United States. FLUXNET is a meta-network summarising several regional or national networks. However, the sites of these networks were typically not intended for validation of satellite land products, so that the chosen locations and surroundings might not be optimal (Fang et al., 2012b) and respective measurements might not get high priority.

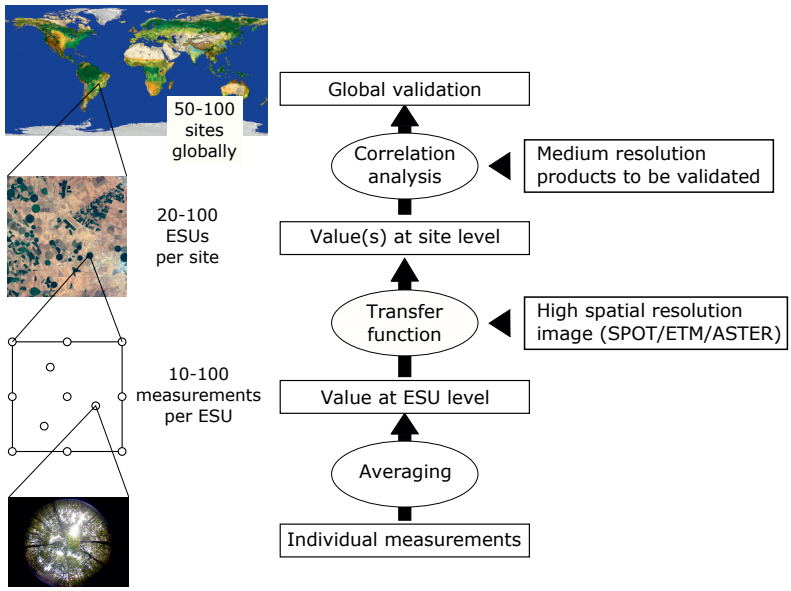

Figure 1.1: Global LAI product validation procedure (remodelled after Morisette et al., 2006). Image credits: ESA (2005), ESA and Université Catholique de Louvain (2010), and Jonckheere et al. (2004).

A range of studies have shown that independent validation data from in situ measurements is essential to evaluate LAI products. They could generally conclude that global LAI products did not meet quality requirements set by GCOS like absolute accuracy of $0.5\,m^2\,m^{-2}$ (Canisius et al., 2010; Fang et al., 2012a; Fang et al., 2012b). This is especially true for forest biomes, where absolute errors are larger and agreement between global datasets is lower compared to other biomes (Fang et al., 2013; Garrigues et al., 2008). Still, due to the available validation data, LAI land surface products in general have reached validation stage 2 of 4 in the CEOS validation hierarchy. This means that "product accuracy is estimated over a significant set of locations and time periods by comparison with reference in situ [...]" (Land Product Validation subgroup, 2019). In order to progress in validation levels and thereby increase scientific soundness of the products, the uncertainty structure associated with the products has to be further evaluated (level 3) and validation needs to be performed regularly (level 4). For this, the total number and the temporal coverage of in situ sites needs to be increased.

Above-Ground Biomass (AGB)

AGB is defined as the "amount of organic matter that is stored in vegetation above the ground level" (Santoro and Cartus, 2018). In contrast to LAI, there are no operational, global AGB products available yet. Product development has been hampered by the lack of systematic observations from suitable space-borne missions. Only the Advanced Land Observation Satellite (ALOS) Phased Array type L-band Synthetic Aperture Radar (PALSAR) missions of the Japan Aerospace Exploration Agency (JAXA) would suit this purpose, but data access is connected to costs, which is a major hurdle on the way to global products (Reiche et al., 2016). Noticeable regional AGB and Growing Stock Volume (GSV) products were prepared for the pan-tropics (Avitabile et al., 2016; Baccini et al., 2012; Saatchi et al., 2011), northern hemisphere (Santoro et al., 2015), and African woodlands and savannahs (Bouvet et al., 2018).

All of the above-mentioned maps rely on extensive databases of ground measurements based on forest inventory plots, which are used both for model calibration and validation. Plot AGB estimates are typically derived with plot tree inventories for which simple tree metrics, such as Diameter at Breast Height (DBH) and tree height are measured (Chave et al., 2005). These metrics are used in combination with Allometric Scaling Equations (ASEs) — also called allometric models — to derive AGB. ASEs in turn need to be established based on empirical relationships between the tree metrics and AGB, for which calibration samples need to be harvested destructively. Final ASEs are species or region specific and wrong application can propagate errors into the AGB product (Yuen et al., 2016).

Despite progress in AGB mapping approaches, Mitchard et al. (2013) found markedly different AGB estimates and patterns between the maps of Saatchi et al. (2011) and

Baccini et al. (2012), with differences only cancelling out when aggregating to the country scale. Next to differences in data sources and processing procedures, different ASEs underlying the training data were discussed as principal reasons for the map differences. This underlines the significant role of ASEs and plot level AGB estimation.

In contrast to the case of LAI, a best practice guideline for AGB product validation is still in preparation. Also, AGB products are only working towards CEOS validation stage 2, which is targeted for 2019 (Land Product Validation subgroup, 2019).

1.4 Innovations in Technology and Data Accessibility as Opportunities for Innovation in Product Validation

As outlined in the previous section (Section 1.3), global vegetation structure product calibration and validation in particular of forests face specific challenges. In summary and with regard to the technical process of validation, these challenges require regular validation data in case of LAI as well as accurate AGB estimation at the tree level combined with scalability of such methods to the plot level. Since technological evolution and data accessibility have ever been fundamental drivers in Earth Observation innovations, forest structure product calibration and validation is no exception to this and recent technologies could improve validation data production.

Concerning ground based systems, automatic sensor systems have been introduced that perform measurements periodically. In the case of LAI, Li et al. (2015b) combined DHP with wireless network technology to automatically acquire LAI of agricultural crops. Crop photos were uploaded to a central server, which allowed continuous remote monitoring. Fan et al. (2018) developed a simple VIS/NIR camera system for ryegrass monitoring. The raw images were radiometrically calibrated to Bidirectional Reflectance Factor (BRF) and multi-linear regression models were established with LAI derived with an LAI-2200. Both systems can provide daily measurements of LAI, but employ downward looking optics and connected processing procedures, and are therefore not immediately suitable for forest applications.

LiDAR

LiDAR has seen a steep increase in forest structure applications, because of its ability for explicit 3D structure retrieval, as indicated by the rise in occurrence of the keyword in scientific publications (Figure 1.2). It is worth noting that LiDAR systems can primarily be divided into two types for which data recording and subsequent analysis techniques differ. These are large-footprint, full-waveform systems like National Aeronautics and Space Administration (NASA)'s Laser Vegetation Imaging Sensor (LVIS) and small-footprint,

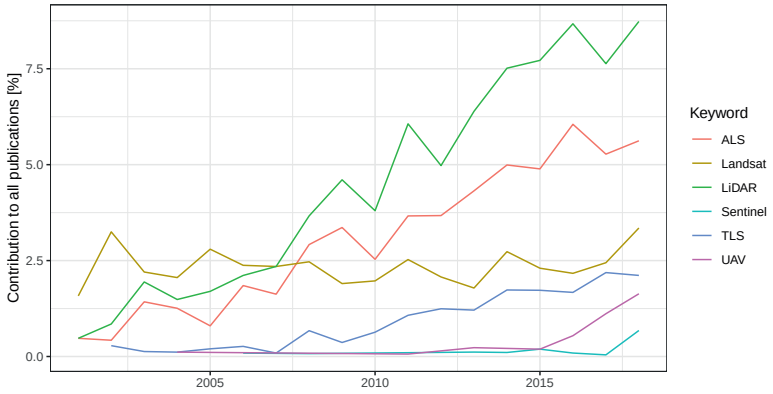

Figure 1.2: Occurrence of selected technologies as keywords in Web of Science publications relative to all publications in connection to forest structure since 2000. Additional to label terms the following synonyms were used: Laser scanning for LiDAR, airborne/terrestrial lidar and airborne/terrestrial laser scanning for ALS/TLS, UAV, UAS, drone and RPAS for Unmanned Aerial Vehicle (UAV). Only the fields Environmental Sciences & Ecology, Forestry, Physical Geography, Imaging Science & Photographic Technology, and Remote Sensing were considered (accessed: 2019-01-29).

discrete return systems of commercial suppliers like RIEGL and Leica. The former require interpretation of the recorded waveform and typically assume a statistical model of the canopy. The latter allow for discovery of discrete elements like individual trees, branches and leaves, and can possibly also simulate full-waveform, space-borne LiDAR (Ristorcelli et al., 2014).

For the estimation of LAI and the vertical distribution of foliage throughout the canopy expressed as Plant Area Volume Density (PAVD), ALS was demonstrated to be an effective tool over large areas (Morsdorf et al., 2006; Zheng and Moskal, 2009) as well as in the context of space-borne missions (Korhonen et al., 2017; Tang et al., 2014). ALS LAI retrieval relies on the gap fraction model, which is also applied with indirect ground-based methods like DHP, but for ALS often with simplifying assumptions. For example, viewing direction is often assumed to be nadir, even though neglecting observation geometry can lead to systematic errors at large scan angles (Liu et al., 2018; Zheng et al., 2017).

ALS has also proven its usability for forest AGB estimation at the plot (Asner and Mascaro, 2014; Kankare et al., 2013), regional (Drake et al., 2002) and national level (Kangas et al., 2018; Nilsson et al., 2017). In contrast to LAI, AGB methods rely on empirical relationships between AGB measured in forest inventory plots and ALS features. In the case of full-waveform, these features are typically some type of canopy height metric like the Height Of Median Energy (HOME) (Drake et al., 2002). Height metrics are also used in the case of discrete return systems (Asner and Mascaro, 2014), but these can

additionally provide Individual Tree Detection (ITD), which can further support AGB estimation (Duncanson et al., 2014; Eysn et al., 2015; Kankare et al., 2013; Koch et al., 2006; Strîmbu and Strîmbu, 2015).

These two fields show the possible synergies between LAI and AGB retrievals, which are both possible from ALS. However, a bottleneck with ALS is data availability. Even though many countries in western Europe, Scandinavia, and North America have regular, national ALS surveys, which are also exploited for infrastructure and natural resource management, only some countries make these datasets publicly available. Additionally, repetition frequencies are too low to track seasonal changes for effective LAI validation. ALS availability is even lower in tropical countries, where 44.3 % of global forest area is situated (Keenan et al., 2015).

The introduction of TLS into forestry applications in the early 2000s was driven by the motivation to measure forest plots in an accurate, rapid and reproducible manner (Liang et al., 2016). Therefore, initial studies focussed on emulating traditional forest inventories by deriving stem maps, DBH and tree height (Bienert et al., 2006; Liang et al., 2016; Simonse et al., 2003). Since then, the number of studies that utilise TLS capabilities has steadily grown (Figure 1.2). Meanwhile, TLS is discussed as a disruptive technology rather than a development (Newnham et al., 2015) in particular in the context of AGB measurements (Disney et al., 2018) as well as forest ecology (Malhi et al., 2018).

AGB estimation by means of TLS is typically achieved by extracting single trees from plot-scale point clouds and subsequently fitting simple geometrical models — usually based on cylinders — to the single tree point clouds (Hackenberg et al., 2014; Raumonen et al., 2013; Stovall et al., 2017). In fact, current studies predominantly focussed on single tree AGB estimation (Calders et al., 2015b; Gonzalez de Tanago et al., 2018; Lau et al., 2018; Momo Takoudjou et al., 2018) due to the challenges of plot-scale tree reconstruction. These challenges are increasingly tackled: improved field protocols allow accurately co-registered plot-scale point clouds (Liu et al., 2017; Tremblay and Béland, 2018; Wilkes et al., 2017), automatic segmentation algorithms can identify individual trees (Burt et al., 2018; Parkan and Tuia, 2015), and automatic foliage identification algorithms can separate photosynthetically active material from woody components (Vicari et al., 2019; Wang et al., 2018). Still, fieldwork is time consuming and requires 3 to 6 days/ha (Wilkes et al., 2017). Thus, plot-scale analysis (Calders et al., 2018a) and direct upscaling to space-borne missions is rare for AGB estimation.

With respect to foliage and LAI, TLS has been adopted as a close approximation to the point quadrat method (Wilson, 1963). In this sense, TLS has been used to estimate gap fraction and subsequently LAI. The distance measurement capability of TLS has also allowed to derive PAVD, which is the vertical distribution of foliage across the canopy (Jupp et al., 2009). The active character is also an advantage over passive ground-based sensors as it provides independence from illumination conditions (Jupp et al., 2009) and

can achieve discrete clumping appraisal through voxelisation (Pimont et al., 2018). Further improvements have been suggested with respect to multi-return TLS signals (Lovell et al., 2011; Newnham et al., 2012), topographic correction of PAVD profiles (Calders et al., 2014), individual tree LAI estimation (Béland et al., 2011; Li et al., 2017), fieldwork protocols (Zheng and Moskal, 2012), treatment of gap fraction underestimation due to partial hits (Hancock et al., 2014), bias treatment in voxelised approaches (Pimont et al., 2018) as well as calibration procedures (Soma et al., 2018).

For the installation in forests, Culvenor et al. (2014) developed an automatic LiDAR-based LAI monitoring system, which combines the advantages of monitoring instruments and TLS. However, the prototype was still prone to malfunctions in early experiments as well as to battery drainage (Griebel et al., 2015). Additionally, rain and moist weather had a negative impact on the recorded LAI, so that rain events need to be identified and filtered from the record (Griebel et al., 2015; Portillo-Quintero et al., 2014). Finally, LiDAR systems tend to have a higher price tag than passive sensors due to their specialised sensors and system configuration, which limits the use in wide range satellite validation.

UAV

UAVs — also called Unmanned Aerial Systems (UASs), Remotely Piloted Aircraft Systems (RPASs) or simply drones — do not provide a fundamentally new class of sensors for vegetation observations, but rather a new perspective that could previously not be filled with ground-based, air- or space-borne sensors. Additionally, entry level commercial UAVs come at an affordable price and have a low requirement in training before first take-off. This opens up new opportunities for applications. On top of the fast growing number of publications in recent years dealing with UAVs (Figure 1.2), a range of reviews tried to categorise and summarise the latest trends: Anderson and Gaston (2013) reviewed UAVs for ecological, Tang and Shao (2015) and Torresan et al. (2016) for forestry, and Pádua et al. (2017) for agroforestry applications. Aasen et al. (2018) provide extensive background information for radiometric and geometric procedures related to UAVs with respect to quality of the observed spectral quantities.

Plot inventories are a typical target of UAV studies in the context of forest structure assessment (Torresan et al., 2016). Here, the strength of fast acquisition with consumer frame-cameras in combination with Structure from Motion (SfM) photogrammetric workflows is exploited. This makes the production of Canopy Height Models (CHMs) possible that can be fed into ITD algorithms (Lisein et al., 2013; Puliti et al., 2015; Sankey et al., 2017). This approach based on passive optical sensors can provide tree height estimation in open canopy forests, which in turn can be used together with ASEs to derive AGB (Lin et al., 2018). However, dense canopy cover prevents visibility of the ground and proper CHM generation in closed forests (Wallace et al., 2016). With respect to LAI, a wide range of studies present procedures to estimate LAI in field crops based on UAVs (Duan

et al., 2014; Roosjen et al., 2018; Roth et al., 2018), but only very few deal with estimation over forests (Chianucci et al., 2016; Tian et al., 2017).

Unmanned Aerial Vehicle Laser Scanning (UAV-LS) is the crossing of LiDAR and UAV technology. An important technological requirement for the development of UAV-LS systems is the accurate, high frequency position and orientation estimation during flight, which can be achieved with miniaturised Inertial Measurement Units (IMUs) (Jaakkola et al., 2010) or inclusion of SfM into the processing workflow (Wallace et al., 2012). An early, custom-built example was presented by Jaakkola et al. (2010) with a theoretical measurement rate of 38 000 points/s. Commercial suppliers provided solutions only very recently. For example, RIEGL offers a system since 2015 with a measurement rate of 500 000 points/s. Due to its canopy penetration capabilities, UAV-LS has found applications for forest structure retrieval, including forest inventory relevant CHM estimation and ITD (Balsi et al., 2018; Guo et al., 2017; Jaakkola et al., 2017; Lin et al., 2011; Wallace et al., 2012; Wallace et al., 2014b), as well as DBH and AGB estimation (Jaakkola et al., 2017). Guo et al. (2017) additionally derived LAI for three study sites, but this was not validated against independent data sources.

General challenges for UAV operation still lie in rapidly changing regulations and fragmented regulations across countries, despite well-coordinated regulations of other air-traffic participants (Stöcker et al., 2017; Torresan et al., 2016). In forests, required safety regulations like Visual Line of Sight (VLOS) add to this problem. In the future and following fast development in the private and commercial sectors, regulations will probably consolidate. Additionally, regulations and technology that allow relay systems — observing and controlling one UAV from another one closer to the observer — could extend the operational envelope especially in forests.

Open Data

Next to the access to ground- and low altitude-based technology, access to data from space-borne missions was and is a major driver for innovations in forest structure retrieval and validation. The price of such data products gains importance when dealing with longer time series and larger areas for which data is required, and both dimensions are desirable for robust validation approaches. There have been two noticeable events in this context. First, the opening of the Landsat archive in 2008 (Wulder et al., 2012) and second, the launch of the Copernicus Sentinels relevant for land applications starting with Sentinel-1A in 2014 (Torres et al., 2012).

1.5 Research Objectives

The main objective of this thesis is to explore new technologies for forest structure biophysical variable estimation that enable timely, repeatable and cost-effective calibration

and validation of EO products. The work is focussing on LAI as a measure of total canopy foliage and tree structure, defined by tree height, DBH and total tree volume. The investigated technologies are ground-based monitoring sensors, open decametric multi-spectral satellite observations as well as UAV-LS. The following research questions were derived in order to reach the main objective:

RQ 1 How can forest LAI be efficiently and automatically monitored over time?

RQ 2 How is prediction performance of hybrid RTM-MLRA forest LAI-retrieval chains affected by their individual processing chain parts?

RQ 3 What is the capability of UAV-LS to estimate canopy height and DBH?

RQ 4 How can UAV-LS contribute to tree volume assessment?

1.6 Thesis Structure

In order to fulfil the objectives of this thesis, the experimental Speulderbos Reference Site has been established in the Veluwe forest area in the Netherlands (Brede et al., 2016). All fieldwork related to the studies in this thesis were performed at this site.

In Chapter 2, automatic monitoring of foliage dynamics is tested with the PAI Autonomous System from Transmittance Sensors at 57° (PASTiS-57) system. The test is split in two parts: first, RTM experiments are employed to explore the validity of the general retrieval algorithm with respect to assumptions on the canopy's architecture. Second, a field experiment is performed and PASTiS-57 observations are compared to light-independent retrievals of a time series of TLS acquisitions as well as the space-borne MODIS LAI product. (Research Question 1)

Chapter 3 tests how new decametric space-borne missions like Landsat and Sentinel-2 can estimate the seasonal development of forest LAI. For this, RTMs and MLRAs are combined. Single modules in the processing work-flow are examined in order to identify the importance of single modules as well as which factors perform most successful. The results are benchmarked against a time series based on TLS acquisitions and litter trap LAI estimates. (Research Question 2)

In Chapter 4 a novel UAV-LS system is tested with respect to production of CHM and single tree DBH estimation. Both variables can be used in combination with ASEs to estimate AGB. The resulting products are compared to TLS-derived estimates. (Research Question 3)

Chapter 5 adopts a state-of-the-art Quantitative Structure Model (QSM) to test with the UAV-LS data in order to explicitly model single trees and estimate individual tree volume. The QSM work-flow is modified by using control cylinders instead of control circles in order to accommodate the lower point density of the UAV-LS compared to

TLS. The UAV-LS volume estimates are compared to TLS based modelling results. (Research Question 4)

Chapter 6 summarises the main findings of this thesis, and discusses implications and opportunities for further research.

Chapter 2

Monitoring Forest Phenology and Leaf Area Index with the Automatic, Low-Cost Transmittance Sensor PASTiS-57

This chapter is based on:

B. Brede, J.-P. Gastellu-Etchegorry, N. Lauret, F. Baret, J. Clevers, J. Verbesselt, and M. Herold (2018). "Monitoring Forest Phenology and Leaf Area Index with the Autonomous, Low-Cost Transmittance Sensor PASTiS-57". *Remote Sensing* 10.7, 1032. DOI: 10.3390/RS10071032

Abstract

Land Surface Phenology (LSP) and Leaf Area Index (LAI) are important variables that describe the photosynthetically active phase and capacity of vegetation. Both are derived on the global scale from optical satellite sensors and require robust validation based on in situ sensors at high temporal resolution. This study assesses the PAI Autonomous System from Transmittance Sensors at 57° (PASTiS-57) instrument as a low-cost transmittance sensor for simultaneous monitoring of LSP and LAI in forest ecosystems. In a field experiment, spring leaf flush and autumn senescence in a Dutch beech forest were observed with PASTiS-57 and illumination independent, multi-temporal Terrestrial Laser Scanning (TLS) measurements in five plots. Both time series agreed to less than a day in Start Of Season (SOS) and End Of Season (EOS). LAI magnitude was strongly correlated with a Pearson correlation coefficient of 0.98. PASTiS-57 summer and winter LAI were on average $0.41\,\mathrm{m^2\,m^{-2}}$ and $1.43\,\mathrm{m^2\,m^{-2}}$ lower than TLS. This can be explained by previously reported overestimation of TLS. Additionally, PASTiS-57 was implemented in the Discrete Anisotropic Radiative Transfer (DART) Radiative Transfer Model (RTM) model for sensitivity analysis. This confirmed the robustness of the retrieval with respect to non-structural canopy properties and illumination conditions. Generally, PASTiS-57 fulfilled the Committee on Earth Observing Satellites (CEOS) Land Product Validation (LPV) requirement of 20 % accuracy in LAI for a wide range of biochemical and illumination conditions for turbid medium canopies. However, canopy non-randomness in discrete tree models led to strong biases. Overall, PASTiS-57 demonstrated the potential of automatic devices for monitoring of phenology and LAI at daily temporal resolution as required for validation of satellite products that can be derived from ESA Copernicus' optical missions, Sentinel-2 and -3.

2.1 Introduction

Vegetation phenology describes the "timing of seasonal developmental stages in plant life cycles including bud burst, canopy growth, flowering, and senescence [...]" (Kimball, 2014). This includes the start, end and length of the photosynthetically active phase in the year. A mechanistic understanding of controls on these events is still lacking for most biomes (Richardson et al., 2013). This leads to a general misrepresentation of vegetation temporal behaviour in global circulation models and uncertainty in vegetation-climate feedbacks. Standardised, wide-spread observations are paramount for the quantification of phenology and climate feedbacks.

Proximal sensing techniques such as phenocams or webcams allow high revisit frequency and objective analysis techniques (Browning et al., 2017; Keenan et al., 2014; Richardson et al., 2009). They are based on the principle that changes in canopy biophysical and -chemical composition, which go along with leaf development and senescence, alter its radiative regime. Most often exploited is the decrease of reflectance in the visible wavelengths due to absorption for photosynthesis and the increase in the Near-Infrared (NIR) due to reflecting properties of leaves. The latter effect can be exploited when sensors also record NIR (Petach et al., 2014; Soudani et al., 2012). This can be done for example with tower-based proximal sensing. However, these sensors are often not standardised in terms of measurement protocols (Balzarolo et al., 2011).

Apart from this, the change in reflective behaviour is also utilised to detect phenological events over large areas with satellite-borne sensors (Che et al., 2014; Zhang et al., 2003). The spatially aggregated, temporal behaviour of plants over larger areas that are observed from space is referred to as LSP (Kimball, 2014). In contrast to ground-based systems, space-borne missions have the advantage to use only single or few sensors, which makes it easier to derive comparable products.

The case is similar for another quantitative vegetation property, the LAI. It is defined as the one-sided leaf area per unit of ground surface area (Chen and Black, 1992). Hence, it quantifies the amount of leaves that are available for photosynthesis during the photoperiod. Similar to LSP, LAI can be inferred from ground-based and space-borne instruments, but also from air-borne sensors (Casas et al., 2014; Frampton et al., 2013; Koetz et al., 2005) and Unmanned Aerial Vehicles (UAVs) (Chianucci et al., 2016; Roosjen et al., 2018). Ground-based LAI observations are typically performed with consumer-grade cameras equipped with fish-eye lenses, referred to as Digital Hemispherical Photography (DHP) (Jonckheere et al., 2004). This method relies on gap fraction theory to infer LAI (Weiss et al., 2004). Most often, observations with a viewing zenith angle of 57.5°, the so-called hinge angle, are analysed, where impact of the Leaf Angle Distribution (LAD) on gap fraction is minimal. Other hand-held instruments are also available. However, in general, ground-based instruments for LAI are used manually and in campaigns that cover larger

areas to capture the extent of satellite scenes (Frampton et al., 2013). Regular re-sampling of the same locations is possible, but labour-intensive (Lang et al., 2017; Lukasová et al., 2014).

In the context of Earth observation satellite missions and programmes, such as NASA's MODerate-resolution Imaging Spectroradiometer (MODIS) or ESA's Sentinel-3 mission (Berger et al., 2012; Donlon et al., 2012), both LSP and LAI spatial products require robust quality ground-based validation. This demands monitoring devices that match land product's temporal resolution, potentially able to record LAI at high resolution so that LSP can be inferred from the time series. Low-cost devices would be preferred to allow deployment over larger areas and at many sites.

The PASTiS-57 is a candidate to fulfil these requirements. It was developed by Institut national de la recherche agronomique (INRA)-Hiphen (Avignon, France) during the FP7 ImagineS project (`http://fp7-imagines.eu`). Its main application was to support multi-day calibration and validation field campaigns for retrieval of LAI and Fraction Absorbed Photosynthetically Active Radiation (FAPAR) with hectometric resolution space-borne sensors (Latorre et al., 2014; Nestola et al., 2017; Raymaekers et al., 2014; Simic et al., 2012). Recently, it was compared with seasonal measurements of LAI-2200 and DHP in agricultural fields (Fang et al., 2018). Its measurement principle is based on gap fraction theory. Similar to DHP, it exploits the LAD quasi-invariance at the hinge angle. However, a more detailed assessment of its performance characteristics especially with respect to changing illumination conditions and plant biochemical properties has not been presented yet.

In this context, vegetation RTMs can support sensitivity analysis, the definition of new sensors and the development of inversion procedures to translate the radiative signal into canopy variables (Jacquemoud et al., 2009). Generally, vegetation RTMs model the interaction of sun radiation with canopy elements based on the canopy's biophysical and -chemical properties. In this way, they can be exploited to assess the sensors sensitivity to canopy parameters in idealised conditions, i.e. without measurement noise, and for a wide range of possible canopy conditions. For example, the widely used PROSAIL model, a combination of the Scattering by Arbitrarily Inclined Leaves (SAIL) canopy and PROSPECT leaf radiative models, has been exploited to design vegetation indices (Clevers and Verhoef, 1993) and for biophysical parameter retrieval via inversion (Atzberger and Richter, 2012; Campos-Taberner et al., 2016; Rivera et al., 2013). However, SAIL represents the canopy as a homogeneous layer of scatterers. This assumption does not hold for clumped canopies such as forests.

In these cases, a heterogeneous representation that can take into account canopy clumping and non-random structure is more appropriate. The DART model implements this paradigm (Gastellu-Etchegorry et al., 1996). DART applications include canopy biophysical and -chemical parameter retrieval (Banskota et al., 2015; Demarez and Gastellu-Etchegorry,

2000), surface energy budget studies (Gastellu-Etchegorry et al., 2004) and recently chlorophyll fluorescence modelling (Gastellu-Etchegorry et al., 2017). Additionally, DART incorporates the option to implement in-scene sensors such as hemispherical or pinhole cameras (Gastellu-Etchegorry et al., 2017). This provides the option to test arbitrary sensor designs.

The aim of this study has been twofold: (i) testing the ground-based transmittance sensor PASTiS-57 for monitoring LSP and LAI in a forest stand with daily frequency; and (ii) assessing the sensor's sensitivity to canopy properties other than LAI and their interactions by means of RTM experiments, thereby testing the robustness of the measurement principle to different canopy conditions. This study is structured as follows: The PASTiS-57 sensor is presented in detail in Section 2.2.1. Section 2.2.2 describes the field data collection and analysis. Section 2.2.3 elaborates on implementation of the sensor in DART, the set up of the synthetic canopy and how sensitivity analysis was conducted. Results are presented in Section 2.3 and discussed in Section 2.4. Section 2.5 summarises the results and lists implications for future sensor design.

2.2 Materials and Methods

2.2.1 PASTiS-57 Instrument

The PASTiS-57 consists of a weather proof, battery powered datalogger with 6 photodiode-based sensors (Figure 2.1). The sensors are fixed to a viewing zenith angle of 57.5°, sensitive in the blue spectral region to minimise canopy multiple scattering and have different lengths of wire for sensor distribution around the data-logger. The logger is battery powered and can automatically collect data at 1 min interval for up to four months. Intervals of 2 min and 5 min are also possible. Radiation is recorded with uncalibrated Digital Number (DN) in the interval 0–4000, whereas larger DNs are treated as unreliable due to saturation effects. The signal can be calibrated with dedicated Photosynthetically-Active Radiation (PAR) sensors (Latorre et al., 2014). However, a more practical approach is to utilise the relative signal by installing one device above the canopy, which serves as reference for incoming radiation, and another device below the canopy, which represents the observations. In this way, many plots can be served by one reference sensor, as long as it is within a distance where illumination conditions can be assumed comparable. The observed signal is the spectral directional transmittance τ for each sensor:

$$\tau = \frac{DN_{below\ canopy}}{DN_{above\ canopy}} \tag{2.1}$$

Figure 2.1: The PASTiS-57 instrument installed in the Speulderbos site: (A) With the opened data-logger box, the six sensors can be seen on top, a spare cable is curled up at the back of the data-logger, and two D-cell batteries for power supply in the box; and (B) two PASTiS-57 installed at the centre of Plot C (centre marker not visible).

2.2.2 Field Experiment

Study Area and Field Data Collection

PASTiS-57 sensors have been installed at the Speulderbos Fiducial Reference site in the Veluwe forest area (N52°15.15′ E5°42.00′), The Netherlands (Brede et al., 2016) (`www.wur.eu/fbprv`). This site represents a maturing stand of mixed European beech (*Fagus sylvatica*), pedunculate oak (*Quercus robur*) and sessile oak (*Quercus petraea*) with few understorey. The trees were initially planted in 1835. Nowadays, the stand has a density of around 200 trees/ha.

PASTiS-57 instruments were installed in the centres of five plots. For redundancy, each plot was equipped with two devices (Figure 2.2). Contrary to previous studies where sensors were put onto the ground, the individual sensors in this study have been mounted on top of the data logger on a plastic board to face the NE, E, SE, SW, W and NW directions. Each PASTiS-57 unit was fixed at 1.30 m above ground at an iron rod, aligned to north with a magnetic compass and levelled with a bubble level. Another two devices have been mounted at the top of a 42 m high scaffold tower approximately 550 m west of Plot A to record above canopy reference downward radiation. Campaigns were conducted in spring 2016 during leaf flush, autumn 2016 during leaf senescence, and summer and autumn 2017. Campaigns were programmed with 2 min interval in 2016 and 1 min interval in 2017.

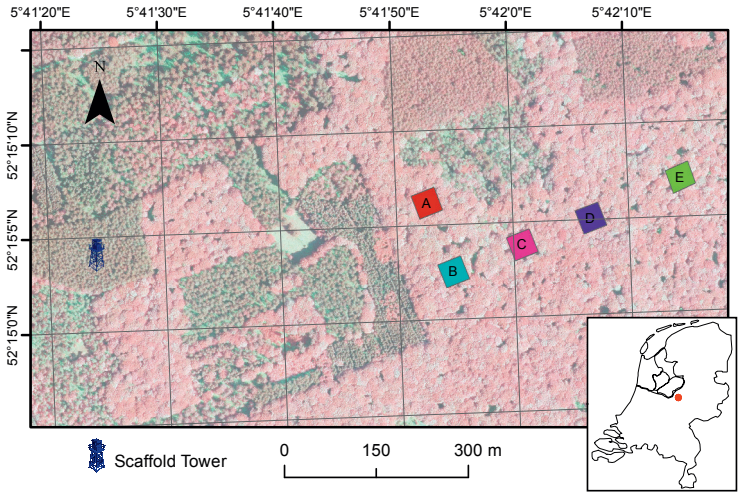

Figure 2.2: Map of the study site with the scaffold tower where reference instruments were placed and the five sampling plots. Background is an airborne false-colour composite of 2013. The location of the study site within The Netherlands is marked on the inset.

Plant Area Index (PAI) Retrieval

It should be noted that many proximal sensing techniques cannot distinguish between foliage and woody canopy elements. The PAI includes both classes, while LAI refers only to photosynthetically active plant tissue (Calders et al., 2015c; Woodgate et al., 2016). In the following, PAI refers to observed plant area, while LAI refers to the actual quantity of green leaf area. Typically, LAI retrieval from below canopy sensors such as DHP uses gap fraction theory (Leblanc et al., 2005; Weiss et al., 2004). For this, the canopy is assumed as a uniform cloud of randomly oriented, black facets ($\rho = 0$, $\tau = 0$). In this case, the gap fraction is related to LAI based on Beer–Lambert's law:

$$P(\theta) = e^{-G(\theta)\Omega(\theta)L/\cos\theta} \tag{2.2}$$

where θ is the viewing zenith angle, $P(\theta)$ the canopy gap fraction in direction θ, $G(\theta)$ the projection of unit foliage in the θ direction, which characterizes the foliage angular distribution, $\Omega(\theta)$ the clumping index that describes the non-randomness of the canopy and L the LAI. $P(\theta)$ has been variably interpreted as gap fraction in the case of DHP (Weiss et al., 2004), hit probability in the case of lidar sensors (Calders et al., 2014; Jupp et al., 2009) or transmittance in the case of PASTiS-57 (Nestola et al., 2017; Raymaekers et al., 2014).

For canopy clumping estimation, the method of Lang and Xiang (LX) (Lang and Xiang, 1986) and the six different viewing directions of each PASTiS-57 instrument were exploited. The LX method assumes that within a segment the foliage is random and it contains

gaps. In the case of PASTiS-57 the instantaneous field of view of a single sensor can be interpreted as a segment. In that case, canopy clumping can be described as:

$$\Omega(\theta) = \frac{\ln \overline{P(\theta)}}{\overline{\ln P(\theta)}} \tag{2.3}$$

where $\overline{P(\theta)}$ is the mean gap fraction of all segments and $\overline{\ln P(\theta)}$ the logarithm of the mean gap fraction of all segments. "The reasoning behind this technique is that since the [LAI] is related to the natural logarithm of the gap fraction, the average LAI should follow the logarithm average of the gap fraction" (Leblanc et al., 2005). In this sense, the denominator in Equation (2.3) normalises the gap fraction by the logarithm. Using this definition for clumping, replacing $P(\theta)$ with PASTiS-57 measured transmittance τ_{PASTIS} and exploiting the near constant value of the G-function at $\theta = 57.5°$ for many LAD reduces Equation (2.2) to

$$L = \frac{-1.075 \ln(\tau_{PASTIS})}{\Omega} \tag{2.4}$$

The goal of this study was to produce daily observations of LAI, from which phenological parameters can be derived. Earlier studies in forests showed that sub-daily retrievals with PASTiS-57 based on Equation (2.4) produce results with strong, high frequency noise with ± 0.5 LAI amplitude (Lecerf et al., 2010). Therefore, raw readings require appropriate quality filters to be applied. Here, these filters were based on experience gathered while investigating the raw time series. The primary result was that high frequency noise stems from changing illumination conditions that violate the assumptions for the retrieval.

Firstly, broken cloud cover can result in different sky illumination conditions at the location of the reference and the observation sensors. Here, this was counteracted by aggregating via averaging of the 1 min transmission readings to a daily time series. Secondly, strong cloudiness reduces the radiation reaching the forest floor, especially at the north-facing sensors, resulting in below canopy DN of 0, which are interpreted as infinite PAI (Equation (2.4)) and do not match the assumptions behind the clumping appraisal. Therefore, DN readings of 0 for the below canopy sensors were removed from the time series. Thirdly, large canopy gaps result in direct illumination on the below canopy sensor, which violates the assumption of diffuse illumination and produces high DN readings. These conditions are only of short duration when the sun moves over the specific gap. Even the NW and NE sensors experience these conditions when canopy elements are overly strong illuminated through canopy gaps and result in recorded high transmission. To counteract this effect, all DN exceeding the 95th daily percentile were removed.

Reference Datasets

Next to PASTiS-57 records, a multi-temporal campaign with a RIEGL VZ-400 TLS (RIEGL LMS GmbH, Horn, Austria) was conducted at the Speulderbos site. This scanner

has shown good results for monitoring phenology (Calders et al., 2015c). The main advantage of TLS as a gap fraction sensor is its independence from illumination conditions (Calders et al., 2018b; Hancock et al., 2014; Jupp et al., 2009). This results in high precision time series, i.e. with low noise in the temporal domain. On the other side, partial hits lead to underestimation of gap fraction by these kind of sensors (Hancock et al., 2014; Vaccari et al., 2013). Partial hits result from objects that only partially cover the laser instantaneous field of view, but are registered as full interceptions by the waveform analysis methods of commercial suppliers to maximise point cloud density. In this way, gap fraction is underestimated and, consequently, PAI is overestimated. In addition, wet canopy conditions have to be avoided for the sampling, because water droplets on canopy elements absorb the laser beam, thereby apparently increasing gap fraction.

In total 45 sampling events were conducted. The sampling strategy was to focus efforts during change periods, i.e. SOS and EOS, and to avoid rain conditions. For each sampling event, the scanner was mounted on a surveying tripod in each centre of the five plots, at a maximum distance of 3 m from the respective PASTiS-57 devices. $P(\theta)$ was derived from the hemispherical scans by taking into account the multi-return capability of the scanner (Calders et al., 2014). The hinge angle was approximated with the 55° to 60° region, which is a typical strategy (Calders et al., 2014; Calders et al., 2015c; Jupp et al., 2009).

Apart from the ground-based TLS time series, MODIS Collection 6 MCD15A3H LAI products were retrieved (Myneni et al., 2015; Myneni et al., 2011). MCD15A3H is a four-day composite product based on inversion of a vegetation RTM. Its eight-day companion product was validated to Stage 2 according to the LPV subgroup (`https://lpvs.gsfc.nasa.gov/`). However, the four-day product was preferred over the eight-day product as the goal here included estimating temporal metrics, thus denser samples were important.

The samples were retrieved from the Application for Extracting and Exploring Analysis Ready Samples (APPEARS) service of the US Geological Survey (`https://lpdaacsvc.cr.usgs.gov/appeears/`) for the period 1 January 2016 until 28 February 2018 and for the 500 m pixel centred at the Speulderbos site. This means that the MCD15A3H samples also included forest patches other than beech, i.e. some mixed species stand included in the Speulderbos site. After downloading, the time series was filtered with the accompanying quality flags to allow only good quality LAI retrievals. After visual inspection it was clear that some outliers in summer with LAI below $3\,m^2\,m^{-2}$ occurred, which have been excluded as well.

Phenological Model Fitting

LSP can be modelled with logistic functions (Kimball, 2014; Zhang et al., 2003). These mathematically simple models are fitted piecewise to time series of vegetation indices or LAI to describe the spring growth and autumn senescence periods (Calders et al., 2015c). From these models LSP indicators like SOS and EOS can be derived. Here, a logistic

model was used (Calders et al., 2015c; Zhang et al., 2003):

$$PAI(t) = \frac{U - L}{1 + e^{-k(t-t_m)}} + L \tag{2.5}$$

where t is time (expressed as Day Of Year (DOY)), U the upper asymptote ($m^2\,m^{-2}$), L the lower asymptote ($m^2\,m^{-2}$), k the growth rate (d^{-1}) and t_m the inflection point, where k is maximal (DOY). The model was fitted with a non-linear least squares routine implemented in the `nls` function of the R `stats` package (Bates and Watts, 1988; R Core Team, 2014). Separate sigmoids were estimated for the spring 2016 and autumn 2017 periods. In addition to the model parameters' best estimates, non-linear least squares estimate also produces prediction intervals. Finally, SOS and EOS were estimated as the time of the year when the fitted model reached the 95 % upper and lower prediction interval for the L and U parameter, respectively. This fitting strategy was applied separately to the PASTiS-57, TLS and MODIS time series, and results were compared.

2.2.3 Radiative Transfer Model Experiments

In-scene sensors in DART can be implemented as frame cameras with arbitrary viewing direction and properties (see Figure 2.3 for an example), and record at-sensor spectral radiance for any number of spectral bands with any bandwidths ($W\,m^{-2}\,sr^{-1}\,\mu m^{-1}$). For this study, the frame camera characteristic was not exploited, but only the integrated radiance over the whole sensor FOV was regarded similar to the PASTiS-57 photo-diodes. As in the field set up (Section 2.2.2), in this simulation the 6 PASTiS-57 sensors were directed in the NE, E, SE, SW, W and NW directions with a viewing zenith angle of 57.5°. In the DART scene, one device consisting of six sensors was positioned below, another above the simulated canopy, so that canopy transmittance could be calculated in the same way as in the field experiment (Equation (2.1)). The PASTiS-57 spectral response curve is not exactly known, so a blue waveband centred at 490 nm with 20 nm bandwidth (FWHM) was chosen. Additionally, bands centred in the green (560 nm), red (665 nm) and NIR (865 nm) were tested following the specifications of the Sentinel-2 MultiSpectral Instrument (MSI) (Drusch et al., 2012). These additional bands allowed judging the instrument performance in the case photo-diodes would have been chosen that are sensitive in another spectral region.

Two scenarios were set up to test different canopy parameters. In both, only the sensitivity of PASTiS-57 to change in LAI was investigated, but not to the temporal evolution. This is justified with the direct dependence of temporal sensitivity on the sensitivity to LAI. The first scenario modelled the canopy as a turbid medium, which is in accordance to gap fraction theory that is underlying the LAI retrieval (Section 2.2.2). This scenario was intended to test the retrieval robustness to different illumination conditions as well as variation in biophysical and -chemical canopy composition. Table 2.1 summarises the parameters and their chosen values. For each case, one typical and two extreme cases were chosen.

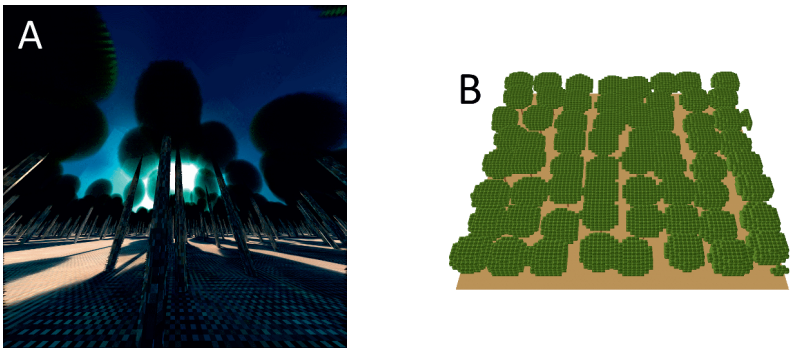

Figure 2.3: DART sample scene: (**A**) True colour image sample for below-canopy sensor in DART. The viewing zenith angle is 57.5°, but the field of view is extended compared to the sensors used in the modelling to give an overview of the scene. (**B**) Top view of the created mock-up with 50 trees.

All parameters were varied in a full grid approach, resulting in a total of 450 simulations. For this experiment, clumping was not investigated ($\Omega = 1$) because the canopy was homogeneous in all directions. The solar azimuth angle was kept constant at 180°. The simulated sensors were analysed with respect to their prediction performance of the true LAI. The results were compared with the Global Climate Observing System (GCOS) requirement for LAI retrieval accuracy, which is 20 % as well as the accuracy goal for agricultural meteorology applications identified by the WMO, which is 5 % (Fernandes et al., 2014). The Relative Error (RE) was chosen as accuracy metric and calculated as:

$$RE = \frac{PAI_{simulated\ PASTIS} - LAI_{DART}}{LAI_{DART}} \tag{2.6}$$

where LAI_{DART} is the DART input LAI and $PAI_{simulated\ PASTIS}$ the PAI derived with the simulated PASTiS-57. Using this formulation, positive REs meant overestimation of the PASTiS-57-derived PAI.

During analysis of the results of these RTM simulations, a systematic bias in PAI estimation has been identified. This could be linearly modelled with the form $PAI = aLAI + b + \epsilon$ independently for each LAD ($p < 0.01$). For assessment of this error's impact on LSP metrics estimation, PAI in Equation (2.5) was replaced with the linear bias model and solved for t. The comparison of this with the unbiased estimation of t gave the expected error in LSP metric. Since the analytic solution was complex, the impact of the relative error was assessed numerically by testing a range of values for U, L and k. In the case of U and L extreme combinations were tested, i.e. $L = 0$ and $U \in \{1, 2, ...10\}$. In the case of k, estimates from the field derived models were used (Section 2.2.2), i.e. $k \in \{0.5, -0.08\}$.

Table 2.1: Biophysical, biochemical and illumination parameters and values used for turbid DART experiments.

Parameter	Values	Unit
Leaf Area Index (LAI)	1, 2, ..., 10	$m^2\,m^{-2}$
Leaf Angle Distribution (LAD)	spherical, erectrophile, planophile extremophile, plagiophile	-
Chlorophyll a and b (C_{ab})	20, 50, 80	$\mu g\,cm^{-2}$
Solar Zenith Angle (SZA)	0, 57.5, 80	°

Values for t_m were not necessary, because it cancels out when only considering the difference between two estimates.

The second scenario was intended to test the retrieval performance with respect to canopy non-randomness. For this, discrete trees were modelled with ellipsoid crowns with 10 m diameter and 5 m height, and trunks with 40 cm diameter. The number of trees per scene was varied between 50 and 400 trees on a scene of 80 m×80 m. Illumination and canopy biochemical parameters were held constant with a spherical LAD, 50 µg cm^{-2} C_{ab} and SZA of 57° to extract the effect of clumping alone.

2.3 Results

2.3.1 Field Experiment

Figure 2.4 shows the raw DN recordings of two sampling days, one before SOS, one after leaf flush in summer. For both days, averages were clearly lower than reference readings above the canopy, resulting in average canopy transmittance of 29.1 % and 0.9 % before and after the start of season, respectively. Another feature was the high number of 0 DN readings at early and late hours of the day after leaf flush, which made up 25.7 % of all observations on that day. At these times, the SZA is typically large, so that the direct path through the canopy is long and not sufficient radiation reaches the below canopy sensors. In contrast to this, the SW sensor on the reference device experienced saturation in the afternoon, probably due to direct illumination. Overall, the two days showed high agreement in temporal evolution, indicating similar impact of changes in illumination. These stem from the course of the sun, resulting in the rise and fall of readings over the course of the day, and from clouds and stems, causing high frequency changes.

A full PAI time series for all three campaigns derived from a device on Plot C can be seen in Figure 2.5. While the difference between the single sensors was only marginal, the impact of the filtering was clearly visible. The naive retrieval resulted in strong, high frequency noise with positive spikes and a Lag 1 Auto-Correlation Coefficient (ACC1) of

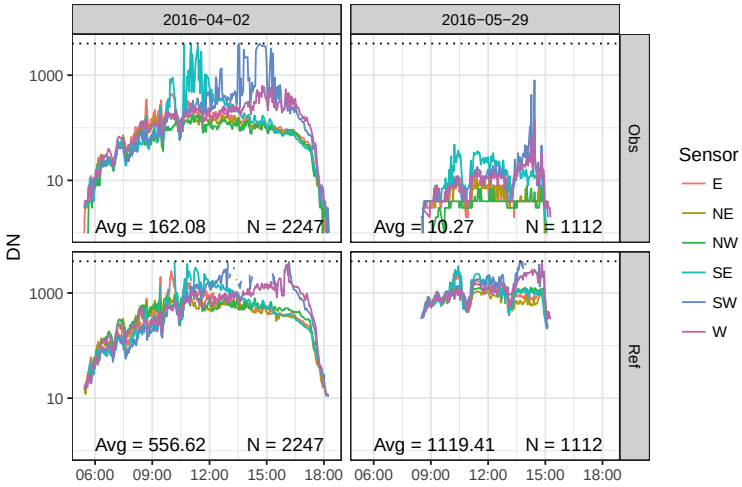

Figure 2.4: Recordings of two sampling days for one device in Plot A. Upper panels are the observations below the canopy, lower panels are reference readings from above the canopy. DN axis is on log-scale. Dotted horizontal line is saturation point at 4000 DN. Discontinued lines on lower panel reach saturation. Only pairs for which the observation did not reach 0 DigitalNumber were considered.

0.93. The noise after filtering was modest and evolved equally around a mean course of PAI with ACC1 of 0.97. The former resulted from situations under full canopy in summer, when the below-canopy sensors had 0 DN readings. This results in theoretically infinite PAI according to Equation (2.4). When comparing the two years, an earlier decrease in PAI could be observed in 2017. This can be explained with the natural variability of EOS. This results from different wind loads, which is the main force to defoliate the trees once the leaves have died.

In Figure 2.6 PASTiS-57 and TLS estimated PAI are plotted together for the dynamic phases of the yearly phenology, which are spring leaf flush and autumn senescence. Overall, PASTiS-57 and TLS showed high agreement in temporal development. Both sensors' time series reflect the fast leaf development during spring and the longer senescence period in autumn. The TLS sampling intervals were not sufficient to record the fast changes in spring, especially between the sampling events of 4 May 2016 and 12 May 2016 when PAI increased by $1.86\,m^2\,m^{-2}$ on average within eight days. The PASTiS-57 with their daily interval could closely follow the development.

Considering the magnitude, both sensors agreed strongly with a Pearson correlation coefficient of 0.98. However, PASTiS-57 retrievals were lower in winter by $1.44\,m^2\,m^{-2}$ compared to TLS. This was likely due to the different sensing techniques. In case of PASTiS-57, backward scattering from woody elements increases recorded radiation at the

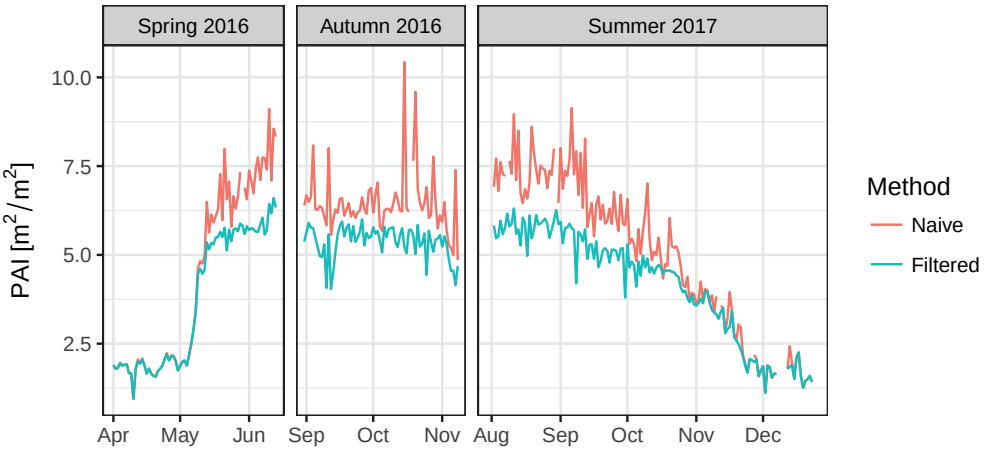

Figure 2.5: All campaigns of one instrument in Plot C before (Naive) and after application of filtering (Filtered).

below canopy sensors, thus decreases PAI estimates. In the case of TLS, the partial hits are mainly responsible for the sensitivity to the recording of canopy elements. For both instruments, PAI > 1.5 in winter pointed to the large influence of woody material on the retrievals. In contrast to this, PASTiS-57 average and TLS agreed in summer to within $0.74\,\mathrm{m^2\,m^{-2}}$.

Parameter estimates for the fitted phenological models are summarised in Tables 2.2 and 2.3. A total of 21 and 40 samples for each plot were used for TLS and MODIS, respectively. Concerning the upper and lower asymptotes U and L, PASTiS-57 showed significantly lower estimates compared to TLS in all plots. For both spring and autumn campaigns, PASTiS-57 U and L were on average $0.41\,\mathrm{m^2\,m^{-2}}$ and $1.43\,\mathrm{m^2\,m^{-2}}$ lower than TLS, reflecting the difference in acquisition mechanism. Compared to MODIS, PASTiS-57 U and L were $0.19\,\mathrm{m^2\,m^{-2}}$ lower and $0.97\,\mathrm{m^2\,m^{-2}}$ higher, respectively. Again, this reflects the different nature of the retrieval algorithms. MODIS LAI makes use of top of canopy reflectance and is stronger utilising the NIR signal. This makes it less sensitive to woody material in the canopy, thus MODIS LAI showed generally lower values than PASTiS-57.

Furthermore, PASTiS-57 agreed very well with TLS in terms of SOS with an average difference of less than a day. EOS was estimated on average 22 days later by TLS. However, agreement among TLS plots was low with a range of 29 days in EOS. More samples during winter would have been necessary to decrease the estimation error. Moreover, PASTiS-57 achieved the lowest estimation standard error on the sigmoid inflection points t_m. This was made possible by the high temporal density of the PASTiS-57 time series. Additionally, PASTiS-57 agreed well with MODIS SOS to within 2 days. As in the case of TLS, EOS

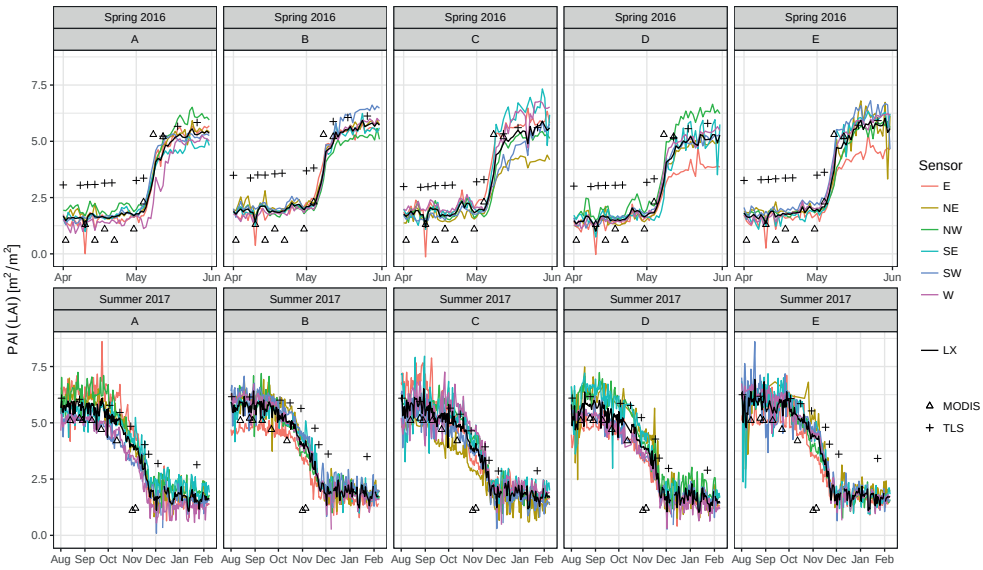

Figure 2.6: Comparison of PASTiS-57 and TLS derived PAI for single sensors (coloured) and Land and Xiang clumping correction (LX), and MODIS LAI for five plots during the spring 2016 and summer 2017 campaigns.

estimation of MODIS was impaired. Only for MODIS, persistent cloud cover — which is common in autumn in The Netherlands — prevented frequent observations.

2.3.2 Radiative Transfer Model Experiments

The DART RTM experiments permitted to have control over all canopy and illumination parameters, and to model abstract canopies. Figure 2.7 summarises the results for the turbid medium canopy case. Most influential was the choice of the spectral band. For instance, NIR retrievals were generally more than 75 % lower than true LAI. This strong misinterpretation stems from the retrieval assumption of black leaves, which is not fulfilled in the NIR. In fact, leaves typically transmit around 45 % of incoming radiation in this band. This leads to higher recorded radiation below canopy and underestimation of LAI. Additionally, the RE was larger at small SZA. This could be explained by a smaller optical path through the canopy at small SZA, which leads to increased below-canopy recorded radiation compared to what would be expected for black leaves. These effects could also be observed to some degree in the green spectral band, where leaves typically transmit >10 %.

In contrast, the blue and red bands were less compromised. They both underestimated true LAI by maximum 40.0 % and on average by 14.2 % and 14.5 %, respectively. Thus, the average accuracy was within the GCOS threshold accuracy of 20 %. Leaf absorption

Table 2.2: Phenological model fitting results for the spring 2016 campaign with parameter mean estimates and their 95 % standard error. U is the upper asymptote ($m^2\,m^{-2}$), L the lower asymptote ($m^2\,m^{-2}$), k the growth rate (d^{-1}), t_m the inflection point (DOY) and SOS the Start Of Season (DOY). MODIS results refer to all plots and represent LAI in case of U and L.

Parameter	A	B	C	D	E
U_{PASTIS}	5.31 (±0.04)	5.65 (±0.04)	5.46 (±0.05)	5.09 (±0.05)	5.67 (±0.05)
U_{TLS}	5.82 (±0.03)	6.10 (±0.03)	5.72 (±0.04)	5.62 (±0.04)	5.99 (±0.03)
U_{MODIS}	5.63 (±0.15)	–	–	–	–
L_{PASTIS}	1.63 (±0.03)	1.94 (±0.03)	1.85 (±0.04)	1.57 (±0.03)	1.75 (±0.04)
L_{TLS}	3.10 (±0.02)	3.51 (±0.03)	3.02 (±0.03)	3.03 (±0.03)	3.32 (±0.02)
L_{MODIS}	0.80 (±0.09)	–	–	–	–
k_{PASTIS}	0.43 (±0.03)	0.49 (±0.04)	0.54 (±0.06)	0.48 (±0.04)	0.44 (±0.03)
k_{TLS}	0.41 (±0.03)	0.52 (±0.05)	0.47 (±0.04)	0.43 (±0.04)	0.31 (±0.02)
k_{MODIS}	0.77 (±0.26)	–	–	–	–
$t_{m,PASTIS}$	129.5 (±0.2)	129.3 (±0.2)	129.3 (±0.2)	129.2 (±0.2)	129.1 (±0.2)
$t_{m,TLS}$	130.0 (±0.3)	128.6 (±0.4)	129.3 (±0.4)	129.5 (±0.4)	130.9 (±0.3)
$t_{m,MODIS}$	126.0 (±0.5)	–	–	–	–
SOS_{PASTIS}	117.9	119.5	121.0	119.6	118.4
SOS_{TLS}	118.2	119.9	119.7	119.2	115.8
SOS_{MODIS}	120.9	–	–	–	–

is strongest at these wavelengths due to absorption by chlorophyll, so that the canopy comes close to the approximation of black facets. Typical transmittance for these spectral regions is <2 % and reflectance <4 %. This is why blue channels of digital cameras are recommended for LAI retrieval (Jonckheere et al., 2005; Lang et al., 2017). Nonetheless, even these low values in ρ and τ led to higher detected radiation at the sensor compared to what would be expected with black leaves, so that canopy transmittance was overestimated, which leads to underestimation of PAI.

Within the blue and red spectral bands most variation was across the different LADs. While the spherical LAD underestimated true LAI by an average of 2.8 % and a maximum of 11.0 % in the blue, simulated canopies with planophile LADs resulted in average and maximum underestimation of 38.2 % and 40.0 %, respectively. In the latter case, the deviation of the G-function value from 0.5 and transmitting properties of the leaves probably interacted to increase the deviation from true LAI.

Apart from this, underestimation was generally increasing with true LAI. This means that at higher LAI more radiation was reaching the sensor than expected by the model, i.e. canopy transmittance is larger than expected. This effect could be created by multiple

Table 2.3: Same as Table 2.2, but for the autumn 2017 campaign referring to the EOS (DOY).

Parameter	A	B	C	D	E
U_{PASTIS}	5.69 (±0.04)	5.72 (±0.03)	5.64 (±0.05)	5.49 (±0.05)	5.79 (±0.04)
U_{TLS}	6.06 (±0.08)	6.07 (±0.08)	6.00 (±0.13)	6.05 (±0.12)	6.15 (±0.10)
U_{MODIS}	5.06 (±0.11)	–	–	–	–
L_{PASTIS}	1.59 (±0.04)	1.80 (±0.04)	1.69 (±0.05)	1.55 (±0.05)	1.64 (±0.04)
L_{TLS}	3.05 (±0.10)	3.43 (±0.14)	2.74 (±0.17)	2.78 (±0.18)	3.34 (±0.16)
L_{MODIS}	0.65 (±0.09)	–	–	–	–
k_{PASTIS}	−0.08 (±0.00)	−0.08 (±0.00)	−0.07 (±0.00)	−0.08 (±0.01)	−0.09 (±0.01)
k_{TLS}	−0.08 (±0.01)	−0.12 (±0.02)	−0.07 (±0.01)	−0.10 (±0.02)	−0.09 (±0.02)
k_{MODIS}	−0.16 (±0.02)	–	–	–	–
$t_{m,PASTIS}$	307.6 (±0.7)	307.8 (±0.7)	307.5 (±1.0)	309.8 (±1.0)	311.7 (±0.7)
$t_{m,TLS}$	307.2 (±1.9)	317.4 (±2.0)	307.4 (±3.0)	314.4 (±2.6)	316.7 (±2.6)
$t_{m,MODIS}$	292.5 (±1.7)	–	–	–	–
EOS_{PASTIS}	250.0	250.4	243.2	256.2	262.8
EOS_{TLS}	258.8	288.4	263.7	280.8	281.4
EOS_{MODIS}	269.0	–	–	–	–

scattering in the canopy. According to the gap fraction model assumption there are no scattering processes within the canopy. Radiation is only absorbed or transmitted without interaction. However, the DART simulated leaves had $\tau > 0$, which allows radiation to go through leaves. The more leaves there are, the stronger the mismatch between gap fraction and DART model.

Concerning C_{ab}, pairwise Student's t-tests between any of the C_{ab} levels showed no significant differences in LAI estimation ($p > 0.95$) and differences were below 0.1 %. This showed that the direct influence of C_{ab} on LAI estimation was very low.

Finally, SZA had minor overall impact on the retrievals. This was on average 0.9 % in the blue band between SZA 0° and 57.5°. However, the difference was larger for spherical and erectophile LADs. The extreme case was at LAI 10, where the relative error for 0° and 57.5° differed by 5.1° and 9.7° for spherical and erectophile LADs, respectively.

When translating the impact of the bias in LAI retrieval on LSP metrics, erectophile LADs delivered the largest error with 1.9 days later estimation of EOS. Spherical, planophile, extremophile and plagiophile LADs resulted in 1.5 days, 0.8 days, 1.0 days and 1.1 days later EOS, respectively. SOS estimation showed lower errors with on average 0.1 days. This means EOS as the generally slower process experiences larger errors in LSP metric retrieval based on the LAI bias error. It should be noted that this difference was based on the particular phenological model used here (Section 2.2.2), but models based on sigmoid functions in general should experience errors on the same order of magnitude.

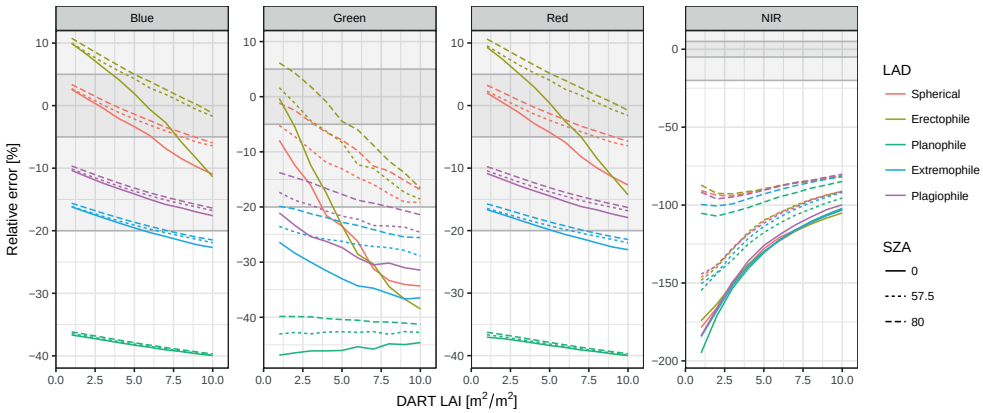

Figure 2.7: DART model results for turbid canopy representation for west facing sensors. Positive errors mean over-estimation by the retrieval. Light grey and darker grey areas are the 20 % and 5 % accuracy requirement of GCOS, respectively (Fernandes et al., 2014).

RTM results for the heterogeneous scenario are presented in Figure 2.8. Tree density was significantly altering retrieval performance in scenarios with <200 trees and LAI > $5\,m^2\,m^{-2}$. This led to underestimation of up to 69.4 % at true LAI $10\,m^2\,m^{-2}$ and a scene with 50 trees. For these scenarios the present leaf mass was concentrated in few crowns, so that the assumption of a homogeneous canopy did not hold and LAI was underestimated. The clumping correction after Lang and Xiang (Lang and Xiang, 1986) could account for some of these effects, but could only reduce the underestimation to 55.1 % in the case of 50 trees. In those cases, the assumption of a random foliage distribution within the sensor FOV was violated. Actually, the horizontal FOV of the PASTiS-57 is large compared to the solid angles that camera pixels represent. The clumping correction after Lang and Xiang (Lang and Xiang, 1986) corresponds rather to the small FOVs represented by camera pixels.

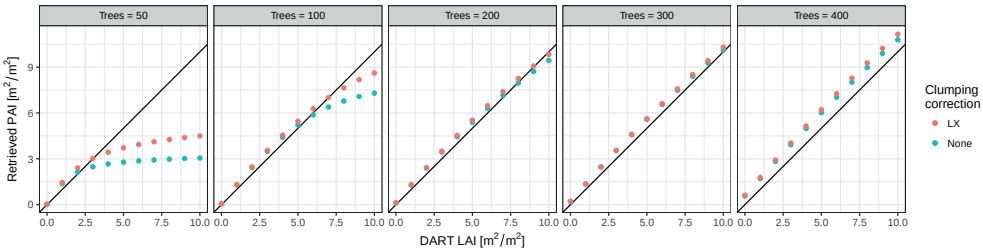

Figure 2.8: DART model results of discrete canopy representation for five different tree densities (horizontal panels in number of trees). Retrieval without (None) and with clumping correction after Lang and Xiang (LX) (Lang and Xiang, 1986).

2.4 Discussion

Ground-validation of LSP and LAI require high temporal density canopy observations. This study explored the PASTiS-57 instrument for automatic monitoring of phenology and PAI in a Dutch beech forest. DART RTM experiments helped to evaluate sensing mechanism of the PASTiS-57 in relation to changes in canopy biochemical and structural properties other than LAI.

The field experiments showed very good temporal agreement with illumination independent TLS and MODIS LAI products when temporal density of these reference products was high. Biases in PAI magnitude were attributed to differences in sensing mechanism. The field observations required filtering and aggregating the readings to daily time series to reduce high frequency noise, especially during full canopy coverage in summer. This noise can be partially tracked back to the sensor's radiometric resolution of 4000 DN. Considering Equation (2.4), the change in PAI per DN, which is the sensitivity to signal digitisation, is inversely proportional to the DN. This is because the first derivative of Equation (2.4) with respect to τ is proportional to the inverse of τ: $L' \propto -\frac{1}{\tau}$. This can result in differences as large as $0.75\,\mathrm{m^2\,m^{-2}}$ between DN observation readings of 1 and 2 when the reference sensor is close to saturation (Figure 2.9). Radiometric sensitivity also impacts the maximum PAI that can be recorded. In the case of PASTiS-57, it lies at $8.91\,\mathrm{m^2\,m^{-2}}$ with a single measurement. Modern digital cameras typically offer digitisation up to 14 bit for raw images, resulting in 16 384 grey levels, so that theoretically $10.43\,\mathrm{m^2\,m^{-2}}$ can be retrieved. Therefore, a higher signal bit depth improves the sensitivity to high LAI as well as maximum retrievable LAI. In the case of the field experiment, the maximum summer PAI was $\sim 6\,\mathrm{m^2\,m^{-2}}$ (Figure 2.5), which was within the theoretical range.

The RTM experiments confirmed the principles underlying the retrievals. In particular, below canopy transmittance measurements in blue and red spectral bands have a high

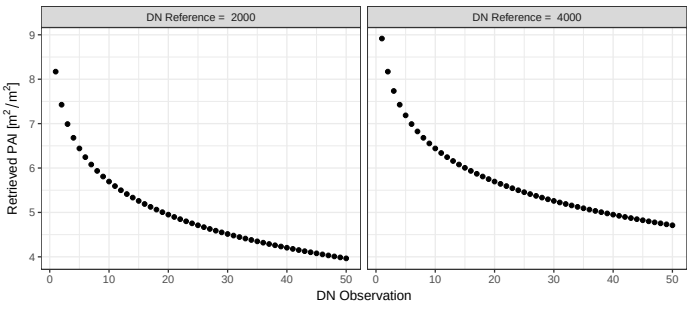

Figure 2.9: Sensitivity of PASTiS-57 PAI due to digitisation at low observation readings (DN) for two levels of reference readings.

sensitivity to canopy structure and are robust against variation in biochemical composition and illumination conditions. This is not the case for top of canopy reflectance measuring sensors, i.e. tower based or satellite sensors, which often exploit the NIR. These are much more dependent on C_{ab} and illumination angle (Jacquemoud et al., 2009).

However, heterogeneous scenarios confirmed the strong effect of canopy non-randomness on LAI estimation. In particular in case of low tree density scenarios, which violate the homogeneous canopy assumption more than dense canopies with closed cover, LAI was strongly underestimated. Clumping correction after Lang and Xiang (Lang and Xiang, 1986) counteracted this effect somewhat. Other clumping correction strategies exist, but these usually require estimation of gap size distribution (Gonsamo and Pellikka, 2009; Leblanc et al., 2005). This is possible with DHP, but not with pointing devices, such as PASTiS-57. Therefore, a strategy for field measurements would be to employ multiple PASTiS-57 instruments per plot. Alternatively, a new sensor design based on low-cost micro-computers equipped with fish-eye cameras could be tested. Such an imaging sensor could also retrieve LAD concurrently with LAI (Weiss et al., 2004).

Another disadvantage of the single-band, pointing device design of the PASTiS-57 is the lack of options to distinguish woody and foliage canopy elements. Gower et al. (1999) list ranges of 7 % to 34 % of wood area index contribution to PAI based on a literature review. Previous studies proposed solutions to this problem with multi-band imaging sensors, including NIR (Kucharik et al., 1997) or imaging sensors combined with radiative transfer modelling (Woodgate et al., 2016). Another way is multi-temporal estimation by using the winter measured PAI as branch area index and subtract it from the summer measured PAI. However, this neglects radiative interaction processes when both elements are present in the canopy (i.e. occlusion of leaves by branches) and is not agreed on (Bréda, 2003). The lack of consolidated correction methods has also led to a prevalent neglect of correction (Bréda, 2003; Woodgate et al., 2016). This topic needs to be addressed with dedicated devices, i.e. dual-wavelength lidar (Howe et al., 2015).

In the context of sensor simulation, DART proved to be a versatile tool. Especially the option to simulate arbitrary sensors allowed the implementation of the PASTiS-57 sensor in this study. Although sensor simulation with RTMs is not new, below canopy sensor simulations have been restricted to DHP (Gonsamo and Pellikka, 2009) or TLS (Grau et al., 2017; North, 1996). Another advantage of DART was the option to simulate heterogeneous canopies, which is crucial for forest radiative transfer modelling.

Next to considerations concerning the retrieval principle, thoughts should be given to practical instrument design choices. For instance, the power supply with batteries is a good choice for remote sites and proved to provide electricity for ∼1 year. However, close to field stations constant power could be supplied via the electricity grid or from centrally organised solar cells to prevent power loss and missing observations. A permanent data-link to the logger and upload to cloud servers could help to identify sensor problems

and monitor results in real-time. Furthermore, the contamination of the sensors with water, falling leaves or needles, or with insects should be taken care of in a long-term deployment. In sites with substantial understorey, sensors could be deployed at different heights and below understorey plants to sample the vertical profile. In addition, sensors at larger heights might be able to focus on the foliage and prevent large stems to be in the FOV.

In the context of a set-up in larger, permanent sample sites, the representative area of PASTiS-57 should be considered to determine the number of required devices. In this respect, PASTiS-57 is comparable to other below-canopy sensors such as DHP and Licor LAI-2000 that measure τ at the hinge angle. Therefore, the diameter of the measurement area is $2\times$ canopy height $/ \tan(57.5°)$. This results in a diameter of 32 m for a 25 m high canopy, as is the case for Speulderbos. Considering geo-location error of 1 pixel (Drusch et al., 2012) this would be representative for Sentinel-2 10 m resolution bands. However, replicates need to be installed per plot to improve precision in the case of LAI validation (Fernandes et al., 2014). In the case of Sentinel-3 — when considering geo-location error — a footprint of 1000 m would need to be covered. Locations should be sampled to account for the site heterogeneity, i.e. number of species, differences in canopy structure and presence/variability of understorey.

Furthermore, low-cost, passive sensors such as PASTiS-57 can be combined with light-independent monitoring. For instance, Culvenor et al. (2014) presented a monitoring lidar system that samples the hinge angle, similar to the TLS used in this study. These systems are more cost and maintenance intense, but offer opportunities for inter-comparison and benchmarking, also with traditional manual sampling methods. Such a combination of sensors would offer the option of high precision light-independent sensors for site central areas and low-cost sensors for covering larger areas. This would provide the instrument infrastructure necessary for continuous validation of LSP and LAI products, as required by validation Stage 4 of the GCOS LPV group (Fernandes et al., 2014).

2.5 Conclusions

Robust tracking of the phenological cycle and thereby connected canopy biophysical conditions requires sampling techniques with high temporal resolution. This study assessed the ground-based, automatic, cost-efficient PASTiS-57 instrument in both field and RTM experiments for its performance in forest SOS, EOS and LAI estimation. The instrument design supported acquisition of yearly time series at up to 1 min raw data resolution with low maintenance effort. The choice of the blue spectral region and a viewing angle of 57.5° was found to be robust for a range of canopy biochemical and illumination conditions, thereby focussing on changes in canopy structure, mainly LAI. However, clumping assessment in irregular canopies was limited by the low number of sensors per instrument and the sensors' pointing measurements. In addition, the restriction to a viewing angle of 57.5°

alone does not allow retrieval of LAD together with LAI, as is possible with DHP. Future studies should compare PASTiS-57 with other phenology monitoring devices and develop combinations of instruments as site concepts. Other sensor designs could be tested, i.e. based on imaging sensors.

Chapter 3

Impact of Retrieval Scheme Features on Forest LAI Prediction with Sentinel-2A MSI, Landsat 7 ETM+ and Landsat 8 OLI

This chapter is based on:

B. Brede, J. Verrelst, J.-P. Gastellu-Etchegorry, J. Clevers, L. Goudzwaard, J. den Ouden, J. Verbesselt, and M. Herold (in preparation). "Impact of Retrieval Scheme Features on Forest LAI Prediction with Sentinel-2A MSI, Landsat 7 ETM+ and Landsat 8 OLI"

Abstract

ESA's Sentinel-2A (S2A) mission is already providing time series that allow the characterisation of dynamic vegetation, especially when combined with the NASA/USGS Landsat 7 (L7) and Landsat 8 (L8) missions. Hybrid retrieval schemes combining non-parametric Machine Learning Regression Algorithms (MLRAs) and vegetation Radiative Transfer Models (RTMs) were proposed as fast and accurate methods to infer biophysical parameters such as Leaf Area Index (LAI) from these data streams. However, the exact design of optimal retrieval schemes is rarely discussed. Additionally, studies focused on agricultural applications, thereby ignoring forest areas.

In this study the impact of five retrieval scheme features on LAI prediction performance of MultiSpectral Instrument (MSI), Enhanced Thematic Mapper Plus (ETM+) and Operational Land Imager (OLI) observations was analysed over a Dutch beech forest site for a one year period. The retrieval scheme features were the (1) addition of prior knowledge of leaf chemistry, (2) the choice of RTM, (3) the addition of Gaussian noise to RTM produced training data, (4) possibility of using Solar Zenith Angle (SZA) as an additional MLRA training feature, and (5) the choice of MLRA. The features were varied in a full grid resulting in 960 inversion models in order to find the overall impact on performance as well as possible interactions among the features. A combination of a Terrestrial Laser Scanning (TLS) time series with litter-trap derived LAI served as validation of the temporal LAI development. Results showed that the most important feature was the addition of absolute noise, which improved the median prediction Root Mean Square Error (RMSE) by $1.09\,\mathrm{m^2\,m^{-2}}$ when 5 % noise was added compared to inversions without noise. The best inversion model achieved an RMSE of $0.90\,\mathrm{m^2\,m^{-2}}$ and explained 86.3 % of the variance of the reference time series. The available observations for the test site also showed that combined observations of multiple missions are required to capture dynamic vegetation in order to generate an LAI product at decametric resolution. The results presented here show that more investigation of noise in hybrid retrieval schemes is necessary to optimise model performance.

3.1 Introduction

Vegetation represents a primary component in Earth's terrestrial carbon cycle, with respect to its role both as a source of CO_2 through respiration and as a sink of CO_2 through photosynthesis (Beer et al., 2010). Its photosynthetic capacity is a function of available leaf area, which can be quantified in terms of LAI. LAI is the leaf area per horizontally projected ground area (Chen and Black, 1992) and it was acknowledged as an Essential Climate Variable (ECV) with high priority in the European Space Agency (ESA)'s Global Monitoring for Environmental Security (GMES) program (Malenovský et al., 2012) and is a focus area of the Committee on Earth Observing Satellites (CEOS) Working Group on Calibration and Validation (WGCV) Land Product Validation (LPV) subgroup (Morisette et al., 2006).

The Sentinel-2 mission was awaited for the purpose of estimation of biophysical parameters such as LAI. Its higher spatial resolution, higher revisit frequency and additional red edge bands are emphasised as potentials for performance advances when compared to the Landsat missions. Agricultural preparation campaigns such as SEN3Exp and SicilyS2EVAL offered measurements to gain insight in its spectral opportunities (Delegido et al., 2011; Frampton et al., 2013; Richter et al., 2012; Verrelst et al., 2012). The SPOT5 Take5 campaign delivered a dataset with a 5-day revisit time to explore the temporal domain (Campos-Taberner et al., 2016). The domain of forest remote sensing has not seen this extent of targeted preparation campaigns. Nevertheless, approaches are advancing to make use of the Sentinel-2 open data in terms of biophysical parameter estimation (Korhonen et al., 2017). All these campaigns underlined that Sentinel-2 has high potential for estimation of LAI and Chlorophyll a and b (C_{ab}) in diverse canopies.

In parallel with the advances in sensor technology and data availability, MLRAs were introduced as retrieval techniques (Baret et al., 2007; Durbha et al., 2007; Lazaro-Gredilla et al., 2014; Verrelst et al., 2015a; Verrelst et al., 2012). Their main advantage is their ability to map the non-linear relationship between canopy parameters and the reflectance signal, and their fast mapping speed compared to look-up tables (Verrelst et al., 2015a). Especially Gaussian Process Regression (GPR) – a kernel-based MLRA – showed good results and could achieve the 10 % precision for C_{ab} retrieval required by the Global Climate Observing System (GCOS) (Verrelst et al., 2012). Like traditional retrieval techniques, MLRAs require a database of biophysical parameters and their associated reflectance signal to learn the mapping. This database can originate from field observations, but also from vegetation RTMs. RTMs encode the parameter-reflectance relationship based on physical laws, which makes them universally applicable. Verrelst et al. (2015a) conclude that MLRAs and RTMs combined in training schemes have potential for implementation in operational processing chains for retrieving biophysical parameters. These schemes are referred to as hybrid training schemes.

Turbid medium RTMs, which approximate the vegetation canopy as one homogeneous layer, dominate all kinds of inversion schemes (e.g. Baret et al., 2007; Haboudane et al., 2004). Among these RTMs, PROSAIL – a combination of the PROSPECT leaf and the SAIL canopy model (Jacquemoud et al., 2009) – is one of the most widely used. The main reasons for the use of turbid medium models are their fast processing speed and the low number of input parameters. However, PROSAIL does not agree well with geometrically explicit RTMs in the case of heterogeneous scenes (Widlowski et al., 2007). As modelling capabilities have outrun means to collect ground truth for complex canopies, a final evaluation of the differences remains open (Widlowski et al., 2015). On the other hand, so-called emulators make it possible to build fast surrogates for complex models (Verrelst et al., 2016). For that, a complex physical model is replaced with a statistical learning model that was trained on input-output combinations of the physical model. This makes it practically possible to exploit heterogeneous RTMs in operational contexts.

Considering these developments together – decametric observations from Sentinel-2 and Landsat, fast mapping with MLRA algorithms and fast radiative transfer modelling with emulators – a decametric LAI product would be possible. Such a product would offer better opportunities to monitor ecosystems in fragmented landscapes than comparable products on hectometric scale like the MODerate-resolution Imaging Spectroradiometer (MODIS) (Myneni et al., 2011) and CYCLOPES (Baret et al., 2007) LAI products.

The aim of this study was to compare different hybrid retrieval schemes that make combined use of S2A MSI, L7 ETM+ and L8 OLI observations for forest LAI retrieval. Features in the retrieval scheme were altered in a fully-factorised way to explore their effects. Performance statistics for the realisations were derived to identify which features influence performance most. Apart from this, features were analysed in terms of their extrapolation potential and interactions with other features.

Section 3.2 describes the available field and space-borne data used for prediction and validation. Section 3.3.1 introduces the training ensembles and the remaining of Section 3.3 elaborates the training choices. In Section 3.4 all results are presented and discussed. The conclusions derived can be found in Section 3.5.

3.2 Data

3.2.1 Study Site

This study focussed on the Speulderbos Fiducial Reference site in the Veluwe forest area (N52°15.15′ E5°42.00′), The Netherlands (Brede et al. 2016, `www.wur.eu/fbprv`). In an earlier forest inventory the site was equipped with a 40 m spaced wooden pole grid, which was geo-located with Real Time Kinematic (RTK) GPS and land surveying methods. This grid served to define the five plots A to E (Figure 3.1). The plot locations were chosen

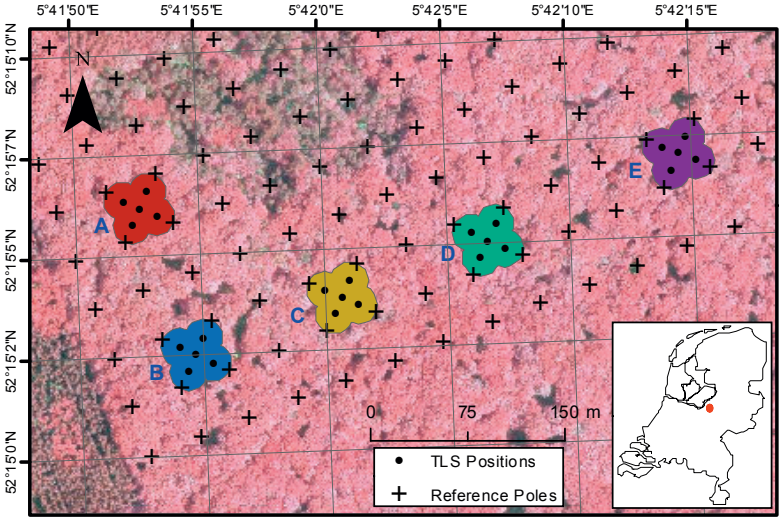

Figure 3.1: Speulderbos study site with TLS scan positions and polygons representing the five plots. Background image is an airborne false-colour composite of 2013. The inset shows the location of the study site within the Netherlands.

with a distance of at least 80 m between them. This distance is four times the image registration error according to S2A mission definition (Drusch et al., 2012).

The stand is predominantly composed of European beech (*Fagus sylvatica*). A few specimens of pedunculate oak (*Quercus robur*) and sessile oak (*Quercus petraea*) can be found as well. In the understorey few specimens of evergreen European holly (*Ilex aquifolium*) can be found with heights of <7 m: 1 each in plots A, B, and E. The stand was created as a plantation in 1835 and left unmanaged from then on, so that dominant trees are of even age. Recruitment took only place in canopy openings caused by falling trees as was the case in plot D. This was reflected by the total number of stems, which was 1059 ha^{-1} in plot D compared to 280 ha^{-1}, 250 ha^{-1}, 280 ha^{-1} and 202 ha^{-1} in plots A, B, C and E, respectively, as determined in a forest inventory in 2013/2014. Basal area was 43.0 m^2 ha^{-1}, 42.5 m^2 ha^{-1}, 31.4 m^2 ha^{-1}, 34.8 m^2 ha^{-1} and 37.2 m^2 ha^{-1} for plots A, B, C, D, and E, respectively.

3.2.2 Field Data

During a field campaign with temporally dense sampling a TLS time series was acquired. The five plots were revisited 28 times with a RIEGL VZ-400 scanner (RIEGL LMS GmbH, Horn, Austria). Sample dates were chosen in an opportunistic way with an increased intensity during leaf flush and senescence. Rain events and wet canopy conditions were avoided as wet canopy elements tend to absorb the laser pulses thereby introducing a bias in

the estimation of gap fraction. In each plot the same five positions were scanned resulting in a total of 25 positions per field visit. The positions were arranged in a star shape with a centre position determined according to the wooden poles and four positions at the corners of imaginary squares with 20 m edge length. For each position the tripod was levelled. The individual point clouds were processed with the `PyLidar` package (`http://pylidar.org`) based on the methodology developed by Calders et al. (2015c). This includes the derivation of gap fraction by counting pulses that exited the canopy versus all pulses fired in the *hinge angle* region, which was approximated by the zenith angle region between 50° and 60°. Terrain correction for vertical profiles as proposed by Calders et al. (2014) was not used because only total canopy Plant Area Index (PAI) values were required, which is indifferent to the terrain. Finally, PAI was derived as follows:

$$PAI = -1.1 \log(P_{gap}(57.5°)) \tag{3.1}$$

where $P_{gap}(57.5°)$ is the gap fraction at the hinge angle. PAI is defined as the one sided surface area of all plant material per unit area ground surface (Calders et al., 2015c). This is different from LAI, which only includes foliage material.

Additionally, 25 litter traps were installed in the area to directly measure LAI per season. In each plot five traps were positioned close to the TLS sampling points. Their construction was based on recommendations of the CTFS Global Forest Carbon Research Initiative Litterfall Monitoring Protocol, version March 2010 (`http://www.ctfs.si.edu/data/documents/Litter_Protocol_20100317.pdf`). Each trap consisted of a PVC pipe bent to a circle with an area of 0.7 m^2 and holding a plastic net. The net allows water to drain and prevent decomposition of the litter content. For each trap the pipe circles were levelled to assure correct surface area and are held in place 1 m over the ground with four wooden poles.

Litter was collected six times in 2016 over the course of the season. Litter was collected with paper bags; sorted by species and components, i.e. leaves, twigs, and husks; dried for at least 24 h at 65 °C; and weighted. Specific Leaf Area (SLA) – the unit area of leaf per unit mass – was estimated based on sub-samples of 100 leaves of each litter collection. The total leaf area per trap for the whole season was then inferred from the total collected dry leaf weights taking into account the litter trap surface area. Plot level LAI was estimated as the mean of the single traps.

Apart from these canopy structural measurements, the leaf chemistry was monitored over the course of the year. For this purpose two beech trees between plot A and B were rigged with ropes and climbed four times at different points of leaf development. On each tree five branches were cut off at each sampling event from near the crown top. From each branch five leaves were sampled randomly when no differences in development stage were visible. Especially during the last sampling event, the leaves showed different stages of senescence. In that case the leaves were sampled to represent the abundance of the respective senescence

stage on the branch. Leaf reflectance spectra were acquired with a Fieldspec Pro 3 (ASD Incorporated, Boulder, CO, USA) equipped with an integration sphere. Additionally, the same leaves were sampled with a Minolta SPAD-500 chlorophyll meter (Spectrum Technologies, Inc., Plainfield, IL, USA). For this four SPAD measurements per leaf were averaged. The sampling resulted in a total of 173 reflectance spectra.

3.2.3 Sentinel-2A MSI, Landsat ETM+ and OLI

S2A MSI was primarily designed for land cover and disaster monitoring, but also for retrieval of biophysical parameters like Fraction Absorbed Photosynthetically Active Radiation (FAPAR), LAI and Fractional vegetation cover (FCover) (Drusch et al., 2012). Operational products incorporate the Top Of Atmosphere (TOA) Bidirectional Reflectance Factor (BRF) and recently the Surface Reflectance (SR) BRF for Europe. Table 3.1 gives an overview of the MSI spectral bands.

S2A MSI TOA BRF products for tile T31UFT were downloaded from the Copernicus Open Access Hub (`https://scihub.copernicus.eu/`) for the period of January 2016 until December 2016. The relative orbits R008 and R051 both include the Speulderbos site, thereby doubling the number of observations compared to single orbit observation. TOA BRF products were further processed with sen2cor 2.4.0 (`http://step.esa.int/main/third-party-plugins-2/sen2cor/`) to derive SR BRF products. During further processing 60 m bands (B01, B09, B10) were excluded, because they are heavily affected by atmospheric conditions and therefore were not provided in surface reflectance products. Cloud and quality screening was performed manually under consideration of the scene classification delivered with sen2cor. For this Normalised Difference Vegetation Index (NDVI) time series for the extracted observations were inspected. Potentially cloud free dates were identified as high values in the time series and the respective images were checked.

Since the opening of the Landsat Archive in 2008, Landsat products experienced a steady growth in range of studies and applications (Wulder et al., 2012). In particular the provision of atmospherically corrected data made physical-based and time series approaches feasible with the potential to scale up to a global dimension. This included retrieval of biochemical leaf properties (Houborg et al., 2015), canopy biophysical parameters (Ganguly et al., 2012; Li et al., 2015a), and time series based deforestation monitoring (Dutrieux et al., 2015; Reiche et al., 2015). However, specific application to forest LAI retrieval has been limited.

For this study, L7 ETM+ and L8 OLI SR BRF products at Worldwide Reference System (WRS) row 24 and WRS path 197 and 198 were obtained as on-demand download products provided by the USGS Earth Resources Observation and Science (EROS) Center Science Processing Architecture (ESPA) On Demand Interface (`https://landsat.usgs.gov/landsat-surface-reflectance-high-level-data-products`). Both Landsat time

Table 3.1: Spectral band specifications for bands and missions used in this study (band centres and widths in nm), bands used for atmospheric correction were omitted (Drusch et al., 2012; Irons et al., 2012).

Domain	Landsat 7 ETM+			Landsat 8 OLI			Sentinel-2A MSI		
	Name	Center	Width	Name	Center	Width	Name	Center	Width
VIS	B1	485	70	B2	482	60	B2	490	65
	B2	560	80	B3	561	57	B3	560	35
	B3	660	60	B4	654	37	B4	665	30
NIR	B4	835	13	B5	864	28	B5	705	15
							B6	740	15
							B7	783	20
							B8	842	115
							B8A	865	20
SWIR	B5	1650	20	B6	1608	84	B11	1610	90
	B7	2220	260	B7	2200	187	B12	2190	180

series profited from two orbits from which Speulderbos can be observed. Clouds and cloud shadows were identified in the same manner as for MSI and with the support of the pixel quality layer delivered with Landsat Collection 1 products.

All space-borne observations were extracted from the SR products based on polygons representing the plots. These polygons were produced considering the circular field of view of the TLS at the five scan positions within each plot (Figure 3.1). Each position was buffered with a circle of 14.4 m radius, which corresponds to the top of canopy of the approximated tree height of 25 m. The combined area of the circles represented the plots. For each plot and SR product, pixels overlaying each plot were averaged with weights according to their overlap with the plot polygon.

3.3 Methods

3.3.1 Ensemble Overview

The inversion in this study generally followed a hybrid scheme (Verrelst et al., 2015a; Verrelst et al., 2015b):

1. A vegetation RTM was run in forward mode to create a database of training samples, i.e. biophysical parameters served as input for the RTM to predict spectral BRFs. These parameters were varied to cover multiple canopy conditions.

2. A specific amount of Gaussian noise was added to the spectra to prevent the MLRA from over-fitting and simulate observation noise.

3. Multiple MLRAs were trained on the database to learn the inverse mapping, i.e. from spectral bands to biophysical parameter. Model tuning was performed on a part of the generated database, while the rest was used for testing of the trained model.

4. The MLRAs were applied to the observed spectra to predict the desired biophysical parameter. MLRAs performance was compared.

In this study, features in the training scheme were altered to test their impact on the prediction performance. The following list gives an overview and introduces reference terms under which the feature domains were treated:

- Biochemical Prior: Using leaf biochemical parameters inferred from field spectroscopy observations to restrict the RTM input parameter space (label: *prior knowledge*) versus using a free range (label: *free*) (2 alternatives).
- RTM: Two underlying, structurally contrasting RTMs were tested: turbid medium PROSAIL (SAIL 4 coupled with PROSPECT 5) and structurally-explicit Discrete Anisotropic Radiative Transfer (DART) (with PROSPECT 5) (2 alternatives).
- Noise scenario: Using multiple noise levels for two types of noise each (4 and 5 alternatives).
- SZA: Using the SZA as an additional learning feature (label: *SZA*) or not (label: *no SZA*) (2 alternatives).
- MLRA: Using multiple MLRAs: Ordinary Least Squares (OLS), Multi-Layer Perceptron (MLP), Regression Tree (RT), Support Vector Regression (SVR), Kernel Ridge Regression (KRR), GPR (6 alternatives).

Each unique combination of these features is referred to as a realisation in the following, while realisations with the same feature were summarised as ensembles. For example, a realisation may have used *biochemical prior knowledge*, DART, specific levels of noise, SZA and OLS. And all realisations that implement DART make up the an ensemble. All possible combinations of the list above were tested, resulting in 960 realisations. Training was performed independently for each mission and predictions were combined later to form one time series per realisation. An independent per mission performance assessment was not conducted, because effective number of observations varied strongly between the missions and thus would not allow fair comparison.

3.3.2 Leaf Biochemical Parameter Estimation

For retrieval of leaf chemical properties, the collected field spectral samples (Section 3.2.2) were inverted with a gradient descent approach utilising the PROSPECT 5 model as implemented in the R package `hsdar` (`https://cran.r-project.org/web/packages/hsdar`) (Feret et al., 2008; Lehnert et al., 2016). The quasi-Newton method after Byrd

et al. (1995) that allows box constraints was chosen. The parameter ranges given in Table 3.2 were chosen as constraints. Results were inspected to identify biochemical compounds whose abundance was stable over the season and could be assumed fixed over the course of the year.

3.3.3 RTMs and Training Database Creation

Two contrasting canopy RTMs were used to represent different levels of canopy complexity. One was PROSAIL, which is a turbid medium model, i.e. it treats the canopy as a homogeneous medium. It is a combination of the PROSPECT leaf and the SAIL canopy bidirectional reflectance model (Jacquemoud et al., 2009). It has been widely used in the fields of agriculture, plant physiology and ecology, including estimation of biophysical parameters (Atzberger and Richter, 2012; Baret et al., 2007; Campos-Taberner et al., 2016; Lauvernet et al., 2008). In this study PROSAIL 5B as implemented in the R package `hsdar` was used.

On the other hand, the DART model is a voxel-based flux-tracing model that allows building complex 3D scenes including vegetation canopies (Gastellu-Etchegorry et al., 1996; Gastellu-Etchegorry et al., 2017). DART contains a PROSPECT module to simulate leaf reflectance and transmission. Applications of DART can be found in the fields of surface energy budget studies (Gastellu-Etchegorry et al., 2004) and forest biophysical parameter retrieval (Banskota et al., 2015; Demarez and Gastellu-Etchegorry, 2000; Malenovský et al., 2013), where its advantages of explicitly modelling 3D structure were exploited. DART can be obtained from CESBIO with free licences for publicly funded research and teaching.

As both RTMs use PROSPECT 5 as underlying leaf model, they have many common parameters. Table 3.2 gives an overview of the used parameter ranges. In case of *free* realisations, ranges were adopted from the literature (Verrelst et al., 2015b). In case of *prior knowledge* realisations, the values were estimated with field spectroscopy as described in Section 3.3.2. The range of sun zenith angles is based on the geographic location of the Speulderbos site. Since ETM+, OLI and MSI have narrow fields of view of 15°, 15° and 21°, respectively, view zenith angle and relative azimuth angles were assumed 0. This was found a reasonable assumption for mid and high latitudes (Nagol et al., 2015). Soil spectra were estimated from MSI barren, winter observations. BRFs were extracted as described above and averaged over all sites. Sensor spectral response curves were approximated as Gaussian with centre wavelength and Full Width at Half Maximum (FWHM) according to published specifications (Table 3.1). In this way, in fact three models were trained, one for each sensor.

The DART scene was built of five trees as squared, repetitive scene with 10 m edge length and grid size of 1 m horizontal and 0.5 m vertical cell size. This means the scene was duplicated along the edges. The trees' heights and diameters were roughly approximated

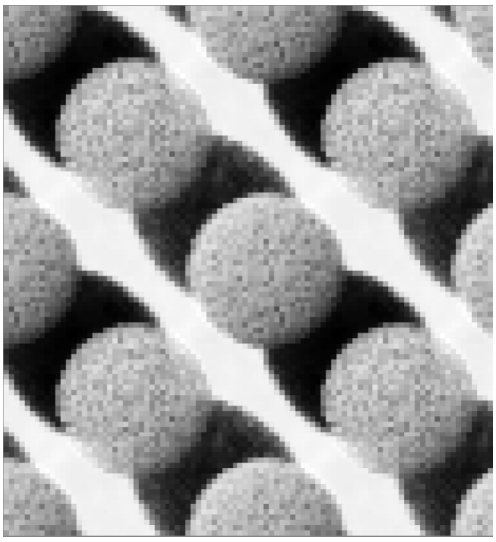

Figure 3.2: Nadir view of DART sample scene that is used to represent the heterogeneous canopy. The centre scene with 5 trees is replicated along the edges. Colour is reflectance with low values black and high values white.

with TLS point clouds (Table 3.2, Section 3.2.2). However, the trees were based on generic forms consisting of 8-faceted stems and ellipsoidal crowns. The stems had a diameter of 0.5 m below and 0.25 m within the crown. The crown leaf volume was simulated as turbid medium cells. TLS was not used to build 3D tree models in order to keep the number of input parameters minimal. For fast computation an emulator was built to replace actual DART simulations (Verrelst et al., 2016). For this, 2500 samples of DART input parameters were drawn with Latin hypercube sampling according to the *free* option in Table 3.2. Then, the same MLRAs as for the inversion were trained to predict the single spectral bands of ETM+, OLI and MSI. The best performing MLRA was identified according to the lowest RMSE in a five-fold cross-validation. The application of this emulator decreased the computation speed from approximately 33 s to 0.005 s per sample. On the other hand, PROSAIL required 0.003 s per sample.

In total, 2500 parameter samples were drawn with Latin hypercube sampling using uniform distributions to evenly cover the parameter space for all parameters with range specifications. Of these 2500, 30 % were modified to represent barren, winter conditions. This means all leaf chemical parameters and LAI were set to 0.

3.3.4 RTM Sensitivity Analysis

In order to assess the importance of the RTM input parameters (Table 3.2) on the single spectral outputs, a global sensitivity analysis of the RTMs was conducted. Such

Table 3.2: RTM parameters with their symbols, units, ranges (in case of *free* realisations) and estimated values (in case of *prior knowledge* realisations; based on PROSPECT inversion of sampled leaf spectra, Section 3.3.2).

	Model parameter	Unit	Free	Best estimate
Leaf parameters: PROSPECT-5B				
N	Leaf structure index	-	1 - 2.5	1.27
C_{ab}	Leaf chlorophyll content	$\mu g\,cm^{-2}$	0 - 80	-
Car	Leaf carotenoid content	$\mu g\,cm^{-2}$	0 - 20	8.60
C_m	Leaf dry matter content	$g\,cm^{-2}$	0.001 - 0.025	0.00263
C_w	Leaf equivalent water thickness	cm	0.002 - 0.025	0.0053
C_{brown}	Brown pigment content	-	0 - 1	-
Canopy parameters: SAIL4 and DART				
LAI	Leaf area index	$m^2\,m^{-2}$	0 - 8	0 - 8
θ_s	Sun zenith angle	°	27.5 - 80	27.5 - 80
θ_o	View zenith angle	°	0	0
ϕ	Sun-sensor azimuth angle	°	0	0
LAD	Leaf angle distribution	-	Plagiophile	Plagiophile
Canopy parameters: SAIL4				
α_{soil}	Soil wet/dry factor	-	0	0
$hspot$	Hot spot parameter	-	0	0
Canopy parameters: DART				
$TreeHeight$	Tree height	m	20	-
$CrownDiameter$	Tree crown diameter	m	5 - 9	-
$CrownHeight$	Tree crown height	m	7	-

an approach also helps to gauge how good input parameters can be estimated from spectral outputs. The approach here generally followed the approach of Verrelst et al. (2016) based on Sobol' sensitivity indices (Jansen, 1999; Sobol', 1990) modified by Saltelli et al. (2010) and as implemented in the R package `sensitivity` (`https://cran.r-project.org/web/packages/sensitivity`). Here, only the total effect indices were considered that describe the sensitivity of the model output to an input parameter and its interactions with other parameters. The sum of the sensitivity indices with respect to all input parameters varies per spectral band output. Therefore, indices were normalised to sum up to 1 to ease comparison across spectral band outputs. Furthermore, only bands of MSI were taken into account, because they cover the same spectral domains as ETM+ and OLI (Table 3.1).

3.3.5 Noise Scenarios

The addition of noise to the RTM-generated spectral bands has multiple purposes: it simulates errors of radiometric calibration, atmospheric noise and residuals from the atmospheric correction, but to some extent also bridges between the simplified representation of the RTM and the actual radiometric behaviour of the canopy (Baret et al., 2007). Generally, noise prevents the inverse model from over-fitting on the training database. However, an accurate quantification of all error terms in the sensing process remains difficult (Baret et al., 2007). Verrelst et al. (2014) added up to 20 % Gaussian noise to the reflectance spectra in a look-up table approach to find optimal performance results.

In this study two types of noise were tested: multiplicative wavelength-independent (MI) and additive wavelength-independent (AI) noise (Weiss and Baret, 2016). MI is dependent on the BRF. Its term is larger for NIR compared to red spectral bands for typical vegetation spectral responses. MI and AI were added to the RTM spectral bands:

$$\rho' = \rho_{RTM} + \rho_{RTM} \cdot \epsilon_{MI} + \epsilon_{AI} \tag{3.2}$$

where ρ' is the noise contaminated spectral band, ρ_{RTM} is the RTM spectral band output, ϵ_{MI} the MI noise term with $\epsilon_{MI} \sim \mathcal{N}(0, \sigma_{MI})$ and ϵ_{AI} the AI noise term with $\epsilon_{AI} \sim \mathcal{N}(0, \sigma_{AI})$. Apart from noise free, realisations with MI noise of 0.05, 0.1, 0.2 and 0.3, and AI noise of 0.05, 0.1 and 0.2 were tested. The additional MI noise level of 0.3 was added after analysis showed an increasing performance up to 0.2. The 0.05 noise level was motivated by the Sentinel-2 mission requirement for SR BRFs of 5 % error (Drusch et al., 2012), and the other were pessimistic variations. However, as mentioned before the noise term has multiple purposes, so that the mission requirements can only be an indication.

3.3.6 Solar Zenith Angle

Illumination conditions greatly affect the reflectance of canopies (Brede et al., 2015; Jacquemoud et al., 2009; Morton et al., 2014). As the SZA changes over the course of the year, the internal canopy shadowing varies. Furthermore, SZA is an easy to obtain feature as it is solely a function of location and time. Therefore, SZA was incorporated in the training scheme to test if it improves LAI prediction. SZA was calculated for local overpass times of the respective missions with the R package `RAtmosphere` (Teets (2003), `https://cran.r-project.org/web/packages/RAtmosphere`). For the respective realisations, it was treated as an extra training feature next to spectral bands.

3.3.7 Machine Learning Regression Algorithms

Studies on MLRA typically test a range of algorithms to explore their respective (dis)advantages and cross-comparison results. This was adopted in this study as well. All

models were trained to predict LAI, while the independent variables depended on the learning realisation. Multi-variate OLS regression was chosen as a benchmark method. For neural networks the classic MLP was used (e.g. Baret et al., 2007). In particular this was the implementation of the Stuttgart Neural Network Simulator in the R package `RSNNS` (`https://cran.r-project.org/web/packages/RSNNS`). Networks with $n + 1$ neurons in a single hidden layer were trained, where n corresponded to the number of independent variables. Random Forest was selected as a RT algorithm (Belgiu and Drăgu, 2016; Breiman, 2001) and used as implemented in the R `ranger` package (`https://cran.r-project.org/web/packages/ranger`). The forests were grown with 500 trees.

Furthermore, three kernel-based methods were used. This type of regression methods translates the – possibly non-linear – regression problem from the parameter space into a higher dimensional feature space, where it can be solved linearly. Kernel functions implement a notion of similarity function. SVR, KRR and GPR with Radial Basis Function (RBF) kernels were tested here. The kernel σ hyperparameter was estimated with the `sigest` function from the `kernlab` package. Although developed to estimate σ for SVR, results in initial tests were promising for KRR and GPR. For further reading on MLRAs in biophysical parameter estimation the reader is referred to Verrelst et al. (2015a).

The general work-flow for MLRA application typically involves splitting of the feature database to tune model parameters. Here, five-fold cross-validation was performed during the tuning process. This was based on the training dataset, which held 2500 samples of the RTM-based database. Next, the model performance for the best tuned parameters was evaluated with the test dataset, which held 500 samples of the RTM based database. This set was never seen by the models during training. Finally, the models were applied on the actual sensor observations and compared with the validation dataset (Section 3.3.8). However, as we inverted observations of three different sensors, in fact for each realisation three separate models were trained.

3.3.8 Ensemble Analysis & Validation

In order to analyse how well the MLRAs were able to learn the RTM-produced band-LAI relationships the test error was consulted. However, this error represents only the theoretical performance in case the RTM produces true results for the scene and the induced noise properties correspond to the noise of the actual spectral observations.

For validation purposes the advantages of the TLS time series – i.e. high precision due to independence of illumination conditions (Calders et al., 2018b; Jupp et al., 2009) – was combined with the direct estimation of LAI with the litter-traps. Litter-traps are considered among the most accurate methods in terms of absolute LAI for forest canopies (Jonckheere et al., 2004). This approach follows the suggestion of Woodgate et al. (2015) to calibrate TLS with other techniques. Specifically, the TLS time series was scaled with

the litter-trap total LAI separately for each plot:

$$LAI_i = \frac{PAI_{TLS,i} - min(PAI_{TLS})}{max(PAI_{TLS})} \cdot LAI_{LT} \tag{3.3}$$

where LAI_i is the LAI at time i, PAI_{TLS} is the TLS derived PAI time series and LAI_{LT} is the litter-trap LAI. The observations were averaged per plot and linearly interpolated to obtain a continuous time series.

For each realisation the time series of predicted LAI was compared with this validation time series. The performance metric was the RMSE:

$$RMSE = \sqrt{\frac{1}{t}\sum_{i=1}^{t}(LAI_{realisation,i} - LAI_{valid,i})^2} \tag{3.4}$$

where t is the length of the time series, and $LAI_{realisation,i}$ and $LAI_{valid,i}$ the realisation and validation LAI at time i, respectively.

3.4 Results & Discussion

3.4.1 Validation Time Series

Figure 3.3 shows the derived validation time series. The seasonal pattern with a fast spring leaf flush in May and autumn leaf falling in November dominated the temporal behaviour. Calders et al. (2015c) observed this speed in spring leaf flush for a mixed oak forest in the Netherlands. Maximum LAI of $6.1\,m^2\,m^{-2}$ was reached on May 26 in plot A. Plot B and E showed LAI values just below $6.0\,m^2\,m^{-2}$. Plot C had a larger gap in its centre so that overall LAI was lower there. Measured LAI for plot D was about 2 units lower with a peak of $3.2\,m^2\,m^{-2}$. This was due to the age composition of this plot, which was dominated by younger trees. The maximum LAI compares well with the results of Leuschner et al. (2006), who measured LAI by litter-traps in 23 mature Beech stands in Germany. They found an average LAI of $7.4\,m^2\,m^{-2}$ with a range between 5.6 to 9.5 $m^2\,m^{-2}$.

Another feature is the slow decrease in LAI starting in August that could be observed in all plots. After the 2016 growing season few, brown leaves were still remaining on the trees until new leaves flushed in 2017. Overall, the obtained time series show the expected dynamic behaviour of the canopy during spring and autumn.

With respect to the uncertainty of the validation data, the standard deviation of the mean for the litter-trap samples was calculated as $0.43\,m^2\,m^{-2}$, $0.25\,m^2\,m^{-2}$, $0.41\,m^2\,m^{-2}$, $0.32\,m^2\,m^{-2}$ and $0.24\,m^2\,m^{-2}$ for plots A to E, respectively. GCOS specified an accuracy of $0.5\,m^2\,m^{-2}$ as a target for LAI products for local and regional applications (Fernandes et al., 2014). However, this is the requirement for the final LAI products, so that the achieved

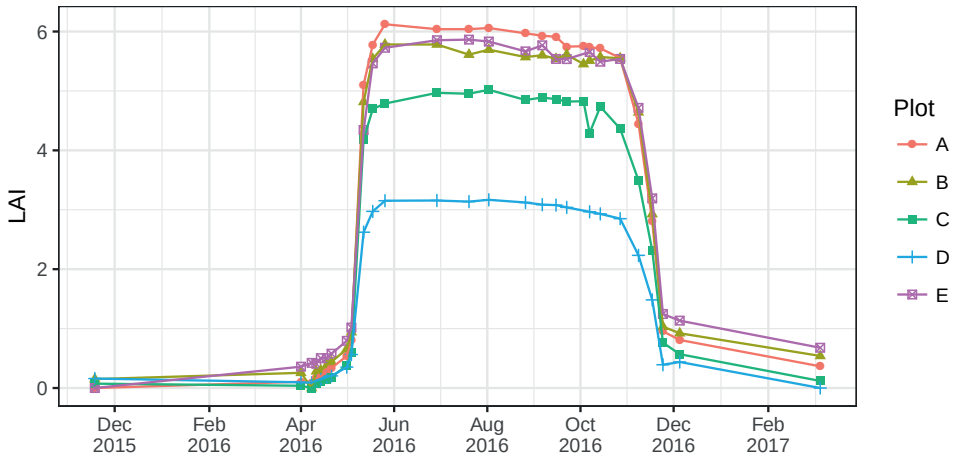

Figure 3.3: Speulderbos LAI time series for 2016 derived from TLS, points are observations. Lines are linear interpolations. Interpolations for outside of the measurement campaign were performed with the values from the previous and next year, which are added to the graph for clarity.

uncertainties are rather high for a validation measurement. This affected especially the realisation evaluations in terms of RMSE.

Nonetheless, the used TLS-based approach was found to be very suitable from an acquisition point of view. The active illumination source leads to independence of cloud and sun conditions, which is useful when frequent acquisitions have to be made. Passive devices are restricted to operations under full cloud cover or clear sky (Jonckheere et al., 2004). On the other hand, sampling was restricted by rain and wet canopy conditions, because liquid water absorbs the laser energy, which leads to overestimation of gap fraction and ultimately underestimation of LAI.

3.4.2 Leaf Biochemical Parameters Retrieval

The leaf chemistry assessment indicated that some leaf components remained stable over the course of the season, while others showed a dynamic behaviour, resulting in multi-modal distributions (Figure 3.4). The static ones were the N parameter, the dry matter content C_m, and to some extent the equivalent water thickness C_w. The mean of the carotenoids remained stable, but its variance was increasing at the last sampling day. C_{ab} showed clear dynamics, with a strong decrease during the last sampling day. When compared to the readings of the SPAD meter, C_{ab} retrievals showed a quadratic relationship (Figure 3.5), which is confirmed by other studies (Buddenbaum et al., 2015; Percival et al., 2008). This strong relationship supports the validity of the C_{ab} retrievals, and thereby the retrieval of the other biochemical constituents since they were inverted simultaneously. On the basis

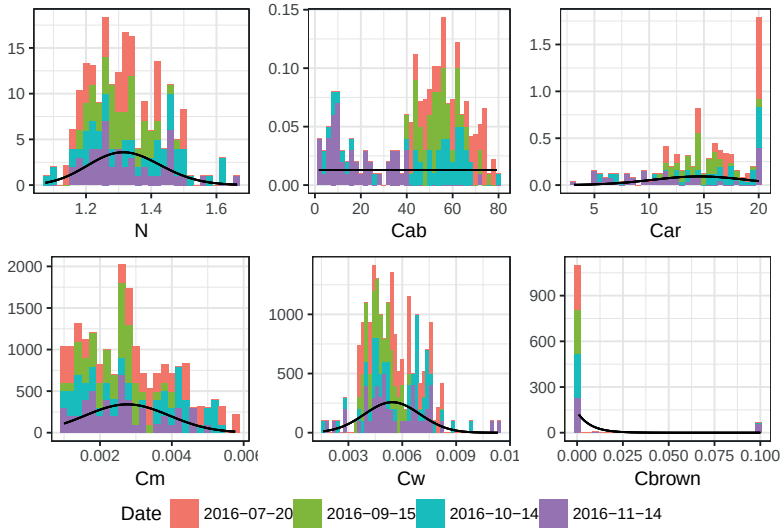

Figure 3.4: Leaf chemical properties based on PROSPECT inversions of 173 leaf samples. Stacks are coloured by acquisition date. Solid lines are fitted probability density functions. Ordinate axis is kernel density.

of these results it was decided to constrain the training with fixed, central values of the N parameter, Car, C_w and C_m, but vary C_{ab} and C_{brown} as given in Table 3.2.

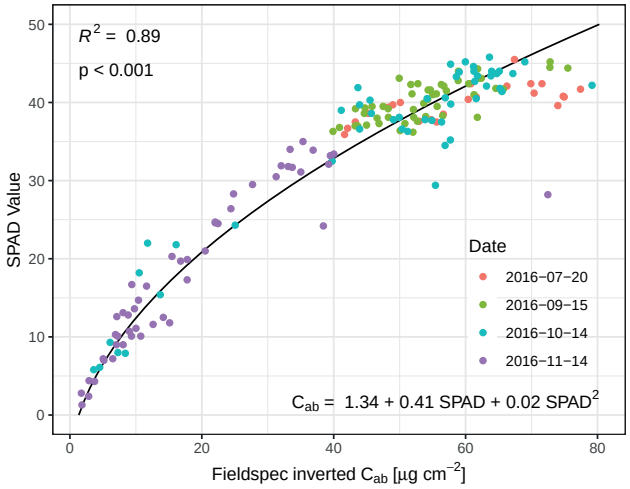

Figure 3.5: Comparison of Fieldspec inverted C_{ab} with SPAD meter value taken from the same leaf samples. Solid line, R^2, p-value and formula correspond to the quadratic fit. Dates correspond to the leaf sampling dates.

3.4.3 Satellite-based Spectral Observations

Of the 64 dates in 2016 when MSI observations of the Speulderbos site were available, 21 dates yielded usable observations, which is 32.8 % of all. Figure 3.6 shows the bands B04 and B8A, which are the red and NIR spectral bands (Table 3.1) and hold most information on change in canopy characteristics. The automatic scene classification could identify most of the cloud affected conditions with an accuracy of 91.6 %. Overall, the time series depicted the start of season in April and May: the red reflectance decreased over all plots from 0.059 ± 0.003 on May 1 to 0.022 ± 0.001 on May 11 due to absorption by chlorophyll. At the same time, reflectance in band B8A increased from 0.188 ± 0.008 to 0.406 ± 0.014, which can be attributed to the leaves' characteristic scattering behaviour. During late summer, the overall temporal course remained stable with a slightly decreasing trend. This trend could also be observed in the validation time series (Figure 3.3). An exception was July 17, when B8A reflectance jumped to 0.526 ± 0.023. There were no clouds over the plots on that day, but clouds close-by probably caused adjacency effects.

In case of the two Landsat missions, 41 and 42 observation dates were available of which 8 (17.1 %) and 9 (15.8 %) were usable for ETM+ and OLI, respectively (Figure 3.7). The pixel quality bits for cloud occurence indicated at least medium confidence, which appeared to indicate clear sky conditions after checking the corresponding images. As for MSI, these could mostly be found during the spring green-up and late summer periods.

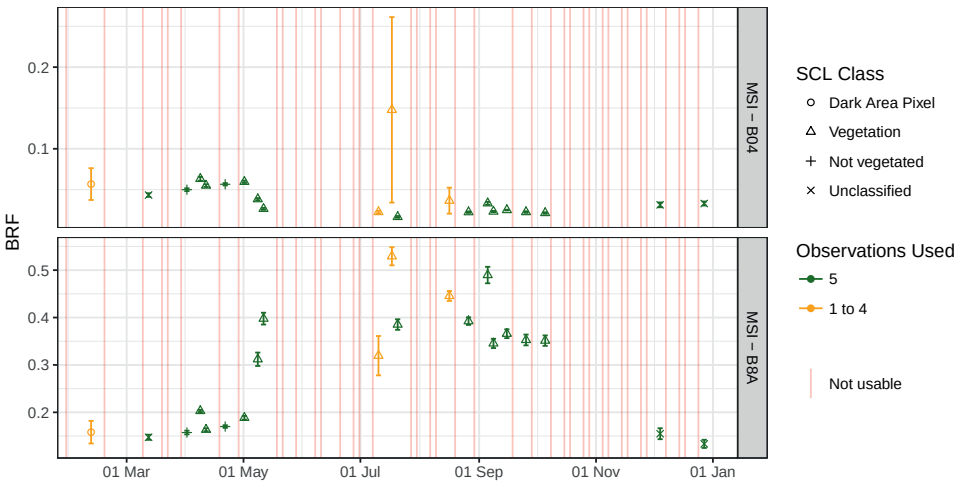

Figure 3.6: Observed BRFs for S2A MSI red and NIR band over the year 2016 for the five Speulderbos plots (see Figure 3.1). Points represent average BRF over the five sites, error bars one standard deviation. Colour codes the number of plots for which the observations were useful (clear sky). SCL class refers to the mode of all Scene Classifications given by sen2cor over the five plots.

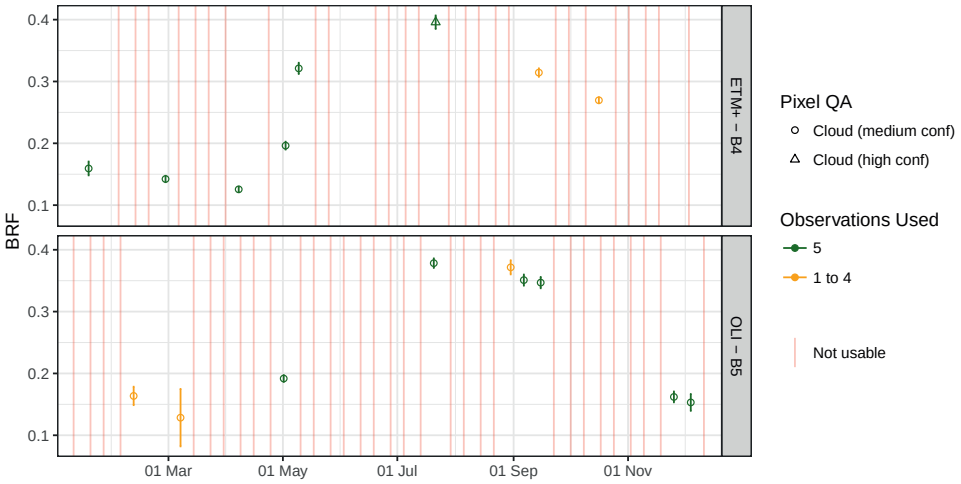

Figure 3.7: Same as Figure 3.6, but for Landsat 7 ETM+ and Landsat 8 OLI. Pixel QA refers to the pixel quality bits. Six observations were discarded, because they exceeded a reflectance of 1.

Cloud conditions, represented by bits set to high confidence cloud, were identified with an accuracy of 85.9 %.

In September, when multiple observations of MSI and OLI were available, they produced comparable SR BRFs when excluding September 5. Only the SWIR bands produced small, but significant differences. This gives confidence in comparable behaviour of SR BRFs and to combine observations from these sensors. However, for a detailed comparison the spectral response functions of the sensors and the used atmospheric processors need to be taken into account e.g. Doxani et al., 2018. In fact, for optimal inter-operability the S2A and Landsat products should be harmonised before combined processing.

3.4.4 RTM Sensitivity

PROSAIL's and DART's sensitivity to their input parameters is depicted in Figure 3.8. In case of PROSAIL, BRFs in the visible bands were primarily driven by C_{ab} with a contribution of 74.8 % and 49.4 % in B03 and B04, respectively. This extended into the first red edge band B05, but strongly decreased to 6.1 % at B06. In the red edge and NIR bands LAI was the most important parameter with a relative contribution of 68.5 % for bands B06 to B8A on average. This sensitivity is the reason why LAI retrieval relies on the NIR domain. The SWIR bands were mostly dependent on leaf water content C_w, which had 52.8 % and 46.2 % contribution in B11 and B12, respectively. These results are in line with those of Jacquemoud et al. (2009).

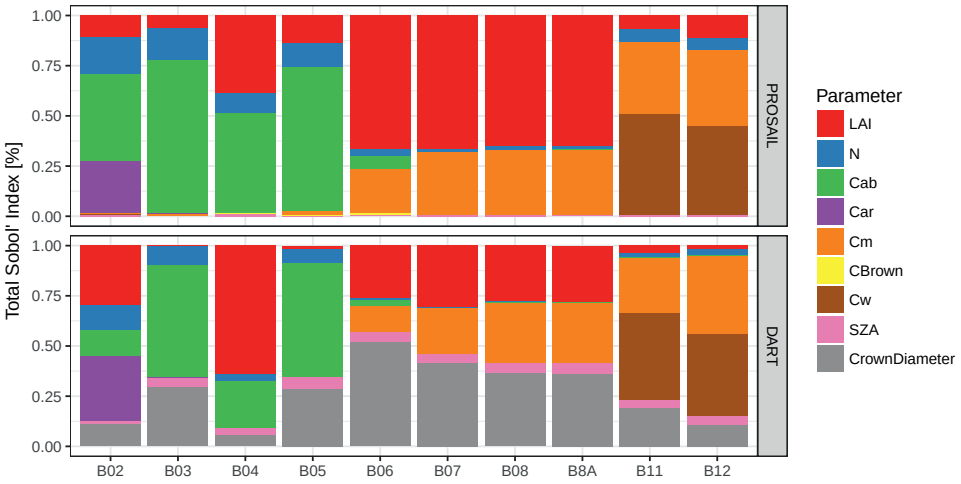

Figure 3.8: Global sensitivity of S2A MSI spectral bands to PROSAIL and DART input parameters. Total Sobol' Indices were normalised per band to sum up to 1. For band specifications see Table 3.1.

On the other hand, DART's output sensitivity was dominated by canopy structural parameters (LAI and CrownDiameter) in the NIR spectral outputs. The contribution of LAI was maximal in B04 with 64.1 %, while that of crown diameter was maximal in B06 with 52.2 %. Their combined contribution was minimal in B12 with 12.7 %. In contrast to PROSAIL, DART showed some sensitivity towards SZA, which was 5.1 % on average in bands B05 to B8A. This reflects the effect of shadowing and DART's vertical heterogeneous character.

3.4.5 Impact of Training Scheme Features on Prediction Performance

This section presents the single inversion scheme features and their role for predicting LAI. Since the RMSE results were not normal distributed, the median was calculated for all realisations that implemented the specific feature. In this way the feature's role can be evaluated. It should also be noted that per default RMSE refers to the validation error. Only in some cases the training error was evaluated, but this is always explicitly mentioned.

Table 3.3 summarises the effects of all features on the validation RMSE. The feature with the strongest influence on performance in terms of RMSE was the adding of AI noise to the RTM generated spectral outputs. Adding 5 % AI noise decreased the median RMSE from $2.32\,\mathrm{m^2\,m^{-2}}$ for no noise to $1.23\,\mathrm{m^2\,m^{-2}}$. Realisations with 5 % AI noise also achieved the overall lowest RMSE. The second-most important feature was the choice of MLRA. Here, realisations varied between RMSE of $1.95\,\mathrm{m^2\,m^{-2}}$ for MLP, and RMSE of $1.50\,\mathrm{m^2\,m^{-2}}$

Table 3.3: Validation median RMSE for training features. Per feature all realisations were summarised that implement that feature.

Feature	Realisation	Median RMSE
Leaf chemical prior	Free range	1.48
	Prior	2.09
RTM	PROSAIL	1.93
	DART	1.48
MI Noise	0 %	1.71
	5 %	1.69
	10 %	1.71
	20 %	1.65
	30 %	1.63
AI Noise	0 %	2.32
	5 %	1.23
	10 %	1.37
	20 %	1.75
SZA	Without SZA	1.69
	With SZA	1.65
MLRA	OLS	1.72
	MLP	1.95
	RT	1.57
	SVR	1.50
	KRR	1.65
	GPR	1.59

for SVR. Restraining the training database with prior information on leaf biochemical contents generally decreased prediction performance.

The following sections present the performance results of all training features in more detail and elaborate on their first order interactions, whereas typically only the strongest interaction is discussed. Interactions were investigated by comparing the respective groups of realisations that implement the features. For example, if feature A has two realisations A1 and A2, and its strongest first order interaction feature B has B1 and B2, all realisations that implement them (A1/B1, A1/B2, A2/B1, A2/B2) were compared to each other. The strongest interaction was identified as the one that varies performance in terms of validation RMSE the most after the feature under consideration.

Leaf Biochemical Prior

Figure 3.9 summarises how the leaf biochemical prior information affected the training results in terms of RMSE with violin plots. These plots have the advantage of not reducing distributions to their statistical moments as box-plots do, but to display the full distributions. This makes them particularly suitable for non-normal data, as was the case for most of the distributions here. They are basically vertical smoothed density estimate plots that are symmetric around the vertical axis. This means they become wider at values where more observations occurred. The choice for a particular RTM was identified as the strongest interaction with the leaf biochemical prior choice.

PROSAIL performance was generally more affected by introducing prior information than DART performance: median RMSE decreased from 1.90 to 1.39 $\mathrm{m^2\,m^{-2}}$ when prior information was included in the test data sets, while it increased from 1.45 to 2.37 $\mathrm{m^2\,m^{-2}}$ in case of the validation data. The former can be explained by the sensitivity of PROSAIL to biochemical parameters C_{ab}, C_m and C_w (Section 3.4.4). Using prior information effectively decreases the parameter input space that the model has to learn, thereby

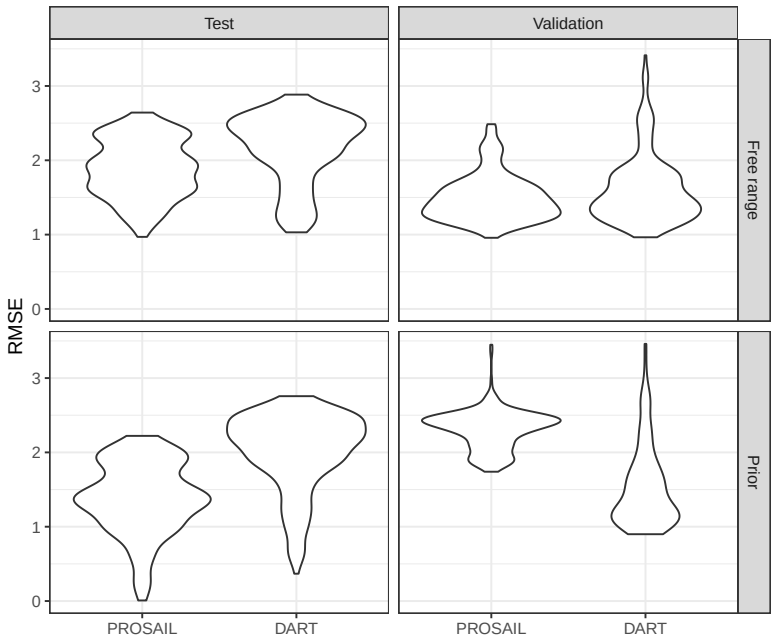

Figure 3.9: Impact of using leaf biochemical prior information on RMSE performance for DART and PROSAIL. All violin areas are scaled to be the same. In case of the validation results, 36 realisations were trimmed with RMSE larger than $3.5\,\mathrm{m^2\,m^{-2}}$, because they prevented proper display.

making it easier for the model. This also made it possible to reach testing RMSE as low as $0.01\,m^2\,m^{-2}$. However, inversion of actual observations was impaired by the constraint of the leaf chemical parameter space. This may be due to the fact that leaves were only sampled from two beech trees, while oak was also present and environmental conditions may change the chemical composition throughout the study area. Additionally, the way the constraint was implemented — as mean estimates allowing no deviation — may also play a role.

Contrary to this, the DART inversion performance was less sensitive to leaf biochemical parameters (Section 3.4.4). Median performance in terms of RMSE was similar at $2.31\,m^2\,m^{-2}$ and $2.16\,m^2\,m^{-2}$ for test data and improved slightly with a decrease in RMSE from 1.51 to 1.43 $m^2\,m^{-2}$ for the validation data set when introducing leaf chemical information. Thus, reducing the input parameter space had a small positive effect during training and validation.

RTM Choice

Among other features, Figure 3.10 compares the inverse model realisation in terms of their used RTM. Both testing error, i.e. the error based on RTM produced samples, and validation error, i.e. the error based on the validation time series for the Speulderbos site, are shown. Overall, PROSAIL and DART achieved a median RMSE of $1.64\,m^2\,m^{-2}$ and $2.19\,m^2\,m^{-2}$, while the validation RMSE was $1.93\,m^2\,m^{-2}$ and $1.48\,m^2\,m^{-2}$, respectively. The lower performance of DART on the testing samples can be explained with its additional freely varying parameter, the crown diameter. However, with this parameter came the capability to model crown gaps (Figure 3.2), which led to the better performance in terms of validation RMSE.

Apart from the overall better median RMSE of DART, using this RTM generally decreased spread of error for realisations that also implemented some AI noise larger than 0 %. The validation RMSE standard deviation for those realisation was $0.50\,m^2\,m^{-2}$ for PROSAIL and $0.33\,m^2\,m^{-2}$ for DART. In case of 5 % AI noise the difference was even larger with $0.58\,m^2\,m^{-2}$ for PROSAIL and $0.17\,m^2\,m^{-2}$ for DART. This means that choosing this combination reduced the importance for a particular choice of the other training features.

There were realisations for which the testing RMSE was larger than the validation RMSE. In fact, this was the case for 43.3 % and 77.7 % of the PROSAIL and DART cases, respectively. Under circumstances where data of the same origin would have been used, this would be unlikely to occur, especially in scenarios with added noise. However, training in this study was based on RTM output and validation on field acquired data.

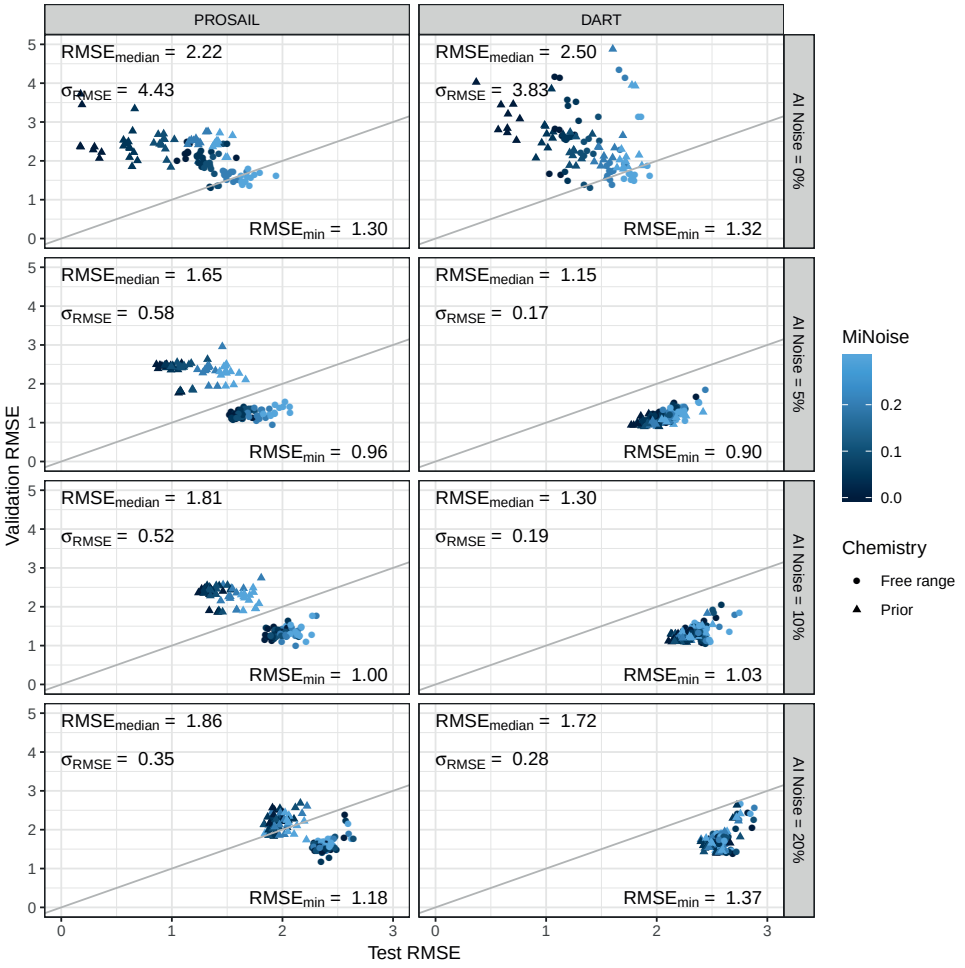

Figure 3.10: Prediction performance in terms of testing and validation RMSE in dependence of the chosen RTM, AI and MI noise level, and bio-chemical prior. $RMSE_{median}$, σ_{RMSE} and $RMSE_{min}$ refer to the validation error in the respective panel cell. Grey line is 1:1 line. In case of the validation results, 14 realisations were trimmed with RMSE larger than $10\,\mathrm{m^2\,m^{-2}}$ (all with 0 % AI noise), because they prevented proper display.

Noise Scenarios

Both the AI and MI noise had different effects on the testing and validation error. Generally testing errors increased with increasing noise. In the case of AI from $1.30\,m^2\,m^{-2}$ for 0 % to $2.46\,m^2\,m^{-2}$ median RMSE for 20 % AI noise, and in the case of MI from $1.88\,m^2\,m^{-2}$ for 0 % to $2.07\,m^2\,m^{-2}$ median RMSE for 20 % MI noise. This showed the general effect of the noise to blur the relationship between spectral output and associated LAI, and prevent the MLRA to learn the true RTM produced pattern.

However, AI noise was generally more successful at reducing validation RMSE (Table 3.3): it decreased median RMSE by $1.09\,m^2\,m^{-2}$ (from $2.32\,m^2\,m^{-2}$ for 0 % AI noise to $1.23\,m^2\,m^{-2}$ for 5 % AI noise). MI noise reduced median RMSE only by $0.08\,m^2\,m^{-2}$ (from $1.71\,m^2\,m^{-2}$ for 0 % MI noise to $1.63\,m^2\,m^{-2}$ for 20 % MI noise).

Considering AI noise alone, the addition of any in comparison to no AI noise strongly changed the distribution of realisations in terms of RMSE (Figure 3.10). This did not only include the best, but also low performing results. More precisely, AI noise prevented occurrence of very bad results. For the 0 % AI noise level worst performance reached up to $29.29\,m^2\,m^{-2}$ and the 95 % quantile lay at $10.3\,m^2\,m^{-2}$, while for 5 % these statistics were $2.96\,m^2\,m^{-2}$ and $2.47\,m^2\,m^{-2}$, respectively. Here, the added noise prevented the MLRA from over-fitting on clean RTM simulations.

Noise was also found an important training scheme element in PROSAIL-Look Up Table (LUT)-based inversions of observations from agricultural crops by Rivera et al. (2013) and Verrelst et al. (2014). They added up to 50 % and 30 % noise to PROSAIL spectra, respectively, but did not specify how the error was implemented. However, the required magnitude of noise corresponds to the MI noise in this study, which was optimal at 20 to 30 %. Baret et al. (2007) added 0.04 absolute Gaussian white (AI) noise in a global retrieval scheme based on PROSAIL. This is in line with the optimal 5 % AI noise in this study. Koetz et al. (2005) adopted a wavelength-dependent, relative noise term of maximal 10 % in the 444 nm band. Both Koetz et al. (2005) and Baret et al. (2007) based their choice for a specific noise level on experience of observation errors, but do not evaluate other possibilities.

Baret et al. (2007) argued that the quantification of the error term is difficult, as it includes errors stemming from the radiometric calibration of the sensor, Bidirectional Reflectance Distribution Function (BRDF) normalisation, atmospheric correction, cloud residuals and the RTM representativeness for the actual canopy. Additionally, the interaction of these single terms plus the properties of the used MLRA in an inversion scheme complicates the choice based on experience of errors of the sub-systems. Surely, it is more practical to conduct a sensitivity analysis over validation samples rather than characterising the sensor-inversion system in detail. Moreover, noise terms need to be defined properly to compare them across studies.

SZA

As shown in Table 3.3, realisations that made use of SZA as an extra training feature achieved overall $0.04\,m^2\,m^{-2}$ smaller median RMSE than realisations that did not include SZA. A Wilcoxon signed-rank test confirmed that the two groups differed significantly ($p < 0.01$). This difference was most prominent with the multiple MLRAs. For example, SVR benefited strongest with a decrease in median RMSE by $0.07\,m^2\,m^{-2}$. This can be explained by the richer feature space that the MLRAs had available for learning. Additionally, SZA correlated with the general phenological patterns of the study area with low SZA in summer.

Strategies to include SZA into inversion schemes of multi-temporal observations are not consolidated yet. Koetz et al. (2005) computed independent LUTs for different observation dates and consequently SZAs, but they did not investigate the error that would occur if they would not have done so. However, training separate models for multi-temporal time series with multiple observations per year is undesirable due to computational load and the checks that would be necessary to ensure consistent model properties. Campos-Taberner et al. (2016) conducted PROSAIL inversions over a full season of L8 OLI, L7 ETM+ and Satellite Pour l'Observation de la Terre (SPOT) High Resolution Geometric (HRG) sensor data and they mention solar-sensor geometry as inputs for PROSAIL, but do not elaborate how these parameters were dealt with in the training database. Baret et al. (2007) Weiss et al. (2007) included SZA as a training feature in their neural network based inversion for the VEGETATION based CYCLOPES LAI product, but again did not evaluate this strategy. However, as the CYCLOPES product has global extents, it spans several degrees of latitude, leading to different regimes of illumination dynamics over the year. Thus, SZA was given importance in past studies and showed some importance here as well, but has not been yet evaluated for global LAI products. At least adding SZA as an additional training feature is an easy implementable option. Also, SZA is efficient to compute, as only the location and observation time are needed to calculate it. However, interactions with other parameters that change over the time of the year such as soil background and LAI itself also need to be considered.

MLRA

As demonstrated in the discussion of the other training features, the choice for a specific MLRA was not the most important factor affecting validation performance in this study (Table 3.3). However, studies employing MLRA typically compare various algorithms e.g. Campos-Taberner et al., 2016; Verrelst et al., 2012. Figure 3.11 gives an overview over all realisations grouped by their used MLRA. The MLRAs reached best (and median) RMSE of 1.03 (1.72), 0.90 (1.57), 0.90 (1.95), 0.96 (1.50), 0.92 (1.65) and 0.91 (1.59) $m^2\,m^{-2}$ in case of OLS, RT, MLP, SVR, KRR and GPR, respectively. Hence, even though RT and MLP produced the best, SVR produced the overall best realisations. Maximum

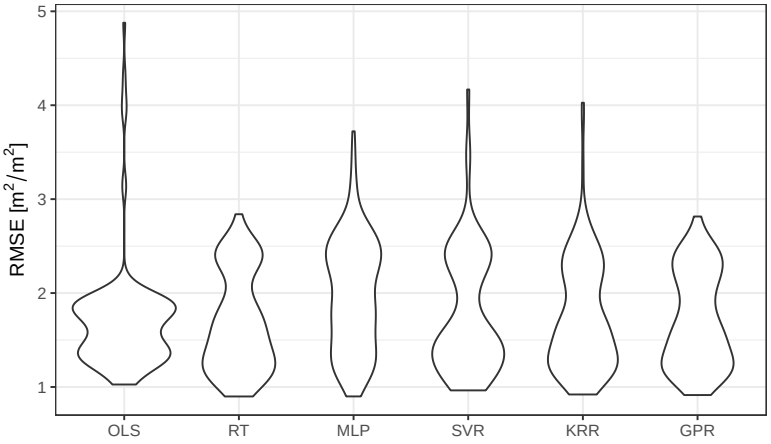

Figure 3.11: Violin plots of prediction performance for the different MLRAs. It should be noted that 24 realisations were trimmed with RMSE larger than $5.0\,\mathrm{m^2\,m^{-2}}$ (17 for OLS and 7 for KRR), because they prevented proper display.

differences among the MLRAs in median RMSE of $0.45\,\mathrm{m^2\,m^{-2}}$ were found between SVR and MLP realisations. There were also 17 realisations using OLS and 7 using KRR that exceeded RMSE of $5\,\mathrm{m^2\,m^{-2}}$, all of which were training without noise applied to the training spectral features.

Apart from the MLRA validation, performance processing time is an important property especially for routine and large scale production. The time required for the training of the described realisations in this study was on average 0.03 s, 7.18 s, 2.29 s, 3.17 s, 125.37 s and 123.81 s for the OLS, RT, MLP, SVR, KRR and GPR, respectively. This is in contrast to Verrelst et al. (2012) who found KRR and GPR required around the tenth of the time of a neural network or an SVR. However, their models were implemented with Matlab, while this study used R. Additionally, the implementations of RT, SVR, KRR and GPR in this study could make use of parallelisation. Concerning time required for prediction of 10 000 random samples the models needed 0.08 s, 0.09 s, 0.09 s, 0.15 s, 0.30 s and 0.19 s in the case of OLS, RT, MLP, SVR, KRR and GPR, respectively. Hence, implementation details and optimisation can play a significant role in processing time.

3.4.6 Best Performing Feature Combination

Figure 3.12 shows the best performing realisation that reached RMSE of $0.90\,\mathrm{m^2\,m^{-2}}$. It was built with a RT based on a DART produced database restricted with prior information from the leaf sampling, 5 % AI and 5 % MI noise, and without SZA as additional training feature. Maximum LAI of $5.68\,\mathrm{m^2\,m^{-2}}$ was reached in plot A on July 17. LAI before May 1 was on average $(0.16 \pm 0.34)\,\mathrm{m^2\,m^{-2}}$, and thereafter $(4.63 \pm 0.63)\,\mathrm{m^2\,m^{-2}}$ until

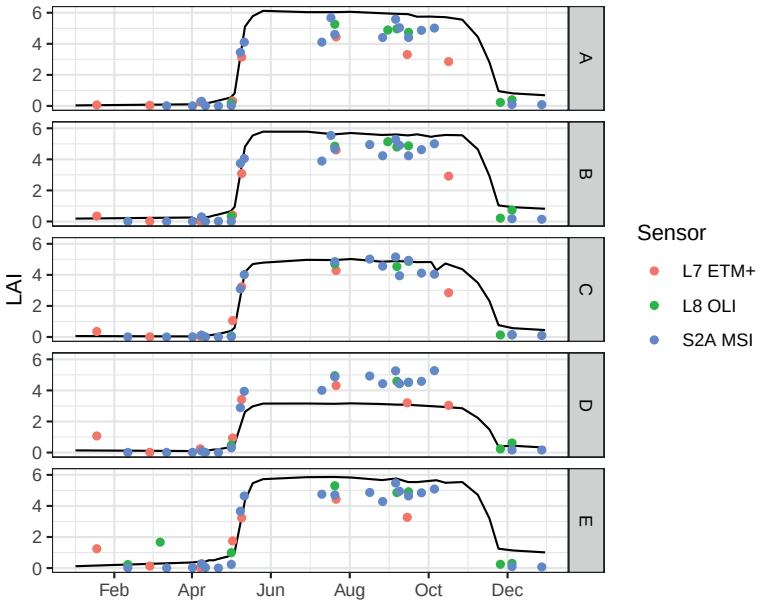

Figure 3.12: Best performing realisation in terms of RMSE over the 2016 study period. Black solid line is the validation time series.

end of October. The predicted LAI explained 86.3 % of variation of the reference time series.

In general these results for a single time series are in the range of previously published results. Schlerf and Atzberger (2006) achieved $0.66\,\mathrm{m^2\,m^{-2}}$ with a two-band combination chosen from simulated Landsat TM bands over a Norway Spruce site. For beech canopies within the same site Schlerf and Atzberger (2012) report $2.12\,\mathrm{m^2\,m^{-2}}$ RMSE with a multi-spectral, near-nadir viewing set-up. Both studies used the INFORM RTM to create the training database (Atzberger, 2000).

However, as can be observed in Figure 3.12, the predictions showed different biases for the single plots. In fact, summer LAI was underestimated on average by $1.07\,\mathrm{m^2\,m^{-2}}$ in plots A, B and E, and overestimated by $1.38\,\mathrm{m^2\,m^{-2}}$ in plot D. The bias in plot D could result from the structure of the plot, which consisted of more young trees compared to the other plots. The position of the litter traps was chosen close to the TLS scan positions, which were possibly not representative for the whole of the plot. Additionally, RMSE as the choice of error metric during retrieval evaluation does not allow the assessment of bias. In fact, additional error metrics would be needed to characterise the bias as well as temporal consistency of the time series.

3.5 Conclusions

The Sentinel-2 mission provides a new science-grade data stream for monitoring of dynamic vegetation behaviour. Together with other missions like Landsat 7, 8 and future Landsat 9 a characterisation of temporal dynamics in biophysical parameters becomes possible at decametric resolution. Accurate retrieval and a universal processing work-flow for potential Sentinel-2 and Landsat harmonised biophysical products remains a challenge. Previous studies identified MLRAs combined with RTMs in hybrid retrieval schemes as a potential solution. This study investigated the impact of multiple properties of such schemes on the retrieval performance for LAI over a Dutch beech forest site.

Addition of AI noise on the RTM spectral database was found to be most important for prediction performance with a difference of $1.09\,\mathrm{m^2\,m^{-2}}$ in median RMSE compared to no noise. A level of 5 % was optimal in this study. On the other hand, MI noise showed less improvements. Added noise helps the MLRAs to generalise and prevent over-fitting on the pure RTM output. Previous studies did not investigate the effect of different noise definitions and some did not report precisely how noise was defined. With respect to its importance, a clear definition and careful sensitivity analysis should be paramount for future studies.

The choice for the heterogeneous DART RTM in comparison with the turbid medium PROSAIL model resulted in a median RMSE difference of $0.45\,\mathrm{m^2\,m^{-2}}$. An additional advantage of DART in this study was the lower spread of performance of other inversion scheme features, i.e. DART led to more consistent inversion schemes. The choice of a specific MLRA was found to be less critical in terms of prediction performance. However, MLRAs varied significantly in run-time, also depending on the implementation and code optimisation. When choosing a particular MLRA these secondary benefits should be weighted together with the expected accuracy.

Chapter 4

Comparing RIEGL RiCOPTER UAV LiDAR Derived Canopy Height and DBH with Terrestrial LiDAR

This chapter is based on:

B. Brede, A. Lau, H. M. Bartholomeus, and L. Kooistra (2017). "Comparing RIEGL RiCOPTER UAV LiDAR Derived Canopy Height and DBH with Terrestrial LiDAR". *Sensors* 17.10, 2371. DOI: 10.3390/s17102371

Supplementary materials to this chapter can be found in the online publication.

Abstract

In recent years, LIght Detection And Ranging (LiDAR) and especially Terrestrial Laser Scanning (TLS) systems have shown the potential to revolutionise forest structural characterisation by providing unprecedented 3D data. However, manned Airborne Laser Scanning (ALS) requires costly campaigns and produces relatively low point density, while TLS is labour intense and time demanding. Unmanned Aerial Vehicle Laser Scanning (UAV-LS) can be the way in between. In this study, we present first results and experiences with the RIEGL RiCOPTER with VUX®-1UAV UAV-LS system and compare it with the well tested RIEGL VZ-400 TLS system. We scanned the same forest plots with both systems over the course of two days. We derived Digital Terrain Models (DTMs), Digital Surface Models (DSMs) and finally Canopy Height Models (CHMs) from the resulting point clouds. UAV-LS CHMs were on average 11.5 cm higher in five plots with different canopy conditions. This showed that TLS could not always detect the top of canopy. Moreover, we extracted trunk segments of 58 trees for UAV-LS and TLS simultaneously, of which 39 could be used to model Diameter at Breast Height (DBH). UAV-LS DBH showed a high agreement with TLS DBH with a correlation coefficient of 0.98 and Root Mean Square Error (RMSE) of 4.24 cm. We conclude that RiCOPTER has the potential to perform comparable to TLS for estimating forest canopy height and DBH under the studied forest conditions. Further research should be directed to testing Unmanned Aerial Vehicle (UAV)-borne LiDAR for explicit 3D modelling of whole trees to estimate tree volume and subsequently Above-Ground Biomass (AGB).

4.1 Introduction

LiDAR has become a valuable source of information to assess vegetation canopy structure. This is especially true for complex forest canopies that limit manual and destructive sampling. These capabilities are investigated to replace traditional forest plot inventories (Liang et al., 2016), but even more if they can deliver additional information that is not captured with traditional inventories (Newnham et al., 2015). One particular important variable in this context is AGB which makes up an essential part of the forest carbon pool. TLS has the potential to accurately measure AGB on a plot scale (Calders et al., 2015b; Gonzalez de Tanago et al., 2018), while ALS from manned aircraft can serve as means to up-scale plot measurements to the landscape level. This is particularly interesting for calibration and validation activities of space-borne missions aiming at AGB assessment like ESA's BIOMASS (Le Toan et al., 2011) and NASA's GEDI (`https://science.nasa.gov/missions/gedi`) missions. Another important derivative of LiDAR point clouds is vertical forest canopy structure, which is linked to biodiversity (Eitel et al., 2016; Wallis et al., 2016).

ALS is typically acquired from manned aircraft, thereby covering large areas, but requiring substantial financial capital and available infrastructure. Acquisition density is typically in the order of 1 to 10 points/m^2, depending on flight altitude and scanner configuration. A straight-forward application for ALS point clouds is the generation of DTMs and DSMs, and derivation of canopy height by considering the difference between those two. More advanced products take into account the waveform of the returning pulses and reconstruct canopy attributes from that (Morsdorf et al., 2009). However, the relatively low density of ALS point clouds forces to approach actual canopy structure from a statistical point of view where each resolution cell contains a sample of the population of possible returns. In this respect, ALS products can be treated as 2.5D raster layers.

On the other hand, TLS produces point clouds with such a density—millions of points per scan position—that single canopy elements like stems and branches can be resolved. Geometrical models serve to reconstruct the 3D tree architecture, and allow estimation of wood volume and derivation of AGB (Calders et al., 2015b; Hackenberg et al., 2014; Raumonen et al., 2013) and other stand characteristics. A hard requirement for this approach is accurate co-registration of several point clouds acquired from different scan positions in the forest, which leads to time demanding field campaigns, mostly in the order of 3 to 6 days/ha (Wilkes et al., 2017). Therefore, it is questionable if TLS in its current form will replace operational plot inventories, or rather supply higher quality information for selected samples (Newnham et al., 2015).

Independent from the developments of LiDAR instruments, UAVs have found use as platforms for various types of sensors in forestry and many other fields (Colomina and Molina, 2014; Torresan et al., 2016). Especially the introduction of affordable, ready-to-use

systems on the consumer market has been boosting applications and widened the user community. Even consumer-grade RGB cameras in combination with dedicated software packages can serve for the production of high-resolution orthomosaics and surface models derived with Structure from Motion (SfM) techniques. More sophisticated prototype sensors also allow the production of hyperspectral images (Suomalainen et al., 2014). One of the most favourable aspects of UAVs as sensor platforms is their low demand in infrastructure, high mapping speed and price advantage compared to manned aircraft. The implementation of legal regulations for professional UAV users remains a hot topic however (Colomina and Molina, 2014).

Recently, LiDAR sensors have been mounted on UAVs to combine the advantages of LiDAR and UAV technology. A variety of custom build systems with different degrees of off-the-shelf components were tested to derive forest inventory metrics. Jaakkola et al. (2010) probably build the first UAV LiDAR system, the Finish Geodetic Institute (FGI) Sensei, integrating an Ibeo Lux and Sick LMS151 profile scanner. During test flights the Sensei produced point clouds with 100 to 1500 points/m^2 and could be successfully used to detect single trees. Another custom build system based on the Ibeo Lux scanner was presented by Wallace et al. (2012). During tests it produced point clouds with up to 50 points/m^2, but with a relatively low airborne time of 3 to 5 min owed to the capacity of the UAV. This same system was employed to conduct surveys of forest plots, and terrain and under-storey height, tree location, tree height, crown area and volume could be derived (Wallace et al., 2014b). Chisholm et al. (2013) constructed another light-weight LiDAR UAV system that did not require any means of positioning or orientation system, but rather used pattern-matching algorithms to produce a point cloud. However, due to assumptions in the processing the system and the low range of the laser scanner of 30 m had to be flown below canopy. They could successfully estimate DBH for their open grove study site. Wei et al. (2017) employed the commercially available HawkScan1200, consisting of a VUX®-1LR scanner and Applanix AP20 Inertial Measurement Unit (IMU), and mapped a 60 km^2 area with a point density of 0.5 points/m^2 to perform vegetation filtering and DTM generation on the resulting point cloud.

Overall, these systems showcase that principal technological challenges such as component miniaturisation and suitable post-processing have been overcome in the recent years. Important forest inventory metrics like tree height, location and DBH could be derived. Nonetheless, custom-build systems have not yet achieved point density counts in same the order of magnitude as TLS. This would open up opportunities that are at the forefront of LiDAR research in forestry, such as explicit structural modelling to precisely estimate AGB (Calders et al., 2015b; Raumonen et al., 2013). Moreover, even though custom build systems are low cost, at the same time they are typically not easily available for use by a wider audience.

The aim of this paper is to present the commercially available RIEGL RiCOPTER system and the work flow to process the acquired data. In a field experiment we concurrently collected RiCOPTER and TLS data in a forest site containing different canopy architectures. We compared the two point clouds in respect to their point distributions, different elevation models derived from both point clouds and estimates of DBH. With this comparison we want to test if the RiCOPTER performs comparable to TLS field acquisition.

4.2 RIEGL RiCOPTER with VUX®-1UAV

4.2.1 System Specifications

The RIEGL RiCOPTER with VUX®-1UAV (RIEGL Laser Measurement Systems GmbH, Horn, Austria) is an integrated UAV and sensor system. The RiCOPTER is a battery-driven octocopter with an empty weight (no batteries and equipment) of 9 kg that can carry a payload of up to 8 kg. For safety reasons it has two flight controller units. In case of system failure of the main controller, the backup takes over immediately. Together with the VUX®-1UAV scanner (3.75 kg), the system controller (0.9 kg), the IMU (0.7 kg) and optional cameras the total system weights just under 25 kg; hence, it is possible to operate it under light UAV regulations in many European countries (Torresan et al., 2016). The batteries allow flight times of up to 30 min at 30 km h^{-1} maximum cruise speed. This allows flying multiple overlapping flight lines to increase target coverage. However, during mapping of forest plots flight time and speed need to be reduced to guarantee flight safety and adequate point density.

The VUX®-1UAV is a survey-grade laser scanner that is mounted underneath the RiCOPTER. It uses a rotating mirror with a rotation axis in flight direction to direct the laser pulses and achieve an across-track Field Of View (FOV) of 330° perpendicular to the flight direction. This means that lateral flight line overlap is only restricted by the maximum operating range of the laser. Overall its attributes are comparable to the terrestrial VZ-400 despite its lower weight (Table 4.1). It should be noted that both operate at a wavelength of 1550 nm, which makes them eye-safe and sensitive to the same types of canopy elements. An Applanix AP20 IMU attached to the VUX®-1UAV and Global Navigation Satellite System (GNSS) antennas on top of the RiCOPTER record flight orientation and GNSS data. Apart from these devices and sensors essential for processing, two consumer-grade Sony Alpha-6000 system cameras can be mounted on the VUX®-1UAV. During later processing the point clouds can be overlaid with the RGB colour information from these cameras. The on-board instrument controller manages all sensors' data streams and includes a 220 GB SSD storage, which is sufficient for several missions.

Next to the RiCOPTER system a ground station is necessary for mission planning and in-flight coordination. Planar or spherical Ground Control Points (GCPs) should be set

Table 4.1: VZ-400 and VUX®-1UAV main characteristics.

Characteristic	VZ-400 [1]	VUX-1UAV [2]
Maximum Pulse Repition Rate (PRR) (kHz)	300	550
Maximum effective measurement rate (kHz)	120	500
Minimum—Maximum range (m)	1.5—350 [3]	3—920 [4]
Accuracy—Precision (mm)	5—3	10—5
Laser wavelength (nm)	1550	1550
Beam divergence (mrad)	0.3	0.5
Weight (kg) [5]	9.6	3.75

[1] high speed mode, incl. online waveform processing; [2] 550 kHz mode; [3] at target $\rho \geq 0.9$; [4] at target $\rho \geq 0.6$; [5] without battery and tilt mount.

out in the field before flight to support co-registration during processing. These targets do not necessarily need to be geolocated in case only internal point cloud registration is to be optimised. However, they should have an adequate size of >0.5 m—depending on flight altitude and scanning speed—to be properly covered. In case sufficient planar surfaces are available in the study area, these can also be used. However, this is typically not the case for forest plots.

4.2.2 Operations

Necessary legal requirements for professional operations are similar to other UAV operations and mainly involve RiCOPTER registration as an aircraft in the country of operations as well as the training and licensing of the pilot. Both processes can partly run in parallel and can take up to several months. Additional to regular licensing the pilot should also become familiar with the flight behaviour of the RiCOPTER, since it is considerably larger than typical mini-UAV. Also the proper operation of the two independent flight controllers needs to be trained. Moreover, operation in forest areas usually requires take off and landing in canopy openings with restricted viewing conditions and options to manoeuvre. Another general preparation includes the identification of a source of base station data that is necessary for processing the acquired data. Additionally, legal requirements for the transportation of the batteries need to be investigated.

Once these general prerequisites are fulfilled, practical mission planning can begin. This mainly involves getting access permissions to the study site especially from the landowner, arranging transport and notifying other airspace users. Furthermore, the weather forecast should be studied with respect to wind, visibility and humidity to identify the best suitable days for mission execution. As for other mini-UAV the RiCOPTER has a legal limit on wind speed up to which take off is allowed, which is $7\,\mathrm{m\,s^{-1}}$ for the Netherlands. However, wind limits are typically stricter in respect to data quality as crown movement hampers

proper co-registration of point clouds from different flight lines, as is also the case for TLS (Wilkes et al., 2017).

Initial flight path planning should be performed in preparation of the field work. The target is a certain point density to be achieved by varying flying speed and altitude, and overlap of flight lines. Nonetheless, not anticipated on-site conditions like single emerging trees or lack of emergency landing locations can demand modification. Transport to the site should take into account the size and weight of the equipment. The RiCOPTER itself is delivered with a transport case of ∼120 cm × 80 cm × 55 cm. The ground station has dimensions ∼55 cm × 45 cm × 20 cm. At the study site, the area should be inspected to identify take-off and landing as well as emergency landing locations, obstacles close the intended flight path and positions for GCPs. After completion the equipment can be set up and the mission executed. After the mission, the raw data is downloaded from the instrument controller.

4.2.3 Data Processing

RIEGL provides a software suite together with the RiCOPTER system to convert the produced raw data into point clouds. Figure 4.1 gives an overview of the required steps. While most of the work can be done in RIEGL's software for airborne and mobile laser scanning, RiPROCESS, the trajectory preprocessing has to be accomplished with third party software, e.g. Applanix POSPac Mobile Mapping Suite. For this purpose additional GNSS base station data has to be acquired. During GNSS post-processing both data streams from the GNSS antennas and the IMU are taken into account to reconstruct the flight trajectory.

For each flown and logged scan line, the raw scan data has to be subjected to waveform analysis during which targets are detected within the stored flight line waveforms. Up to four targets can be detected per pulse. During this process, Multiple Time Around (MTA) range ambiguities have to be taken care of. MTA range ambiguity occurs when pulses are fired before their predecessor pulses can return. MTA 1 range, where no ambiguity can occur because a pulse always returns before the next is fired, is at around 100 m range for a Pulse Repition Rate (PRR) of 550 Hz. Thus MTA range ambiguity needs to be taken care of, but does not result in serious obstacles assuming flying heights below 120 m. The waveform processing detects targets in the scanners own coordinate system. Next, this data is interpreted with help of the trajectory information and the scanner mounting orientation to produce the first point clouds, one per flight line. The within and across flight line registration is already of high quality as experienced by the authors during several missions and would serve when registration error of below 1 m is not an issue.

However, when sub-centimetre accuracy is required, point clouds need to be fine registered. In principal this means to reduce errors in the flight trajectory as the position and orientation error of the RiCOPTER system (cm scale) is much bigger than the range error

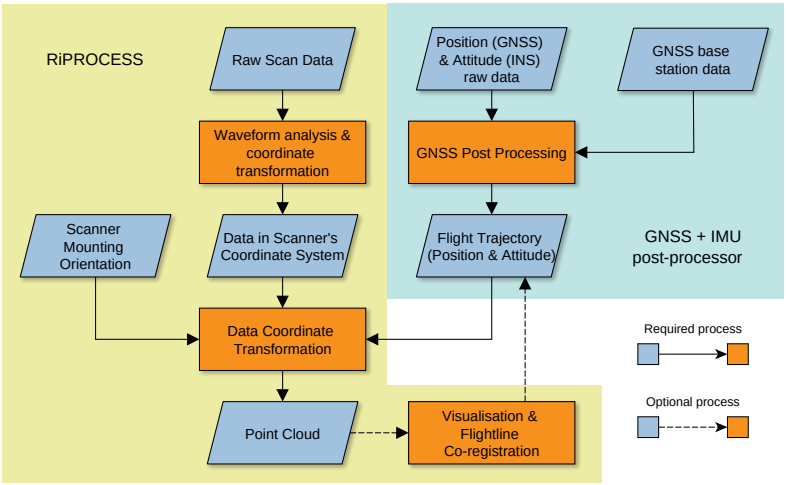

Figure 4.1: RiCOPTER processing flowchart (based on RIEGL LMS GmbH (2017)).

of the scanner (mm scale). This process can include two independent steps. One is the within flight line trajectory optimisation that is handled by the RiPRECISION package within RiPROCESS. Similar to Multi-Station Adjustment (MSA) for TLS (Wilkes et al., 2017) control planes are automatically searched for in the point clouds per flight line. So far this process demands no user interaction. It can be supported by GCPs that have been independently located to within millimetres, e.g. with Real Time Kinematic (RTK) GNSS. However, for forest situations this is impractical as GNSS reception is typically too low under closed canopies to achieve the required accuracy. The other possible optimisation is across flight line optimisation that can be performed with the Scan Data Adjustment (SDA) package within RiPROCESS. It assumes within flight line registration as optimal and only changes the overall position and orientation of flight lines to each other. This can be compared to linking point clouds from single scanning positions in TLS. Here, next to automatically detected planes, also manually digitised control objects, such as planes, spheres and points, can be included to improve the co-registration.

The point cloud processing can be finished off with removal of atmospheric noise, which is visible as returns close to the flight trajectory with typically low reflectivity, and target type classification. Finished point clouds can be exported from RiPROCESS in common file formats, e.g. ASCII and LAS, to continue analysis in dedicated software packages.

4.3 Field Experiment

The field experiment took place at the Speulderbos Fiducial Reference site in the Veluwe forest area (N52°15.15′ E5°42.00′), The Netherlands (Brede et al., 2016) (`www.wur.eu/`

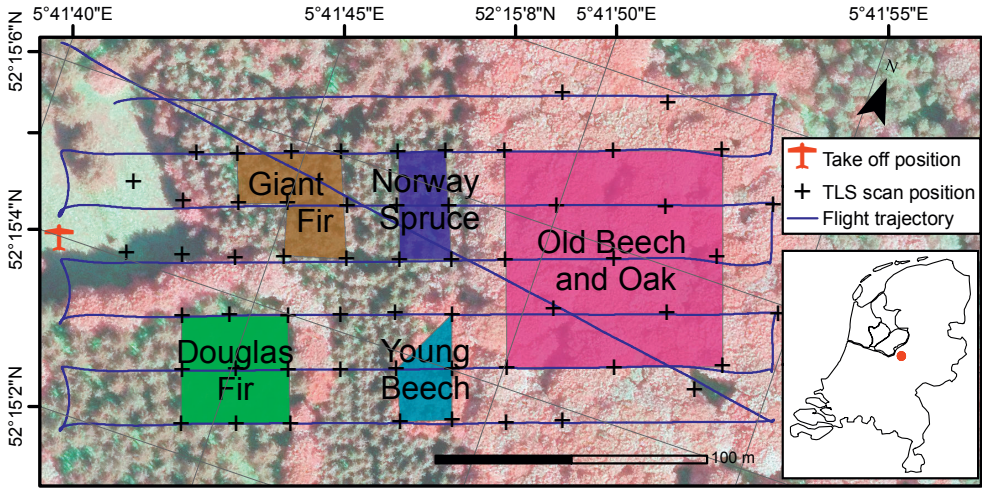

Figure 4.2: Map of the study site with TLS scan positions (crosses), take off position (red plane), flight lines (blue), target areas, study site location in the Netherlands (red dot in inset), airborne false colour composite as background image.

`fbprv`). The core site is established in a stand composed of European Beech (*Fagus sylvatica*) with occasional Pedunculate Oak (*Quercus robur*) and Sessile Oak (*Quercus petraea*), and a very open understorey with only few European Holly (*Ilex aquifolium*) (Figure 4.2). The stand was established in 1835 and had a tree density of 204 trees/ha. At the time of the experiment the overstorey was in the progress of spring bud break and leaf unfolding, so that only few trees carried a full leaf canopy. In an earlier inventory campaign the Beech stand has been equipped with a 40 m spaced wooden pole grid that has also been geo-located with RTK GPS and land surveying techniques to an accuracy of better than 0.5 m.

Additional to the Beech stand, sections of Norway Spruce (*Picea abies*), Giant Fir (*Abies grandis*), young beech and Douglas Fir (*Pseudotsuga menziesii*) have been scanned as well with the goal to capture different forest types in terms of species composition, tree density and canopy architecture. The Norway Spruce and Giant Fir stands were established in 1943 and 1967, respectively, and had no understorey species. However, the plots were relatively dense with 676 Trees/ha and 961 Trees/ha, respectively, and many low branches. The young beech stand was established in 1973 and had a density of 805 Trees/ha. There were no other species present in this stand, but most lower branches were carrying leaves. The Douglas Fir stand had a very open understorey where only few saplings of up to 2 m height could be found. The stand was established in 1959 and has been thinned since then as was obvious through the present stumps.

The total scanned area covered 100 m × 180 m, roughly 2 ha. In the study area, a forest road separates the old beech and oak from the other stands, and a bike path the Giant Fir and Norway Spruce stands. The UAV take-off area was located in an opening east of the stands that was wide enough to allow Visual Line of Sight (VLOS) operations.

TLS data acquisition was completed in the course of two days that were both marked by very low wind speeds ($<3\,m\,s^{-1}$). During the first day the TLS scan position grid was set up. For that the wooden poles in the Beech stand were taken as starting positions. With the help of a theodolite the TLS positions were marked to form a grid of 40 m spacing in the Beech and 20 m spacing in the Douglas Fir stands. Additional positions in the grid centres have been added in the Beech stand. Cylindrical retro-reflective targets were set up for later coarse co-registration of scans (Wilkes et al., 2017). The first 15 positions have been scanned during the first day, the remaining 43 during the second day. All scans were performed with 0.06° scan resolution. Due to the VZ-400's zenithal scan angle range of 30° to 130°, an upward and tilted scan had to be performed per scan location to cover the area directly over the scan position.

To support co-registration of RiCOPTER flight lines 4 large (120 cm × 60 cm) and 8 small (60 cm × 60 cm) ground control panels have been distributed under the trees and next to the take-off site. The panels consist each of 2 equally sized wooden panes connected via piano hinges. When set up the panes form a 90° angle between them, which makes them look like tents. Cars used for transport were deliberately parked on the forest road in the scanning area to provide additional control surfaces for the co-registration. The ground station was erected next to the take off site. The scan lines were designed to maximise lateral overlap and efficiently use air time (Figure 4.2). The RiCOPTER was flown at an altitude of 90 m a.g.l., with a cruise speed of $6\,m\,s^{-1}$. The VUX®-1UAV was operated with the full FOV of 330°, a PRR of 550 kHz and scan speed of 58 lines/s, which resulted in an average rectangular point spacing of ∼8 cm and a point density of 140 points/m^2 for a single flight line at nadir. Mission time for active scan and non-active connection lines was 9 min to cover a distance of ∼2300 m.

4.4 Methods

In case of TLS, the scans were first coarsely co-registered with automatically extracted tie-points based on the retro-reflective cylinders. These registrations had typical registration errors of <5 cm. Afterwards MSA was applied to refine the registration (Wilkes et al., 2017). This approach automatically searches for tie-planes in the scans and iteratively adjusts orientation and position of each scan position to minimise the global fitting error of tie-planes. The resulting standard deviation of the errors over all tie-planes was 0.62 cm. All operations were executed with RIEGL's RiSCAN PRO® software package.

For processing of the RiCOPTER data the work-flow as described in Section 4.2.3 was applied. GNSS data was obtained from 06-GPS (Sliedrecht, The Netherlands) for a virtual base station in the centre of the study site and the period of the campaign to allow GNSS post-processing. RiPRECSION-UAV was applied to optimise within flight line registration. Automatic across-flight line registration with automatic search of tie-planes continuously failed to produce good results, probably due to missing planar surfaces in the study area. Therefore, the GCP panels were manually digitised as tie-planes and used for fine registration. Final standard deviation of the fitting errors of 0.97 cm.

The resulting point clouds from TLS and UAV-LS were co-registered via common tie-planes. These were the manually selected GCP panels. Then different raster products were produced at 0.5 m resolution with LAStools (`https://rapidlasso.com/lastools/`): scan density by counting all hits within a resolution cell, DTMs by selecting the lowest point in a resolution cell, DSMs with the highest, and CHMs by calculating the difference between DTMs and DSMs.

The lower stem parts of individual trees were manually extracted from the TLS and UAV-LS point clouds from the 5 plots (Figure 4.2). For each tree all points at a height of 120 to 140 cm were selected to represent DBH. These subsets were manually inspected for the suitability to fit circles. In case of presence of branches at the DBH height, the corresponding points were further manually removed. Next, circles were fitted to the horizontal coordinates of these points separately for UAV-LS and TLS. An iterative optimisation procedure was used to minimise the euclidean distance between points and circles according to Coope (Coope, 1993) as implemented in R's (`http://www.r-project.org/`) `circular` package. Next to the geometries, the points contained information about the return number and scan angle under which they were recorded. These were analysed to gain more insights which scan conditions can be beneficial to record stem points.

4.5 Results

The acquired TLS and UAV-LS point clouds showed a number of differences. Figure 4.3 shows two sample transects through the Old Beech and Oak area (cf. Figure 4.2). The UAV-LS point cloud clearly had a lower point density in the stem area, while the branch and leaf area appeared to be of comparable density. Nonetheless, single stems as well as larger branches could be made out. It should be noted that even though the images suggest the trees to have a full canopy, this was not the case during the time of acquisition. The canopy level rather has a distinctively different apparent reflectance than stem and ground elements, because partial hits are much more likely in the crown area where branches do not completely fill the laser footprint.

Figure 4.4 gives an overview of point density over the whole of the study site. While UAV-LS point density was highest in tree crowns, visible as mushroom forms in the Old

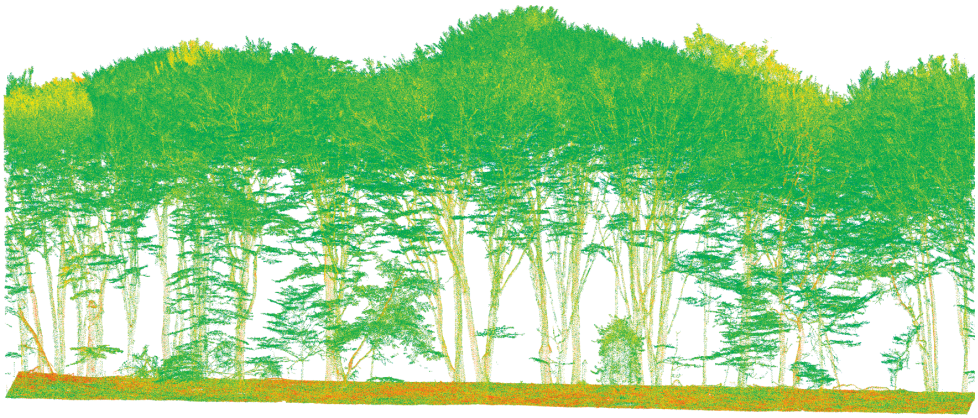

(**a**) ALS

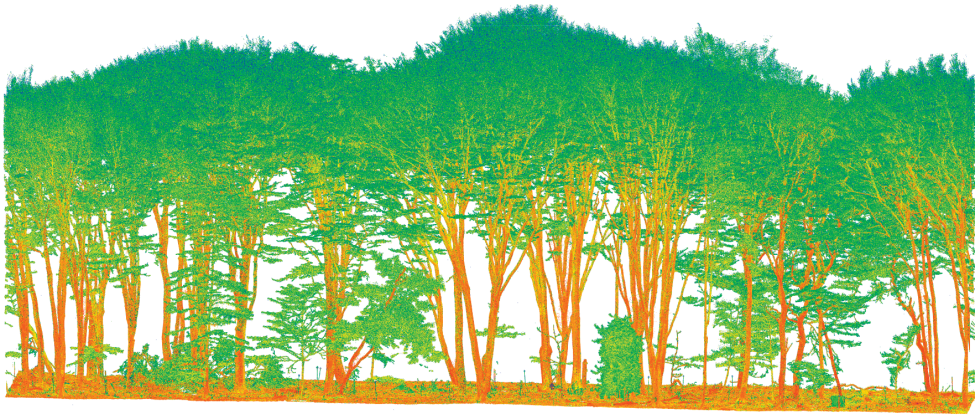

(**b**) TLS

Figure 4.3: Old Beech and Oak point clouds samples from same perspective, coloured according to apparent reflectance (blue = low, green = medium, red high).

Beech and Oak area, TLS point density peaked at stem locations, visible as black specks in the TLS map. Furthermore, higher density areas were created by slight horizontal course corrections of the UAV, which are visible as stripe patterns in the density map, especially in the forest opening in the Northwest. Also more points were observed along the centre line of the plot in WE direction due to the higher overlap of flight lines in that area, i.e. northern and southern flight lines contribute to the centre locations. This can be seen when comparing Beech areas close to WE centre line and Beech in upper right of Figure 4.4, around [160,60] and [210,110], respectively. In case of TLS fewer points were registered around scan positions, which stems from the restriction in zenithal scanning angle of the VZ-400 scanner. Overall, UAV-LS point density was about 2

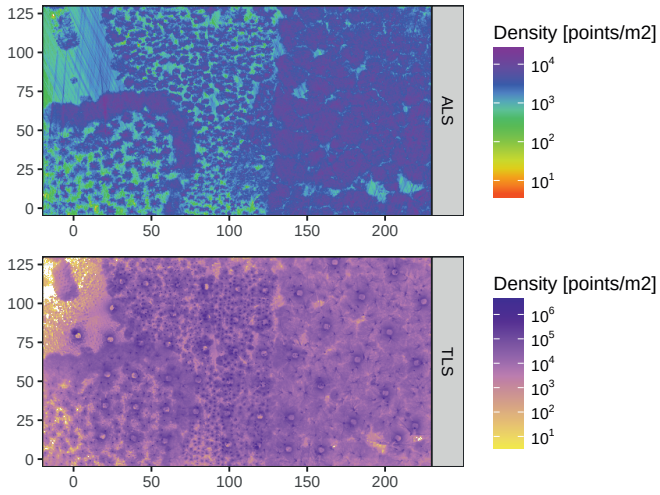

Figure 4.4: ALS and TLS point cloud density maps for whole study site at 0.5 m resolution in project coordinate system.

orders of magnitude lower than TLS for the given scan configurations. It was on average 5344 points/m^2, 3081 points/m^2, 3005 points/m^2, 2965 points/m^2 and 3004 points/m^2 for the Old Beech and Oak, Giant Fir, Norway Spruce, Young Beech, and Douglas Fir plots, respectively.

Figure 4.5 shows vertical return profiles of two focus areas representing different canopy architectures. While the Old Beech and Oak canopy had higher trees of up to 35 m with only few branches on the lower levels, the Norway Spruce canopy had trees up to 30 m and a considerable higher number of small, horizontally oriented branches below the crown level. The distribution of UAV-LS and TLS points was similar for both canopies, but UAV-LS hit relatively more often the upper canopy levels. This is clearly the effect of perspective of the UAV-LS from above and TLS from below the canopy. Considering the distribution of return order in the upper canopy, the Old Beech and Oak canopy showed many more higher order returns than the Norway Spruce canopy. This could be explained by the foliage coverage of the Norway Spruce: while the water in the green needles allowed first order returns, it absorbed too much of the pulse energy to allow higher order return from within the clumped shoots. On the other hand, the not fully developed Old Beech and Oak canopy allowed partially intercepted beams and therefore multiple returns.

Despite the perspective of the UAV-LS above the canopy, it hit the ground level in similar proportions as the TLS relative to all returns. This was clearly possible due to the multi-return capabilities of the VUX®-1UAV scanner. Returns up to 7$^{\text{th}}$ order could be recorded over the whole study area. This is in contrast to the TLS that is dominated

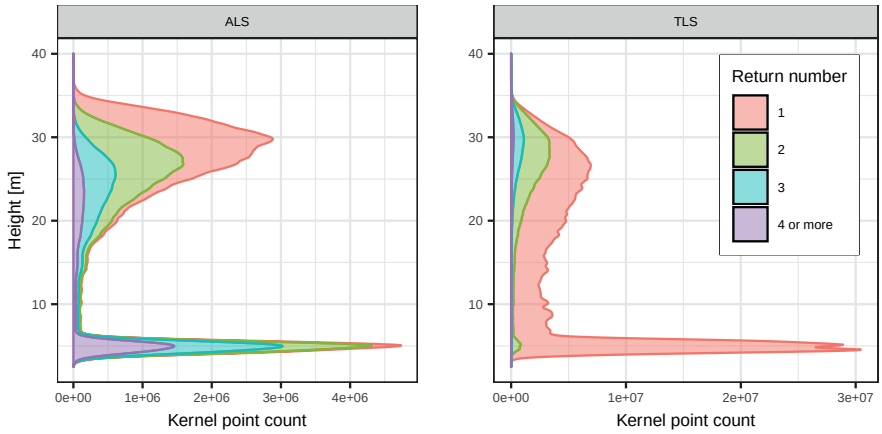

(**a**) Old Beech and Oak

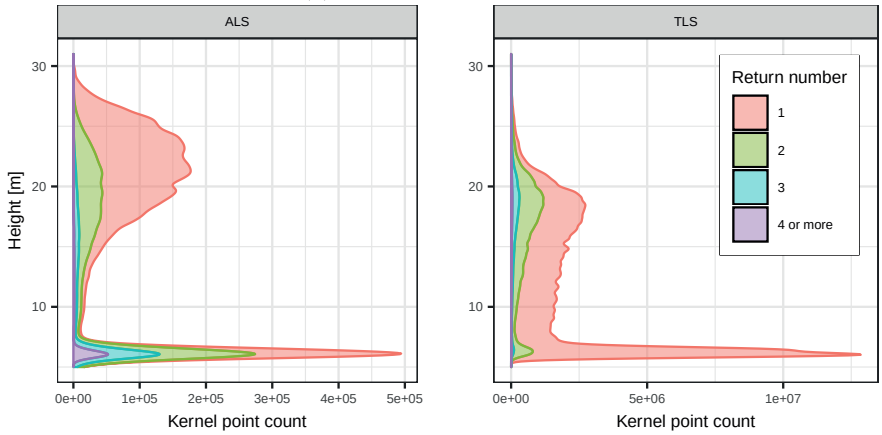

(**b**) Norway Spruce

Figure 4.5: Vertical return density profiles smoothed with Gaussian kernel of all points in two areas of interest (see Figure 4.2), height reference is lowest point found in sub-area.

by 1st order returns, which results from a higher proportion of hard targets like wood and ground elements. The ground returns were spread over some range of heights due to slightly sloped terrain and ground features like dead trees and hollows.

Figure 4.6 shows the CHM difference map. The underlying DTM, DSM and CHM maps can be found in the supplementary material. General agreement between both maps was very high with a dominance of small offsets of $\pm 0.5\,\mathrm{m}$. However, an overall pattern can be observed similar to relieve shading resulting in positive differences in eastern and negative in western directions The pattern is not regular over the whole study area. For instance, it is strong over the Douglas Fir plot in the south-west and less pronounced over the Old

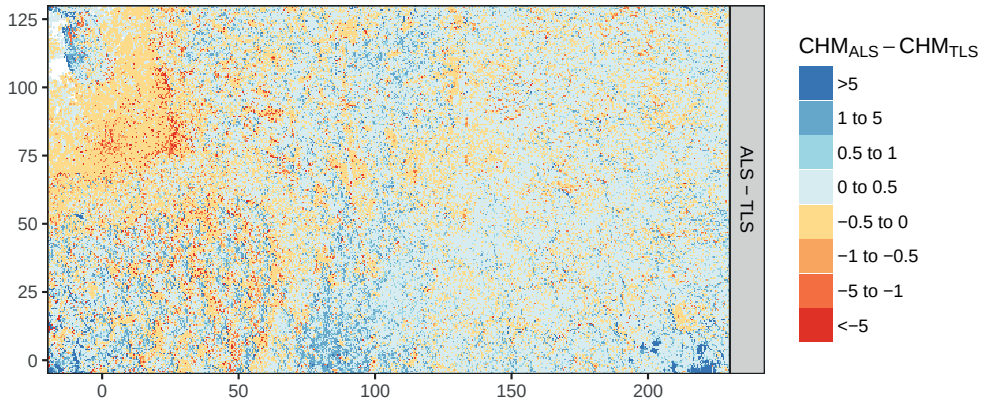

Figure 4.6: Differences in Canopy Height Models (CHMs). Colour height bins were chosen according to histogram and to facilitate evaluation of the sign of the difference.

Beech and Oak plot. This pattern stems from slight mis-registration of the point clouds of about 0.5 to 1 m at the crown level. One major source of error could have been crown movement by wind, a common problem in LiDAR field data acquisition (Wilkes et al., 2017). This would also explain the pronounced pattern in the Douglas Fir plot with its high trees (up to 35 m) that are more susceptible to wind than the lower trees in the other plots. Finally, the TLS did not cover a small area in the Northwest that was occluded by a copse in the middle of the grass patch.

The mis-registration can also be found in the scatterplot of height differences in the plots in Figure 4.7: extreme cases can be found along the x and y axes. They represent cases when either the UAV-LS or the TLS hit the crown and the other the ground. Outliers along the x and y axis represent mainly the western and eastern crowns sides, respectively. Nonetheless, all scatterplots confirm the high agreement of UAV-LS and TLS. However, similar to the vertical profiles (Figure 4.5) also in the case of the CHMs UAV-LS tended to detect higher points in the canopy, resulting in overall higher CHM. For instance, the UAV-LS CHM was 6.1 cm and 12.2 cm higher for the Giant Fir and Old Beech and Oak plots, respectively. The difference for all cells over all plots was 11.5 cm.

Out of the 58 extracted tree stems, 39 were found to be suitable for DBH estimation. Of the accepted 12 trees stems had low level branch points that had to be removed to make the circle fitting possible. The 19 unsuitable trunks would clearly fail to form a circle (17) or had bifurcated trunks that violated the assumption of a single, circular trunk (2). The rejected cases were mainly found in the dense Giant Fir and Norway Spruce plots, and in the Young Beech plot with small overall trunks and branches on the lower canopy levels. Each UAV-LS and TLS point ring contained 40 and 5522 points on average, respectively. Figure 4.8 shows examples of 2 trunks and the resulting fitted circles. In

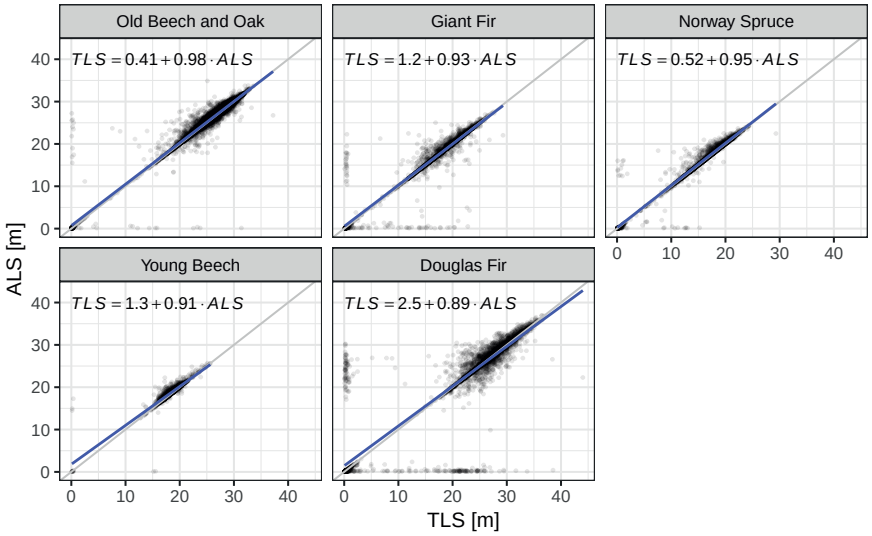

Figure 4.7: Differences in CHM per plot. Ordinary least squares regression lines in blue and formulas. Grey lines are 1:1 lines. Points are transparent to facilitate identification of high density clusters.

both cases there was a large number of TLS points available, while only few UAV-LS points covered the stem at the DBH height and in the case of Douglas Fir it was also only from one direction. However, it was still possible to approximate the stems with circles. In Figure 4.9 the performance of UAV-LS fitted circles in comparison to TLS fits can be seen. Both agree well with a correlation coefficient of 0.98 and RMSE of 4.24 cm, while the range of estimated DBH was 19 to 93 cm. In comparison to TLS UAV-LS estimates were 1.71 cm larger.

Another interesting observation concerned the scan angles and return orders of the UAV-LS points that were available for the DBH estimation. The scan or body across angle is the angle under which a laser pulse was shot from the scanner. It is 0° perpendicular to the rotor arms when mounted, i.e. a scan angle of 0° would describe nadir when the RiCOPTER flies perfectly horizontal. Large positive and negative scan angles result in low incidence angles. Figure 4.10 shows the distribution of scan angles for the sampled points that were used for the DBH estimation. The distributions were strongly bimodal for the Old Beech and Oak, Norway Spruce and Douglas Fir plots with peaks between −20° to −40° and 20° to 40°. The distribution of the Young Beech points were dominated by two trees that were hit from flight lines with the same orientation, resulting in a peak around −30°. Even though the RiCOPTER does not always fly perfectly horizontal, because it has to compensate the wind direction, generally scan angles around 30° to 40° seem to be well suited for detection of trunks. Probably self-occlusion of the observed tree

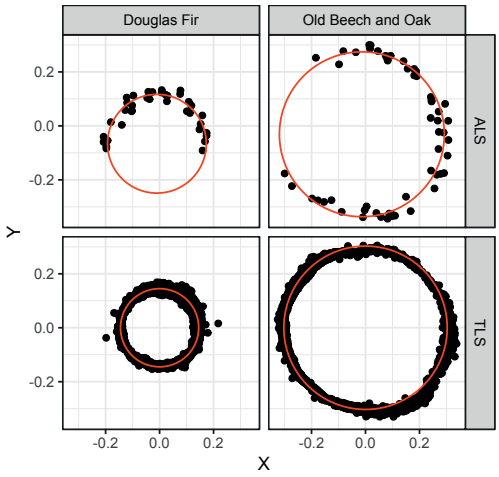

Figure 4.8: Samples of fitted circles to estimate DBH in the x-y-plane, x and y axis in cm.

and occlusion by other trees is minimal at these angles. Furthermore, trunk points were constituted of 14.6% 1st, 25.8% 2nd, 29.4% 3rd, and 30.2% 4th or higher return order. This underlines that the multi-return capability of the VUX®-1UAV was beneficial to observe trunks.

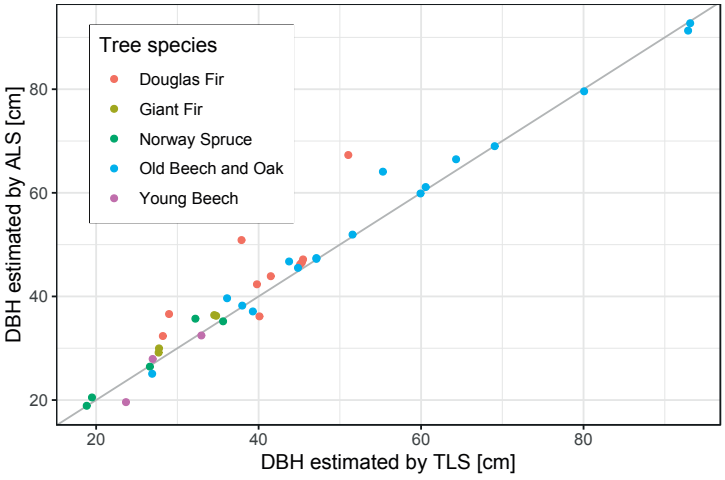

Figure 4.9: DBH of TLS compared to UAV-LS. Grey line is 1:1.

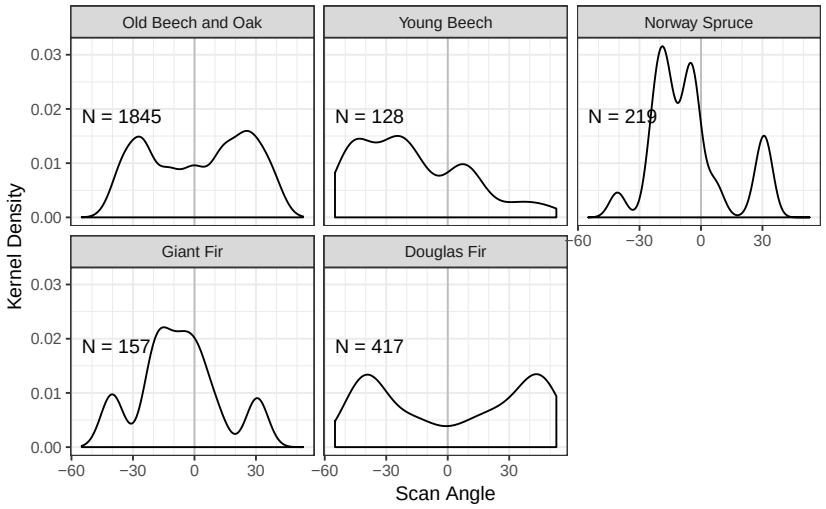

Figure 4.10: UAV-LS scan angles under which the points considered for the DBH estimation were observed. N denotes the number of points for each plot.

4.6 Discussion

Development of LiDAR technology and algorithms in recent years has shown great potential to support forestry practices, in particular geometric characterisation of plots up to unbiased estimation of AGB (Calders et al., 2015b). In this context TLS yields a data source of unprecedented detail and accuracy. However, TLS acquisition can be labour intense and time consuming especially in challenging environments like tropical forests (Wilkes et al., 2017). New UAV-borne LiDAR technology can possibly accelerate these field campaigns and provide a larger coverage.

In this context, the RIEGL RiCOPTER with VUX®-1UAV has proven useful to characterise the Speulderbos forest plot. CHMs were successfully derived and showed good agreement with TLS. Canopy height estimated by the UAV-LS were generally higher. This could be expected by its viewing perspective from above the canopy and the known shortcoming of TLS to not always detect the top of canopy (e.g. Hilker et al. (2010)). However, the difference of on average 11.5 cm falls within the precision of traditional field measurements for tree height of 50 cm (Luoma et al., 2017). Concerning the estimation of individual tree height, Wallace et al. (2014b) found good agreement with field measurements of 0.35 m (mean absolute error) by using point clouds of up to 300 points/m^2 density.

Multi-return and side-looking capabilities proved to be important features of the VUX®-1UAV to scan trunks and estimate DBH for a number of trees under different canopy

conditions (Figure 4.9). While other UAV LiDAR systems are also able to record multiple targets per pulse, not many systems are able to acquire data under larger scan angles (>30° off nadir). Nonetheless, a sufficient number of points could not be collected for all sampled trunks, mainly in the dense, narrow spaced needle-leaf plots. Repeated flights over the same plots with varying flight paths could result in better coverage. The average RMSE of 4.24 cm between TLS and UAV-LS is comparable to reported deviations of TLS and traditional methods of 0.7 to 7.0 cm (RMSE) (Liang et al., 2016). However, the DBH estimation error is still much larger than the precision of traditional methods of ∼0.3 cm (Luoma et al., 2017).

The scan angles that proved optimal to scan the trunk samples (Figure 4.10) have implications for the flight preparation. The targeted plots should be always well covered, possibly with flight lines that overshoot the plot area. For instance if the flight height is at 90 m and the optimal angle is assumed to be 30°, the flight trajectory should overshoot by ∼52 m. However, it is difficult to say how general the optimal scan angles found in this study are. In any way, we found that multiple flight lines, made possible through the long air-borne time, were contributing to a better sampling from different directions. In this respect more lines at faster speed, should be preferred to fewer at lower speed assuming same airborne time. Maximising line crossings and multiple flights should be considered as well. The later will be primarily restricted by the number of battery packs available.

Initial point cloud production of VUX®-1UAV data solely relies on the on-board IMU and GNSS post processing. This is possible because of the IMU's accuracy, which on the other hand results in a large weight for the scanner. This drives the weight of the whole system, since heavier sensors also require larger payload capacity and thus larger UAVs. Together with the system requirement of long endurance this brought the total system weight up to just under the legal limit for mini-UAV (personal communication RIEGL, 2016). This design decision makes it unnecessary to employ algorithms that reconstruct the trajectory in the post-processing as shown in previous studies (Chisholm et al., 2013; Wallace et al., 2012). However, it makes the availability of GNSS base station data a hard requirement that might be difficult to fulfil in remote areas. Also the system weight can be a logistical challenge in such cases.

Even though this study did not aim to conduct full plot inventories, the data shows promising attributes to extend the analysis in that direction. One important step for this would be to detect single trees in all plots. Wallace et al. (2014a) produced detection rates of up to 98% with point clouds of 50 points/m^2 density. Therefore, detection should be achievable with the ∼3000 points/m^2 RiCOPTER point clouds. Based on the detected trees, single tree height can be estimated. However, traditional forest inventory data would be necessary for validation.

Apart from characterising traditional forest metrics, UAV-borne LiDAR could also be utilised as a flexible, higher resolution alternative to manned airborne LiDAR, especially

to study foliage. In that case several published algorithms could be employed (Detto et al., 2015; García et al., 2015; Morsdorf et al., 2006; Tang et al., 2014) and tested if they are applicable on higher density point clouds. Moreover, reliable and mobile systems like the RiCOPTER are suitable for multi-temporal studies (Jaakkola et al., 2010).

4.7 Conclusions

This study presented first results and experiences with the RIEGL RiCOPTER with VUX®-1UAV UAV-LS with its components and processing work flow, and its performance in estimating CHM and DBH compared to TLS. As first steps we compared the RiCOPTER with the well tested RIEGL VZ-400 TLS by deriving CHM and estimating DBH. CHMs showed only small differences that could be explained by the perspective of the RiCOPTER above the canopy, resulting in different vertical detection profiles that facilitate the discovery of highest points in the canopy, which is not always possible with TLS. Additionally, the multi-return and side-looking capabilities of the VUX®-1UAV scanner proved beneficial to detect trunk elements. This feature will be valuable when more sophisticated 3D modelling is to be applied. However, not all sampled tree trunks were sufficiently covered with points, so that more flights or different flight patterns are necessary to achieve better coverage. Overall, the RiCOPTER could produce comparable results to the VZ-400. Further experiments should be directed to test explicit quantitative structural modelling to derive AGB from the RiCOPTER point clouds as well as co-registration strategies of multiple flights and with TLS systems.

Chapter 5

Tree Volume Estimation through UAV Laser Scanning and Quantitative Structure Modelling

This chapter is based on:

B. Brede, K. Calders, A. Lau, P. Raumonen, H. M. Bartholomeus, M. Herold, and L. Kooistra (in review). "Tree Volume Estimation through UAV Laser Scanning and Quantitative Structure Modelling". *Remote Sensing of Environment*

Abstract

Above-Ground Biomass (AGB) product calibration and validation requires ground reference plots at hectometric scales to match space-borne missions' resolution. Traditional forest inventory methods that use allometric equations for single tree AGB estimation suffer from biases and low accuracy, especially when dealing with large trees. Terrestrial Laser Scanning (TLS) and explicit tree modelling show high potential for direct estimates of tree volume, but at the cost of time demanding fieldwork. This study aimed to assess if novel Unmanned Aerial Vehicle Laser Scanning (UAV-LS) could overcome this limitation, while delivering comparable results. For this purpose, the performance of UAV-LS in comparison with TLS for explicit tree modelling was tested in a Dutch temperate forest. In total, 200 trees with Diameter at Breast Height (DBH) ranging from 6 to 91 cm from 5 stands, including coniferous and deciduous species, have been scanned, segmented and subsequently modelled with *TreeQSM*. Direct comparison with TLS derived models showed that UAV-LS was reliably modelling volume of trunks and branches with diameter $\geq$30 cm in the mature beech and oak stand with Concordance Correlation Coefficient (CCC) of 0.85 and Root Mean Square Error (RMSE) of 1.12 m^3. Including smaller branch volume led to a considerable overestimation and decrease in correspondence to CCC of 0.51 and increase in RMSE to 6.59 m^3. Denser stands prevented sensing of trunks and further decreased CCC to 0.36 in the Norway spruce stand. Also small, young trees posed problems by preventing a proper depiction of the trunk circumference and decreased CCC to 0.01. This dependence on stand indicated a strong impact of canopy structure on the UAV-LS volume modelling capacity. Improved flight paths, repeated acquisition flights or alternative modelling strategies could improve UAV-LS modelling performance under these conditions. This study contributes to the use of UAV-LS for fast tree volume and AGB estimation on scales relevant for satellite AGB product calibration and validation.

5.1 Introduction

Terrestrial vegetation contains approximately 450 to 650 PgC, which is on the same order of magnitude as the atmospheric carbon pool (Ciais et al., 2013) and forests make up a significant contribution to the vegetation carbon pool. However, the forest carbon pool is only weakly constrained due to a low and possibly biased number of sample plots worldwide (Houghton et al., 2009). The future ESA BIOMASS (Le Toan et al., 2011) and NASA GEDI (`https://science.nasa.gov/missions/gedi`) missions aim to improve observations of AGB on global scales with a focus on forests. This underpins the space agencies' commitment towards global AGB mapping capabilities.

Even though general relationships between satellite sensor signals and AGB for the intended missions are well established — e.g. exponential relationship for Synthetic Aperture Radar (SAR) backscatter intensity and AGB — specific retrieval models have to be calibrated based on ground reference plots (Baccini et al., 2012; Saatchi et al., 2011; Thiel and Schmullius, 2016). This means calibration at the scale of the satellite's mapping unit are required, which are typically hectometric for AGB. If best practice for validation of geophysical products shall be followed, the observation's geo-location error has to be considered, which usually means to triplicate the calibration unit side length (Fernandes et al., 2014). Additionally, a large number of plots is required to capture the heterogeneity of stand structural characteristics across an area of interest. For example, Saatchi et al. (2011), Baccini et al. (2012) and Mitchard et al. (2014) used data from 4079, 283 and 413 inventory plots to build maps for (pan-)tropical forests, respectively. Furthermore, uncertainty in traditional field inventory biomass assessment based on allometric equations is high. Contributing to this is the limited availability of calibration samples for allometric model generation, which need to be destructively harvested, and wrong application of allometric models outside of the area where they have been developed (Yuen et al., 2016).

Given above-mentioned circumstances, calibration of satellite-based AGB products is already challenging. But in the light of systematic global AGB product validation, a significant number of globally and temporally representative in situ sites, and systematic re-validation of the product's time series is required as envisaged by the Committee on Earth Observing Satellites (CEOS) Land Product Validation (LPV) subgroup. This requires accurate and fast techniques that cover the satellite footprint. Forest inventory techniques can achieve the speed and coverage, but lack accuracy in tropical forests (Disney et al., 2018).

TLS has been proposed as an alternative to traditional inventory techniques for AGB assessment (Disney et al., 2018). Compared to the latter it has shown nearly unbiased AGB estimates, which is particularly critical for large trees (Calders et al., 2015b; Gonzalez de Tanago et al., 2018; Keller et al., 2001). Another advantage of TLS is that it does not

require destructive sampling. Several studies have demonstrated the effectiveness of TLS for AGB assessment (Calders et al., 2015b; Gonzalez de Tanago et al., 2018; Hackenberg et al., 2015; Momo Takoudjou et al., 2018; Rahman et al., 2017; Stoval and Shugart, 2018; Stovall et al., 2017) and best practices for field set-ups begin to be established (Wilkes et al., 2017). Currently, the LPV guideline for good practices in AGB validation is being compiled, which also includes a section on TLS.

However, a drawback of TLS-based AGB inventories is the time consuming field work. For the acquisition of a dataset that allows reliable geometrical modelling, an experienced team requires 3 to 6 days for a 1 ha plot (Wilkes et al., 2017). Good quality data for geometrical modelling means low occlusion of canopy elements, which makes it necessary to use multiple scan locations in the plot and accurately co-register them.

Recently, miniaturisation and advancement in several Unmanned Aerial Vehicle (UAV) components has prepared the ground for the construction of UAV-LS systems. The critical challenge in this context is the high position and orientation accuracy requirement of the scanner at any time during data acquisition. This determines the geometric accuracy of the produced point cloud. In the contrasting case of TLS, positioning of the scanning positions relative to each other is provided with common targets, most often retro-reflectors, and scan positions are limited to tens to few hundreds per plot (Wilkes et al., 2017). For UAV-LS, the position has to be determined several times per second for flight times of up to 30 min to provide the necessary information for accurate target localisation.

Another difference of UAV-LS to TLS is the perspective above the canopy. From this perspective trunks, which contain the largest part of biomass, are at least partly occluded by upper branches or leaves (Brede et al., 2017). Finally, UAV-LS point cloud densities are limited by scanner speed and flight time. Recent UAV-LS systems have produced point clouds with densities of around 50 (Wallace et al., 2012), 1500 (Jaakkola et al., 2010; Mandlburger et al., 2015) and 4000 points/m^2 (Brede et al., 2017). TLS plot scans have typically point densities of tens of thousands points/m^2 (Brede et al., 2017; Wilkes et al., 2017).

Recent forestry related applications with UAV-LS cover Digital Elevation Model (DEM) generation (Wei et al., 2017), Canopy Height Model (CHM) generation, Leaf Area Index (LAI) estimation, AGB estimation via allometric equations based on tree height and crown area (Guo et al., 2017), DBH estimation (Brede et al., 2017; Wieser et al., 2017), tree height estimation and localisation (Wallace et al., 2014b), and tree detection and segmentation (Balsi et al., 2018; Wallace et al., 2014a). With these UAV-LS systems available now, the question can be investigated how UAV-LS point clouds compare to TLS point clouds for explicit structural tree modelling.

The aim of this study was to compare tree volume estimation performance of high density UAV-LS (>1000 points/m^2) with TLS point clouds for different canopy architectures, including deciduous and coniferous species. Tree volume was investigated instead of AGB,

because AGB is a product of tree volume and wood density, the latter being equal for both laser scanning systems. The work flow strongly builds on established TLS methods. This will make fast tree volume estimation possible at the plot scale, and support calibration and validation of future AGB missions at hectometric scale.

5.2 Data

5.2.1 Study Site

This study was performed at the Speulderbos Reference site in the Veluwe forest area (N52°15.15′ E5°42.00′), The Netherlands (Brede et al. 2016, `www.wur.eu/fbprv`). Five stands were investigated (Figure 5.1, Table 5.1). The first and in terms of area largest consisted of maturing European beech (*Fagus sylvatica*) and oak (*Quercus robur*, *Q. petraea*), here referred to as old beech and oak. Crown heights of sampled trees reached up to 32 m, but were 27 m on average. The understorey was sparse with only few seedlings and young trees, and occasional European holly (*Ilex aquifolium*). A forest road separated this beech and oak stand from the second stand consisting of young beech with trees of on average 23 m height. These beeches were markedly different from the old beech stand in terms of age and consequently stem diameter (Table 5.1). Additionally, their branching behaviour was less complex with most tree volume concentrated in the central trunk. In contrast to this, the old beech trees showed more complex structure with major branching occasionally occurring below 10 m height.

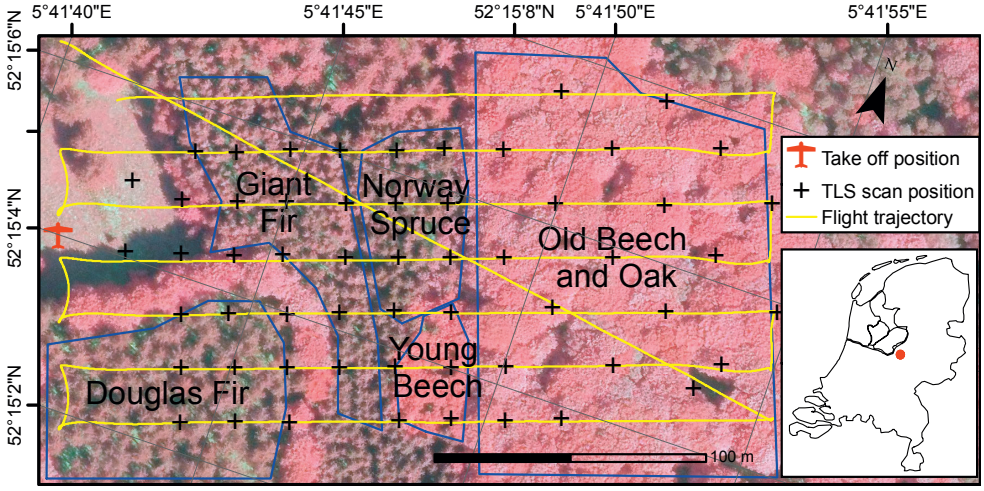

Figure 5.1: Map of the study site with stand locations, TLS scan positions and UAV-LS flight trajectory. Location within the Netherlands marked as red dot on inset map.

Table 5.1: Stand sample characteristics. Tree density was estimated based on manually identified trees in the TLS point cloud, tree height based on segmented tress range in height, and DBH based on optimised TLS Quantitative Structure Models (QSMs).

	Giant fir	Norway spruce	Douglas fir	Young beech	Old beech & oak
Tree density (ha^{-1})	588	714	231	554	142
Minimum tree height (m)	11.3	14.6	18.7	4.6	18.4
Average tree height (m)	21.1	19.9	30.6	16.4	27.2
Maximum tree height (m)	27.4	25.1	35.3	22.5	31.6
Minimum DBH (cm)	11.2	14.4	15.6	6.2	22.9
Average DBH (cm)	28.5	28.5	40.1	21.3	59.2
Maximum DBH (cm)	58.4	46.9	56.5	37.1	91.0

Located north of the young beech stand was the third stand consisting of Norway spruce (*Picea abies*) with maximum tree height of 25 m. Located further east was the fourth stand, a Giant fir (*Abies grandis*) stand with maximum heights of 27 m. Both Norway spruce and Giant fir trees were characterised by numerous small branches along the main stem.

The fifth stand was in the South-East of the study area and consisted of Douglas fir (*Pseudotsuga menziesii*) with maximum tree heights of 35 m, making up the highest trees in the study area. This stand had only little understorey, and had been thinned in recent years as could be recognised by tractor tracks and stumps. Additionally, the lower tree trunks were mostly free of branches.

5.2.2 UAV-LS Data

UAV-LS data was collected with a RIEGL RiCOPTER with VUX®-1UAV (RIEGL Laser Measurement Systems GmbH, Horn, Austria). The VUX®-1UAV is a survey-grade laser scanner with an across-track Field Of View (FOV) of 330° (Table 5.2). UAV-LS data acquisition was conducted in the course of 2 hours (Brede et al., 2017). The take-off site was chosen in the western part of the study area in a clearing, which allowed operation within Visual Line of Sight (VLOS). The study area of 100 m x 180 m was covered with a total of 8 parallel flight lines (Figure 5.1) and one diagonal cross-line.

The collected raw data was processed with the VUX®-1UAV accompanying software package RiPROCESS. This included (i) post-processing of the Global Navigation Satellite System (GNSS) and Inertial Measurement Unit (IMU) records to reconstruct the flight trajectory, (ii) LIght Detection And Ranging (LiDAR) waveform analysis for target detection in scanner geometry and (iii) translation of the detected points into global coordinate system under consideration of the trajectory information. Additionally, single

Table 5.2: VZ-400 and VUX®-1UAV main characteristics

Characteristic	VZ-400[1]	VUX®-1UAV[2]
Maximum Pulse Repition Rate (PRR) (kHz)	300	550
Maximum effective measurement rate (kHz)	120	500
Minimum / Maximum range (m)	1.5 / 350[3]	3 / 920[4]
Accuracy / Precision (mm)	5 / 3	10 / 5
Laser wavelength (nm)	1550	1550
Beam divergence (mrad)	0.35	0.5
Weight (kg)[5]	9.6	3.75

[1]high speed mode, incl. online waveform processing
[2]550 kHz mode [3]at target $\rho \geq 0.9$ [4]at target $\rho \geq 0.6$
[5]without battery and tilt mount

flight geometry was optimised with automatically detected control-planes in the point cloud. Finally, all flight lines were manually fine-registered based on 12 ground control targets, which were placed throughout the study area. A detailed description of the acquisition and processing work-flow is described in Brede et al. (2017). The resulting UAV-LS point cloud had densities between 2965 points/m^2 and 5344 points/m^2 depending on the position of the flight lines and tree heights with an average of 4059 points/m^2.

5.2.3 TLS Data

TLS data was collected with a RIEGL VZ-400 scanner from 58 scan positions during two days (Table 5.2). This scanner was used in several studies dealing with explicit, three-dimensional tree modelling (Lau et al., 2018) and AGB estimation (Calders et al., 2015b; Gonzalez de Tanago et al., 2018). The scan positions were spaced on a 20 m grid across the study area, but with slightly wider spacing in the old beech and oak stand due to good visibility (Figure 5.1). The angular scan resolution was set to 0.06°. Due to the limitation of the VZ-400 to a minimum viewing zenith angle of 30°, a second scan was performed at each position with a 90° tilted scanner to capture the canopy directly above the scan position. Retro-reflective targets were placed in between scan positions to facilitate co-registration. Fine-registration between positions was achieved with RIEGL's multi-station adjustment routine built into the RiSCAN PRO software (Wilkes et al., 2017). This automatically searches for planar surfaces in the point clouds and uses them for co-registration between the point clouds. The final TLS point cloud was co-registered to the UAV-LS point cloud with the help of five Ground Control Points (GCPs) distributed over the study area.

5.3 Methods

5.3.1 Tree Segmentation

In recent years, several automatic tree segmentation algorithms for Airborne Laser Scanning (ALS) have been proposed (Duncanson et al., 2014; Heinzel and Huber, 2016; Parkan and Tuia, 2018). However, understorey trees are usually hard to detect (Eysn et al., 2015). Also, methods based on the CHM potentially separate elements from trees especially when crowns are inter-locked. This was particularly the case with the old beech and oak stand. As tree segmentation in this study needed to be of best quality to leave tree architecture in place, a semi-automatic procedure was chosen that took advantage of both UAV-LS and TLS data sets.

The segmentation was essentially a marker-based inverse watershed segmentation (Koch et al., 2006) followed by manual correction. Tree trunks were manually identified to serve as initial markers with Quantum GIS 2.18 (QGIS Development Team, `https://qgis.org`) based on 0.2 m resolution TLS point density maps. The tree trunks were clearly visible in this map as they were hit often and cover only a small ground area compared to upper branches and crowns. A 0.2 m resolution CHM was derived as the difference between DEM and Digital Surface Model (DSM) based on the UAV-LS point cloud (Brede et al., 2017). Then, the inverse watershed segmentation implemented in the `R ForestTools` package (`https://cran.r-project.org/web/packages/ForestTools/`) was applied based on the TLS markers and UAV-LS CHM. Only crowns with a height of at least 5 m were considered for the automatic segmentation. The single segmented trees were exported into single files for inspection. UAV-LS and TLS points were exported in the same file, but marked with different labels for later filtering.

From the range of automatically segmented trees, sample trees for later modelling were selected. The selection took into account the tree species as given by the location in the plots (Figure 5.1) as well as tree size indicated by the trunk and crown size. The goal was to maximise the range of sizes to evaluate tree volume modelling with small and large trees. Next, the single tree point clouds were manually inspected and points not belonging to the specific tree were removed. In some cases, neighbouring trees had to be inspected together to transfer significant branch points from one to the other. The co-registration allowed to segment the UAV-LS and TLS point clouds together. Also, tree and branch identification was much easier with the TLS than with the UAV-LS point clouds. Additionally, points representing ground were removed. Finally, UAV-LS and TLS points were separated based on their labels. All manual work was performed by the same operator to assure comparable quality over all the selected trees. CloudCompare 2.10 was used in this analysis (`http://cloudcompare.org`) to perform the 3D work.

5.3.2 Point Cloud Foliage Filtering and Density Normalisation

In the next step, the point clouds were filtered and normalised. During the filtering foliage was removed, as this was not focus of thsi study. Also, foliage is not modelled with *TreeQSM* and can only be recognised by the routine to a limited extent. Filtering was especially important for the coniferous species in the study area, but also some of the deciduous trees already showed young leaves. Density normalisation is a necessary step prior to 3D model fitting, as the model routines assume equal density of the point clouds across the tree. In this study, this assumption was particularly violated by the UAV-LS data with a much higher number of hits in the upper crown (Brede et al., 2017).

Foliage filtering was based on a supervised Random Forest classification (Belgiu and Drăgu, 2016; Breiman, 2001; Zhu et al., 2018). For this, training samples representing hard (trunk, branches) and soft (leaves) tissue were manually selected from the tree point clouds. Based on the radiometric properties of these points, individual models were trained for each plot, and separately for UAV-LS and TLS, resulting in a total of 10 models. Radiometric features were apparent reflectance, RIEGL deviation number — a measure of pulse waveform deviation from the expected shape (Calders et al., 2017) — and return characteristic (i.e. first, intermediate, last return). Other studies proposed to involve additional geometric features such as local neighbourhood relationships to improve classification results (Wang et al., 2018; Zhu et al., 2018). However, classification accuracy based solely on radiometric features was considered sufficient for hard tissue candidate selection in this study as these already provided good classification results.

For each Random Forest model, 2000 samples were picked for both soft and hard tissue for training. Model performance was checked with a 5-fold cross-validation. The final models were trained on all 4000 samples to produce the class probability rather than the class. In the filtering step, only points with a hard tissue probability of more than 90 % were selected for each tree. During the density normalisation the class probability was utilised as a selection criterion. The points were segmented into voxels and within each voxel the point with the highest hard tissue probability was selected. The grid size for TLS was 2.5 cm, which closely follows Calders et al. (2018a) and recommendations by Wilkes et al. (2017). The UAV-LS grid size was set to 10 cm, which is in line with the lower density of the UAV-LS point clouds.

5.3.3 Tree Modelling with *TreeQSM*

Explicit 3D cylinder models of trees were produced with *TreeQSM* in this study. *TreeQSM* was introduced as a way to effectively fit cylinder models to detailed TLS point clouds, taking into account tree inherent structure like connectivity, branching and branch tapering (Raumonen et al., 2013). Additionally, *TreeQSM* neither makes assumptions based on tree species nor distinguishes between deciduous and coniferous tree architectures. *TreeQSM* was used in several studies to automatically produce 3D tree models, and estimate

tree volume and subsequently AGB (Calders et al., 2015b; Gonzalez de Tanago et al., 2018).

The *TreeQSM* fitting procedure is extensively explained in Raumonen et al. (2013), Calders et al. (2015b) and Gonzalez de Tanago et al. (2018). Essentially, tree modelling is performed in two main steps. First, the point cloud is segmented into trunk and individual branches. The segmentation uses small subsets or patches in two phases. In the first phase large constant size patches with radius PatchDiameter1 are used across the tree. This segmentation serves to identify the tree's coarse architecture and branches. In the second phase, a finer cover with patch size varying from PatchDiameter2Min to PatchDiameter2Max determines the final branch topology. In the second main step, the branch geometry is reconstructed by least squares fitting of cylinders.

PatchDiameter2Min (PD2Min) plays a central role in the *TreeQSM* tuning, as it defines the smallest possible features that will be modelled. Hence, it has to be adapted to the smallest features that can be resolved with the data available. Additionally, there is a random component in the initialisation of the patches. This makes it necessary to run the same parameter settings multiple times for each tree and aggregate the produced models, which provides a measure of modelling confidence.

In this study, PatchDiameter1 (PD1) was kept constant for all trees. In the case of UAV-LS and TLS, it was chosen as 20 cm and 18 cm, respectively. PD2Min was varied from 2 to 31 cm in steps of 2 cm for UAV-LS and 2 to 11 cm in steps of 0.5 cm for TLS. PatchDiameter2Max (PD2Max) was varied from 10 to 70 cm in steps of 10 cm for UAV-LS and between 10 to 14 cm for TLS. The variation was conducted in a full-grid approach and each parameter combination was run 10 times, to derive statistics about the modelling uncertainty of the respective parameter set.

5.3.4 Best Fit QSM Identification

Although *TreeQSM* produces inherently valid models with respect to topology and tapering for a range of input parameters, the best fitting model for a given point cloud has to be identified independently. Calders et al. (2015a) proposed an automatic framework for parameter tuning that was successfully applied to TLS data in Calders et al. (2015b) and Calders et al. (2018a). This framework is based on selecting segments along the trunk and fitting circles to each via least squares optimisation. These circles provide a robust measure of the trunk diameter at the respective height. Then, the QSM is selected that matches the circle radii best. This procedure has the advantage that the circles deliver measures of the trunk that are independent from the QSM. However, in a previous study circle fitting at DBH height for 19 out of 58 trees (33 %) was unsuccessful for the dataset used in this study due to too low point density (Brede et al., 2017).

Therefore, the procedure of Calders et al. (2015a) was adapted to use cylinders instead, which are the extension of circles into the third dimension. This has the advantage to take more space and potentially more points into account, thereby overcoming the problem of low point density at specific positions at the trunk for the UAV-LS data. For the purpose of cylinder fitting, three to six straight parts of the trunk or big branches were manually selected from each tree. The parts had to contain at least 10 returns to be taken into consideration for cylinder fitting. Cylinders were fitted in two steps: first, the orientation of each cylinder was estimated based on point normals and Hough transformation (Rabbani and Heuvel, 2005). Then, the points were projected onto the plane that was orthogonal to the cylinder central axis. This allowed to estimate radius and central axis with least squares circle fitting.

Based on the radii of these derived control cylinders the tuning followed the framework of Calders et al. (2015a) per tree, and independently for UAV-LS and TLS. For all QSMs, the QSM cylinders that were closest to the control cylinder centres were identified. The maximum allowed angle and distance between QSM and control cylinder were 15° and 50 cm, respectively. Per *TreeQSM* parameter combination, the QSM model cylinder radii r_{QSM} were related to the control cylinder radii $r_{control}$: $\Delta r = 1 - (r_{control} - r_{QSM})/r_{control}$. The absolute average over all control cylinders was defined as c_{match}. Subsequently, the mean $\overline{c_{match}}$, standard deviation σ_c and coefficient of variation CV_c were derived. Then the parameter combination with the largest PD2Min was chosen where $CV_c < CV_{threshold}$ and $\overline{c_{match}} > c_{conformity}$, where $c_{conformity} = 5 \times \min(CV_c)$ and $c_{conformity} = 0.95$. If no such parameter set existed, the parameter set with the lowest CV_c was selected. If no control cylinders could be derived from the segments, the model with the parameter set with the lowest standard deviation in volume was chosen.

5.3.5 QSM Comparison

For the assessment of UAV-LS correspondence to TLS QSMs total volume across samples in a stand, CCC — a measure for the agreement of two methods measuring the same quantity (Lin, 1989) — was used. RMSE was used to quantify the magnitude of the deviation of modelled volume and Mean Signed Difference (MSD) to assess the bias. The averaged Coefficient of Variation (CV) across samples of a stand gave an indication of the model uncertainty.

In order to get further insights into how the estimated volume was distributed over the vertical dimension of QSMs, vertical volume distribution profiles were computed. For this, volume was summed up across 30 height layers relative to the maximum height and to the total volume of each individual tree. The height layers were defined by the minimum and maximum height coordinate of each segmented TLS tree point cloud. This allowed comparison across all trees within the same stand as well as across stands.

5.4 Results

5.4.1 Tree Segmentation

The CHM was segmented based on 767 manually selected markers (Figure 5.2). Some of the sampled tree point clouds also included additional non-dominant understorey trees, especially in the old beech and oak plot. These trees were also considered for the further processing. In total, 40 trees per stand were selected, summing up to a total of 200.

5.4.2 Foliage Filtering

Table 5.3 summarises the foliage identification performance for the UAV-LS and TLS point clouds. All models achieved classification accuracies ≥ 0.71, while all except UAV-LS in the Norway spruce stand and in the young beech stand achieved accuracies ≥ 0.91. The Norway spruce trees seemed to provide challenges due to their high number of small branches close to the trunks, which resulted in only few trunk returns. These were prone to be higher order returns, which could lead to degradation in the reflectance signal in the selected training data. In the case of the young beech trees, the trunks were small in diameter even though they were more sparsely covered by branches than for example the Norway spruce. However, the small trunk surfaces might have led to partial returns at the trunk edges, which also could have effects on the reflectance signal. Nonetheless, classification accuracy was generally high, and UAV-LS and TLS showed comparable results.

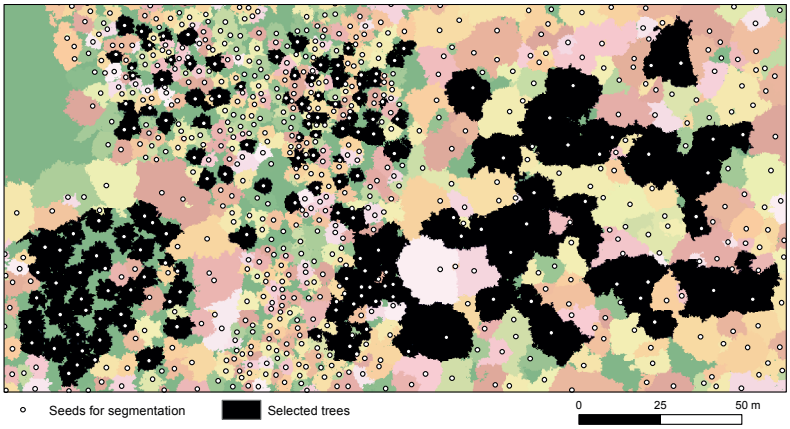

Figure 5.2: Manually selected seeds for watershed segmentation, segmented CHM and selected trees for 3D modelling in project coordinate system. Some selected segments contained more than one tree and some contained none.

Table 5.3: Classification performance for point cloud filtering from 5-fold cross-validation.

Stand	Accuracy UAV-LS	Accuracy TLS
Douglas fir	0.96	0.95
Giant fir	0.91	0.95
Norway spruce	0.71	0.93
Old beech and oak	0.94	0.92
Young beech	0.82	0.88

5.4.3 Control Cylinders

Cylinder fitting was successful for at least one cylinder for all TLS-based tree point clouds and in 185 out of 200 cases (92.5 %) for the UAV-LS. Figure 5.3 summarises the estimated cylinder diameters compared with TLS. Generally, cylinders could be fitted best for the old beech and oak trees with CCC of 0.99 and RMSE of 2.3 cm in diameter. Foliage was least developed in this stand, exposing trunks, so that they could be sampled well from above.

Giant fir and Norway spruce control cylinders were estimated about equally with CCC of 0.96 and 0.93, and RMSE of 2.38 cm and 2.26 cm, respectively. However, for 6 and 5 trees no control cylinders could be successfully fitted, respectively. The foliage and small branches of these species shielded their trunks, which made already the cylinder selection in the TLS point cloud difficult during manual segmentation.

In the case of young beech trees, four individuals could not produce acceptable control cylinders. UAV-LS fitting performance compared to TLS was lower with CCC of 0.88 and RMSE of 3.69 cm when compared to the old beech trees. The young beech stand was relatively open, but tree diameters were small, so that the chance of trunk hits was much lower than for larger trees. Additionally, UAV-LS estimated cylinders were on average 1.18 cm larger compared to TLS. This was due to cylinders only partially covered with points.

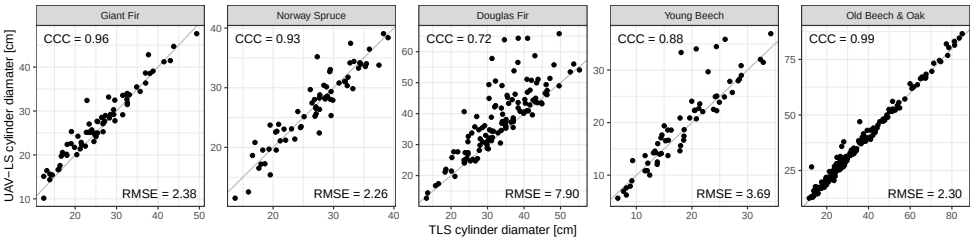

Figure 5.3: UAV-LS estimated cylinder diameter compared to TLS. Grey lines are 1:1.

The effect of partial coverage was even stronger in the Douglas fir stand due to its position in the corner of the plot. This position prevented good visibility of the trunks from the last diagonally crossing flight line (Figure 5.1). In combination with the relatively large trunks this led to the largest RMSE of all plots of 7.90 cm and on average 4.71 cm larger cylinder diameters compared to TLS.

5.4.4 QSM Comparison

Figure 5.4 and 5.5 compare acquired (segmented) point clouds, normalised point clouds and QSM samples for the largest beech tree found in the study area and a Douglas fir, respectively. In both cases, UAV-LS delivered sufficient points to visually delineate the lower part of the trunk, i.e. the volume of the trunk could be delineated clearly on all sides. The normalisation with foliage filtering typically removed a significant part of points, especially in the upper crown area. For TLS, this were 92.7 % and 94.9 % of the points in case of the beech and the Douglas fir, respectively. For UAV-LS, 77.6 % and 88.8 % of the points were removed, respectively. However, the identification of foliage in the UAV-LS point clouds seemed to be less effective, despite high cross-validation classification accuracy between 0.71 and 0.96 (Table 5.3). Also, the UAV-LS normalised point clouds did not show upper branches as clearly, compared to the TLS normalised point cloud. This means branches could be recognised, but only after careful checking and turning of the point cloud. Also, some branch surfaces were not sampled completely, so that guessing the occupied volume visually was more difficult. A consequence of this incompleteness is that the QSM derived from UAV-LS resulted in a much less coherent upper crown modelling: cylinders did not follow natural growth directions and a much higher number of cylinders was fitted than seemed necessary, when compared to TLS.

Considering all sampled trees, UAV-LS tree volume estimation in comparison to TLS volume varied markedly across the different stands in the study area (Figure 5.6). As was the case in the control cylinder diameter estimation (Section 5.4.3), UAV-LS based old beech and oak QSMs showed overall the closest correspondence to TLS based QSMs in terms of volume with CCC of 0.51. Additionally, the modelling uncertainty expressed as mean CV was lowest among all stands with a value of 0.10. The structural characteristics of this stand were probably the most favourable for UAV-LS sampling of all the considered stands. The relatively wide spacing between individuals, the large trunks with reconstructed DBH of up to 91.0 cm and the comparably low shielding of lower canopy elements by upper branches and foliage when seen from above had a positive effect on volume estimation. However, UAV-LS volume estimates for large specimen in this stand were positively biased as indicated by the MSD of 3.44 m^3. This bias in combination with the fact that the old beech and oak stand contained the largest trees in the study area produced the largest RMSE among all stands of 6.59 m^3. Inspecting the distribution of the volume over differently sized cylinders gave further insights how this could be traced to differently sized branches (Figure 5.8): Considering only large cylinders with diameter $\geq$30 cm resulted

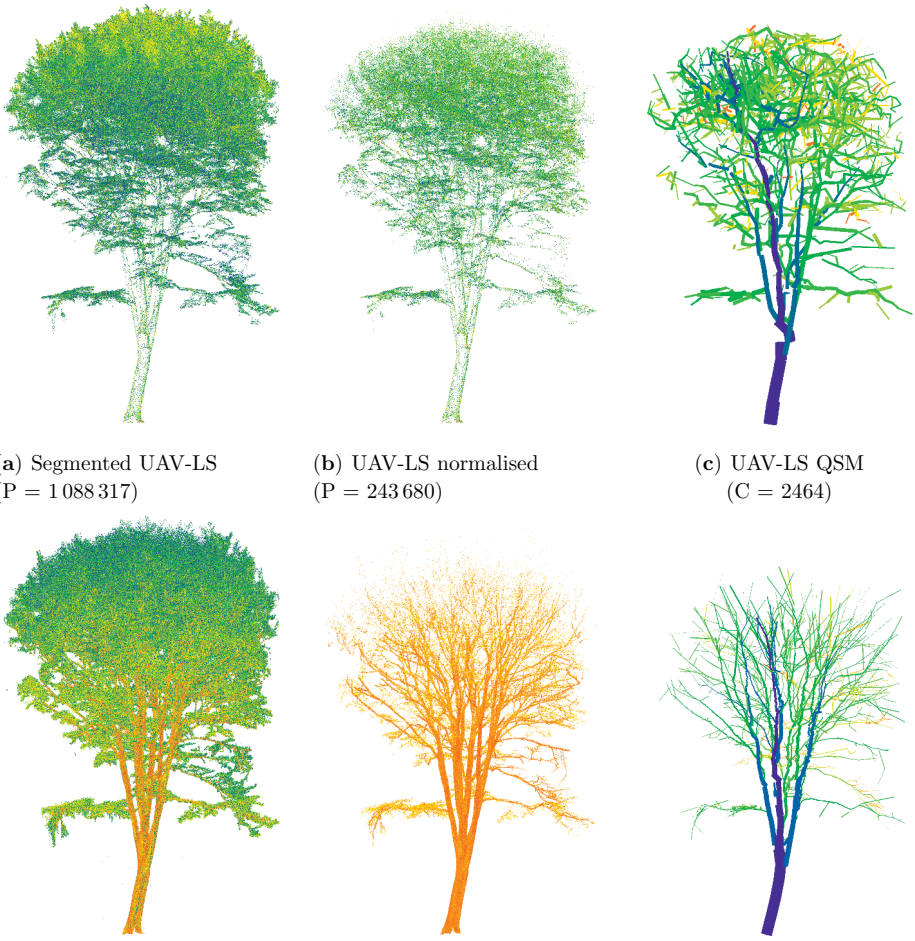

(**a**) Segmented UAV-LS (P = 1 088 317)

(**b**) UAV-LS normalised (P = 243 680)

(**c**) UAV-LS QSM (C = 2464)

(**d**) Segmented TLS (P = 4 626 368)

(**e**) TLS normalised (P = 337 326)

(**f**) TLS QSM (C = 3471)

Figure 5.4: Tree segmentation, point density normalisation and QSM example for beech. Point cloud colour represents reflectance (blue = low, green = intermediate, red = high), QSM colour refers to branching order. Scale bar in metre. Number of points P or cylinders C in caption.

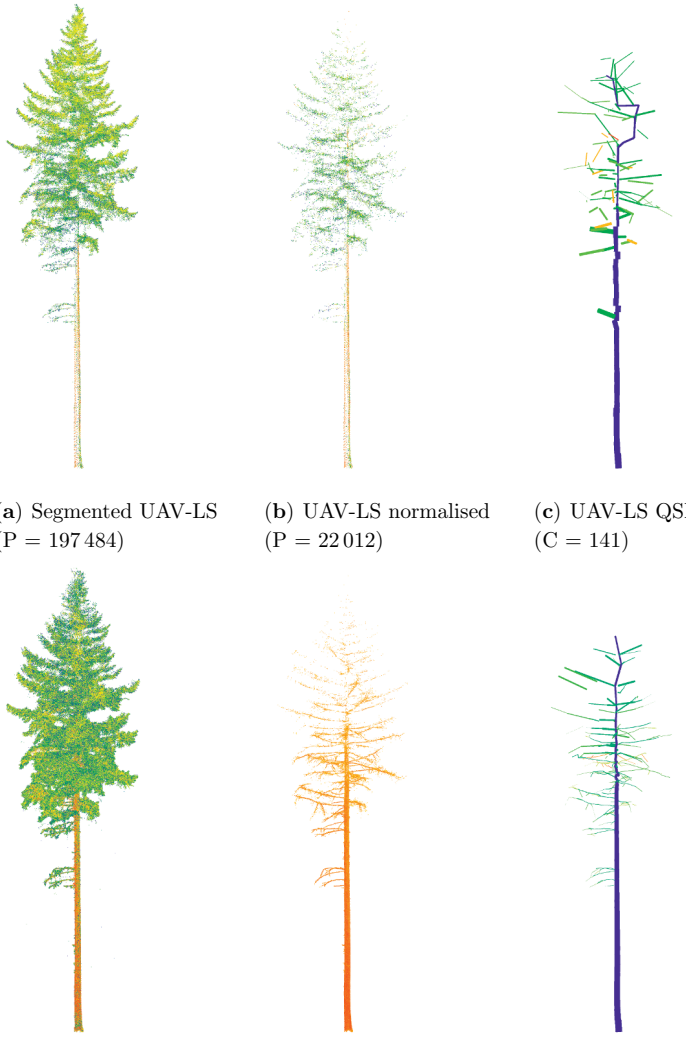

(**a**) Segmented UAV-LS (P = 197 484)

(**b**) UAV-LS normalised (P = 22 012)

(**c**) UAV-LS QSM (C = 141)

(**d**) Segmented TLS (P = 1 613 021)

(**e**) TLS normalised (P = 81 888)

(**f**) TLS QSM (C = 588)

Figure 5.5: Same as Figure 5.4, but for a Douglas fir.

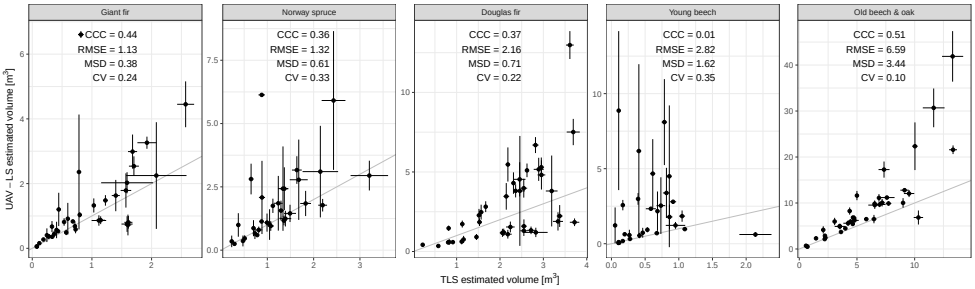

Figure 5.6: Tree volume reconstruction for UAV-LS compared to TLS. Error bars represent 1 standard deviation of the 10 QSM realisations. Grey lines are 1:1 match. CV is mean UAV-LS coefficient of variance. Positive MSD means overestimation by UAV-LS. RMSE and MSD in m^3.

in high correspondence between UAV-LS and TLS with CCC> 0.85, RMSE as low as 0.65 m^3 and MSD as low as 0.1 m^3. But taking smaller cylinders into account, considerably degraded UAV-LS volume estimates for this stand in terms of all performance metrics. CCC of minimum 0.42, and RMSE and MSD of maximum 6.70 m^3 and 3.57 m^3, respectively, were reached. Furthermore, it was possible to trace the differences between UAV-LS and TLS volume estimates to the vertical distribution of cylinder volume (Figure 5.7). It could be seen that UAV-LS overestimated volume in the upper half of trees with an average contribution of this part of 41.3 % to the total tree volume for UAV-LS compared to 27.6 % for TLS. The reason for this could be observed in the sample (Figure 5.4), but also in all other old beech and oak trees' QSMs. The upper crown was modelled as a large number of small cylinders that were apparently not corresponding to real branches. Probably the quality of the point clouds was not sufficient in terms of point count and point registration accuracy.

Apart from these general observations for the old beech and oak stand, an outlier could be observed when only considering large cylinders (Figure 5.8). This specimen was located at the southern edge of study area. Inspecting the point cloud together with QSM realisations revealed that the stem was not modelled with cylinders as large as those of the TLS QSM, but with many smaller cylinders. The UAV-LS point cloud mainly contained points from one side of the tree and trunk, which were not sufficient to model the whole circumference. The most southern UAV-LS flight line was nearly directly over this tree effectively preventing registration of points on the southern trunk sites. The corresponding UAV-LS point cloud covered only the trunk surfaces facing into the plot, which resulted in a QSM with undersized trunk cylinders.

The Douglas fir comprised the second largest trees in the study area with DBH of up to 56.5 cm diameter. It was most similar to old beech and oak stand with respect to canopy openesses. Nonetheless, UAV-LS reconstruction was less successful here with lower CCC

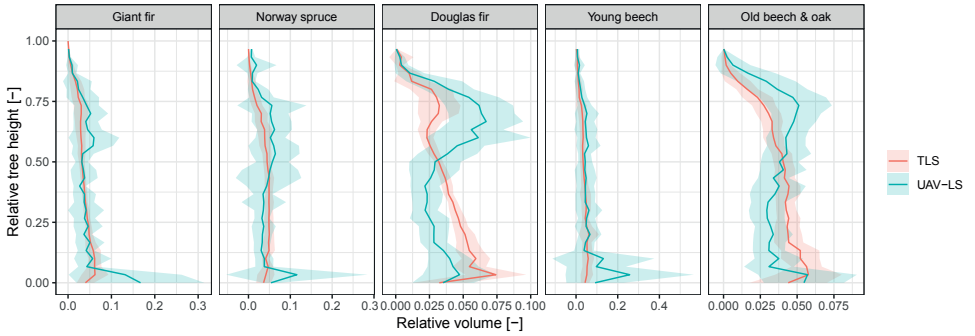

Figure 5.7: QSM volume aggregated over height. Solid centre lines represent the mean volume contribution of a height layer to the total tree volume. Relative tree height was based on the TLS point cloud height range. Coloured ribbons indicate 1 standard deviation from the mean. Each panel summarises all modelled trees of the corresponding stand.

of 0.37 and higher CV of 0.22. The bias in terms of MSD was with 0.71 m^3 substantially lower than for the old beech and oak. However, this stemmed mainly from the cancelling effect of two groups, for which volume was over- and underestimated, respectively. The overestimation could be traced to the same mechanism as in the old beech and oak stand. The crown tended to be modelled with a high number of small cylinders. The effect on the vertical distribution of volume was even stronger than in the old beech and oak stand, with 49.1 % of the total volume in the upper half of the tree in the case of UAV-LS compared to 25.7 % in the case of TLS (Figure 5.7). The group of underestimated trees turned out to be positioned at the southern and south-western edges of the study area. Here, the effect was the same as for the single outlier in the old beech and oak stand. This means due to the location of the flight lines, the trees' southern sides could not be sensed from

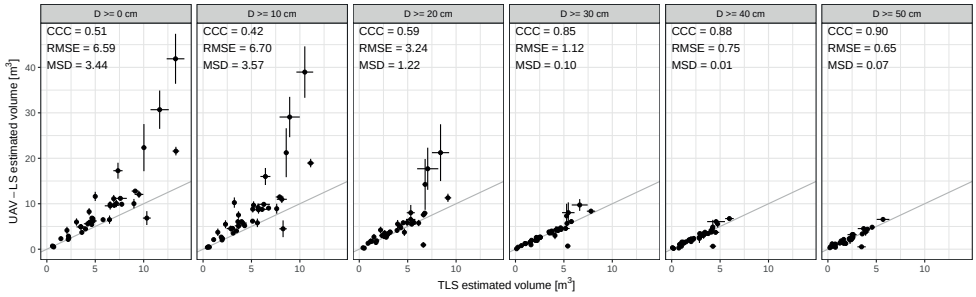

Figure 5.8: Accumulative tree volume for different diameter bins reconstruction for UAV-LS compared to TLS for old beech and oak trees. Error bars represent 1 standard deviation of the 10 QSM realisations. Grey lines are 1:1 match. Positive MSD means overestimation by UAV-LS. RMSE and MSD in m^3.

the UAV resulting in incomplete point clouds and QSMs with many small instead of few properly sized cylinders for trunks.

In the case of giant fir, UAV-LS agreed with TLS reconstructed models with CCC of 0.44 and RMSE of 1.13 m^3. Outliers could not be explained by their position within the stand as was the case for the Douglas fir trees. In fact, this stand could be observed from a UAV-LS flight line outside of the plot in the North plus from the diagonal cross line (Figure 5.1), which provided better observations from multiple directions. The vertical distribution of volume indicated a similar bias as was the case for old beech, oak and Douglas fir, but with a much lower magnitude across the tree vertical profiles (Figure 5.7). The upper halves of trees contained 35.5 % in the case of UAV-LS, while this was 25.6 % for TLS.

Despite the similar levels of agreement of UAV-LS modelled control cylinders with TLS control cylinders between giant fir and Norway spruce (Section 5.4.3), Norway spruce modelled QSMs showed less agreement in terms of QSM volume with CCC of 0.36 and RMSE of 1.32 m^3. Also, Norway spruce QSM models showed less modelling confidence than giant fir QSMs in terms of a higher CV of 0.33 for Norway spruce and 0.24 for giant fir. The denser tree coverage of the Norway spruce could be an explanation for that (Table 5.1), as it results in mutual shielding of trees from above canopy view points and therefore observation of lower and larger tree elements by UAV-LS. Additionally, the higher tree density leads to a lower number of points per tree.

The young beech stand showed the lowest comparability between UAV-LS and TLS QSMs with CCC of 0.01. Especially the RMSE of 2.14 m^3 indicated low modelling performance with respect to the maximum individual TLS QSM volume of 0.84 m^3. In particular, volume was generally overestimated with a MSD of 1.62 m^3. When inspecting the corresponding point clouds, it became clear that the point density on the trunk and branch surfaces was too low to actually represent the volume of the individuals, i.e. points formed lines for trunks instead of covering them on multiple sites. In contrast to the old beeches, the young beech trees were positioned much denser (Table 5.1) and had already almost flushed all their leaves, which hindered visibility of the lower canopy elements.

5.5 Discussion

5.5.1 Tree Segmentation

Overall, UAV-LS point clouds show potential in combination with semi-automatic segmentation of trees. Even young trees in the understorey of the old beech and oak could be identified. If a fully automatic approach is desired to achieve fast plot scale results, it can be said that recent automatic algorithms have moved away from incremental adaptation of initial algorithms and make more use of the characteristics of LiDAR data (Duncanson

et al., 2014; Eysn et al., 2015; Zhen et al., 2016). Algorithms exploit more and more the full vertical profile of high density ALS point clouds (Strîmbu and Strîmbu, 2015) and can even deliver segmentation uncertainty (Parkan and Tuia, 2018). Wallace et al. (2014a) achieved detection rates of up to 98 % with another UAV-LS system that produced point clouds with 50 points/m^2. This suggests that automatic detection and segmentation with the dataset underlying this study has the potential to achieve excellent segmentation results. These approaches should be targeted in the future.

5.5.2 Foliage Filtering

The foliage classification cross-validation with UAV-LS based on manually selected training samples generally produced high accuracies in this study (Table 5.3). However, a certain extent of foliage points remained that were subsequently modelled as small branches (Figure 5.4 and 5.5). This portion was larger for UAV-LS than for TLS and led to a much higher number of small cylinders in the upper crown for UAV-LS. Previous TLS-based studies using *TreeQSM* have skipped leaf-wood separation, but still achieved high correspondence with destructively measured AGB (Calders et al., 2015b; Gonzalez de Tanago et al., 2018; Lau et al., 2018). Together this suggests that foliage filtering prior to wood volume assessment with *TreeQSM* based on UAV-LS will require a higher attention in the future.

For improved classification of foliage, new classification approaches based on geometric features, e.g. local cluster orientation, have been proposed to overcome the ambiguity of radiometric LiDAR features (Vicari et al., 2019; Wang et al., 2018; Zhu et al., 2018). However, these methods rely on high density TLS point clouds and tests with lower density point clouds are still to be performed (Vicari et al., 2019). This is especially relevant for UAV-LS as observation geometry, point registration accuracy and point cloud density markedly differ from TLS. Another alternative for the whole volume estimation work-flow for coniferous species could be a hybrid approach as suggested by Stovall et al. (2017): they model stems of coniferous *Pinus contorta* explicitly with cylinders and make use of allometric relationships to estimate branch and needle biomass. Unfortunately, such an approach would require the establishment of an extensive database for foliage density allometric relationships.

5.5.3 QSM Modelling

The tree modelling performance of UAV-LS compared to TLS in this study needs to be regarded in the context of the challenges to produce accurate point clouds from a UAV platform. Four principal mechanisms come into question that have a stronger affect on UAV-LS point cloud accuracy than on TLS. First, the overall LiDAR sensor ranging accuracy and precision is lower for the VUX®-1UAV than the VZ400 (Table 5.2). This is likely to be the general case for miniaturised LiDAR sensors. However, LiDAR ranging

accuracy is typically the smallest error source in the whole point cloud production chain, both for UAV-LS and TLS. It can only be improved by exchanging the LiDAR sensor with a higher quality device.

Second, the larger beam divergence of the VUX®-1UAV additionally decreases point cloud accuracy. For example, at an average canopy height of 20 m and a flight height of 90 m the VUX®-1UAV produces an effective footprint of 3.5 cm at the top of the canopy, while this is 1.4 cm for the VZ400. This larger footprint leads to larger ambiguity in the point registration, hence lower spatial accuracy. As for the LiDAR ranging accuracy, beam divergence is bound to the system in use. Nevertheless, the effective divergence can be reduced by flying at lower altitudes. In forest set-ups, the flight height lower limit is restricted by the tree height and UAV observing opportunities from openings for VLOS operation.

Third, the free moving mounting of the LiDAR on a UAV produces many more degrees of freedom for the scanner positioning and orientation. In this study, the trajectory was sampled at 200 Hz for a flight time of approximately 20 min, resulting in roughly 240 000 positions. For the TLS only 118 positions — 58 upright and 58 tilted — had to be estimated. For accurate co-registration of scan lines and scan positions, planar features extracted from the point clouds are usually used to achieve the fine registration (Wilkes et al., 2017). TLS point clouds with higher point density provide more opportunities to find those features, such as even trunk surfaces or ground patches. These have to be larger in size for UAV-LS with a lower point cloud density and are therefore rarer in forests. Additionally, UAV-LS registration has to be optimised within flight lines, which can be regarded as the equivalent to scan positions in TLS. Positioning and orientation errors can be controlled to some extent with the flight path planning, with straight flight lines delivering best results, and by avoiding weather conditions with strong gusts that abruptly change flight speed and orientation.

Fourth, the perspective of the TLS from below the canopy favours correct modelling of the trunk and lower branches. UAV-LS point clouds are less dense in this region, leading to higher uncertainty in cylinder fitting. These modelling errors at lower heights can propagate into higher areas of the canopy. Especially the upper crown becomes very difficult to model under these conditions.

All together, the above-mentioned factors determine a threshold on the diameter for modelling of branches. Here, a diameter of 30 cm appeared to be the threshold for reliable volume modelling with UAV-LS (Figure 5.8). Different thresholds have been observed in TLS-based studies using cylinder fitting approaches: Hackenberg et al. (2015) found that elements with diameter $\geq$10 cm can be modelled accurately, while elements with diameter $\leq$4 cm were often overestimated. Momo Takoudjou et al. (2018) modelled branches with diameter $\geq$5 cm reliable. However, Lau et al. (2018) found that *TreeQSM* reconstructed

actual branching architecture as opposed to cumulative volume only for branches with diameter ≥30 cm.

Additionally, the above results showed that canopy structure as exemplified by the different stands in this study has a significant impact on UAV-LS QSM modelling capability when modelled with *TreeQSM*. UAV-LS QSMs showed higher agreement in terms of tree volume with TLS in open stands, and decreasing agreement in denser stands or in stands with smaller trees. The direction of this trend can also be observed when using Structure from Motion (SfM) techniques of passive camera systems (Wallace et al., 2017). Still, the detection of small understorey trees and the moderate modelling success even in dense stands speak for the application of UAV-LS in complex vertically structured forests. In comparison to TLS, UAV-LS has the advantage of fast acquisition speed and thereby larger coverage of plot area. In this study, UAV-LS acquisition required 2 h, while TLS took approximately 16 h, which is factor of eight difference. This should be considered together with possible improvements to the UAV-LS processing chain.

There are some ways that possibly improve UAV-LS QSM agreement with TLS. First, repeated flights with point cloud acquisition over the study area would increase the number of points, which increases the chance to collect trunk returns in dense stands such as the giant fir and Norway spruce stands or to penetrate the foliage of the young beech stand. Second, varying flight patterns with different headings would improve the sampling of different trunk sides and prevent edge effects such as those observed for the Douglas firs (Section 5.4.4). Third, additional layout of ground control panels could improve the flight line-to-flight line registration and therefore internal consistency of the point cloud, which could improve the modelling of smaller branches. Fourth, in closed stands like the giant fir or Norway spruce stands fitting procedures that apply more constrains could be utilised. For instance, successful identification and modelling of the trunk as a single large cylinder or cone in these coniferous species would capture the larger part of total tree volume. Also slice-wise fitting as applied in Stovall et al. (2017) for the trunk could deliver more robust results. Pitkänen et al. (2019) present another complementary procedure for coniferous species that applies modelling and quality checking over height slices. UAV-LS control cylinders showed acceptable agreement with CCC of at least 0.93 (Figure 5.3), indicating that a large cylinder or cone-shaped geometry, or slice-wise fits could be successful.

5.6 Conclusions

Recent technological developments have allowed UAV-LS to produce high density point clouds. This study compares UAV-LS explicit tree modelling with a TLS benchmark in terms of tree volume estimation. UAV-LS point cloud acquisition was considerably faster than TLS at scales relevant for satellite AGB calibration and validation. In total, 200 trees of 5 stands have been segmented and automatically modelled. UAV-LS control cylinders, which were used during model selection, generally agreed well with TLS cylinders with

RMSE in diameter between 2.26 cm and 7.90 cm. Full tree volume based on reconstructed QSMs showed differences between the examined stands. Mature beech and oak volumes were reproduced best by UAV-LS with CCC of 0.51 and RMSE of 6.59 m^3. Young beech trees showed lowest correspondence with CCC of 0.01 and RMSE of 2.82 m^3. This pointed to the fact that canopy structure, in this case tree and branch size, branch arrangement and foliage, plays a major role in tree volume estimation capabilities. Also, the impact of flight path planning could be observed to some extent with improved volume modelling when trunks were observed from multiple sites. Future studies should aim to overcome the limitations in dense canopies by increasing the point cloud density through repeated flights and adapting the flight path with respect to maximising viewing angles on the trunks.

Chapter 6

Synthesis

6.1 Main Findings

The overall objective of this thesis was to explore methods that allow efficient observations of forest structure at scales relevant to hectometric space-borne products. For this, Chapter 2 and 3 focussed on production of Leaf Area Index (LAI) high frequency time series, while Chapter 4 and 5 focussed on forest inventory metrics and Above-Ground Biomass (AGB) at hectare scale. In Chapter 1, four research questions were defined. This section summarises the answers to these questions based on the studies performed in Chapter 2 to 5. Section 6.2 reflects on these results in particular with respect to findings of other studies, upcoming developments in the field and their significance for practical validation exercises.

1. How can forest LAI be efficiently and automatically monitored over time?

Timely observations of canopy foliage are necessary in order to validate high frequency, hectometric LAI products. The validation of the time dimension can give additional clues on the sensitivity of the respective product to phenology, another land product (Land Product Validation subgroup, 2019). So far, labour-intensive manual sampling with ground instruments such as Digital Hemispherical Photography (DHP), LiCor LAI-2000 Plant Canopy Analyzer or Tracing Radiation and Architecture of Canopies (TRAC) is recommended for LAI validation (Fernandes et al., 2014). In Chapter 2, the PAI Autonomous System from Transmittance Sensors at 57° (PASTiS-57) — a transmittance system with six individual upward pointing sensors per device — was evaluated using a Radiative Transfer Model (RTM) and a field experiment with respect to automatically monitoring forest LAI and thereby tracking phenological changes.

Considering fieldwork, the PASTiS-57 proofed to be an overall robust sensor. The water-proof housing, long battery life and relative ease of use support long-term and large scale deployment with potentially multiple users. Regular visits were necessary every three months when a 1 minute sampling interval was chosen in order to read out the data. Readout could be carried out for all devices in the chosen study site within 1 hour. In comparison, the production of the Terrestrial Laser Scanning (TLS) validation time series required approximately 4 hours fo each sampling event.

The retrieval algorithm underlying PASTiS-57 is based on the gap fraction theory, which is also used for the manual LAI-2000 instrument. In this sense, PASTiS-57 is compatible with recommended LAI validation practices (Fernandes et al., 2014). Compatibility with previous standards would foster acceptance and introduction into validation campaigns. During the field experiment, PASTiS-57 data showed very high agreement in terms of phenological timing when compared to time series from illumination-independent TLS. LAI magnitude differed between the instruments, but followed directions that were reported earlier when comparing passive sensors and TLS (Woodgate et al., 2015). Future research

should aim to establish inter-calibration procedures between different instruments. Also, the high frequency dynamics of the derived time series in relation to illumination conditions and rain events should be investigated.

Experimental implementation of the PASTiS-57 sensor within the Discrete Anisotropic Radiative Transfer (DART) RTM allowed testing the general sensing principle and showed general robustness under varying Leaf Angle Distribution (LAD), leaf Chlorophyll a and b (C_{ab}) and Solar Zenith Angle (SZA) for homogeneous canopies. Only planophile and erectophile LADs produced larger deviations exceeding 20 % difference from the true value. Heterogeneous stands with explicit tree representations produced larger deviations due to clumping effects, especially with sparse tree cover. The limited number of PASTiS-57 viewing directions prevents proper canopy clumping assessment.

Branch material was not taken into account in the RTM experiments, as trees are modelled following a 'lollipop' model with single straight trunks and a spherical crown. Also in the field experiments, neither PASTiS-57 nor TLS retrievals distinguished foliage from woody material. In fact, this is often not the case for forest LAI validation measurements (Bréda, 2003; Fernandes et al., 2014). Still, the RTM approach proved useful in order to assess the accuracy of the retrieval approach under various canopy configurations. In forest settings, RTM-based approaches sometimes remain the only way of accuracy and uncertainty assessment of biophysical variables (Adams et al., 2016; Nightingale et al., 2018b). Detailed forest reconstructions based on TLS can provide virtual stands that can be exploited for these purposes (Calders et al., 2018a) and foster uncertainty assessment, including the contribution of branch material to the error.

2. How is prediction performance of hybrid RTM-Machine Learning Regression Algorithm (MLRA) forest LAI-retrieval chains affected by their individual processing chain parts?

ESA's Sentinel-2 has been anticipated for operational production of land-cover and biogeophysical variable maps (Drusch et al., 2012). Retrieval of biophysical variables was extensively tested in pre-launch field campaigns with simulated observations in particular for agricultural areas (Atzberger and Richter, 2012; Delegido et al., 2011; Frampton et al., 2013; Verrelst et al., 2015b). Applications in forested areas were mostly attempted post-launch (Korhonen et al., 2017; Majasalmi and Rautiainen, 2016; Vafaei et al., 2018). Even fewer studies investigated the usability of Sentinel-2 for forest structure and in particular LAI (e.g. Korhonen et al., 2017). In combination with the Landsat family of missions, high frequency observations at decametric resolution are possible that can serve to upscale ground-reference measurements as performed in Chapter 2. Chapter 3 investigated an LAI retrieval approach for local, multi-temporal estimation of LAI with Sentinel-2A and Landsat 7/8, and especially how individual elements in the processing chain affect the prediction performance.

Of the investigated elements, adding Additive Independent (AI) noise to the RTM-produced database of spectra had the strongest positive influence on the prediction performance. This procedure was implicitly used in previous studies, and was typically related to the error originating from the sensor and atmospheric correction applied (Baret et al., 2007). However, this has not been systematically evaluated. Also, a clear definition of the error model has typically not been provided. Here, the wavelength independent terms of the noise model of Weiss and Baret (2016) were implemented and error terms were systematically varied. The resulting importance of added noise suggests that noise should be treated as an additional hyper-parameter in the training of hybrid retrieval schemes employing RTMs and MLRAs. Other elements of the inversion processing chain had less impact on the prediction performance. In case of the insertion of a leaf chemical prior, this is particularly important, as the corresponding collection of field data is labour-intensive.

In Chapter 3, LAI retrieval was attempted using as few assumptions on canopy architecture and as few field data as possible. This is relevant in scenarios when only few reference measurements are available and these have to be used for independent validation of the retrieval. However, with an increasing amount of regularly acquired ground data as presented in Chapter 2, data driven approaches can be applied. Additionally, detailed forest scenes can be generated based on TLS forest reconstructions (Calders et al., 2018a), assuming little change of forest macro structure (i.e. standing tree density, branching behaviour) and terrain.

A particular disadvantage of the method presented in Chapter 3 is the need for a homogeneous area. Even though validation efforts in general should preferably be performed in homogeneous areas with small variation in land-cover, decametric sensors such as Sentinel-2 can provide the means to assess the spatial heterogeneity across validations sites, plus their temporal dynamics. This could be exploited to turn formerly unsuitable sites into suitable ones by characterising their spatial characteristics in detail. For heterogeneous sites, a rigid production of a single database for the MLRA learning restricts the approach to a single species composition or land-cover type. Therefore, adaptation strategies to varying macro-structure should be found.

3. What is the capability of UAV-LS to estimate canopy height and DBH?

Unmanned Aerial Vehicle (UAV) technology has evolved rapidly in the last years and applications in forest inventories are being targeted (Torresan et al., 2016). Combining UAV with LIght Detection And Ranging (LiDAR) into Unmanned Aerial Vehicle Laser Scanning (UAV-LS) has been technologically challenging due to the high accuracy requirement of LiDAR sensors with respect to the platform's position and orientation. In Chapter 4, the RiCOPTER with VUX®-1UAV (VUX®-1UAV) was tested with respect to canopy height and Diameter at Breast Height (DBH) estimation.

For this purpose, the UAV-LS derived Canopy Height Model (CHM) and DBH estimates were compared with TLS over a 100 m × 180 m area. UAV-LS produced on average 11.5 cm higher CHMs, which can be explained with TLS possibly not reaching the top of canopy. UAV-LS DBH reached high correlation and a Root Mean Square Error (RMSE) of 4.24 cm compared to TLS. However, DBH could not successfully be estimated for 19 out of 58 sample trees (33 %), especially in dense coniferous stands.

On the one hand, UAV-LS proved to be a very fast tool for the production of the point clouds. The fieldwork required was 2 hours for the UAV-LS acquisition, while the same area required 2 days for the TLS work. The difference would probably be much larger in tropical environments where TLS fieldwork is slowed by understorey and visibility requirements for the setting of the retro-reflective targets (Wilkes et al., 2017). On the other hand, the reduced success in DBH modelling limits the usability of UAV-LS for forest inventories. Intensified flight patterns with larger diversity of flight directions as well as repeated flights should be tested in future studies. Additionally, UAV are typically restricted to Visual Line of Sight (VLOS) operations in forest environments and by aeronautical regulations. This means UAVs can only be operated from large forest openings, where they are visible during the whole flight time.

4. How can UAV-LS contribute to tree volume assessment?

Upcoming space-borne missions focussing on AGB estimation require calibration and validation data, preferably at scales similar to the satellites' footprints. TLS and tree reconstruction is discussed as a breakthrough technology for unbiased estimation of tree volume and subsequently AGB (Calders et al., 2015b; Disney et al., 2018), especially in the case of large tropical trees (Gonzalez de Tanago et al., 2018; Momo Takoudjou et al., 2018). However, fieldwork is tedious and labour-intense. Chapter 5 investigated the UAV-LS RiCOPTER with VUX®-1UAV with respect to explicit tree volume modelling.

In comparison to state-of-the-art TLS volume reconstruction, UAV-LS estimated volume reliably for trunks and branches with diameter ≥30 cm in a mature beech and oak stand. When smaller branches were to be included, UAV-LS generally overestimated total tree volume, mainly due to an excess of small cylinders modelled in the canopies. In the upper parts of the trees, small branches with small inter-element space led to confusion to which branch points belong. This led to higher requirements in terms of point cloud accuracy compared to lower parts of the trees. Additionally, volume estimation differed with stand characteristics. For example, young beech trees that already carried a substantial amount of foliage during the sampling could most often not be modelled correctly due to too low number of points along the lower trunks. Coniferous species with high number of small branches at low heights shielded their trunks and thereby prevented proper modelling.

Overall, the detailed validation of tree reconstructions beyond summarising statistics is difficult. Some previous studies differentiated between branch diameter classes when

comparing TLS reconstruction and destructively harvested sample trees (Hackenberg et al., 2015; Lau et al., 2018; Momo Takoudjou et al., 2018; Stovall et al., 2017). However, actual tree architecture has rarely been validated. This means that model agreement with ground truth was only established on a statistical basis, which is also the case for this study. This hampers detailed analysis of the tree reconstruction accuracy, especially with small branches, and should be addressed in future studies. Another issue that could not be addressed with the dataset available in Chapter 5 was if the poor modelling capability of small branch total volume was due to the lower point density or due to the most likely lower spatial accuracy of the UAV-LS point cloud.

6.2 Reflection and Outlook

This work was motivated by the growing need for rigorous and efficient calibration/validation data and procedures for Earth Observation (EO) land products. Rigorous validation is relevant in the wider context of climate observations and the implementation of the Committee on Earth Observing Satellites (CEOS) targets. Additionally, independent validation data is helpful in the full uncertainty characterisation of land products and validation of traceability chains (Nightingale et al., 2018a). This thesis contributes to these topics in the domain of forest structure variables with a special focus on meeting hectometric EO temporal and spatial resolutions.

The remainder of this section places this thesis' findings in a wider context of developments in the field of forest structure assessment from ground and proximal sensing techniques as well as EO land product calibration/validation. The latter will also expand the discussion towards non-forest vegetation types.

6.2.1 Wood-Leaf-Separation

The differentiation between woody and leaf material is particularly important in the context of LAI estimation in forest environments, because woody material produces a bias in LAI measurements. For example, Hu et al. (2016) found a contribution of 14 to 28 % woody material to Plant Area Index (PAI) across four larch, birch and pine plots. As briefly described in Chapter 2, the differentiation between woody and leafy material is not made by many fast, indirect methods and instruments, such as DHP, LAI2000 plant canopy analyser or PASTiS-57. Proper measurements are therefore too complicated and/or time consuming, and hence skipped. This leads to occasionally labelling PAI measurements as LAI (e.g. Chen et al., 1997). However, the proper definition of the LAI product can be a significant source of error in validation and inter-comparison (Weiss et al., 2007).

A practical approach for deciduous species can be the combined use of litter-traps and indirect methods, as presented in Chapter 3. On the one hand, litter-traps are among the

most accurate direct methods for LAI estimation if spatial sampling is sufficient for the study area (Chen et al., 1997; Jonckheere et al., 2004; Leuschner et al., 2006; Liu et al., 2015). On the other hand, indirect methods can deliver a high temporal resolution of the canopy development. The combination of both approaches delivers accurate, frequent observations of LAI. The high frequency observations from the PASTiS-57 in Chapter 2 could be improved with such an approach.

Measurement of total LAI with litter-traps is not possible in evergreen forests as it is in deciduous forests, because leaves can be exchanged throughout the year, depending on the species. Litter-traps can be adapted to this by simultaneously monitoring leaf growth (Wang et al., 2017). However, this is labour-intensive and requires access to leaf material from different heights in the canopy. Furthermore, multiple species within the plot require separate growth monitoring. This favours indirect methods. In the case of passive sensors, imaging sensors with additional Near-Infrared (NIR) channels can help to differentiate between wood and leaf due to the high transmittance of leaves in the NIR. Kucharik et al. (1998) and Zou et al. (2009) present examples for such devices. Conceptually, both devices retrieve PAI from visible and Woody Area Index (WAI) from NIR images, and then subtract WAI from PAI to derive LAI. Nowadays, NIR-enabled webcams for surveillance become as easily accessible as digital cameras when DHP started to be explored. Alternatively, the transmission filters for digital cameras can be exchanged in order to let NIR radiation pass through and enable NIR photography, as described in several online sources (e.g. Gibson, 2019). However, despite this advantage no significant further research has been conducted on this topic.

Developments with respect to wood-leaf-separation have been more dynamic in the field of TLS, possibly due to relevance of foliage identification for explicit tree modelling (Vicari et al., 2019). For the exploitation of the spectral domain with TLS, only few experimental systems have been presented like the Salford Advanced Laser Canopy Analyser (SALCA) (Danson et al., 2014; Mark Danson et al., 2018) and the Dual-Wavelength Echidna® Lidar (DWEL) (Douglas et al., 2015; Li et al., 2018a; Li et al., 2018b) systems. Both employ lasers around 1065 nm and 1545 nm, the vegetation peak reflectance and water absorption features, respectively (Danson et al., 2014), in order to separate wood from foliage. These instruments are still in development and challenges in the construction of multi-spectral LiDAR, like laser alignment, reflectance calibration and ambiguity of the reflectance signal in case of partial returns, has to be acknowledged (Vicari et al., 2019). Additionally, current devices have limited capabilities with respect to regular or large scale field data acquisition, due to heavy weight, long scanning times and short range. Single-wavelength TLS could also be employed, but the reflectance signal is typically ambiguous and limited for use in very accurate separation of woody and leaf compartments as required for LAI estimation. This is in contrast to the use in Chapter 5, where separation was only targeting candidates with high chance of being wood, instead of an accurate classification.

Alternatively, methods can exploit the geometric domain for wood-leaf-separation. This typically involves production of classification features based on the local point neighbourhood (Ma et al., 2016; Wang et al., 2018) or analysis of the connectivity graph that a tree point cloud represents (Vicari et al., 2019). Based on scans from DWEL instruments, Li et al. (2018a) combine spectral and geometric features in order to highlight the complementing advantages for classification of different canopy parts by using both domains.

From this point in time, it looks most likely that geometric TLS approaches will be favoured in the near future, at least for experimental plots and in the tropics. The lacking use and demonstration of multi-spectral imagers, and relatively wide distribution of commercial single-wavelength TLS plus the successful test of geometric separation algorithms speak for this development. Nonetheless, operational applications like monitoring at ecosystem network sites of for example the Integrated Carbon Observation System (ICOS) requires probably less expensive approaches, as LAI is typically only an auxiliary measurement. This would speak for a renewed and deeper investigation of multi-spectral imagers with fish-eye optics.

6.2.2 Sensor Networks plus Sentinels: Towards Automated LAI Validation

The Global Climate Observing System (GCOS) has set the target to operationalise the generation of 10-day LAI and Fraction Absorbed Photosynthetically Active Radiation (FAPAR) products at 5 km and 50 m by 2020 (WMO, 2016, action T40). The MODerate-resolution Imaging Spectroradiometer (MODIS) LAI/FAPAR product MCD15A3H is already now produced at 4-day interval and 500 m resolution (Myneni et al., 2015). However, Baret et al. (2006) state that validation efforts including multiple sampling events spread over the season are expensive both with respect to time and human resources. This is in contrast to the goal of reaching Land Product Validation (LPV)-subgroup validation stage 4 for LAI, which includes the repeated validation of products. Subsequently also temporal accuracy should be targeted, i.e. timing of onset of growing season and senescence phase. These requirements support the idea of automated sensors within sensor networks and automatic distribution of validation data.

Generally, sensor networks and in particular Wireless Sensor Networks (WSNs) have found numerous applications in various fields such as animal, infrastructure, patient or environmental monitoring (Yick et al., 2008). They consist of several sensor nodes that each contain one or more sensors, a (micro) processor, a power supply and a radio connection. In the context of LAI validation, three levels of networks could be distinguished that are in line with previously agreed validation strategies (Morisette et al., 2006): first, the local level where actual LAI measurements take place and raw data is locally transmitted to a central server node (Figure 6.1). This local network's footprint would correspond to the traditional Elementary Sampling Unit (ESU) (Section 1.3 on page 5). Second, several

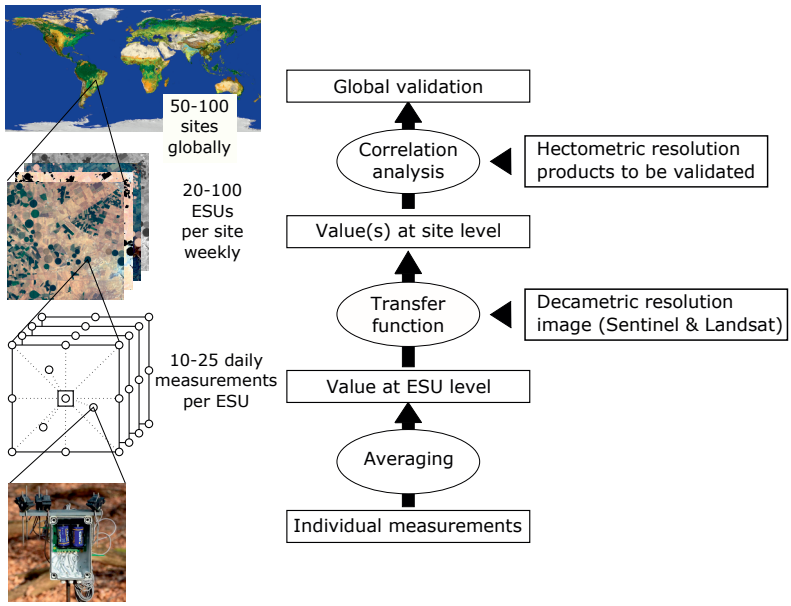

Figure 6.1: Modified global LAI product validation procedure with ground sensors connected via WSNs, and regular Sentinel and Landsat observations for local/regional upscaling. Image credits: ESA (2005), ESA and Université Catholique de Louvain (2010).

local ESU-nodes transmit their data to a data server that represents a validation site. Third, data packages are transmitted from site nodes to central global servers. Such an architecture is not new to environmental monitoring. For example, within RadCalNet, local stations observe atmospheric properties like aerosol properties and automatically produce Top Of Atmosphere (TOA) reflectance factors, which can be accessed via a web-portal (RadCalNet, 2019). The missing core technology to make this approach possible for LAI validation is an accepted automatic sensor.

Such a sensor would need to fulfil certain requirements derived from the common practices for LAI validation (Fernandes et al., 2014). This is primarily the compliance with transmission/gap fraction theory based retrieval, which would support combined use and inter-calibration with accepted sensors in order to produce long records of validation data. Furthermore, such a sensor should allow understorey assessment in forests to adapt to the field of view of space-borne missions. Additionally, wood-leaf-separation (Section 6.2.1) and clumping appraisal (Section 2.4) should be possible to translate gap fraction measurements into effective green LAI. These theoretical features need to be paired with a robust physical sensor design that resists environmental stresses and is easy to handle by a wide range of users. Easy maintenance with respect to repairs in case of physical damage and software

update should also be targeted. Finally, (wireless) communication interfaces are needed for the integration in a WSN, and possibly real-time sensor health and status monitoring.

In this context, the PASTiS-57 fulfils some of these criteria, namely the compliance with accepted retrieval methods, to a limited extent clumping appraisal when operated as a single sensor, and robustness in the field (Chapter 2). Based on the experimental devices by Kucharik et al. (1998) and Zou et al. (2009), NIR imaging sensors could be further explored. In this context, the rapidly developing and easy accessible Raspberry Pi micro-computers combined with NIR-camera modules have some potential. For example, Valle et al. (2017) tested a Raspberry Pi with Pi NoIR NIR-enabled camera module for lettuce PAI estimation and field phenotyping. Kirby et al. (2018) examined distortion properties of the Pi NoIR camera module and compared them with the much used Nikon Coolpix, but did not derive LAI. Additionally, Li et al. (2015b), Bauer et al. (2016), and Fan et al. (2018) designed sensor systems for field crop LAI monitoring, with the system of Li et al. (2015b) including WSN features like remote server upload of data. Qu et al. (2014b) and Qu et al. (2014a) actually designed a local sensor network for LAI and canopy clumping retrieval, and operated it for 2 months in a larch stand. Experiences from these first trials could be exploited to construct WSN systems for unattended data acquisition in forest plots. In larger sites, these systems could be combined with illumination-independent LiDAR-based monitoring systems for inter-calibration (Section 1.4 on page 9).

Based on the data-streams of ground-based WSNs, local to regional LAI maps could be produced regularly (Figure 6.1). With a growing database of ground-based observations, more and more data-driven approaches like MLRAs for regional upscaling can be tested (Verrelst et al., 2012; Verrelst et al., 2015b). Yin et al. (2019) demonstrate such an approach based on the WSN introduced by Qu et al. (2014b) and Gaussian process regression for a 5 km×5 km study area in northern China. These approaches are supported by regular and dense Sentinel-2 observations as well as Landsat 8. C-band Synthetic Aperture Radar (SAR) time series from for example Sentinel-1 have also shown some potential in picking up the phenological development of forests (Rüetschi et al., 2018) and LAI (Manninen et al., 2013), and could support the modelling of the pheno-phases.

6.2.3 UAV for Forest Structure Assessment and Land Product Validation

Opportunities and Challenges for UAV in Forest Structure Assessment

UAVs have experienced an increase in usage in forestry, which is not only documented by an increase in publications (Figure 1.2 on page 10), but also in review articles (Adão et al., 2017; Pádua et al., 2017; Torresan et al., 2016). Major opportunities offered by UAV in forestry applications are their top of canopy perspective in places where infrastructure like scaffold towers is not available and their low acquisition costs. Especially the latter constantly appears as an advantage of UAVs in review studies (Aasen et al., 2018; Adão et al., 2017; Anderson and Gaston, 2013; Colomina and Molina, 2014; Stöcker et al.,

2017; Torresan et al., 2016). Additionally, off-the-shelf software tools, in particular for photogrammetric processing and production of Digital Surface Models (DSMs), have helped UAVs to be explored as a tool in forest applications (e.g. Fraser and Congalton, 2018; Lisein et al., 2013; Wallace et al., 2016; Zarco-Tejada et al., 2014). Hence, Aasen (2017) has coined the adoption of UAVs as a "democratisation of geospatial data acquisition". Of course, UAVs have strongly increased the number of self-enabled EO data producers. But still, quality applications with high demands in terms of radiometric and geometric accuracy require a certain investment in material as well as the respective know-how, which translates into hiring of trained personnel, payment of external companies or time investment in the form of training of present personnel. This also applies to the licensing and maintenance.

Major limitations for UAVs in forestry and other scientific applications still relate to aeronautical regulations. Compared to mature regulations for commercial air-traffic, regulations for UAVs are still in preparation in some countries, need to take into account latest technological developments like autonomous flight behaviour in the case of detect-and-avoid-autopilots and are therefore changing rapidly. A particular challenge for the governing bodies is the consideration of private and recreational UAV users. These users are more prevalent for UAV than for manned aircraft like gliders and ultra-light aircraft due to the low entry level costs for UAV, and can cause harm due to lack of training, experience or knowledge. Additionally, UAV legal frameworks have been developed on a country-level basis and still need international coordination. For example, while the conversion of commercial licences is well regulated and formalised for manned aircraft, conversion or acknowledgement still need to be decided on a case by case basis for UAV licenses.

In practice, UAVs appear not to be an obvious choice for forest applications due to the required clear take-off and landing area, in particular for fixed wing systems. Additionally, aeronautical regulations or technical restrictions may require flights to be carried out within VLOS, which is defined as a maximum distance of 500 m from the observer in the Netherlands for example, and can be very limited in forest environments. Therefore, suitability for given plots has to be estimated before flight operations. In the future, with maturing technology and legislation, these limitations might be mitigated with communication relay systems, in which additional UAV operate as communication links and observers for the primary, sensor-carrying system (de Alcantara Andrade et al., 2018). Such a procedure in combination with Vertical Take-Off and Landing (VTOL) UAV could define the limit of UAV operability in dense forests with minimal options for take-off.

Considering LiDAR-based sensors for UAV in forest structure assessments, there has only been a limited contribution of well suited applications and their limitations to UAV-LS. This took place for Airborne Laser Scanning (ALS) (large scale mapping, CHM and Individual Tree Detection (ITD)) and TLS (up to plot-scale mapping, AGB and explicit

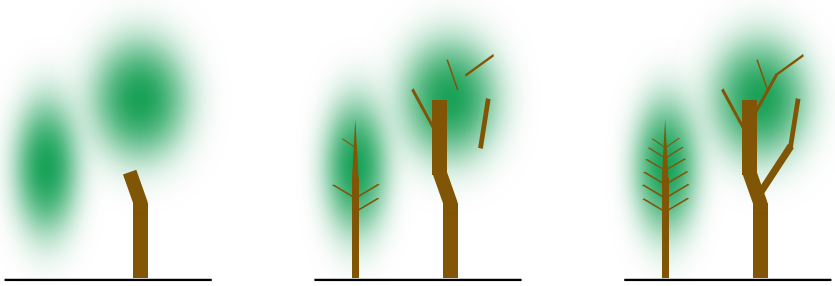

(**a**) Minimal capture of trunks, ALS-like

(**b**) Incomplete capture of trunks and large branches

(**c**) Full 3D geometry, TLS-like

Figure 6.2: Possible levels of detail at which different LiDAR can resolve woody canopy elements (brown) and foliage (green).

tree structure). But it appears likely that UAV-LS will differentiate according to the requirements for detail of the application. This is because the ability to resolve certain canopy elements is primarily driven by the delivered point cloud density and accuracy, which in turn is determined by the quality and price of the UAV-LS system. Custom-built prototypes are located at the low density end of this spectrum and can produce point clouds with densities of $<100\,\text{points/m}^2$ (Wallace et al., 2012, e.g.). Point clouds from these systems are similar to conventional ALS and thus can resolve only large elements like single trees and large trunks, but small branches and leaf material have to be treated as a random medium (Figure 6.2a). Applications are oriented towards low cost substitution of ALS for local plots like CHM production, ITD, and crown parameter estimation (Balsi et al., 2018; Wallace et al., 2014a; Wallace et al., 2014b). In the context of AGB estimation, the derived parameters can be used in Allometric Scaling Equations (ASEs) to derive AGB. In this sense, low cost UAV-LS could help to expand the number of plots in the tropics or extend the spatial footprint of traditional inventory plots. At the same time, low-density UAV-LS could help to retrieve LAI over large plots, because LAI retrieval often relies only on a turbid medium assumption of the canopy, which can be satisfied by low density point clouds.

UAV-LS for Explicit Modelling, AGB and LAI Retrieval

With respect to UAV-LS systems delivering high density point clouds, the principal question will be which level of detail of canopy elements can be resolved. This is particularly relevant with respect to dense, evergreen tropical forests, where new AGB calibration data is most relevant for future space-borne missions. In this context, Chapter 4 and 5 explored the use of the RiCOPTER VUX®-1UAV system similar to how TLS would be used, i.e. deriving full geometric detail (Figure 6.2c), but in a temperate forest with only few foliage during

spring. Another flight campaign took place at the Speulderbos site in the summer of 2017 using similar flight path patterns as in Chapter 4 and 5. The closed canopy did not allow easy manual identification of the trunks in the point clouds. Recently, another campaign with the same RiCOPTER system was conducted in different sub-tropical eucalyptus forests in Australia and showed good penetration for canopies with gaps, but low penetration in closed stands (Harm Bartholomeus, personal communication). Mitigating options like repeated flights need to be tested in dense tropical forests in order to draw final conclusions on the applicability of discrete geometric modelling. Alternatively, strategies that exploit semi-discrete point clouds need to be explored. Semi-discrete in this context refers to point clouds that do not capture the full 3D geometric structure of single trees, but rather random trunks and branches, especially those that are favoured by observation opportunities like canopy openings and sparse understorey, and do not allow to connect single elements due to too large spaces in between (Figure 6.2b). Such a strategy could involve ASE relationships based on branch diameters at arbitrary heights instead of only the DBH. Calibration for those ASE would need to be extracted from TLS reconstructions, as field techniques would be tremendously complicated. However, in practice the advantages of high-end UAV-LS need to be weighed against their disadvantages in the field, which are mainly related to their relatively large size, weight and costs compared to UAVs carrying a multi-spectral camera.

Apart from explicit geometric modelling, high resolution and spatially explicit PAI/LAI retrieval might also require high density UAV-LS. In those cases, voxel-based approaches are needed in contrast to gap fraction approaches to retrieve per voxel Plant Area Volume Density (PAVD) in 3D and subsequently PAI maps (Pimont et al., 2018). The 3D retrieval requires a sufficient number of pulses to reach each voxel in the study area in order to make unbiased and high confidence estimates of PAVD. Pimont et al. (2018) concluded that most estimators found in the literature exhibit substantial uncertainty when the number of pulses that reach a voxel falls below 30. Before this background, Figure 6.3 shows the number of pulses that cross each voxel for the dataset used in Chapter 4 and 5 at two canopy height layers with a similar map extent as Figure 4.2 on page 77. Characteristic stripes perpendicular to the flight paths are recognisable that were produced when the RiCOPTER performed course correction to follow the pre-programmed path. Concerning the count of pulses that cross each voxel, a median of 530 ($Q_1 = 131$, $Q_2 = 1923$) pulses could be found at 25 m a.g.l., while this were only 205 ($Q_1 = 50$, $Q_2 = 577$) at 17.5 m. This reduced to 88 ($Q_1 = 23$, $Q_2 = 239$) at 2.5 m and shows that even for a high density point cloud with 4059 points/m^2 on average a proper characterisation of the lower canopy levels can become challenging when fine spatial resolution and low bias is required.

UAVs for Land Product Validation

UAVs and related sensors have been developed and tested for the estimation of various vegetation and land surface parameters like LAI (Chianucci et al., 2016; Duan et al.,

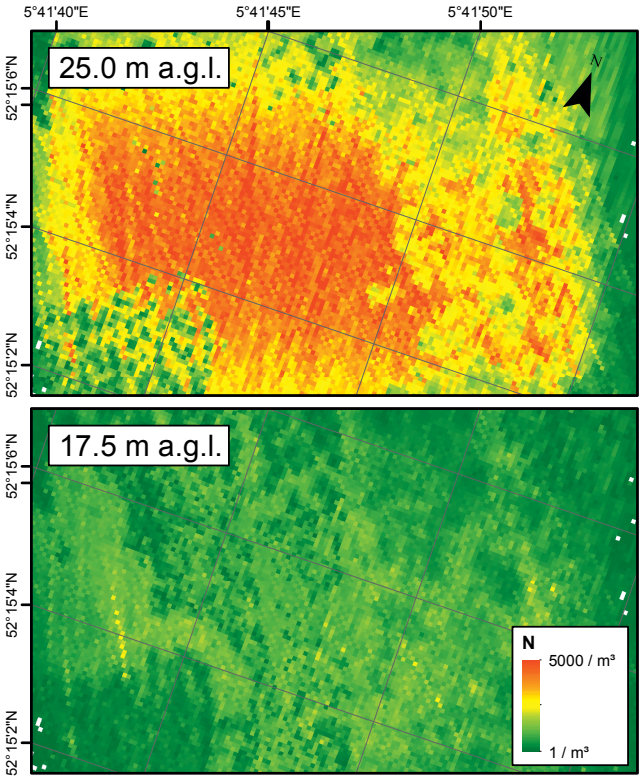

Figure 6.3: Number of pulses (N) crossing each voxel over Speulderbos during early spring campaign at 1 m voxel edge length at different heights above ground level. For the UAV-LS dataset used in Chapter 4 and 5.

2014; Roosjen et al., 2018; Roth et al., 2018; Tian et al., 2017), C_{ab} (Jay et al., 2018; Roosjen et al., 2018), albedo (Boehmler et al., 2018), FAPAR (Tewes and Schellberg, 2018), vegetation indices (Brede et al., 2015; Capolupo et al., 2015), vegetation phenology (Klosterman et al., 2018; Klosterman and Richardson, 2017), forest AGB (Lin et al., 2018; Puliti et al., 2015) and Land Surface Temperature (LST) (Berni et al., 2009; Hoffmann et al., 2016; Reineman et al., 2013; Zarco-Tejada et al., 2012). Best practices for multi- and hyper-spectral data acquisition are being established (OPTIMISE, 2019; SENSECO, 2019). This indicates a level of readiness of UAV-related methods to become trustworthy measurements with traceable uncertainties.

Land product validation exercises often struggle to meet the spatial footprint of the space-borne missions under investigation. This is counteracted with a selection of large-scale homogeneous calibration sites or upscaling with costly airborne imagery. Employing UAVs

could permit alternative validation strategies that bridge the gap between high-quality local point measurements and the space-borne sensor's footprint, or provide stand-alone observations altogether. In fact, the LPV best practice guide for AGB is planned to cover UAV-LS and its possible future developments (Martin Herold, personal communication). Additionally, GCOS suggests to employ UAVs to improve the spatial coverage of albedo measurements (WMO, 2016). For other land products, UAVs applications are similarly straight forward, like Vegetation Indices (VIs) and LST. The major challenges that have to be tackled are the high demands in sensor accuracy and (SI-)traceability. Finally, UAV-based methods could be integrated with automated sensors (Section 6.2.2) in order to provide local, regularly updated products at (sub-)metric resolution.

References

Aasen, H. (2017). "State-of-the-art in UAV remote sensing survey - First insights into applications of UAV sensing systems". *International Archives of the Photogrammetry, Remote Sensing and Spatial Information Sciences - ISPRS Archives* 42.2W6, 1–4. DOI: 10.5194/isprs-archives-XLII-2-W6-1-2017.

Aasen, H., E. Honkavaara, A. Lucieer, and P. Zarco-Tejada (2018). "Quantitative Remote Sensing at Ultra-High Resolution with UAV Spectroscopy: A Review of Sensor Technology, Measurement Procedures, and Data Correction Workflows". *Remote Sensing* 10.7, 1091. DOI: 10.3390/rs10071091.

Adams, J., N. Gobron, J.-l. Widlowski, and C. Mio (2016). "A model-based framework for the quality assessment of surface albedo in situ measurement protocols". *Journal of Quantitative Spectroscopy and Radiative Transfer* 180, 126–146. DOI: 10.1016/j.jqsrt.2016.04.005.

Adão, T., J. Hruška, L. Pádua, J. Bessa, E. Peres, R. Morais, and J. J. Sousa (2017). "Hyperspectral imaging: A review on UAV-based sensors, data processing and applications for agriculture and forestry". *Remote Sensing* 9.11. DOI: 10.3390/rs9111110.

Anderson, K. and K. J. Gaston (2013). "Lightweight unmanned aerial vehicles will revolutionize spatial ecology". *Frontiers in Ecology and the Environment* 11.3, 138–146. DOI: 10.1890/120150.

Asner, G. P. and J. Mascaro (2014). "Mapping tropical forest carbon: Calibrating plot estimates to a simple LiDAR metric". *Remote Sensing of Environment* 140, 614–624. DOI: 10.1016/j.rse.2013.09.023.

Atzberger, C. (2000). "Development of an invertible forest reflectance model The INFORM-Model". In: *A decade of trans-European remote sensing cooperation, Proceedings of the 20th EARSeL Symposium*. Ed. by M. Buchroithner. Dresden, 39–44.

Atzberger, C. and K. Richter (2012). "Spatially constrained inversion of radiative transfer models for improved LAI mapping from future Sentinel-2 imagery". *Remote Sensing of Environment* 120, 208–218. DOI: 10.1016/j.rse.2011.10.035.

Avitabile, V., M. Herold, G. B. Heuvelink, S. L. Lewis, O. L. Phillips, G. P. Asner, J. Armston, P. S. Ashton, L. Banin, N. Bayol, N. J. Berry, P. Boeckx, B. H. de Jong,

B. Devries, C. A. Girardin, E. Kearsley, J. A. Lindsell, G. Lopez-Gonzalez, R. Lucas, Y. Malhi, A. Morel, E. T. Mitchard, L. Nagy, L. Qie, M. J. Quinones, C. M. Ryan, S. J. Ferry, T. Sunderland, G. V. Laurin, R. C. Gatti, R. Valentini, H. Verbeeck, A. Wijaya, and S. Willcock (2016). "An integrated pan-tropical biomass map using multiple reference datasets". *Global Change Biology* 22.4, 1406–1420. DOI: 10.1111/gcb.13139.

Baccini, A., S. J. Goetz, W. S. Walker, N. T. Laporte, M. Sun, D. Sulla-Menashe, J. Hackler, P. S. Beck, R. Dubayah, M. A. Friedl, S. Samanta, and R. A. Houghton (2012). "Estimated carbon dioxide emissions from tropical deforestation improved by carbon-density maps". *Nature Climate Change* 2.3, 182–185. DOI: 10.1038/nclimate1354. arXiv: 1504.00980.

Baccini, A., N. Laporte, S. J. Goetz, M. Sun, and H. Dong (2008). "A first map of tropical Africa's above-ground biomass derived from satellite imagery". *Environmental Research Letters* 3.4. DOI: 10.1088/1748-9326/3/4/045011.

Balsi, M., S. Esposito, P. Fallavollita, and C. Nardinocchi (2018). "Single-tree detection in high-density LiDAR data from UAV-based survey". *European Journal of Remote Sensing* 51.1, 679–692. DOI: 10.1080/22797254.2018.1474722.

Balzarolo, M., K. Anderson, C. Nichol, M. Rossini, L. Vescovo, N. Arriga, G. Wohlfahrt, J. C. Calvet, A. Carrara, S. Cerasoli, S. Cogliati, F. Daumard, L. Eklundh, J. A. Elbers, F. Evrendilek, R. N. Handcock, J. Kaduk, K. Klumpp, B. Longdoz, G. Matteucci, M. Meroni, L. Montagnani, J. M. Ourcival, E. P. Sánchez-Cañete, J. Y. Pontailler, R. Juszczak, B. Scholes, and M. Pilar Martín (2011). "Ground-based optical measurements at European flux sites: A review of methods, instruments and current controversies". *Sensors* 11.8, 7954–7981. DOI: 10.3390/s11087954.

Banskota, A., S. P. Serbin, R. H. Wynne, V. A. Thomas, M. J. Falkowski, N. Kayastha, J. P. Gastellu-Etchegorry, and P. A. Townsend (2015). "An LUT-Based Inversion of DART Model to Estimate Forest LAI from Hyperspectral Data". *IEEE Journal of Selected Topics in Applied Earth Observations and Remote Sensing* 8.6, 3147–3160. DOI: 10.1109/JSTARS.2015.2401515.

Baret, F., O. Hagolle, B. Geiger, P. Bicheron, B. Miras, M. Huc, B. Berthelot, F. Niño, M. Weiss, O. Samain, J. L. Roujean, and M. Leroy (2007). "LAI, fAPAR and fCover CYCLOPES global products derived from VEGETATION. Part 1: Principles of the algorithm". *Remote Sensing of Environment* 110.3, 275–286. DOI: 10.1016/j.rse.2007.02.018.

Baret, F., J. T. Morissette, R. A. Fernandes, J. L. Champeaux, R. B. Myneni, J. Chen, S. Plummer, M. Weiss, C. Bacour, S. Garrigues, and J. E. Nickeson (2006). "Evaluation of the representativeness of networks of sites for the global validation and intercomparison of land biophysical products: Proposition of the CEOS-BELMANIP". *IEEE Transactions on Geoscience and Remote Sensing* 44.7, 1794–1802. DOI: 10.1109/TGRS.2006.876030.

Barraza, V., F. Grings, P. Ferrazzoli, M. Salvia, M. Maas, R. Rahmoune, C. Vittucci, and H. Karszenbaum (2014a). "Monitoring vegetation moisture using passive microwave and optical indices in the dry chaco forest, Argentina". *IEEE Journal of Selected Topics in Applied Earth Observations and Remote Sensing* 7.2, 421–430. DOI: 10.1109/JSTARS.2013.2268011.

Barraza, V., F. Grings, Paolo Ferrazzoli, A. Huete, N. Restrepo-Coupe, J. Beringer, E. V. Gorsel, and H. Karszenbaum1 (2014b). "Behaviour of multitemporal and multisensor passive microwave indices in Southern Hemisphere ecosystems". *Journal of Geophysical Research - Biogeosciences* 119, 2231–2244. DOI: 10.1002/2014JG002626.

Bates, D. M. and D. G. Watts (1988). *Nonlinear Regression Analysis and Its Applications*. New York: John Wiley & Sons, 365.

Bauer, J., B. Siegmann, T. Jarmer, and N. Aschenbruck (2016). "On the potential of Wireless Sensor Networks for the in-situ assessment of crop leaf area index". *Computers and Electronics in Agriculture* 128, 149–159. DOI: 10.1016/j.compag.2016.08.019.

Beer, C., M. Reichstein, E. Tomelleri, P. Ciais, M. Jung, N. Carvalhais, C. Rödenbeck, M. A. Arain, D. Baldocchi, G. B. Bonan, A. Bondeau, A. Cescatti, G. Lasslop, A. Lindroth, M. Lomas, S. Luyssaert, H. Margolis, K. W. Oleson, O. Roupsard, E. Veenendaal, N. Viovy, C. Williams, F. I. Woodward, and D. Papale (2010). "Terrestrial gross carbon dioxide uptake: global distribution and covariation with climate". *Science* 329.5993, 834–838. DOI: 10.1126/science.1184984.

Béland, M., J. L. Widlowski, R. A. Fournier, J. F. Côté, and M. M. Verstraete (2011). "Estimating leaf area distribution in savanna trees from terrestrial LiDAR measurements". *Agricultural and Forest Meteorology* 151.9, 1252–1266. DOI: 10.1016/j.agrformet.2011.05.004.

Belgiu, M. and L. Drăgu (2016). "Random forest in remote sensing: A review of applications and future directions". *ISPRS Journal of Photogrammetry and Remote Sensing* 114, 24–31. DOI: 10.1016/j.isprsjprs.2016.01.011.

Bergen, K. M., S. J. Goetz, R. O. Dubayah, G. M. Henebry, C. T. Hunsaker, M. L. Imhoff, R. F. Nelson, G. G. Parker, and V. C. Radeloff (2009). "Remote sensing of vegetation 3-D structure for biodiversity and habitat: Review and implications for lidar and radar spaceborne missions". *Journal of Geophysical Research: Biogeosciences* 114.4, 1–13. DOI: 10.1029/2008JG000883.

Berger, M., J. Moreno, J. A. Johannessen, P. F. Levelt, and R. F. Hanssen (2012). "ESA's sentinel missions in support of Earth system science". *Remote Sensing of Environment* 120, 84–90. DOI: 10.1016/j.rse.2011.07.023.

Berni, J., P. Zarco-Tejada, L. Suarez, and E. Fereres (2009). "Thermal and Narrowband Multispectral Remote Sensing for Vegetation Monitoring From an Unmanned Aerial Vehicle". *IEEE Transactions on Geoscience and Remote Sensing* 47.3, 722–738. DOI: 10.1109/TGRS.2008.2010457.

Bienert, A., S. Scheller, E. Keane, G. Mullooly, and F. Mohan (2006). "Application of terrestrial laser scanners for the determination of forest inventory parameters". *International Archives of Photogrammetry, Remote Sensing and Spatial Information Sciences* 36.5.

Boehmler, J., S. Loría-Salazar, C. Stevens, J. Long, A. Watts, H. Holmes, J. Barnard, and W. Arnott (2018). "Development of a Multispectral Albedometer and Deployment on an Unmanned Aircraft for Evaluating Satellite Retrieved Surface Reflectance over Nevada's Black Rock Desert". *Sensors* 18.10, 3504. DOI: 10.3390/s18103504.

Bonan, G. B. (2008). "Forests and Climate Change: Forcings, Feedbacks, and the Climate Benefits of Fiorests". *Science* 320.5882, 1444–1449. DOI: 10.1126/science.1155121.

Bongers, F. (2001). "Methods to assess tropical rain forest canopy structure: An overview". *Plant Ecology* 153.1-2, 263–277. DOI: 10.1023/A:1017555605618. arXiv: 0005074v1 [arXiv:astro-ph].

Bouvet, A., S. Mermoz, T. Le Toan, L. Villard, R. Mathieu, L. Naidoo, and G. P. Asner (2018). "An above-ground biomass map of African savannahs and woodlands at 25 m resolution derived from ALOS PALSAR". *Remote Sensing of Environment* 206.November 2017, 156–173. DOI: 10.1016/j.rse.2017.12.030.

Bréda, N. J. J. (2003). "Ground-based measurements of leaf area index: A review of methods, instruments and current controversies". *Journal of Experimental Botany* 54.392, 2403–2417. DOI: 10.1093/jxb/erg263.

Brede, B., H. Bartholomeus, J. Suomalainen, J. Clevers, J. Verbesselt, M. Herold, D. Culvenor, and F. Gascon (2016). "The Speulderbos Fiducial Reference Site for Continuous Monitoring of Forest Biophysical Variables". In: *Living Planet Symposium 2016, Prague, Czech Republic, 9-13 May 2016*. Prague, 5.

Brede, B., K. Calders, A. Lau, P. Raumonen, H. M. Bartholomeus, M. Herold, and L. Kooistra (in review). "Tree Volume Estimation through UAV Laser Scanning and Quantitative Structure Modelling". *Remote Sensing of Environment*.

Brede, B., J.-P. Gastellu-Etchegorry, N. Lauret, F. Baret, J. Clevers, J. Verbesselt, and M. Herold (2018). "Monitoring Forest Phenology and Leaf Area Index with the Autonomous, Low-Cost Transmittance Sensor PASTiS-57". *Remote Sensing* 10.7, 1032. DOI: 10.3390/RS10071032.

Brede, B., A. Lau, H. M. Bartholomeus, and L. Kooistra (2017). "Comparing RIEGL RiCOPTER UAV LiDAR Derived Canopy Height and DBH with Terrestrial LiDAR". *Sensors* 17.10, 2371. DOI: 10.3390/s17102371.

Brede, B., J. Suomalainen, H. Bartholomeus, and M. Herold (2015). "Influence of solar zenith angle on the enhanced vegetation index of a Guyanese rainforest". *Remote Sensing Letters* 6.12, 972–981. DOI: 10.1080/2150704X.2015.1089362.

Brede, B., J. Verrelst, J.-P. Gastellu-Etchegorry, J. Clevers, L. Goudzwaard, J. den Ouden, J. Verbesselt, and M. Herold (in preparation). "Impact of Retrieval Scheme Features on Forest LAI Prediction with Sentinel-2A MSI, Landsat 7 ETM+ and Landsat 8 OLI".

Breiman, L. (2001). "Random forests". *Machine Learning* 45.1, 5–32. DOI: 10.1023/A:1010933404324. arXiv: /dx.doi.org/10.1023{\%}2FA{\%}3A1010933404324 [http:].

Browning, D., J. Karl, D. Morin, A. Richardson, and C. Tweedie (2017). "Phenocams Bridge the Gap between Field and Satellite Observations in an Arid Grassland Ecosystem". *Remote Sensing* 9.10, 1071. DOI: 10.3390/rs9101071.

Buddenbaum, H., O. Stern, B. Paschmionka, E. Hass, T. Gattung, J. Stoffels, J. Hill, and W. Werner (2015). "Using VNIR and SWIR field imaging spectroscopy for drought stress monitoring of beech seedlings". *International Journal of Remote Sensing* 36.18, 4590–4605. DOI: 10.1080/01431161.2015.1084435.

Burt, A., M. Disney, and K. Calders (2018). "Extracting individual trees from lidar point clouds using treeseg". *Methods in Ecology and Evolution*. Ed. by S. Goslee, 1–8. DOI: 10.1111/2041-210X.13121.

Byrd, R. H., P. Lu, J. Nocedal, and C. Zhu (1995). "A Limited Memory Algorithm for Bound Constrained Optimization". *SIAM Journal on Scientific Computing* 16.5, 1190–1208. DOI: 10.1137/0916069.

Calders, K., J. Armston, G. Newnham, M. Herold, and N. Goodwin (2014). "Implications of sensor configuration and topography on vertical plant profiles derived from terrestrial LiDAR". *Agricultural and Forest Meteorology* 194, 104–117. DOI: 10.1016/j.agrformet.2014.03.022.

Calders, K., A. Burt, G. Newnham, M. Disney, S. Murphy, P. Raumonen, M. Herold, D. Culvenor, J. Armston, V. Avitabile, and M. Kaasalainen (2015a). "Reducing uncertainties in above-ground biomass estimates using terrestrial laser scanning". In: *Proceedings of the 2015 SilviLaser, La Grande Motte, France, 28–30 September 2015*, 197–199.

Calders, K., M. I. Disney, J. Armston, A. Burt, B. Brede, N. Origo, J. Muir, and J. Nightingale (2017). "Evaluation of the Range Accuracy and the Radiometric Calibration of Multiple Terrestrial Laser Scanning Instruments for Data Interoperability". *IEEE Transactions on Geoscience and Remote Sensing* 55.5, 2716–2724. DOI: 10.1109/TGRS.2017.2652721.

Calders, K., P. Lewis, M. Disney, J. Verbesselt, and M. Herold (2013). "Investigating assumptions of crown archetypes for modelling LiDAR returns". *Remote Sensing of Environment* 134, 39–49. DOI: 10.1016/j.rse.2013.02.018.

Calders, K., G. Newnham, A. Burt, S. Murphy, P. Raumonen, M. Herold, D. Culvenor, V. Avitabile, M. Disney, J. Armston, and M. Kaasalainen (2015b). "Nondestructive estimates of above-ground biomass using terrestrial laser scanning". *Methods in Ecology and Evolution* 6.2, 198–208. DOI: 10.1111/2041-210X.12301.

Calders, K., N. Origo, A. Burt, M. Disney, J. Nightingale, P. Raumonen, M. Åkerblom, Y. Malhi, and P. Lewis (2018a). "Realistic Forest Stand Reconstruction from Terrestrial LiDAR for Radiative Transfer Modelling". *Remote Sensing* 10.6, 933. DOI: 10.3390/RS10060933.

Calders, K., N. Origo, M. Disney, J. Nightingale, W. Woodgate, J. Armston, and P. Lewis (2018b). "Variability and bias in active and passive ground-based measurements of effective plant, wood and leaf area index". *Agricultural and Forest Meteorology* 252.September 2017, 231–240. DOI: 10.1016/j.agrformet.2018.01.029.

Calders, K., T. Schenkels, H. Bartholomeus, J. Armston, J. Verbesselt, and M. Herold (2015c). "Monitoring spring phenology with high temporal resolution terrestrial LiDAR measurements". *Agricultural and Forest Meteorology* 203, 158–168. DOI: 10.1016/j.agrformet.2015.01.009.

Campbell, G. and J. Norman (1989). "The description and measurement of plant canopy structure". In: *Plant Canopies: Their Growth, Form and Function*. Ed. by G. Russell, B. Marshall, and P. G. Jarvis. Cambridge: Cambridge University Press, 1–20. DOI: 10.1017/CBO9780511752308.002.

Campos-Taberner, M., F. J. García-Haro, G. Camps-Valls, G. Grau-Muedra, F. Nutini, A. Crema, and M. Boschetti (2016). "Multitemporal and multiresolution leaf area index retrieval for operational local rice crop monitoring". *Remote Sensing of Environment* 187, 102–118. DOI: 10.1016/j.rse.2016.10.009.

Canisius, F., R. Fernandes, and J. Chen (2010). "Comparison and evaluation of Medium Resolution Imaging Spectrometer leaf area index products across a range of land use". *Remote Sensing of Environment* 114.5, 950–960. DOI: 10.1016/j.rse.2009.12.010.

Capolupo, A., L. Kooistra, C. Berendonk, L. Boccia, and J. Suomalainen (2015). "Estimating Plant Traits of Grasslands from UAV-Acquired Hyperspectral Images: A Comparison of Statistical Approaches". *ISPRS International Journal of Geo-Information* 4.4, 2792–2820. DOI: 10.3390/ijgi4042792.

Casas, A., D. Riaño, S. L. Ustin, P. Dennison, and J. Salas (2014). "Estimation of water-related biochemical and biophysical vegetation properties using multitemporal airborne hyperspectral data and its comparison to MODIS spectral response". *Remote Sensing of Environment* 148, 28–41. DOI: 10.1016/j.rse.2014.03.011.

Chave, J., C. Andalo, S. Brown, M. A. Cairns, J. Q. Chambers, D. Eamus, H. Fölster, F. Fromard, N. Higuchi, T. Kira, J.-P. Lescure, B. W. Nelson, H. Ogawa, H. Puig, B. Riéra, and T. Yamakura (2005). "Tree allometry and improved estimation of carbon stocks and balance in tropical forests". *Oecologia* 145.1, 87–99. DOI: 10.1007/s00442-005-0100-x.

Che, M., B. Chen, H. Zhang, S. Fang, G. Xu, X. Lin, and Y. Wang (2014). "A New Equation for Deriving Vegetation Phenophase from Time Series of Leaf Area Index (LAI) Data". *Remote Sensing* 6.6, 5650–5670. DOI: 10.3390/rs6065650.

Chen, J. and T. A. Black (1992). "Defining leaf area index for non-flat leaves". *Plant, Cell and Environment* 15, 421–429.

Chen, J., C. Menges, and S. Leblanc (2005). "Global mapping of foliage clumping index using multi-angular satellite data". *Remote Sensing of Environment* 97.4, 447–457. DOI: 10.1016/j.rse.2005.05.003.

Chen, J. M., P. M. Rich, S. T. Gower, J. M. Norman, and S. Plummer (1997). "Leaf area index of boreal forests: Theory, techniques, and measurements". *Journal of Geophysical Research* 102.D24, 29429. DOI: 10.1029/97JD01107.

Chianucci, F., L. Disperati, D. Guzzi, D. Bianchini, V. Nardino, C. Lastri, A. Rindinella, and P. Corona (2016). "Estimation of canopy attributes in beech forests using true colour digital images from a small fixed-wing UAV". *International Journal of Applied Earth Observation and Geoinformation* 47, 60–68. DOI: 10.1016/j.jag.2015.12.005.

Chisholm, R. A., J. Cui, S. K. Y. Lum, and B. M. Chen (2013). "UAV LiDAR for below-canopy forest surveys". *Journal of Unmanned Vehicle Systems* 1.1, 61–68. DOI: 10.1139/juvs-2013-0017.

Ciais, P., C. Sabine, G. Bala, L. Bopp, V. Brovkin, J. Canadell, A. Chhabra, R. DeFries, J. Galloway, M. Heimann, C. Jones, C. L. Quéré, R. Myneni, S. Piao, and P. Thornton (2013). "Carbon and Other Biogeochemical Cycles". In: *Climate Change 2013: The Physical Science Basis. Contribution of Working Group I to the Fifth Assessment Report of the Intergovernmental Panel on Climate Change*. Ed. by T. Stocker, D. Qin, G.-K. Plattner, M. Tignor, S. Allen, J. Boschung, A. Nauels, Y. Xia, V. Bex, and P. Midgle. Cambridge, United Kingdom and New York, NY, USA: Cambridge University Press, 465–570.

Clevers, J. G. P. W. and W. Verhoef (1993). "LAI estimation by means of the WDVI: A sensitivity analysis with a combined PROSPECT-SAIL model". *Remote Sensing Reviews* 7.1, 43–64. DOI: 10.1080/02757259309532165.

Colomina, I. and P. Molina (2014). "Unmanned aerial systems for photogrammetry and remote sensing: A review". *ISPRS Journal of Photogrammetry and Remote Sensing* 92, 79–97. DOI: 10.1016/j.isprsjprs.2014.02.013.

Coope, I. D. (1993). "Circle fitting by linear and nonlinear least squares". *Journal of Optimization Theory and Applications* 76.2, 381–388. DOI: 10.1007/BF00939613.

Culvenor, D., G. Newnham, A. Mellor, N. Sims, and A. Haywood (2014). "Automated In-Situ Laser Scanner for Monitoring Forest Leaf Area Index". *Sensors* 14.8, 14994–15008. DOI: 10.3390/s140814994.

Daily, G. and K. Ellison (2002). *The New Economy Of Nature. The Quest to Make Conservation Profitable*. Washington, Covelo, London: Island Press, 250.

Danson, F. M., R. Gaulton, R. P. Armitage, M. Disney, O. Gunawan, P. Lewis, G. Pearson, and A. F. Ramirez (2014). "Developing a dual-wavelength full-waveform terrestrial laser

scanner to characterize forest canopy structure". *Agricultural and Forest Meteorology* 198-199, 7–14. DOI: 10.1016/j.agrformet.2014.07.007.

de Alcantara Andrade, F. A., C. D. Rodin, A. R. Hovenburg, T. A. Johansen, and R. Storvold (2018). "Path Planning of Multi-UAS Communication Relay by Decentralized MPC". In: *2018 OCEANS - MTS/IEEE Kobe Techno-Oceans (OTO)*. IEEE, 1–8. DOI: 10.1109/OCEANSKOBE.2018.8559333.

Defourny, P., S. Bontemps, N. Bellemans, C. Cara, G. Dedieu, E. Guzzonato, O. Hagolle, J. Inglada, L. Nicola, T. Rabaute, M. Savinaud, C. Udroiu, S. Valero, A. Bégué, J.-F. Dejoux, A. El Harti, J. Ezzahar, N. Kussul, K. Labbassi, V. Lebourgeois, Z. Miao, T. Newby, A. Nyamugama, N. Salh, A. Shelestov, V. Simonneaux, P. S. Traore, S. S. Traore, and B. Koetz (2019). "Near real-time agriculture monitoring at national scale at parcel resolution: Performance assessment of the Sen2-Agri automated system in various cropping systems around the world". *Remote Sensing of Environment* 221, 551–568. DOI: 10.1016/j.rse.2018.11.007.

Delegido, J., J. Verrelst, L. Alonso, and J. Moreno (2011). "Evaluation of Sentinel-2 red-edge bands for empirical estimation of green LAI and chlorophyll content". *Sensors* 11.7, 7063–7081. DOI: 10.3390/s110707063.

Demarez, V. and J. Gastellu-Etchegorry (2000). "A Modeling Approach for Studying Forest Chlorophyll Content". *Remote Sensing of Environment* 71.2, 226–238. DOI: 10.1016/S0034-4257(99)00089-9.

Detto, M., G. P. Asner, H. C. Muller-Landau, and O. Sonnentag (2015). "Spatial variability in tropical forest leaf area density from Multireturn LiDAR and modelling". *Journal of Geophysical Research: Biogeosciences* 120.2, 1–16. DOI: 10.1002/2014JG002774.Received.

Disney, M. I., M. Boni Vicari, A. Burt, K. Calders, S. L. Lewis, P. Raumonen, and P. Wilkes (2018). "Weighing trees with lasers: advances, challenges and opportunities". *Interface Focus* 8.2, 20170048. DOI: 10.1098/rsfs.2017.0048.

Disney, M., P. Lewis, and P. North (2000). "Monte Carlo ray tracing in optical canopy reflectance modelling". *Remote Sensing Reviews* 18.2-4, 163–196. DOI: 10.1080/02757250009532389.

Donlon, C., B. Berruti, A. Buongiorno, M.-H. Ferreira, P. Féménias, J. Frerick, P. Goryl, U. Klein, H. Laur, C. Mavrocordatos, J. Nieke, H. Rebhan, B. Seitz, J. Stroede, and R. Sciarra (2012). "The Global Monitoring for Environment and Security (GMES) Sentinel-3 mission". *Remote Sensing of Environment* 120, 37–57. DOI: 10.1016/j.rse.2011.07.024.

Doughty, C. E. and M. L. Goulden (2008). "Seasonal patterns of tropical forest leaf area index and CO2 exchange". *Journal of Geophysical Research* 113, G00B06. DOI: 10.1029/2007JG000590.

Douglas, E. S., J. Martel, Z. Li, G. Howe, K. Hewawasam, R. A. Marshall, C. L. Schaaf, T. A. Cook, G. J. Newnham, A. Strahler, and S. Chakrabarti (2015). "Finding Leaves in the Forest: The Dual-Wavelength Echidna Lidar". *IEEE Geoscience and Remote Sensing Letters* 12.4, 776–780. DOI: 10.1109/LGRS.2014.2361812.

Doxani, G., E. Vermote, J.-c. Roger, F. Gascon, S. Adriaensen, D. Frantz, O. Hagolle, A. Hollstein, G. Kirches, F. Li, J. Louis, A. Mangin, N. Pahlevan, B. Pflug, and Q. Vanhellemont (2018). "Atmospheric Correction Inter-Comparison Exercise". *Remote Sensing* 10.3, 352. DOI: 10.3390/rs10020352.

Drake, J. B., R. O. Dubayah, D. B. Clark, R. G. Knox, J. Blair, M. A. Hofton, R. L. Chazdon, J. F. Weishampel, and S. Prince (2002). "Estimation of tropical forest structural characteristics using large-footprint lidar". *Remote Sensing of Environment* 79.2-3, 305–319. DOI: 10.1016/S0034-4257(01)00281-4.

Drusch, M., U. Del Bello, S. Carlier, O. Colin, V. Fernandez, F. Gascon, B. Hoersch, C. Isola, P. Laberinti, P. Martimort, A. Meygret, F. Spoto, O. Sy, F. Marchese, and P. Bargellini (2012). "Sentinel-2: ESA's Optical High-Resolution Mission for GMES Operational Services". *Remote Sensing of Environment* 120, 25–36. DOI: 10.1016/j.rse.2011.11.026.

Duan, S. B., Z. L. Li, H. Wu, B. H. Tang, L. Ma, E. Zhao, and C. Li (2014). "Inversion of the PROSAIL model to estimate leaf area index of maize, potato, and sunflower fields from unmanned aerial vehicle hyperspectral data". *International Journal of Applied Earth Observation and Geoinformation* 26.1, 12–20. DOI: 10.1016/j.jag.2013.05.007.

Duncanson, L. I., B. D. Cook, G. C. Hurtt, and R. O. Dubayah (2014). "An efficient, multi-layered crown delineation algorithm for mapping individual tree structure across multiple ecosystems". *Remote Sensing of Environment* 154, 378–386. DOI: 10.1016/j.rse.2013.07.044.

Durbha, S. S., R. L. King, and N. H. Younan (2007). "Support vector machines regression for retrieval of leaf area index from multiangle imaging spectroradiometer". *Remote Sensing of Environment* 107.1-2, 348–361. DOI: 10.1016/j.rse.2006.09.031.

Dutrieux, L. P., J. Verbesselt, L. Kooistra, and M. Herold (2015). "Monitoring forest cover loss using multiple data streams, a case study of a tropical dry forest in Bolivia". *ISPRS Journal of Photogrammetry and Remote Sensing* 107, 112–125. DOI: 10.1016/j.isprsjprs.2015.03.015.

Eitel, J. U., B. Höfle, L. A. Vierling, A. Abellán, G. P. Asner, J. S. Deems, C. L. Glennie, P. C. Joerg, A. L. LeWinter, T. S. Magney, G. Mandlburger, D. C. Morton, J. Müller, and K. T. Vierling (2016). "Beyond 3-D: The new spectrum of lidar applications for earth and ecological sciences". *Remote Sensing of Environment* 186, 372–392. DOI: 10.1016/j.rse.2016.08.018.

ESA (2005). *Proba's view of Barrax test site*. (accessed on 23 January 2019). URL: https://www.esa.int/var/esa/storage/images/esa_multimedia/images/2005/07/

proba_s_view_of_barrax_test_site/9974271-2-eng-GB/Proba_s_view_of_Barrax_test_site.jpg.

ESA and Université Catholique de Louvain (2010). *ESA's 2009 global land cover map.* (accessed on 23 January 2019). URL: http://www.esa.int/var/esa/storage/images/esa_multimedia/images/2010/12/esa_s_2009_global_land_cover_map/9942263-2-eng-GB/ESA_s_2009_global_land_cover_map.jpg.

Eysn, L., M. Hollaus, E. Lindberg, F. Berger, J. M. Monnet, M. Dalponte, M. Kobal, M. Pellegrini, E. Lingua, D. Mongus, and N. Pfeifer (2015). "A benchmark of lidar-based single tree detection methods using heterogeneous forest data from the Alpine Space". *Forests* 6.5, 1721–1747. DOI: 10.3390/f6051721.

Fan, X., K. Kawamura, W. Guo, T. D. Xuan, J. Lim, N. Yuba, Y. Kurokawa, T. Obitsu, R. Lv, Y. Tsumiyama, T. Yasuda, and Z. Wang (2018). "A simple visible and near-infrared (V-NIR) camera system for monitoring the leaf area index and growth stage of Italian ryegrass". *Computers and Electronics in Agriculture* 144.November 2017, 314–323. DOI: 10.1016/j.compag.2017.11.025.

Fang, H., C. Jiang, W. Li, S. Wei, F. Baret, J. M. Chen, J. Garcia-Haro, S. Liang, R. Liu, R. B. Myneni, B. Pinty, Z. Xiao, and Z. Zhu (2013). "Characterization and intercomparison of global moderate resolution leaf area index (LAI) products: Analysis of climatologies and theoretical uncertainties". *Journal of Geophysical Research: Biogeosciences* 118.2, 529–548. DOI: 10.1002/jgrg.20051.

Fang, H., S. Wei, C. Jiang, and K. Scipal (2012a). "Theoretical uncertainty analysis of global MODIS, CYCLOPES, and GLOBCARBON LAI products using a triple collocation method". *Remote Sensing of Environment* 124, 610–621. DOI: 10.1016/j.rse.2012.06.013.

Fang, H., S. Wei, and S. Liang (2012b). "Validation of MODIS and CYCLOPES LAI products using global field measurement data". *Remote Sensing of Environment* 119, 43–54. DOI: 10.1016/j.rse.2011.12.006.

Fang, H., Y. Ye, W. Liu, S. Wei, and L. Ma (2018). "Continuous estimation of canopy leaf area index (LAI) and clumping index over broadleaf crop fields: An investigation of the PASTIS-57 instrument and smartphone applications". *Agricultural and Forest Meteorology* 253-254.February, 48–61. DOI: 10.1016/j.agrformet.2018.02.003.

Feret, J. B., C. François, G. P. Asner, A. A. Gitelson, R. E. Martin, L. P. R. Bidel, S. L. Ustin, G. le Maire, and S. Jacquemoud (2008). "PROSPECT-4 and 5: Advances in the leaf optical properties model separating photosynthetic pigments". *Remote Sensing of Environment* 112.6, 3030–3043. DOI: 10.1016/j.rse.2008.02.012.

Fernandes, R., S. Plummer, J. Nightingale, F. Baret, F. Camacho, H. Fang, S. Garrigues, N. Gobron, M. Lang, R. Lacaze, S. LeBlanc, M. Meroni, B. Martinez, T. Nilson, B. Pinty, J. Pisek, O. Sonnentag, A. Verger, J. Welles, M. Weiss, and J. Widlowski (2014). "Global Leaf Area Index Product Validation Good Practices". In: *Best Practice for*

Satellite-Derived Land Product Validation. Ed. by G. Schaepman-Strub, M. Román, and J. Nickeson. 2.0.1. Land Product Validation Subgroup (WGCV/CEOS), 76. DOI: 10.5067/doc/ceoswgcv/lpv/lai.002.

Frampton, W. J., J. Dash, G. Watmough, and E. J. Milton (2013). "Evaluating the capabilities of Sentinel-2 for quantitative estimation of biophysical variables in vegetation". *ISPRS Journal of Photogrammetry and Remote Sensing* 82, 83–92. DOI: 10.1016/j.isprsjprs.2013.04.007.

Fraser, B. T. and R. G. Congalton (2018). "Issues in Unmanned Aerial Systems (UAS) Data Collection of Complex Forest Environments". *Remote Sensing* 10, 908. DOI: 10.3390/rs10060908.

Ganguly, S., R. R. Nemani, G. Zhang, H. Hashimoto, C. Milesi, A. Michaelis, W. Wang, P. Votava, A. Samanta, F. Melton, J. L. Dungan, E. Vermote, F. Gao, Y. Knyazikhin, and R. B. Myneni (2012). "Generating global Leaf Area Index from Landsat: Algorithm formulation and demonstration". *Remote Sensing of Environment* 122, 185–202. DOI: 10.1016/j.rse.2011.10.032.

García, M., J. Gajardo, D. Riaño, K. Zhao, P. Martín, and S. Ustin (2015). "Canopy clumping appraisal using terrestrial and airborne laser scanning". *Remote Sensing of Environment* 161, 78–88. DOI: 10.1016/j.rse.2015.01.030.

Garrigues, S., R. Lacaze, F. Baret, J. T. Morisette, M. Weiss, J. E. Nickeson, R. Fernandes, S. Plummer, N. V. Shabanov, R. B. Myneni, Y. Knyazikhin, and W. Yang (2008). "Validation and intercomparison of global Leaf Area Index products derived from remote sensing data". *Journal of Geophysical Research* 113.G2, G02028. DOI: 10.1029/2007JG000635.

Gastellu-Etchegorry, J. P., V. Demarez, V. Pinel, and F. Zagolski (1996). "Modeling radiative transfer in heterogeneous 3-D vegetation canopies". *Remote Sensing of Environment* 58.2, 131–156. DOI: 10.1016/0034-4257(95)00253-7.

Gastellu-Etchegorry, J. P., E. Martin, and F. Gascon (2004). "DART: a 3D model for simulating satellite images and studying surface radiation budget". *International Journal of Remote Sensing* 25.1, 73–96. DOI: 10.1080/0143116031000115166.

Gastellu-Etchegorry, J.-P., N. Lauret, T. Yin, L. Landier, A. Kallel, Z. Malenovsky, A. A. Bitar, J. Aval, S. Benhmida, J. Qi, G. Medjdoub, J. Guilleux, E. Chavanon, B. Cook, D. Morton, N. Chrysoulakis, and Z. Mitraka (2017). "DART: Recent Advances in Remote Sensing Data Modeling With Atmosphere, Polarization, and Chlorophyll Fluorescence". *IEEE Journal of Selected Topics in Applied Earth Observations and Remote Sensing* 10.6, 2640–2649. DOI: 10.1109/JSTARS.2017.2685528.

Gibson, A. S. (2019). *How to Convert a Camera to Infrared for Black and White Landscape Photography*. (accessed on 23 January 2019). URL: https://digital-photography-school.com/convert-camera-infrared-black-white-landscape-photography.

Gonsamo, A. and P. Pellikka (2009). "The computation of foliage clumping index using hemispherical photography". *Agricultural and Forest Meteorology* 149.10, 1781–1787. DOI: 10.1016/j.agrformet.2009.06.001.

Gonzalez de Tanago, J., A. Lau, H. Bartholomeus, M. Herold, V. Avitabile, P. Raumonen, C. Martius, R. C. Goodman, M. Disney, S. Manuri, A. Burt, and K. Calders (2018). "Estimation of above-ground biomass of large tropical trees with terrestrial LiDAR". *Methods in Ecology and Evolution* 9.2. Ed. by D. Kriticos, 223–234. DOI: 10.1111/2041-210X.12904.

Gower, S. T., C. J. Kucharik, and J. M. Norman (1999). "Direct and indirect estimation of leaf area index, f(APAR), and net primary production of terrestrial ecosystems". *Remote Sensing of Environment* 70.1, 29–51. DOI: 10.1016/S0034-4257(99)00056-5.

Grau, E., S. Durrieu, R. Fournier, J. P. Gastellu-Etchegorry, and T. Yin (2017). "Estimation of 3D vegetation density with Terrestrial Laser Scanning data using voxels. A sensitivity analysis of influencing parameters". *Remote Sensing of Environment* 191, 373–388. DOI: 10.1016/j.rse.2017.01.032.

Griebel, A., L. T. Bennett, D. S. Culvenor, G. J. Newnham, and S. K. Arndt (2015). "Reliability and limitations of a novel terrestrial laser scanner for daily monitoring of forest canopy dynamics". *Remote Sensing of Environment* 166, 205–213. DOI: 10.1016/j.rse.2015.06.014.

Guo, Q., Y. Su, T. Hu, X. Zhao, F. Wu, Y. Li, J. Liu, L. Chen, G. Xu, G. Lin, Y. Zheng, Y. Lin, X. Mi, L. Fei, and X. Wang (2017). "An integrated UAV-borne lidar system for 3D habitat mapping in three forest ecosystems across China". *International Journal of Remote Sensing* 38.8-10, 1–19. DOI: 10.1080/01431161.2017.1285083.

Haboudane, D., J. R. Miller, E. Pattey, P. J. Zarco-Tejada, and I. B. Strachan (2004). "Hyperspectral vegetation indices and novel algorithms for predicting green LAI of crop canopies: Modeling and validation in the context of precision agriculture". *Remote Sensing of Environment* 90, 337–352. DOI: 10.1016/j.rse.2003.12.013.

Hackenberg, J., C. Morhart, J. Sheppard, H. Spiecker, and M. Disney (2014). "Highly accurate tree models derived from terrestrial laser scan data: A method description". *Forests* 5.5, 1069–1105. DOI: 10.3390/f5051069.

Hackenberg, J., M. Wassenberg, H. Spiecker, and D. Sun (2015). "Non destructive method for biomass prediction combining TLS derived tree volume and wood density". *Forests* 6.4, 1274–1300. DOI: 10.3390/f6041274.

Hancock, S., R. Essery, T. Reid, J. Carle, R. Baxter, N. Rutter, and B. Huntley (2014). "Characterising forest gap fraction with terrestrial lidar and photography: An examination of relative limitations". *Agricultural and Forest Meteorology* 189-190, 105–114. DOI: 10.1016/j.agrformet.2014.01.012.

Hansen, M. C., P. V. Potapov, R. Moore, M. Hancher, S. A. Turubanova, A. Tyukavina, D. Thau, S. V. Stehman, S. J. Goetz, T. R. Loveland, A. Kommareddy, A. Egorov, L.

Chini, C. O. Justice, and J. R. G. Townshend (2013). "High-Resolution Global Maps of 21st-Century Forest Cover Change". *Science* 342.6160, 850–853. DOI: 10.1126/science.1244693.

Heinzel, J. and M. Huber (2016). "Detecting Tree Stems from Volumetric TLS Data in Forest Environments with Rich Understory". *Remote Sensing* 9.1, 9. DOI: 10.3390/rs9010009.

Hilker, T., M. van Leeuwen, N. C. Coops, M. A. Wulder, G. J. Newnham, D. L. B. Jupp, and D. S. Culvenor (2010). "Comparing canopy metrics derived from terrestrial and airborne laser scanning in a Douglas-fir dominated forest stand". *Trees* 24.5, 819–832. DOI: 10.1007/s00468-010-0452-7.

Hoffmann, H., H. Nieto, R. Jensen, R. Guzinski, P. Zarco-Tejada, and T. Friborg (2016). "Estimating evaporation with thermal UAV data and two-source energy balance models". *Hydrology and Earth System Sciences* 20.2, 697–713. DOI: 10.5194/hess-20-697-2016.

Houborg, R., M. McCabe, A. Cescatti, F. Gao, M. Schull, and A. Gitelson (2015). "Joint leaf chlorophyll content and leaf area index retrieval from Landsat data using a regularized model inversion system (REGFLEC)". *Remote Sensing of Environment* 159, 203–221. DOI: 10.1016/j.rse.2014.12.008.

Houghton, R. A., F. Hall, and S. J. Goetz (2009). "Importance of biomass in the global carbon cycle". *Journal of Geophysical Research: Biogeosciences* 114.3, 1–13. DOI: 10.1029/2009JG000935.

Howe, G. A., K. Hewawasam, E. S. Douglas, J. Martel, Z. Li, A. Strahler, C. Schaaf, T. A. Cook, and S. Chakrabarti (2015). "Capabilities and performance of dual-wavelength Echidna® lidar". *Journal of Applied Remote Sensing* 9.1, 095979. DOI: 10.1117/1.JRS.9.095979.

Hu, R., J. Luo, G. Yan, J. Zou, and X. Mu (2016). "Indirect measurement of forest leaf area index using path length distribution model and multispectral canopy imager". *IEEE Journal of Selected Topics in Applied Earth Observations and Remote Sensing* 9.6, 2532–2539. DOI: 10.1109/JSTARS.2016.2569469.

Huete, A. R., K. Didan, Y. E. Shimabukuro, P. Ratana, S. R. Saleska, L. R. Hutyra, W. Yang, R. R. Nemani, and R. Myneni (2006). "Amazon rainforests green-up with sunlight in dry season". *Geophysical Research Letters* 33.6, L06405. DOI: 10.1029/2005GL025583.

Irons, J. R., J. L. Dwyer, and J. A. Barsi (2012). "The next Landsat satellite: The Landsat Data Continuity Mission". *Remote Sensing of Environment* 122, 11–21. DOI: 10.1016/j.rse.2011.08.026.

Quality management systems – Fundamentals and vocabulary (2015). Standard. Geneva, CH: International Organization for Standardization.

Jaakkola, A., J. Hyyppä, A. Kukko, X. Yu, H. Kaartinen, M. Lehtomäki, and Y. Lin (2010). "A low-cost multi-sensoral mobile mapping system and its feasibility for tree

measurements". *ISPRS Journal of Photogrammetry and Remote Sensing* 65.6, 514–522. DOI: 10.1016/j.isprsjprs.2010.08.002.

Jaakkola, A., J. Hyyppä, X. Yu, A. Kukko, H. Kaartinen, X. Liang, H. Hyyppä, and Y. Wang (2017). "Autonomous collection of forest field reference — The outlook and a first step with UAV laser scanning". *Remote Sensing* 9.8, 1–12. DOI: 10.3390/rs9080785.

Jacquemoud, S., W. Verhoef, F. Baret, C. Bacour, P. J. Zarco-Tejada, G. P. Asner, C. François, and S. L. Ustin (2009). "PROSPECT + SAIL models: A review of use for vegetation characterization". *Remote Sensing of Environment* 113, S56–S66. DOI: 10.1016/j.rse.2008.01.026.

Jansen, M. J. (1999). "Analysis of variance designs for model output". *Computer Physics Communications* 117.1, 35–43. DOI: 10.1016/S0010-4655(98)00154-4.

Jay, S., F. Baret, D. Dutartre, G. Malatesta, S. Héno, A. Comar, M. Weiss, and F. Maupas (2018). "Exploiting the centimeter resolution of UAV multispectral imagery to improve remote-sensing estimates of canopy structure and biochemistry in sugar beet crops". *Remote Sensing of Environment*. DOI: 10.1016/j.rse.2018.09.011.

Jonckheere, I., S. Fleck, K. Nackaerts, B. Muys, P. Coppin, M. Weiss, and F. Baret (2004). "Review of methods for in situ leaf area index determination Part I. Theories, sensors and hemispherical photography". *Agricultural and Forest Meteorology* 121.1-2, 19–35. DOI: 10.1016/j.agrformet.2003.08.027.

Jonckheere, I., K. Nackaerts, B. Muys, and P. Coppin (2005). "Assessment of automatic gap fraction estimation of forests from digital hemispherical photography". *Agricultural and Forest Meteorology* 132.1-2, 96–114. DOI: 10.1016/j.agrformet.2005.06.003.

Jones, M. O., L. A. Jones, J. S. Kimball, and K. C. McDonald (2011). "Satellite passive microwave remote sensing for monitoring global land surface phenology". *Remote Sensing of Environment* 115.4, 1102–1114. DOI: 10.1016/j.rse.2010.12.015.

Jones, M. O., J. S. Kimball, L. A. Jones, and K. C. McDonald (2012). "Satellite passive microwave detection of North America start of season". *Remote Sensing of Environment* 123, 324–333. DOI: 10.1016/j.rse.2012.03.025.

Jupp, D. L. B., D. S. Culvenor, J. L. Lovell, G. J. Newnham, A. H. Strahler, and C. E. Woodcock (2009). "Estimating forest LAI profiles and structural parameters using a ground-based laser called 'Echidna'". *Tree physiology* 29.2, 171–81. DOI: 10.1093/treephys/tpn022.

Kangas, A., R. Astrup, J. Breidenbach, J. Fridman, T. Gobakken, K. T. Korhonen, M. Maltamo, M. Nilsson, T. Nord-Larsen, E. Næsset, and H. Olsson (2018). "Remote sensing and forest inventories in Nordic countries – roadmap for the future". *Scandinavian Journal of Forest Research* 33.4, 397–412. DOI: 10.1080/02827581.2017.1416666.

Kankare, V., M. Vastaranta, M. Holopainen, M. Räty, X. Yu, J. Hyyppä, H. Hyyppä, P. Alho, and R. Viitala (2013). "Retrieval of forest aboveground biomass and stem

volume with airborne scanning LiDAR". *Remote Sensing* 5.5, 2257–2274. DOI: 10.3390/rs5052257.

Keenan, R. J., G. A. Reams, F. Achard, J. V. de Freitas, A. Grainger, and E. Lindquist (2015). "Dynamics of global forest area: Results from the FAO Global Forest Resources Assessment 2015". *Forest Ecology and Management* 352, 9–20. DOI: 10.1016/j.foreco.2015.06.014. arXiv: 9605103 [cs].

Keenan, T. F., B. Darby, E. Felts, O. Sonnentag, M. A. Friedl, K. Hufkens, J. O'Keefe, S. Klosterman, J. W. Munger, M. Toomey, and A. D. Richardson (2014). "Tracking forest phenology and seasonal physiology using digital repeat photography: A critical assessment". *Ecological Applications* 24.6, 1478–1489. DOI: 10.1890/13-0652.1.

Keller, M., M. Palace, and G. Hurtt (2001). "Biomass estimation in the Tapajos National Forest, Brazil". *Forest Ecology and Management* 154.3, 371–382. DOI: 10.1016/S0378-1127(01)00509-6.

Kimball, J. (2014). "Vegetation Phenology". In: *Encyclopedia of Remote Sensing*. Ed. by E. G. Njoku. Encyclopedia of Earth Sciences Series. New York, NY: Springer New York, 886–890. DOI: 10.1007/978-0-387-36699-9.

Kirby, J., L. Chapman, and V. Chapman (2018). "Assessing the Raspberry Pi as a low-cost alternative for acquisition of near infrared hemispherical digital imagery". *Agricultural and Forest Meteorology* 259.May, 232–239. DOI: 10.1016/j.agrformet.2018.05.004.

Klosterman, S., E. Melaas, J. Wang, A. Martinez, S. Frederick, J. O'Keefe, D. A. Orwig, Z. Wang, Q. Sun, C. Schaaf, M. Friedl, and A. D. Richardson (2018). "Fine-scale perspectives on landscape phenology from unmanned aerial vehicle (UAV) photography". *Agricultural and Forest Meteorology* 248.October 2017, 397–407. DOI: 10.1016/j.agrformet.2017.10.015.

Klosterman, S. and A. D. Richardson (2017). "Observing spring and fall phenology in a deciduous forest with aerial drone imagery". *Sensors* 17.12, 1–17. DOI: 10.3390/s17122852.

Koch, B. (2010). "Status and future of laser scanning, synthetic aperture radar and hyperspectral remote sensing data for forest biomass assessment". *ISPRS Journal of Photogrammetry and Remote Sensing* 65.6, 581–590. DOI: 10.1016/j.isprsjprs.2010.09.001.

Koch, B., U. Heyder, and H. Weinacker (2006). "Detection of Individual Tree Crowns in Airborne Lidar Data". *Photogrammetric Engineering & Remote Sensing* 72.4, 357–363. DOI: 10.14358/PERS.72.4.357.

Koetz, B., F. Baret, H. Poilvé, and J. Hill (2005). "Use of coupled canopy structure dynamic and radiative transfer models to estimate biophysical canopy characteristics". *Remote Sensing of Environment* 95.1, 115–124. DOI: 10.1016/j.rse.2004.11.017.

Korhonen, L., Hadi, P. Packalen, and M. Rautiainen (2017). "Comparison of Sentinel-2 and Landsat 8 in the estimation of boreal forest canopy cover and leaf area index". *Remote Sensing of Environment* 195, 259–274. DOI: 10.1016/j.rse.2017.03.021.

Kucharik, C. J., J. M. Norman, L. M. Murdock, and S. T. Gower (1997). "Characterizing canopy nonrandomness with a multiband vegetation imager (MVI)". *Journal of Geophysical Research* 102.D24, 29455. DOI: 10.1029/97JD01175.

Kucharik, C. J., J. M. Norman, and S. T. Gower (1998). "Measurements of branch area and adjusting leaf area index indirect measurements". *Agricultural and Forest Meteorology* 91.1-2, 69–88. DOI: 10.1016/S0168-1923(98)00064-1.

Land Product Validation subgroup (2019). *Land Product Validation subgroup Portal*. (accessed on 23 January 2019). URL: https://lpvs.gsfc.nasa.gov.

Lang, A. and Y. Xiang (1986). "Estimation of leaf area index from transmission of direct sunlight in discontinuous canopies". *Agricultural and Forest Meteorology* 37.3, 229–243. DOI: 10.1016/0168-1923(86)90033-X.

Lang, M., T. Nilson, A. Kuusk, J. Pisek, L. Korhonen, and V. Uri (2017). "Digital photography for tracking the phenology of an evergreen conifer stand". *Agricultural and Forest Meteorology* 246.May, 15–21. DOI: 10.1016/j.agrformet.2017.05.021.

Latorre, C., F. Camacho, F. De la Cruz, R. Lacaze, M. Weiss, and F. Baret (2014). "Seasonal monitoring of FAPAR over the Barrax cropland site in Spain, in support of the validation of PROBA-V products at 333 m". In: *Fourth Recent Advances in Quantitative Remote Sensing*. 1, 1–6.

Lau, A., L. P. Bentley, C. Martius, A. Shenkin, H. Bartholomeus, P. Raumonen, Y. Malhi, T. Jackson, and M. Herold (2018). "Quantifying branch architecture of tropical trees using terrestrial LiDAR and 3D modelling". *Trees* 32.5, 1219–1231. DOI: 10.1007/s00468-018-1704-1.

Lauvernet, C., F. Baret, L. Hascoët, S. Buis, and F. X. Le Dimet (2008). "Multitemporal-patch ensemble inversion of coupled surface-atmosphere radiative transfer models for land surface characterization". *Remote Sensing of Environment* 112.3, 851–861. DOI: 10.1016/j.rse.2007.06.027.

Lazaro-Gredilla, M., M. K. Titsias, J. Verrelst, and G. Camps-Valls (2014). "Retrieval of Biophysical Parameters With Heteroscedastic Gaussian Processes". *IEEE Geoscience and Remote Sensing Letters* 11.4, 838–842. DOI: 10.1109/LGRS.2013.2279695.

Le Toan, T., S. Quegan, M. W. J. Davidson, H. Balzter, P. Paillou, K. Papathanassiou, S. Plummer, F. Rocca, S. Saatchi, H. Shugart, and L. Ulander (2011). "The BIOMASS mission: Mapping global forest biomass to better understand the terrestrial carbon cycle". *Remote Sensing of Environment* 115.11, 2850–2860. DOI: 10.1016/j.rse.2011.03.020.

Leblanc, S. G., J. M. Chen, R. Fernandes, D. W. Deering, and A. Conley (2005). "Methodology comparison for canopy structure parameters extraction from digital hemispherical

photography in boreal forests". *Agricultural and Forest Meteorology* 129.3-4, 187–207. DOI: 10.1016/j.agrformet.2004.09.006.

Lecerf, R., F. Baret, J. Hanocq, O. Marloie, M. Rautiainen, M. Mottus, J. Heiskanen, and P. Stenberg (2010). "PASTIS 57: Autonomous light sensors for PAI continuous monitoring. Principles, calibration and application to vegetation phenology". In: *AGU Fall Meeting Abstracts 12/2010*.

Lehnert, L. W., H. Meyer, and J. Bendix (2016). *hsdar: Manage, analyse and simulate hyperspectral data in R*. R package version 0.5.1.

Leuschner, C., S. Voß, A. Foetzki, and Y. Clases (2006). "Variation in leaf area index and stand leaf mass of European beech across gradients of soil acidity and precipitation". *Plant Ecology* 186.2, 247–258. DOI: 10.1007/s11258-006-9127-2.

Li, W., M. Weiss, F. Waldner, P. Defourny, V. Demarez, D. Morin, O. Hagolle, and F. Baret (2015a). "A Generic Algorithm to Estimate LAI, FAPAR and FCOVER Variables from SPOT4_HRVIR and Landsat Sensors: Evaluation of the Consistency and Comparison with Ground Measurements". *Remote Sensing* 7.11, 15494–15516. DOI: 10.3390/rs71115494.

Li, X., Q. Liu, R. Yang, H. Zhang, J. Zhang, and E. Cai (2015b). "The Design and Implementation of the Leaf Area Index Sensor". *Sensors* 15.3, 6250–6269. DOI: 10.3390/s150306250.

Li, Y., Q. Guo, Y. Su, S. Tao, K. Zhao, and G. Xu (2017). "Retrieving the gap fraction, element clumping index, and leaf area index of individual trees using single-scan data from a terrestrial laser scanner". *ISPRS Journal of Photogrammetry and Remote Sensing* 130, 308–316. DOI: 10.1016/j.isprsjprs.2017.06.006.

Li, Z., M. Schaefer, A. Strahler, C. Schaaf, and D. Jupp (2018a). "On the utilization of novel spectral laser scanning for three-dimensional classification of vegetation elements". *Interface Focus* 8.2. DOI: 10.1098/rsfs.2017.0039.

Li, Z., A. Strahler, C. Schaaf, D. Jupp, M. Schaefer, and P. Olofsson (2018b). "Seasonal change of leaf and woody area profiles in a midlatitude deciduous forest canopy from classified dual-wavelength terrestrial lidar point clouds". *Agricultural and Forest Meteorology* 262.February, 279–297. DOI: 10.1016/j.agrformet.2018.07.014.

Liang, X., V. Kankare, J. Hyyppä, Y. Wang, A. Kukko, H. Haggrén, X. Yu, H. Kaartinen, A. Jaakkola, F. Guan, M. Holopainen, and M. Vastaranta (2016). "Terrestrial laser scanning in forest inventories". *ISPRS Journal of Photogrammetry and Remote Sensing* 115, 63–77. DOI: 10.1016/j.isprsjprs.2016.01.006.

Lin, J., M. Wang, M. Ma, and Y. Lin (2018). "Aboveground Tree Biomass Estimation of Sparse Subalpine Coniferous Forest with UAV Oblique Photography". *Remote Sensing* 10.11, 1849. DOI: 10.3390/rs10111849.

Lin, L. I.-K. (1989). "A Concordance Correlation Coefficient to Evaluate Reproducibility". *Biometrics* 45.1, 255. DOI: 10.2307/2532051.

Lin, Y., J. Hyyppa, and A. Jaakkola (2011). "Mini-UAV-Borne LIDAR for Fine-Scale Mapping". *IEEE Geoscience and Remote Sensing Letters* 8.3, 426–430. DOI: 10.1109/LGRS.2010.2079913.

Lisein, J., M. Pierrot-Deseilligny, S. Bonnet, and P. Lejeune (2013). "A photogrammetric workflow for the creation of a forest canopy height model from small unmanned aerial system imagery". *Forests* 4.4, 922–944. DOI: 10.3390/f4040922.

Liu, J., A. K. Skidmore, S. Jones, T. Wang, M. Heurich, X. Zhu, and Y. Shi (2018). "Large off-nadir scan angle of airborne LiDAR can severely affect the estimates of forest structure metrics". *ISPRS Journal of Photogrammetry and Remote Sensing* 136, 13–25. DOI: 10.1016/j.isprsjprs.2017.12.004.

Liu, J., X. Liang, J. Hyyppä, X. Yu, M. Lehtomäki, J. Pyörälä, L. Zhu, Y. Wang, and R. Chen (2017). "Automated matching of multiple terrestrial laser scans for stem mapping without the use of artificial references". *International Journal of Applied Earth Observation and Geoinformation* 56, 13–23. DOI: 10.1016/j.jag.2016.11.003.

Liu, Z., X. Wang, J. M. Chen, C. Wang, and G. Jin (2015). "On improving the accuracy of digital hemispherical photography measurements of seasonal leaf area index variation in deciduous broadleaf forests". *Canadian Journal of Forest Research* 45, 721–731. DOI: 10.1139/cjfr-2014-0351.

Lovell, J. L., D. L. B. Jupp, E. van Gorsel, J. Jimenez-Berni, C. Hopkinson, and L. Chasmer (2011). "Foliage profiles from ground based waveform and discrete point lidar". In: *Proceedings of the SilviLaser 2011 Conference. Oct. 16– 20, Hobart, Tasmania.*

Lukasová, V., M. Lang, and J. Škvarenina (2014). "Seasonal Changes in NDVI in Relation to Phenological Phases, LAI and PAI of Beech Forests". *Baltic Forestry* 20.2, 248–262.

Luoma, V., N. Saarinen, M. A. Wulder, J. C. White, M. Vastaranta, M. Holopainen, and J. Hyyppä (2017). "Assessing precision in conventional field measurements of individual tree attributes". *Forests* 8.2, 1–16. DOI: 10.3390/f8020038.

Ma, L., G. Zheng, J. U. H. Eitel, T. S. Magney, and L. M. Moskal (2016). "Determining woody-to-total area ratio using terrestrial laser scanning (TLS)". *Agricultural and Forest Meteorology* 228-229, 217–228. DOI: 10.1016/j.agrformet.2016.06.021.

Majasalmi, T. and M. Rautiainen (2016). "The potential of Sentinel-2 data for estimating biophysical variables in a boreal forest: a simulation study". *Remote Sensing Letters* 7.5, 427–436. DOI: 10.1080/2150704X.2016.1149251.

Malenovský, Z., L. Homolová, R. Zurita-Milla, P. Lukeš, V. Kaplan, J. Hanuš, J. P. Gastellu-Etchegorry, and M. E. Schaepman (2013). "Retrieval of spruce leaf chlorophyll content from airborne image data using continuum removal and radiative transfer". *Remote Sensing of Environment* 131, 85–102. DOI: 10.1016/j.rse.2012.12.015.

Malenovský, Z., E. Martin, L. Homolová, J. P. Gastellu-Etchegorry, R. Zurita-Milla, M. E. Schaepman, R. Pokorný, J. G. Clevers, and P. Cudlín (2008). "Influence of woody elements of a Norway spruce canopy on nadir reflectance simulated by the DART model at very high spatial resolution". *Remote Sensing of Environment* 112.1, 1–18. DOI: 10.1016/j.rse.2006.02.028.

Malenovský, Z., H. Rott, J. Cihlar, M. E. Schaepman, G. García-Santos, R. Fernandes, and M. Berger (2012). "Sentinels for science: Potential of Sentinel-1, -2, and -3 missions for scientific observations of ocean, cryosphere, and land". *Remote Sensing of Environment* 120, 91–101. DOI: 10.1016/j.rse.2011.09.026.

Malhi, Y., T. Jackson, L. Patrick Bentley, A. Lau, A. Shenkin, M. Herold, K. Calders, H. Bartholomeus, and M. I. Disney (2018). "New perspectives on the ecology of tree structure and tree communities through terrestrial laser scanning". *Interface Focus* 8.2, 20170052. DOI: 10.1098/rsfs.2017.0052.

Mandlburger, G., M. Hollaus, P. Glira, M. Wieser, U. Riegl, and M. Pfennigbauer (2015). "First examples from the RIEGL VUX-SYS for forestry applications". In: *Proceedings of Silvilaser*. La Grande Motte, France, 105–107.

Manninen, T., P. Stenberg, M. Rautiainen, and P. Voipio (2013). "Leaf Area Index Estimation of Boreal and Subarctic Forests Using VV/HH ENVISAT/ASAR Data of Various Swaths". *IEEE Transactions on Geoscience and Remote Sensing* 51.7, 3899–3909. DOI: 10.1109/TGRS.2012.2227327.

Mark Danson, F., F. Sasse, and L. A. Schofield (2018). "Spectral and spatial information from a novel dual-wavelength full-waveform terrestrial laser scanner for forest ecology". *Interface Focus* 8.2. DOI: 10.1098/rsfs.2017.0049.

Meroni, M., R. Colombo, and C. Panigada (2004). "Inversion of a radiative transfer model with hyperspectral observations for LAI mapping in poplar plantations". *Remote Sensing of Environment* 92.2, 195–206. DOI: 10.1016/j.rse.2004.06.005.

Mitchard, E. T., T. R. Feldpausch, R. J. Brienen, G. Lopez-Gonzalez, A. Monteagudo, T. R. Baker, S. L. Lewis, J. Lloyd, C. A. Quesada, M. Gloor, H. ter Steege, P. Meir, E. Alvarez, A. Araujo-Murakami, L. E. Aragão, L. Arroyo, G. Aymard, O. Banki, D. Bonal, S. Brown, F. I. Brown, C. E. Cerón, V. Chama Moscoso, J. Chave, J. A. Comiskey, F. Cornejo, M. Corrales Medina, L. Da Costa, F. R. Costa, A. Di Fiore, T. F. Domingues, T. L. Erwin, T. Frederickson, N. Higuchi, E. N. Honorio Coronado, T. J. Killeen, W. F. Laurance, C. Levis, W. E. Magnusson, B. S. Marimon, B. H. Marimon Junior, I. Mendoza Polo, P. Mishra, M. T. Nascimento, D. Neill, M. P. Núñez Vargas, W. A. Palacios, A. Parada, G. Pardo Molina, M. Peña-Claros, N. Pitman, C. A. Peres, L. Poorter, A. Prieto, H. Ramirez-Angulo, Z. Restrepo Correa, A. Roopsind, K. H. Roucoux, A. Rudas, R. P. Salomão, J. Schietti, M. Silveira, P. F. de Souza, M. K. Steininger, J. Stropp, J. Terborgh, R. Thomas, M. Toledo, A. Torres-Lezama, T. R. Van Andel, G. M. van der Heijden, I. C. Vieira, S. Vieira, E. Vilanova-Torre, V. A. Vos, O. Wang, C. E. Zartman,

Y. Malhi, and O. L. Phillips (2014). "Markedly divergent estimates of Amazon forest carbon density from ground plots and satellites". *Global Ecology and Biogeography* 23.8, 935–946. DOI: 10.1111/geb.12168.

Mitchard, E. T., S. S. Saatchi, A. Baccini, G. P. Asner, S. J. Goetz, N. L. Harris, and S. Brown (2013). "Uncertainty in the spatial distribution of tropical forest biomass: A comparison of pan-tropical maps". *Carbon Balance and Management* 8.1, 1–13. DOI: 10.1186/1750-0680-8-10.

Momo Takoudjou, S., P. Ploton, B. Sonké, J. Hackenberg, S. Griffon, F. de Coligny, N. G. Kamdem, M. Libalah, G. I. Mofack, G. Le Moguédec, R. Pélissier, and N. Barbier (2018). "Using terrestrial laser scanning data to estimate large tropical trees biomass and calibrate allometric models: A comparison with traditional destructive approach". *Methods in Ecology and Evolution* 9.4. Ed. by S. McMahon, 905–916. DOI: 10.1111/2041-210X.12933. arXiv: 0608246v3 [arXiv:physics].

Morisette, J. T., F. Baret, J. L. Privette, R. B. Myneni, J. E. Nickeson, S. Garrigues, N. V. Shabanov, M. Weiss, R. A. Fernandes, S. G. Leblanc, M. Kalacska, G. A. Sánchez-Azofeifa, M. Chubey, B. Rivard, P. Stenberg, M. Rautiainen, P. Voipio, T. Manninen, A. N. Pilant, T. E. Lewis, J. S. Iiames, R. Colombo, M. Meroni, L. Busetto, W. B. Cohen, D. P. Turner, E. D. Warner, G. W. Petersen, G. Seufert, and R. Cook (2006). "Validation of global moderate-resolution LAI products: A framework proposed within the CEOS land product validation subgroup". *IEEE Transactions on Geoscience and Remote Sensing* 44.7, 1804–1814. DOI: 10.1109/TGRS.2006.872529.

Morsdorf, F., B. Kötz, E. Meier, K. I. Itten, and B. Allgöwer (2006). "Estimation of LAI and fractional cover from small footprint airborne laser scanning data based on gap fraction". *Remote Sensing of Environment* 104.1, 50–61. DOI: 10.1016/j.rse.2006.04.019.

Morsdorf, F., C. Nichol, T. Malthus, and I. H. Woodhouse (2009). "Assessing forest structural and physiological information content of multi-spectral LiDAR waveforms by radiative transfer modelling". *Remote Sensing of Environment* 113.10, 2152–2163. DOI: 10.1016/j.rse.2009.05.019.

Morton, D. C., J. Nagol, C. C. Carabajal, J. Rosette, M. Palace, B. D. Cook, E. F. Vermote, D. J. Harding, and P. R. J. North (2014). "Amazon forests maintain consistent canopy structure and greenness during the dry season". *Nature* 506, 221–224. DOI: 10.1038/nature13006.

Morton, D. C., J. Rubio, B. D. Cook, J.-P. Gastellu-Etchegorry, M. Longo, H. Choi, M. Hunter, and M. Keller (2016). "Amazon forest structure generates diurnal and seasonal variability in light utilization". *Biogeosciences* 13.7, 2195–2206. DOI: 10.5194/bg-13-2195-2016.

Myneni, R., Y. Knyazikhin, and T. Park (2015). *MCD15A3H MODIS/Terra+Aqua Leaf Area Index/FPAR 4-day L4 Global 500m SIN Grid V006 [Data set]*. NASA EOSDIS Land Processes DAAC. DOI: 10.5067/MODIS/MCD15A3H.006.

Myneni, R., Y. Knyazikhin, and N. Shabanov (2011). "Leaf Area Index and Fraction of Absorbed PAR Products from Terra and Aqua MODIS Sensors: Analysis, Validation, and Refinement". In: *Land Remote Sensing and Global Environmental Change – NASA's Earth Observing System and the Science of ASTER and MODIS*. Ed. by B. Ramachandran, C. O. Justice, and M. J. Abrams. New York, Dordrecht, Heidelberg, London: Springer. Chap. 27, 603–633.

Nagol, J. R., J. O. Sexton, D.-H. Kim, A. Anand, D. Morton, E. Vermote, and J. R. Townshend (2015). "Bidirectional effects in Landsat reflectance estimates: Is there a problem to solve?" *ISPRS Journal of Photogrammetry and Remote Sensing* 103, 129–135. DOI: 10.1016/j.isprsjprs.2014.09.006.

Nestola, E., J. Sánchez-Zapero, C. Latorre, F. Mazzenga, G. Matteucci, C. Calfapietra, and F. Camacho (2017). "Validation of PROBA-V GEOV1 and MODIS C5 & C6 fAPAR products in a deciduous beech forest site in Italy". *Remote Sensing* 9.126. DOI: 10.3390/rs90201026.

Newnham, G. J., J. D. Armston, K. Calders, M. I. Disney, J. L. Lovell, C. B. Schaaf, A. H. Strahler, and F. M. Danson (2015). "Terrestrial Laser Scanning for Plot-Scale Forest Measurement". *Current Forestry Reports* 1.4, 239–251. DOI: 10.1007/s40725-015-0025-5.

Newnham, G., N. Goodwin, J. Armston, J. Muir, and D. Culvenor (2012). "Comparing time-of-flight and phase-shift terrestrial laser scanners for characterising topography and vegetation density in a forest environment". *Proceedings of the SilviLaser 2012, Vancouver, Canada, 16-19 September 2012*.

Nightingale, J., K. F. Boersma, J. P. Muller, S. Compernolle, J. C. Lambert, S. Blessing, R. Giering, N. Gobron, I. D. Smedt, P. Coheur, M. George, J. Schulz, and A. Wood (2018a). "Quality assurance framework development based on six new ECV data products to enhance user confidence for climate applications". *Remote Sensing* 10.8. DOI: 10.3390/rs10081254.

Nightingale, J., N. Origo, S. Douglas, and J. Ryder (2018b). "FRM for land surface parameters: Validation with a Metrology perspective". In: *Land Product Validation and Evolution 2018, 27 Feb - 1 Mar 2018, ESA/ESRIN Frascati, Italy*. Frascati, Italy.

Nilsson, M., K. Nordkvist, J. Jonzén, N. Lindgren, P. Axensten, J. Wallerman, M. Egberth, S. Larsson, L. Nilsson, J. Eriksson, and H. Olsson (2017). "A nationwide forest attribute map of Sweden predicted using airborne laser scanning data and field data from the National Forest Inventory". *Remote Sensing of Environment* 194, 447–454. DOI: 10.1016/j.rse.2016.10.022.

North, P. (1996). "Three-dimensional forest light interaction model using a Monte Carlo method". *IEEE Transactions on Geoscience and Remote Sensing* 34.4, 946–956. DOI: 10.1109/36.508411.

OPTIMISE (2019). *ESSEM COST Action ES1309 OPTIMISE – Innovative optical Tools for proximal sensing of ecophysiological processes*. (accessed on 25 February 2019). URL: http://optimise.dcs.aber.ac.uk/.

Pádua, L., J. Vanko, J. Hruška, T. Adão, J. J. Sousa, E. Peres, and R. Morais (2017). "UAS, sensors, and data processing in agroforestry: a review towards practical applications". *International Journal of Remote Sensing* 38.8-10, 1–43. DOI: 10.1080/01431161.2017.1297548.

Pan, Y., R. A. Birdsey, O. L. Phillips, and R. B. Jackson (2013). "The Structure, Distribution, and Biomass of the World's Forests". *Annual Review of Ecology, Evolution, and Systematics* 44.1, 593–622. DOI: 10.1146/annurev-ecolsys-110512-135914.

Pardini, M., M. Tello, V. Cazcarra-Bes, K. P. Papathanassiou, and I. Hajnsek (2018). "L- and P-Band 3-D SAR Reflectivity Profiles Versus Lidar Waveforms: The AfriSAR Case". *IEEE Journal of Selected Topics in Applied Earth Observations and Remote Sensing* 11.10, 3386–3401. DOI: 10.1109/JSTARS.2018.2847033.

Parkan, M. and D. Tuia (2015). "Individual tree segmentation in deciduous forests using geodesic voting". In: *IEEE International Geoscience and Remote Sensing Symposium (IGARSS)*. IEEE, 637–640. DOI: 10.1109/IGARSS.2015.7325844.

– (2018). "Estimating Uncertainty of Point-Cloud Based Single-Tree Segmentation with Ensemble Based Filtering". *Remote Sensing* 10.2, 335. DOI: 10.3390/rs10020335.

Percival, G. C., I. P. Keary, and K. Noviss (2008). "The potential of a chlorophyll content SPAD meter to quantify nutrient stress in foliar tissue of sycamore (Acer pseudoplatanus), English oak (Quercus robur), and European beech (Fagus sylvatica)". *Arboriculture and Urban Forestry* 34.2, 89–100.

Petach, A. R., M. Toomey, D. M. Aubrecht, and A. D. Richardson (2014). "Monitoring vegetation phenology using an infrared-enabled security camera". *Agricultural and Forest Meteorology* 195-196, 143–151. DOI: 10.1016/j.agrformet.2014.05.008.

Pimont, F., D. Allard, M. Soma, and J.-L. Dupuy (2018). "Estimators and confidence intervals for plant area density at voxel scale with T-LiDAR". *Remote Sensing of Environment* 215.June, 343–370. DOI: 10.1016/j.rse.2018.06.024. arXiv: RSE10796.

Pitkänen, T. P., P. Raumonen, and A. Kangas (2019). "Measuring stem diameters with TLS in boreal forests by complementary fitting procedure". *ISPRS Journal of Photogrammetry and Remote Sensing* 147.March 2018, 294–306. DOI: 10.1016/j.isprsjprs.2018.11.027.

Portillo-Quintero, C., A. Sanchez-Azofeifa, and D. Culvenor (2014). "Using VEGNET In-Situ Monitoring LiDAR (IML) to Capture Dynamics of Plant Area Index, Structure and Phenology in Aspen Parkland Forests in Alberta, Canada". *Forests* 5.5, 1053–1068. DOI: 10.3390/f5051053.

Puliti, S., H. Olerka, T. Gobakken, and E. Næsset (2015). "Inventory of Small Forest Areas Using an Unmanned Aerial System". *Remote Sensing* 7.8, 9632–9654. DOI: 10.3390/rs70809632.

Qu, Y., L. Fu, W. Han, Y. Zhu, and J. Wang (2014a). "MLAOS: A multi-point linear array of optical sensors for coniferous foliage clumping index measurement". *Sensors* 14.5, 9271–9289. DOI: 10.3390/s140509271.

Qu, Y., W. Han, L. Fu, C. Li, J. Song, H. Zhou, Y. Bo, and J. Wang (2014b). "LAINet - A wireless sensor network for coniferous forest leaf area index measurement: Design, algorithm and validation". *Computers and Electronics in Agriculture* 108, 200–208. DOI: 10.1016/j.compag.2014.08.003.

R Core Team (2014). *R: A Language and Environment for Statistical Computing*. Vienna: R Foundation for Statistical Computing.

Rabbani, T. and F. V. D. Heuvel (2005). "Efficient Hough Transform for Automatic Detection of Cylinders in Point Clouds". *ISPRS Workshop on Laser Scanning* 3, 60–65. DOI: 10.1.1.118.1736.

RadCalNet (2019). *RadCalNet – Homepage*. (accessed on 19 February 2019). URL: https://www.radcalnet.org.

Rahman, M. Z. A., M. A. A. Bakar, K. A. Razak, A. W. Rasib, K. D. Kanniah, W. H. W. Kadir, H. Omar, A. Faidi, A. R. Kassim, and Z. A. Latif (2017). "Non-destructive, laser-based individual tree aboveground biomass estimation in a tropical rainforest". *Forests* 8.3. DOI: 10.3390/f8030086.

Raumonen, P., M. Kaasalainen, M. Åkerblom, S. Kaasalainen, H. Kaartinen, M. Vastaranta, M. Holopainen, M. Disney, and P. Lewis (2013). "Fast Automatic Precision Tree Models from Terrestrial Laser Scanner Data". *Remote Sensing* 5.2, 491–520. DOI: 10.3390/rs5020491.

Raymaekers, D., A. Garcia, C. Di Bella, M. Beget, C. Llavallol, P. Oricchio, J. Straschnoy, M. Weiss, and F. Baret (2014). "SPOT-VEGETATION GEOV1 biophysical parameters in semi-arid agro-ecosystems". *International Journal of Remote Sensing* 35.7, 2534–2547. DOI: 10.1080/01431161.2014.883096.

Reiche, J., R. Lucas, A. L. Mitchell, J. Verbesselt, D. H. Hoekman, J. Haarpaintner, J. M. Kellndorfer, A. Rosenqvist, E. A. Lehmann, C. E. Woodcock, F. M. Seifert, and M. Herold (2016). "Combining satellite data for better tropical forest monitoring". *Nature Climate Change* 6.2, 120–122. DOI: 10.1038/nclimate2919.

Reiche, J., J. Verbesselt, D. Hoekman, and M. Herold (2015). "Fusing Landsat and SAR time series to detect deforestation in the tropics". *Remote Sensing of Environment* 156, 276–293. DOI: 10.1016/j.rse.2014.10.001.

Reigber, A. and A. Moreira (2000). "First demonstration of airborne SAR tomography using multibaseline L-band data". *IEEE Transactions on Geoscience and Remote Sensing* 38.5, 2142–2152. DOI: 10.1109/36.868873.

Reineman, B. D., L. Lenain, N. M. Statom, and W. K. Melville (2013). "Development and Testing of Instrumentation for UAV-Based Flux Measurements within Terrestrial and Marine Atmospheric Boundary Layers". *Journal of Atmospheric and Oceanic Technology* 30.7, 1295–1319. DOI: 10.1175/JTECH-D-12-00176.1.

Richardson, A. D., B. H. Braswell, D. Y. Hollinger, J. P. Jenkins, and S. V. Ollinger (2009). "Near-surface remote sensing of spatial and temporal variation in canopy phenology". *Ecological Applications* 19.6, 1417–1428. DOI: 10.1890/08-2022.1.

Richardson, A. D., T. F. Keenan, M. Migliavacca, Y. Ryu, O. Sonnentag, and M. Toomey (2013). "Climate change, phenology, and phenological control of vegetation feedbacks to the climate system". *Agricultural and Forest Meteorology* 169, 156–173. DOI: 10.1016/j.agrformet.2012.09.012.

Richter, K., T. B. Hank, F. Vuolo, W. Mauser, and G. D'Urso (2012). "Optimal exploitation of the Sentinel-2 spectral capabilities for crop leaf area index mapping". *Remote Sensing* 4.3, 561–582. DOI: 10.3390/rs4030561.

RIEGL LMS GmbH (2017). *RIEGL LMS RiProcess for RIEGL Scan Data*. (accessed on 13 September 2017). URL: http://www.riegl.com/uploads/tx_pxpriegldownloads/11_Datasheet_RiProcess_2016-09-16_03.pdf.

Ristorcelli, T., D. Hamoir, and X. Briottet (2014). "Simulating Space Lidar Waveforms From Smaller-Footprint Airborne Laser Scanner Data for Vegetation Observation". *IEEE Geoscience and Remote Sensing Letters* 11.2, 534–538. DOI: 10.1109/LGRS.2013.2273801.

Rivera, J. P., J. Verrelst, G. Leonenko, and J. Moreno (2013). "Multiple cost functions and regularization options for improved retrieval of leaf chlorophyll content and LAI through inversion of the PROSAIL model". *Remote Sensing* 5, 3280–3304. DOI: 10.3390/rs5073280.

Roosjen, P. P., B. Brede, J. M. Suomalainen, H. M. Bartholomeus, L. Kooistra, and J. G. Clevers (2018). "Improved estimation of leaf area index and leaf chlorophyll content of a potato crop using multi-angle spectral data – potential of unmanned aerial vehicle imagery". *International Journal of Applied Earth Observation and Geoinformation* 66, 14–26. DOI: 10.1016/j.jag.2017.10.012.

Roth, L., H. Aasen, A. Walter, and F. Liebisch (2018). "Extracting leaf area index using viewing geometry effects – A new perspective on high-resolution unmanned aerial system photography". *ISPRS Journal of Photogrammetry and Remote Sensing* 141, 161–175. DOI: 10.1016/j.isprsjprs.2018.04.012.

Rüetschi, M., M. E. Schaepman, and D. Small (2018). "Using Multitemporal Sentinel-1 C-band Backscatter to Monitor Phenology and Classify Deciduous and Coniferous Forests in Northern Switzerland". *Remote Sensing* 10.1, 55. DOI: 10.3390/rs10010055.

Saatchi, S. S., N. L. Harris, S. Brown, M. Lefsky, E. T. A. Mitchard, W. Salas, B. R. Zutta, W. Buermann, S. L. Lewis, S. Hagen, S. Petrova, L. White, M. Silman, and A. Morel (2011). "Benchmark map of forest carbon stocks in tropical regions across three continents". *Proceedings of the National Academy of Sciences* 108.24, 9899–9904. DOI: 10.1073/pnas.1019576108.

Saleska, S. R., K. Didan, A. R. Huete, and H. R. da Rocha (2007). "Amazon forests green-up during 2005 drought". *Science* 318.5850, 612. DOI: 10.1126/science.1146663.

Saltelli, A., P. Annoni, I. Azzini, F. Campolongo, M. Ratto, and S. Tarantola (2010). "Variance based sensitivity analysis of model output. Design and estimator for the total sensitivity index". *Computer Physics Communications* 181.2, 259–270. DOI: 10.1016/j.cpc.2009.09.018.

Samanta, A., Y. Knyazikhin, L. Xu, R. E. Dickinson, R. Fu, M. H. Costa, S. S. Saatchi, R. R. Nemani, and R. B. Myneni (2012). "Seasonal changes in leaf area of Amazon forests from leaf flushing and abscission". *Journal of Geophysical Research* 117.G1, G01015. DOI: 10.1029/2011JG001818.

Sankey, T., J. Donager, J. McVay, and J. B. Sankey (2017). "UAV lidar and hyperspectral fusion for forest monitoring in the southwestern USA". *Remote Sensing of Environment* 195, 30–43. DOI: 10.1016/j.rse.2017.04.007.

Santoro, M., A. Beaudoin, C. Beer, O. Cartus, J. E. Fransson, R. J. Hall, C. Pathe, C. Schmullius, D. Schepaschenko, A. Shvidenko, M. Thurner, and U. Wegmüller (2015). "Forest growing stock volume of the northern hemisphere: Spatially explicit estimates for 2010 derived from Envisat ASAR". *Remote Sensing of Environment* 168, 316–334. DOI: 10.1016/j.rse.2015.07.005.

Santoro, M. and O. Cartus (2018). "Research Pathways of Forest Above-Ground Biomass Estimation Based on SAR Backscatter and Interferometric SAR Observations". *Remote Sensing* 10, 608. DOI: 10.3390/rs10040608.

Schlerf, M. and C. Atzberger (2006). "Inversion of a forest reflectance model to estimate structural canopy variables from hyperspectral remote sensing data". *Remote Sensing of Environment* 100.3, 281–294. DOI: 10.1016/j.rse.2005.10.006.

– (2012). "Vegetation Structure Retrieval in Beech and Spruce Forests Using Spectrodirectional Satellite Data". *IEEE Journal of Selected Topics in Applied Earth Observations and Remote Sensing* 5.1, 8–17. DOI: 10.1109/JSTARS.2012.2184268.

SENSECO (2019). *COST Action CA17134 SENSECO – Optical synergies for spatiotemporal SENsing of Scalable ECOphysiological traits*. (accessed on 25 February 2019). URL: http://www.senseco.eu/.

Simic, A., F. Baret, M. Weiss, R. Lecerf, A. Alessandrini, J.-F. Hanocq, and O. Marloie (2012). "Production of the high resolution maps of biophysical variables based on SPOT imagery and in-situ measurements generated by PASTIS 57 for Hyytiala, Finland". In: *IEEE International Geoscience and Remote Sensing Symposium*. Munich, Germany: IEEE, 7655–7658. DOI: 10.1109/IGARSS.2012.6351854.

Simonse, M., T. Aschoff, H. Spiecker, and M. Thies (2003). "Automatic Determination of Forest Inventory Parameters Using Terrestrial Laserscanning". In: *ScandLaser Scientific Workshop on Airborne Laser Scanning of Forests*, 251–257.

Sims, D. A., A. F. Rahman, E. F. Vermote, and Z. Jiang (2011). "Seasonal and inter-annual variation in view angle effects on MODIS vegetation indices at three forest sites". *Remote Sensing of Environment* 115.12, 3112–3120. DOI: 10.1016/j.rse.2011.06.018.

Sobol', I. (1990). "On sensitivity estimation for nonlinear mathematical models". *Mathematical Modeling* 2, 112–118.

Soma, M., F. Pimont, S. Durrieu, and J.-L. Dupuy (2018). "Enhanced Measurements of Leaf Area Density with T-LiDAR: Evaluating and Calibrating the Effects of Vegetation Heterogeneity and Scanner Properties". *Remote Sensing* 10, 1580. DOI: 10.3390/rs10101580.

Soudani, K., G. Hmimina, N. Delpierre, J. Y. Pontailler, M. Aubinet, D. Bonal, B. Caquet, A. de Grandcourt, B. Burban, C. Flechard, D. Guyon, A. Granier, P. Gross, B. Heinesh, B. Longdoz, D. Loustau, C. Moureaux, J. M. Ourcival, S. Rambal, L. Saint André, and E. Dufrêne (2012). "Ground-based Network of NDVI measurements for tracking temporal dynamics of canopy structure and vegetation phenology in different biomes". *Remote Sensing of Environment* 123, 234–245. DOI: 10.1016/j.rse.2012.03.012.

Stöcker, C., R. Bennett, F. Nex, M. Gerke, and J. Zevenbergen (2017). "Review of the current state of UAV regulations". *Remote Sensing* 9.5, 33–35. DOI: 10.3390/rs9050459.

Stoval, A. and H. H. Shugart (2018). "Improved Biomass Calibration and Validation With Terrestrial LiDAR: Implications for Future LiDAR and SAR Missions". *IEEE Journal of Selected Topics in Applied Earth Observations and Remote Sensing* 11.9. DOI: 10.1109/JSTARS.2018.2803110.

Stovall, A. E. L., A. G. Vorster, R. S. Anderson, P. H. Evangelista, and H. H. Shugart (2017). "Non-destructive aboveground biomass estimation of coniferous trees using terrestrial LiDAR". *Remote Sensing of Environment* 200.January, 31–42. DOI: 10.1016/j.rse.2017.08.013.

Strîmbu, V. F. and B. M. Strîmbu (2015). "A graph-based segmentation algorithm for tree crown extraction using airborne LiDAR data". *ISPRS Journal of Photogrammetry and Remote Sensing* 104, 30–43. DOI: 10.1016/j.isprsjprs.2015.01.018.

Suomalainen, J., N. Anders, S. Iqbal, G. Roerink, J. Franke, P. Wenting, D. Hünniger, H. Bartholomeus, R. Becker, and L. Kooistra (2014). "A Lightweight Hyperspectral

Mapping System and Photogrammetric Processing Chain for Unmanned Aerial Vehicles". *Remote Sensing* 6.11, 11013–11030. DOI: 10.3390/rs61111013.

Tang, H., M. Brolly, F. Zhao, A. H. Strahler, C. L. Schaaf, S. Ganguly, G. Zhang, and R. Dubayah (2014). "Deriving and validating Leaf Area Index (LAI) at multiple spatial scales through lidar remote sensing: A case study in Sierra National Forest, CA". *Remote Sensing of Environment* 143, 131–141. DOI: 10.1016/j.rse.2013.12.007.

Tang, L. and G. Shao (2015). "Drone remote sensing for forestry research and practices". *Journal of Forestry Research* 26.4, 791–797. DOI: 10.1007/s11676-015-0088-y.

Teets, D. (2003). "Predicting sunrise and sunset times". *The College Mathematics Journal* 34.4, 317–321.

Tewes, A. and J. Schellberg (2018). "Towards Remote Estimation of Radiation Use Efficiency in Maize Using UAV-Based Low-Cost Camera Imagery". *Agronomy* 8.2, 16. DOI: 10.3390/agronomy8020016.

Thiel, C. and C. Schmullius (2016). "The potential of ALOS PALSAR backscatter and InSAR coherence for forest growing stock volume estimation in Central Siberia". *Remote Sensing of Environment* 173, 258–273. DOI: 10.1016/j.rse.2015.10.030.

Tian, J., L. Wang, X. Li, H. Gong, C. Shi, R. Zhong, and X. Liu (2017). "Comparison of UAV and WorldView-2 imagery for mapping leaf area index of mangrove forest". *International Journal of Applied Earth Observation and Geoinformation* 61.May, 22–31. DOI: 10.1016/j.jag.2017.05.002.

Torres, R., P. Snoeij, D. Geudtner, D. Bibby, M. Davidson, E. Attema, P. Potin, B. Rommen, N. Floury, M. Brown, I. N. Traver, P. Deghaye, B. Duesmann, B. Rosich, N. Miranda, C. Bruno, M. L'Abbate, R. Croci, A. Pietropaolo, M. Huchler, and F. Rostan (2012). "GMES Sentinel-1 mission". *Remote Sensing of Environment* 120, 9–24. DOI: 10.1016/j.rse.2011.05.028.

Torresan, C., A. Berton, F. Carotenuto, S. F. Di Gennaro, B. Gioli, A. Matese, F. Miglietta, C. Vagnoli, A. Zaldei, and L. Wallace (2016). "Forestry applications of UAVs in Europe: a review". *International Journal of Remote Sensing* 38.8-10, 2427–2447. DOI: 10.1080/01431161.2016.1252477.

Tremblay, J.-F. and M. Béland (2018). "Towards operational marker-free registration of terrestrial lidar data in forests". *ISPRS Journal of Photogrammetry and Remote Sensing* 146, 430–435. DOI: 10.1016/j.isprsjprs.2018.10.011.

Vaccari, S., M. van Leeuwen, K. Calders, N. C. Coops, and M. Herold (2013). "Bias in lidar-based canopy gap fraction estimates". *Remote Sensing Letters* 4.4, 391–399. DOI: 10.1080/2150704X.2012.742211.

Vafaei, S., J. Soosani, K. Adeli, H. Fadaei, H. Naghavi, T. D. Pham, and D. T. Bui (2018). "Improving accuracy estimation of Forest Aboveground Biomass based on incorporation

of ALOS-2 PALSAR-2 and Sentinel-2A imagery and machine learning: A case study of the Hyrcanian forest area (Iran)". *Remote Sensing* 10.2. DOI: 10.3390/rs10020172.

Valle, B., T. Simonneau, R. Boulord, F. Sourd, T. Frisson, M. Ryckewaert, P. Hamard, N. Brichet, M. Dauzat, and A. Christophe (2017). "PYM: A new, affordable, image-based method using a Raspberry Pi to phenotype plant leaf area in a wide diversity of environments". *Plant Methods* 13.1, 1–17. DOI: 10.1186/s13007-017-0248-5.

Verrelst, J., M. E. Schaepman, B. Koetz, and M. Kneubühler (2008). "Angular sensitivity analysis of vegetation indices derived from CHRIS/PROBA data". *Remote Sensing of Environment* 112, 2341–2353. DOI: 10.1016/j.rse.2007.11.001.

Verrelst, J., G. Camps-Valls, J. Muñoz-Marí, J. P. Rivera, F. Veroustraete, J. G. Clevers, and J. Moreno (2015a). "Optical remote sensing and the retrieval of terrestrial vegetation bio-geophysical properties - A review". *ISPRS Journal of Photogrammetry and Remote Sensing* 108, 273–290. DOI: 10.1016/j.isprsjprs.2015.05.005.

Verrelst, J., J. Muñoz, L. Alonso, J. Delegido, J. P. Rivera, G. Camps-Valls, and J. Moreno (2012). "Machine learning regression algorithms for biophysical parameter retrieval: Opportunities for Sentinel-2 and -3". *Remote Sensing of Environment* 118, 127–139. DOI: 10.1016/j.rse.2011.11.002.

Verrelst, J., J. P. Rivera, G. Leonenko, L. Alonso, and J. Moreno (2014). "Optimizing LUT-based RTM inversion for semiautomatic mapping of crop biophysical parameters from Sentinel-2 and -3 data: Role of cost functions". *IEEE Transactions on Geoscience and Remote Sensing* 52.1, 257–269. DOI: 10.1109/TGRS.2013.2238242.

Verrelst, J., J. P. Rivera, J. Moreno, and G. Camps-Valls (2013). "Gaussian processes uncertainty estimates in experimental Sentinel-2 LAI and leaf chlorophyll content retrieval". *ISPRS Journal of Photogrammetry and Remote Sensing* 86, 157–167. DOI: 10.1016/j.isprsjprs.2013.09.012.

Verrelst, J., J. P. Rivera, F. Veroustraete, J. Muñoz-Marí, J. G. Clevers, G. Camps-Valls, and J. Moreno (2015b). "Experimental Sentinel-2 LAI estimation using parametric, non-parametric and physical retrieval methods - A comparison". *ISPRS Journal of Photogrammetry and Remote Sensing* 108, 260–272. DOI: 10.1016/j.isprsjprs.2015.04.013.

Verrelst, J., N. Sabater, J. Rivera, J. Muñoz-Marí, J. Vicent, G. Camps-Valls, and J. Moreno (2016). "Emulation of Leaf, Canopy and Atmosphere Radiative Transfer Models for Fast Global Sensitivity Analysis". *Remote Sensing* 8.8, 673. DOI: 10.3390/rs8080673.

Vicari, M. B., M. Disney, P. Wilkes, A. Burt, K. Calders, and W. Woodgate (2019). "Leaf and wood classification framework for terrestrial LiDAR point clouds". *Methods in Ecology and Evolution*. Ed. by R. Freckleton, 1–15. DOI: 10.1111/2041-210X.13144.

Villard, L., T. Le Toan, D. H. Tang Minh, S. Mermoz, and A. Bouvet (2016). "Forest Biomass From Radar Remote Sensing". *Land Surface Remote Sensing in Agriculture and Forest*, 363–425. DOI: 10.1016/B978-1-78548-103-1.50009-1.

Wallace, L., S. Hillman, K. Reinke, and B. Hally (2017). "Non-destructive estimation of above-ground surface and near-surface biomass using 3D terrestrial remote sensing techniques". *Methods in Ecology and Evolution* 8.11. Ed. by D. Kriticos, 1607–1616. DOI: 10.1111/2041-210X.12759.

Wallace, L., A. Lucieer, Z. Malenovský, D. Turner, and P. Vopěnka (2016). "Assessment of forest structure using two UAV techniques: A comparison of airborne laser scanning and structure from motion (SfM) point clouds". *Forests* 7.3, 1–16. DOI: 10.3390/f7030062.

Wallace, L., A. Lucieer, and C. S. Watson (2014a). "Evaluating tree detection and segmentation routines on very high resolution UAV LiDAR data". *IEEE Transactions on Geoscience and Remote Sensing* 52.12, 7619–7628. DOI: 10.1109/TGRS.2014.2315649.

Wallace, L., A. Lucieer, C. Watson, and D. Turner (2012). "Development of a UAV-LiDAR system with application to forest inventory". *Remote Sensing* 4.6, 1519–1543. DOI: 10.3390/rs4061519.

Wallace, L., R. Musk, and A. Lucieer (2014b). "An assessment of the repeatability of automatic forest inventory metrics derived from UAV-borne laser scanning data". *IEEE Transactions on Geoscience and Remote Sensing* 52.11, 7160–7169. DOI: 10.1109/TGRS.2014.2308208.

Wallis, C. I., D. Paulsch, J. Zeilinger, B. Silva, G. F. Curatola Fernández, R. Brandl, N. Farwig, and J. Bendix (2016). "Contrasting performance of Lidar and optical texture models in predicting avian diversity in a tropical mountain forest". *Remote Sensing of Environment* 174.January, 223–232. DOI: 10.1016/j.rse.2015.12.019.

Wang, D., J. Brunner, Z. Ma, H. Lu, M. Hollaus, Y. Pang, and N. Pfeifer (2018). "Separating Tree Photosynthetic and Non-Photosynthetic Components from Point Cloud Data Using Dynamic Segment Merging". *Forests* 9.5, 252. DOI: 10.3390/f9050252.

Wang, R., J. M. Chen, Z. Liu, and A. Arain (2017). "Evaluation of seasonal variations of remotely sensed leaf area index over five evergreen coniferous forests". *ISPRS Journal of Photogrammetry and Remote Sensing* 130, 187–201. DOI: 10.1016/j.isprsjprs.2017.05.017.

Wei, L., B. Yang, J. Jiang, G. Cao, and M. Wu (2017). "Vegetation filtering algorithm for UAV-borne lidar point clouds: a case study in the middle-lower Yangtze River riparian zone". *International Journal of Remote Sensing* 38.8-10, 1–12. DOI: 10.1080/01431161.2016.1252476.

Weiss, M., F. Baret, G. J. Smith, I. Jonckheere, and P. Coppin (2004). "Review of methods for in situ leaf area index (LAI) determination Part II. Estimation of LAI, errors and sampling". *Agricultural and Forest Meteorology* 121.1-2, 37–53. DOI: 10.1016/j.agrformet.2003.08.001.

Weiss, M. and F. Baret (2016). *S2ToolBox Level 2 products: LAI, FAPAR, FCOVER.* Version 1.1. URL: http://step.esa.int/docs/extra/ATBD_S2ToolBox_L2B_V1.1.pdf.

Weiss, M., F. Baret, S. Garrigues, and R. Lacaze (2007). "LAI and fAPAR CYCLOPES global products derived from VEGETATION. Part 2: validation and comparison with MODIS collection 4 products". *Remote Sensing of Environment* 110.3, 317–331. DOI: 10.1016/j.rse.2007.03.001.

White, J. C., N. C. Coops, M. A. Wulder, M. Vastaranta, T. Hilker, and P. Tompalski (2016). "Remote Sensing Technologies for Enhancing Forest Inventories: A Review". *Canadian Journal of Remote Sensing* 8992.December, 1–23. DOI: 10.1080/07038992.2016.1207484.

Widlowski, J. L., C. Mio, M. Disney, J. Adams, I. Andredakis, C. Atzberger, J. Brennan, L. Busetto, M. Chelle, G. Ceccherini, R. Colombo, J. F. Côté, A. Eenmäe, R. Essery, J. P. Gastellu-Etchegorry, N. Gobron, E. Grau, V. Haverd, L. Homolová, H. Huang, L. Hunt, H. Kobayashi, B. Koetz, A. Kuusk, J. Kuusk, M. Lang, P. E. Lewis, J. L. Lovell, Z. Malenovský, M. Meroni, F. Morsdorf, M. Mõttus, W. Ni-Meister, B. Pinty, M. Rautiainen, M. Schlerf, B. Somers, J. Stuckens, M. M. Verstraete, W. Yang, F. Zhao, and T. Zenone (2015). "The fourth phase of the radiative transfer model intercomparison (RAMI) exercise: Actual canopy scenarios and conformity testing". *Remote Sensing of Environment* 169, 418–437. DOI: 10.1016/j.rse.2015.08.016.

Widlowski, J. L., M. Taberner, B. Pinty, V. Bruniquel-Pinel, M. Disney, R. Fernandes, J. P. Gastellu-Etchegorry, N. Gobron, A. Kuusk, T. Lavergne, S. Leblanc, P. E. Lewis, E. Martin, M. Mõttus, P. North, W. Qin, M. Robustelli, N. Rochdi, R. Ruiloba, C. Soler, R. Thompson, W. Verhoef, M. M. Verstraete, and D. Xie (2007). "Third Radiation Transfer Model Intercomparison (RAMI) exercise: Documenting progress in canopy reflectance models". *Journal of Geophysical Research: Atmospheres* 112.9, 1–28. DOI: 10.1029/2006JD007821.

Wieser, M., G. Mandlburger, M. Hollaus, J. Otepka, P. Glira, and N. P. Id (2017). "A Case Study of UAS Borne Laser Scanning for Measurement of Tree Stem Diameter". *Remote Sensing* 9.11, 1–11. DOI: 10.3390/rs9111154.

Wilkes, P., A. Lau, M. I. Disney, K. Calders, A. Burt, J. Gonzalez de Tanago, H. Bartholomeus, B. Brede, and M. Herold (2017). "Data Acquisition Considerations for Terrestrial Laser Scanning of Forest Plots". *Remote Sensing of Environment* 196, 140–153. DOI: 10.1016/j.rse.2017.04.030.

Wilson, J. W. (1963). "Estimation of foliage denseness and foliage angle by inclined point quadrats". *Australian Journal of Botany* 11.1, 95–105. DOI: 10.1071/BT9630095.

WMO (2016). *GCOS-200 – The Global Observing System for Climate: Implementation Needs*. (accessed on 23 January 2019). URL: https://unfccc.int/sites/default/files/gcos_ip_10oct2016.pdf.

Woodgate, W., J. D. Armston, M. Disney, S. D. Jones, L. Suarez, M. J. Hill, P. Wilkes, and M. Soto-Berelov (2016). "Quantifying the impact of woody material on leaf area index

estimation from hemispherical photography using 3D canopy simulations". *Agricultural and Forest Meteorology* 226-227, 1–12. DOI: 10.1016/j.agrformet.2016.05.009.

Woodgate, W., S. D. Jones, L. Suarez, M. J. Hill, J. D. Armston, P. Wilkes, M. Soto-Berelov, A. Haywood, and A. Mellor (2015). "Understanding the variability in ground-based methods for retrieving canopy openness, gap fraction, and leaf area index in diverse forest systems". *Agricultural and Forest Meteorology* 205, 83–95. DOI: 10.1016/j.agrformet.2015.02.012.

Wulder, M. A., J. G. Masek, W. B. Cohen, T. R. Loveland, and C. E. Woodcock (2012). "Opening the archive: How free data has enabled the science and monitoring promise of Landsat". *Remote Sensing of Environment* 122, 2–10. DOI: 10.1016/j.rse.2012.01.010.

Xiao, X., S. Hagen, Q. Zhang, M. Keller, and B. Moore (2006). "Detecting leaf phenology of seasonally moist tropical forests in South America with multi-temporal MODIS images". *Remote Sensing of Environment* 103.4, 465–473. DOI: 10.1016/j.rse.2006.04.013.

Yang, X., J. Tang, J. F. Mustard, J. Wu, K. Zhao, S. Serbin, and J. E. Lee (2016). "Seasonal variability of multiple leaf traits captured by leaf spectroscopy at two temperate deciduous forests". *Remote Sensing of Environment* 179, 1–12. DOI: 10.1016/j.rse.2016.03.026.

Yick, J., B. Mukherjee, and D. Ghosal (2008). "Wireless sensor network survey". *Computer Networks* 52.12, 2292–2330. DOI: 10.1016/j.comnet.2008.04.002. arXiv: 1011.1529.

Yin, G., A. Verger, Y. Qu, W. Zhao, B. Xu, Y. Zeng, K. Liu, J. Li, and Q. Liu (2019). "Retrieval of High Spatiotemporal Resolution Leaf Area Index with Gaussian Processes, Wireless Sensor Network, and Satellite Data Fusion". *Remote Sensing* 11.3, 244. DOI: 10.3390/rs11030244.

Yuen, J. Q., T. Fung, and A. D. Ziegler (2016). "Review of allometric equations for major land covers in SE Asia: Uncertainty and implications for above- and below-ground carbon estimates". *Forest Ecology and Management* 360, 323–340. DOI: 10.1016/j.foreco.2015.09.016.

Zarco-Tejada, P. J., R. Diaz-Varela, V. Angileri, and P. Loudjani (2014). "Tree height quantification using very high resolution imagery acquired from an unmanned aerial vehicle (UAV) and automatic 3D photo-reconstruction methods". *European Journal of Agronomy* 55, 89–99. DOI: 10.1016/j.eja.2014.01.004.

Zarco-Tejada, P., V. González-Dugo, and J. Berni (2012). "Fluorescence, temperature and narrow-band indices acquired from a UAV platform for water stress detection using a micro-hyperspectral imager and a thermal camera". *Remote Sensing of Environment* 117, 322–337. DOI: 10.1016/j.rse.2011.10.007.

Zhang, X., M. A. Friedl, C. B. Schaaf, A. H. Strahler, J. C. F. Hodges, F. Gao, B. C. Reed, and A. Huete (2003). "Monitoring vegetation phenology using MODIS". *Remote Sensing of Environment* 84.3, 471–475. DOI: 10.1016/S0034-4257(02)00135-9.

Zhen, Z., L. J. Quackenbush, and L. Zhang (2016). "Trends in automatic individual tree crown detection and delineation-evolution of LiDAR data". *Remote Sensing* 8.4, 1–26. DOI: 10.3390/rs8040333.

Zheng, G., L. Ma, J. U. H. Eitel, W. He, T. S. Magney, L. M. Moskal, and M. Li (2017). "Retrieving Directional Gap Fraction, Extinction Coefficient, and Effective Leaf Area Index by Incorporating Scan Angle Information From Discrete Aerial Lidar Data". *IEEE Transactions on Geoscience and Remote Sensing* 55.1, 577–590. DOI: 10.1109/TGRS.2016.2611651.

Zheng, G. and L. M. Moskal (2009). "Retrieving Leaf Area Index (LAI) Using Remote Sensing: Theories, Methods and Sensors". *Sensors* 9.4, 2719–2745. DOI: 10.3390/s90402719.

– (2012). "Spatial variability of terrestrial laser scanning based leaf area index". *International Journal of Applied Earth Observation and Geoinformation* 19.1, 226–237. DOI: 10.1016/j.jag.2012.05.002.

Zhu, X., A. K. Skidmore, R. Darvishzadeh, K. O. Niemann, J. Liu, Y. Shi, and T. Wang (2018). "Foliar and woody materials discriminated using terrestrial LiDAR in a mixed natural forest". *International Journal of Applied Earth Observation and Geoinformation* 64.September 2017, 43–50. DOI: 10.1016/j.jag.2017.09.004.

Zou, J., G. Yan, L. Zhu, and W. Zhang (2009). "Woody-to-total area ratio determination with a multispectral canopy imager". *Tree Physiology* 29.8, 1069–1080. DOI: 10.1093/treephys/tpp042.

Summary

Forests play a crucial role in the functioning of the Earth's climate system, through their role in the carbon, energy and water cycles. The accurate description and quantification of their physical structure is essential to understand these roles, predict their behaviour under future climate change and adapt management practices accordingly. Remote sensing in particular from space-borne platforms is attractive for large area assessment of forest structure due to its cost-effectiveness, repeatability and objectiveness. However, the remote sensing signal is by nature ambiguous and needs to be interpreted with solid understanding of the underlying radiative mechanisms and uncertainties need to be rigorously quantified with independent ground data. The remote sensing community has produced a range of biophysical products describing vegetation and forest structure as well as best practice guidelines for their validation. However, the full implementation of anticipated products, including systematic repetition of validation across multiple sites (Committee on Earth Observing Satellites (CEOS) Land Product Validation (LPV) stage 4), is still to be concluded. A major challenge in this context is the provision of long-term validation data sets, which need to be cost-effective, repeatable and fast to acquire in the field.

This thesis aims to investigate new ways of validation that meet the temporal and/or spatial scales of global forest structure products from space-borne missions with hectometric resolution. The particular focus is on Leaf Area Index (LAI) and Above-Ground Biomass (AGB) as metrics of physical forest structure. For the purpose of this thesis, the Speulderbos Reference site in the Veluwe forest area (The Netherlands) was established, where ground and Unmanned Aerial Vehicle (UAV)-borne sensors were tested.

In Chapter 2, the automatic, passive optical sensor PAI Autonomous System from Transmittance Sensors at 57° (PASTiS-57) was tested for its suitability to monitor forest phenology and Plant Area Index (PAI), the total one-sided area of plant material per unit ground. For this, Radiative Transfer Model (RTM) experiments with turbid media and heterogeneous scenes were employed. PASTiS-57 generally meets the CEOS LPV requirement of 20 % accuracy over a wide range of biochemical and illumination conditions for turbid medium canopies. However, canopy non-randomness in discrete tree models led to strong biases. In a field experiment, PASTiS-57 compared well in terms of phenological

timing with Terrestrial Laser Scanning (TLS)-based PAI time series. PASTiS-57 represents a cost-effective way to continuously monitor PAI in forests.

In Chapter 3, decametric resolution Sentinel-2 and Landsat 7/8 observations were analysed with hybrid LAI retrieval algorithms, which combine RTMs with Machine Learning Regression Algorithms (MLRAs). Several combinations of RTMs, MLRAs, and modifications to the processing chain were tested in order to assess their performance to predict a ground-based LAI time series, created from combined TLS and litter trap data. Most important for the success of the processing chain was the addition of a certain level of Gaussian noise to the RTM-produced database prior to MLRA training. With this processing chain, decametric resolution optical missions can produce reference LAI products for inter-comparison with hectometric products. Alternatively, the higher resolution can help to scale up small plot-based ground validation data.

In Chapter 4, a novel Unmanned Aerial Vehicle Laser Scanning (UAV-LS), the RiCOPTER with VUX®-1UAV laser scanner, was used to estimate canopy height and Diameter at Breast Height (DBH). TLS was used to derive reference datasets for both variables. Canopy height was comparable between both sensors with a slight underestimation for TLS, which was expected due to occlusion of the upper canopy when seen from below and hence lower TLS canopy heights. DBH was derived for the first time from UAV-LS data and compared well with TLS derived DBH. However, a part of the UAV-LS samples could not produce a meaningful estimate of DBH based on the extracted point cloud segment due to low point density. Repeated overpasses could counteract this to some degree. In this context, UAV-LS can support fast, plot-scale assessment of these two variables.

In Chapter 5, the capabilities of UAV-LS are further explored in terms of explicit 3D modelling in order to estimate tree volume, which is the first step to retrieve tree AGB. For this purpose, 3D cylinder models were fitted to the segmented single trees with the *TreeQSM* routine. The resulting models were compared with TLS-based models and analysed separately for five different stands with varying architectures, including deciduous and coniferous species. UAV-LS was generally very successful in modelling large, deciduous trees, while coniferous trees with low branches and foliage as well as small trees proved more difficult. If successful, UAV-LS can provide the means to produce plot-scale assessment of woody volume and subsequently AGB at a fraction of time needed for TLS surveys.

This thesis investigates new ways of forest structure product validation with techniques and sensors that meet the temporal and/or spatial resolution of hectometric space-borne missions.

Acknowledgements

I am grateful that my PhD thesis worked out as it did despite my different ideas of how it would be at the start. Learning how to deal with changes to the plan was among the important lessons I learned in the process. There were a range of people who helped me to deal with the new situations.

First in line to give my thanks to is my promotor Martin Herold for giving me the opportunity to pursue a PhD. From the start, you had the trust to send me to international expert meetings where I represented our group. But foremost, I am thankful for the freedom you gave me to explore new topics and extend my work to UAVs when the RiCOPTER arrived in our group.

To my co-promotors, Jan Clevers and Jan Verbesselt, I am thankful for your critical thinking along in our meetings and comments on manuscripts. Additional thanks to Jan Clevers for your support in formal university matters and your fast reviews on manuscripts whenever I needed them.

Science is a team sport and I am grateful for the teams I had for the different fields I played on. Especially Harm, who supported planning and conducting all the field work. Lammert, I felt honoured when you asked my to join the first RiCOPTER training and with that opened new research opportunities for me, which tremendously helped this dissertation. Jean-Philippe and Nicolas, thank you for the very good and fast support with DART. My collaboration with you made me realise that the value of good software is not only the software itself, but good support coming with it. Juha, thank you for opening my eyes to the art of field reflectance measurements. Jan den Ouden and Leo, thank you for your help in Speulderbos. Henk and Jappe, thank you for helping out with UAV piloting.

Besides direct support, I benefited from a friendly and welcoming working environment. Simon, thanks for being a good companion on the train rides home and fruitful discussions about what matters in science. Mathieu, thanks for introducing me to the beauty of the Ardennes. Kalkidan, thanks for showing me the tasty Ethiopian cuisine. More thanks go to past and present members of the GRS group, with whom I could share a coffee and good talk: Adugna, Agnieszka, Aldo, Alvaro, Andrei, Anne, Arend, Arnan, Arnold, Arun, Astrid, Benni, Brice, Corné, Dainius, Daniela, Deborah, Diego, Eliakim, Erika R, Erika S,

Eskender, Federico, Giulia, Gustavo, Jalal, João, Johannes B, Johannes E, Johannes R, John, Jose, Konstantin, Lala, Lukasz, Marcello, Marian, Marston, Michi, Milutin, Nandika, Niki, Panpan, Patric, Peter, Qijun, Robert, Ron, Sabina, Samantha, Sarah, Shivangi, Sylvain, Sytze, Valerio, Willy, Ximena and Yang. Special thanks are reserved for Truus and Antoinette. Thank you for being patient with me filling in the thousands of forms for all kinds of purposes and whenever I wrecked another rental car.

Of course, all this wouldn't have been possible without the support from my family. Ralf und Katrin, Mama und Papa, danke, für die Werte und Fähigkeiten, die ihr mich gelehrt habt und den Freiraum und das damit verbundene Vertrauen, das ihr mir gegeben habt. Ronald, trotz unserer Unterschiede merke ich doch, wie gut es ist, einen Bruder wie dich zu haben. Irgendwie hast du auch einen Anteil an diesem Buch.

Last, but not least, I want to thank my own small family, Anna and Clara. Anna, we had an amazing journey so far, starting at the thresholds of our childhood homes. It was great to take all the steps and make decisions together, and make it work out to find places to study and work close to each other despite our different professional interests. Clara, you will probably only read this in a few years, but you already taught me so many things about life and myself. I am endlessly thankful for our decision to have you.

About the Author

Benjamin Brede was born on March 11, 1988 in Halle (Saale), Germany. He spent his childhood and youth in the village of Brenz in northern Germany, and visited the local primary school. Benjamin completed his high-school education in nearby Neustadt-Glewe. During high-school years, he developed an interest for photography, trained volleyball in two local clubs, wrote local newspaper articles around youth topics, and enjoyed the outdoors through cycling and canoeing.

Following his interests in Earth related and environmental topics, Benjamin started a Bachelor of Science programme in Geography at Philipps University of Marburg in 2008. Specializing in physical geography and following a minor in information science sparked his interest in quantitative environmental research. His BSc thesis dealt with cloud mapping from a ground based infrared scanner and was published as a peer reviewed journal article. During his BSc studies, Benjamin continued to play volleyball in the local volleyball team VfL Marburg 1860 and participated in local competitions.

For his MSc studies, Benjamin moved to Wageningen to start the Master Geo-Information Science in 2012. His MSc thesis dealt with the Amazon greening effect during dry seasons, for which results were presented on an international conference. For his MSc minor thesis, Benjamin conducted UAV and TLS fieldwork in tropical rainforests in Guyana. The results were published as a peer-reviewed journal article. Benjamin completed his MSc studies in 2015.

After finishing the MSc, he took the opportunity to start a PhD in Wageningen. During his PhD time, Benjamin supported TLS fieldwork in tropical forests in Ghana and Ethiopia, took part in the Sentinel-2 validation team meetings, acquired the Dutch professional UAV pilot license and co-organised the WUR PE&RC R-Users meetings.

Benjamin's recent research interests include new technologies for quantifying vegetation properties with focus on UAVs and LiDAR, and linking local scale field to global satellite observations.

Peer-reviewed Journal Publications

Besnard, S., N. Carvalhais, M. A. Arain, A. Black, **B. Brede**, N. Buchmann, J. Chen, J. G. P. W. Clevers, L. P. Dutrieux, F. Gans, M. Herold, M. Jung, Y. Kosugi, A. Knohl, B. E. Law, E. Paul-Limoges, A. Lohila, L. Merbold, O. Roupsard, R. Valentini, S. Wolf, X. Zhang, and M. Reichstein (2019). "Memory effects of climate and vegetation affecting net ecosystem CO2 fluxes in global forests". *PLOS ONE* 14.2. Ed. by D. Hui, e0211510. DOI: 10.1371/journal.pone.0211510.

Brede, **B.**, J.-P. Gastellu-Etchegorry, N. Lauret, F. Baret, J. Clevers, J. Verbesselt, and M. Herold (2018a). "Monitoring Forest Phenology and Leaf Area Index with the Autonomous, Low-Cost Transmittance Sensor PASTiS-57". *Remote Sensing* 10.7, 1032. DOI: 10.3390/RS10071032.

Brede, **B.**, A. Lau, H. M. Bartholomeus, and L. Kooistra (2017b). "Comparing RIEGL RiCOPTER UAV LiDAR Derived Canopy Height and DBH with Terrestrial LiDAR". *Sensors* 17.10, 2371. DOI: 10.3390/s17102371.

Brede, **B.**, J. Suomalainen, H. Bartholomeus, and M. Herold (2015b). "Influence of solar zenith angle on the enhanced vegetation index of a Guyanese rainforest". *Remote Sensing Letters* 6.12, 972–981. DOI: 10.1080/2150704X.2015.1089362.

Brede, **B.**, B. Thies, J. Bendix, and U. Feister (2017c). "Spatiotemporal High-Resolution Cloud Mapping with a Ground-Based IR Scanner". *Advances in Meteorology* 2017, 1–11. DOI: 10.1155/2017/6149831.

Calders, K., M. I. Disney, J. Armston, A. Burt, **B. Brede**, N. Origo, J. Muir, and J. Nightingale (2017). "Evaluation of the Range Accuracy and the Radiometric Calibration of Multiple Terrestrial Laser Scanning Instruments for Data Interoperability". *IEEE Transactions on Geoscience and Remote Sensing* 55.5, 2716–2724. DOI: 10.1109/TGRS.2017.2652721.

Decuyper, M., K. A. Mulatu, **B. Brede**, K. Calders, J. Armston, D. M. Rozendaal, B. Mora, J. G. Clevers, L. Kooistra, M. Herold, and F. Bongers (2018). "Assessing the structural differences between tropical forest types using Terrestrial Laser Scanning". *Forest Ecology and Management* 429.May, 327–335. DOI: 10.1016/j.foreco.2018.07.032.

Mulatu, K. A., M. Decuyper, **B. Brede**, L. Kooistra, J. Reiche, B. Mora, and M. Herold (2019). "Linking Terrestrial LiDAR Scanner and Conventional Forest Structure Measurements with Multi-Modal Satellite Data". *Forests* 10.3, 291. DOI: 10.3390/f10030291.

Roosjen, P. P., **B. Brede**, J. M. Suomalainen, H. M. Bartholomeus, L. Kooistra, and J. G. Clevers (2018). "Improved estimation of leaf area index and leaf chlorophyll content of a potato crop using multi-angle spectral data – potential of unmanned aerial vehicle imagery". *International Journal of Applied Earth Observation and Geoinformation* 66, 14–26. DOI: 10.1016/j.jag.2017.10.012.

Wagner, F. H., B. Hérault, D. Bonal, C. Stahl, L. O. Anderson, T. R. Baker, G. S. Becker, H. Beeckman, D. Boanerges Souza, P. C. Botosso, D. M. J. S. Bowman, A. Bräuning, **B. Brede**, et al. (2016). "Climate seasonality limits leaf carbon assimilation and wood productivity in tropical forests". *Biogeosciences* 13.8, 2537–2562. DOI: 10.5194/bg-13-2537-2016.

Wilkes, P., A. Lau, M. I. Disney, K. Calders, A. Burt, J. Gonzalez de Tanago, H. Bartholomeus, **B. Brede**, and M. Herold (2017). "Data Acquisition Considerations for Terrestrial Laser Scanning of Forest Plots". *Remote Sensing of Environment* 196, 140–153. DOI: 10.1016/j.rse.2017.04.030.

Other Scientific Publications

Bartholomeus, H., **B. Brede**, A. Lau, and L. Kooistra (2017). "Capturing forest structure using UAV based lidar". In: *International Conference on Unmanned Aerial Vehicles in Geomatics UAV-g 2017, Sept 4-7, 2017*. Bonn, Germany.

Brede, **B.**, J. Verbesselt, L. Dutrieux, and M. Herold (2015a). "Performance of the Enhanced Vegetation Index to Detect Inner-annual Dry Season and Drought Impacts on Amazon Forest Canopies". In: *ISPRS - International Archives of the Photogrammetry, Remote Sensing and Spatial Information Sciences*. Vol. XL-7/W3, 337–344. DOI: 10.5194/isprsarchives-XL-7-W3-337-2015.

Brede, **B.**, H. Bartholomeus, J. Suomalainen, J. Clevers, J. Verbesselt, M. Herold, D. Culvenor, and F. Gascon (2016a). "The Speulderbos Fiducial Reference Site for Continuous Monitoring of Forest Biophysical Variables". In: *Living Planet Symposium 2016, Prague, Czech Republic, 9-13 May 2016*. Prague, 5.

Brede, **B.**, J. Clevers, J. Verbesselt, M. Herold, J. Verrelst, and F. Gascon (2017a). "Multi-sensor LAI and Cab retrieval for a Dutch Beech forest site". In: *Remote Sensing of Fluorescence, Photosynthesis and Vegetation Status*. Frascati, Italy.

Brede, **B.**, E. Hamunyela, M. Herold, F. Gascon, and F. M. Seifert (2016b). "Sentinel-2 for Forest Monitoring". In: *1st Sentinel-2 Validation Team Meeting*. Frascati, Italy.

Brede, **B.**, E. Hamunyela, J. Verbesselt, and M. Herold (2018b). "Sentinel-2 for Forest Phenology and Forest Degradation Monitoring". In: *2nd Sentinel-2 Validation Team Meeting*. Frascati, Italy.

Brede, **B.**, J. Suomalainen, P. P. Roosjen, H. Aasen, L. Kooistra, H. M. Bartholomeus, J. G. Clevers, and M. Herold (2018c). "Opportunities of UAV based Sensing for Vegetation Land Product Validation". In: *Land Product Validation and Evolution*. Frascati, Italy.

Brede, **B.**, J. Verrelst, J.-P. Gastellu-Etchegorry, J. G. Clevers, J. Verbesselt, and M. Herold (2017d). "Benchmarking Radiative Transfer Model inversion schemes to estimate Leaf Area Index of a Dutch Beech Forest Site". In: *Recent Advances in Quantitative Remote Sensing V*. Valencia, Spain.

Kooistra, L., H. Bartholomeus, S. Mucher, H. Kramer, J. Franke, C. Ivushkin, and **B. Brede** (2018). "Capturing crop height over the growing season from UAV based LiDAR". In: *EurAgEng 2018, Wageningen, 8-12 July 2018*. Wageningen, The Netherlands.

Wang, N., H. Bartholomeus, L. Kooistra, J. Suomalainen, **B. Brede**, M. Novani, D. Masiliunas, and J. Clevers (2019). "Measuring Temporal Patterns of Crop Sun-induced Chlorophyll Fluorescence at Canopy and Plot Scale". In: *11th EARSeL Workshop on Imaging Spectroscopy, 6-8 Feb 2019*. Brno, Czech Republic.

PE&RC Training and Education Statement

With the training and education activities listed below the PhD candidate has complied with the requirements set by the C.T. de Wit Graduate School for Production Ecology and Resource Conservation (PE&RC) which comprises of a minimum total of 32 ECTS (= 22 weeks of activities)

Review of literature (4.5 ECTS)

- Leaf Area Index Products based on Satellite Observations: Retrieval Methods & Validation (2016)

Writing of project proposal (4.5 ECTS)

- A Multi-Sensor Approach for Next Generation Forest Biophysical Satellite Products (2015)

Post-graduate courses (6.1 ECTS)

- 6th ESA Land Training, University of Agronomic Science and Veterinary Medicine (USAMV), Bucharest (2015)
- DART Training 2017; CNRS, Toulouse (2017)
- Bayesian Statistics; PE&RC (2016)
- Machine Learning for Spatial Data; PE&RC (2017)

Laboratory training & working visits (5.0 ECTS)

- BNUC-L RPAS license; EuroURC & IL&T (2016)
- UAV Lidar remote sensing with the RIEGL RiCopter system; RIEGL LMS GmbH (2016)

Invited review of (unpublished) journal manuscript (15.0 ECTS)

- IEEE Transactions on Geoscience and Remote Sensing (2x, 2017 – 2018)
- International Journal of Applied Earth Observation and Geoinformation (2018)
- International Journal of Biometeorology (2x, 2018)
- International Journal of Remote Sensing (2015)
- Optics Express (2018)
- Remote Sensing (7x, 2015 – 2018)
- Surveys in Geophysics (2018)

Competence strengthening / skills courses (5.2 ECTS)

- Data Management Planning; PE&RC (2015)
- Reviewing a Scientific Paper; PE&RC (2016)
- Project and Time Management; PE&RC (2017)
- R for Big Data; PE&RC (2017)
- Writing Grant Proposals; PE&RC (2017)
- Research Integrity; PE&RC (2017)

PE&RC Annual meetings, seminars and the PE&RC weekend (2.4 ECTS)

- PE&RC First Years Weekend (2015)
- PE&RC Day (2016)
- PE&RC Midterm Weekend (2017)
- PE&RC Last Years Weekend (2018)

Discussion groups / local seminars / other scientific meetings (9.0 ECTS)

- Remote Sensing Thematic Group Meeting; WUR (2015 – 2019)
- R User Meeting; WUR (2017 – 2019)

International symposia, workshops and conferences (24.1 ECTS)

- International Symposium on Remote Sensing of Environment (ISRSE-36); poster presentation; Berlin, Germany (2015)
- S2 Expert User Meeting; oral presentation; Frascati, Italy (2015)
- ESA Living Planet 2016; poster presentation; Prague, Czech Republic (2016)
- IDEAS+ CalVal workshop; oral presentation; Frascati, Italy (2016)
- 1st Sentinel-2 Validation Team Meeting; oral presentation; Frascati, Italy (2016)
- Remote Sensing of Fluorescence, Photosynthesis and Vegetation Status 2017; poster presentation; Frascati, Italy (2017)
- IDEAS+ CalVal workshop; oral presentation; Lille, France (2017)
- Recent Advances in Quantitative Remote Sensing (RAQRS V); poster presentation; Valencia, Spain (2017)
- IDEAS+ CalVal workshop; oral presentation; Frascati, Italy (2017)

- 2nd Sentinel-2 Validation Team Meeting; poster presentation; Frascati, Italy (2018)
- Land Product Validation and Evolution (LPVE 2018); oral presentation; Frascati, Italy (2018)
- IDEAS+ CalVal workshop; oral presentation; Davos, Switzerland (2018)
- NCG Symposium; oral presentation; Wageningen, the Netherlands (2018)
- ESA Living Planet 2019; poster presentation; Milan, Italy (2019)
- IDEAS+ CalVal workshop; oral presentation; Wageningen, The Netherlands (2019)

Lecturing / supervision of practical's / tutorials (3.0 ECTS)

- Geo-scripting (2016)
- Remote Sensing (2016, 2017)

Supervision of MSc students (2.0 ECTS)

- Assessment of tree detection and height estimation by AHN-2 point cloud data (2018)
- Building a Raspberry Pi Prototype for Continuous Forest Canopy Monitoring (2019)

This work was carried out as part of the IDEAS+ contract funded by ESA/ESRIN.

Cover image: UAV-LS point density over the Speulderbos site